การศึกษาโครงสร้างและหน้าที่ของเอนไซม์ไคติเนส เอ จากเชื้อแบคทีเรีย
Vibrio carchariae

นางชมภูนุช ส่งสิริฤทธิกุล

STRUCTURAL AND FUNCTIONAL

CHARACTERIZATION OF CHITINASE A FROM

Vibrio carchariae

Chomphunuch Songsiriritthigul

A Thesis Submitted in Partial Fulfillment of the Requirements for

the Degree of Doctor of Philosophy in Biochemistry

Suranaree University of Technology

Academic Year 2007

STRUCTURAL AND FUNCTIONAL CHARACTERIZATION OF

CHITINASE A FROM *Vibrio carchariae*

Suranaree University of Technology has approved this thesis submitted in partial fulfillment of the requirements for the Degree of Doctor of Philosophy.

Thesis Examining Committee

_____

(Assoc. Prof. Dr. Malee

Tangsathitkulchai)

Chairperson

_____

(Asst. Prof. Dr. Wipa Suginta)

Member (Thesis Advisor)

_____

(Prof. Dr. Dietmar Haltrich)

Member

_____

(Assoc. Prof. Dr. James R. Ketudat-

Cairns)

Member

_____

(Dr. Rodjana Opassiri)

Member

_____   _____

(Assoc. Prof. Dr. Saowanee Rattanaphani) (Assoc. Prof. Dr. Sompong Thammathaworn)

Vice Rector for Academic Affairs   Dean of Institute of Science

ชมภูนุช ส่งสิริฤทธิกุล : การศึกษาโครงสร้างและหน้าที่ของเอนไซม์ไคติเนส เอ จากเชื้อ
แบคทีเรีย *Vibrio carchariae* (STRUCTURAL AND FUNCTIONAL
CHARACTERIZATION OF CHITINASE A FROM *Vibrio carchariae*)
อาจารย์ที่ปรึกษา : ผู้ช่วยศาสตราจารย์ ดร.วิภา สุจินต์, 236 หน้า.

ไคติเนส เอ จากเชื้อ *Vibrio carchariae* เป็นเอ็นโดไคติเนสทำหน้าที่สลายไคตินให้ได้
ผลิตผลสุดท้ายคือ $GlcNAc_2$ เพื่อนำไปสู่ความเข้าใจกลไกการเร่งปฏิกิริยาของเอนไซม์ให้ดีขึ้น จึงได้
ทำการตกผลึกเอนไซม์สี่ชนิด ได้แก่ ผลึกโปรตีนดั้งเดิม ผลึกโปรตีนกลายพันธุ์ E315M ผลึก
เชิงซ้อนของโปรตีนกลายพันธุ์ E315M กับสารตั้งต้น NAG_5 และ NAG_6 และทำการวัดการหักเห
ของแสงเอกซเรย์ได้ความละเอียดถึง 2.00 Å 1.70 Å 1.72 Å และ 1.80 Å พบว่าโครงสร้างสามมิติ
ของเอนไซม์ไคติเนส เอ มีสามองค์ประกอบหลักได้แก่ หน่วยจับสารตั้งต้นที่ปลาย N   หน่วยย่อย
สลายสารตั้งต้นมีโครงสร้างเป็น $(\beta/\alpha)_8$-TIM-barrel   และหน่วยแทรกระหว่างหน่วยย่อยสลายมี
โครงสร้างเป็น $\alpha+\beta$ หน่วยย่อยสลายมีลักษณะเป็นร่องยาวลึกขนาด 33 Å × 14 Å มีปลายเปิด
ทั้งสองด้าน และมีบริเวณจับกับสารตั้งต้นประกอบด้วยหกบริเวณย่อย ตั้งแต่ -4 (ด้านนอนรีดิวซิง)
จนถึง +2 (ด้านรีดิวซิง) โครงสร้างของ E315M-NAG_5 แสดงให้เห็นว่าน้ำตาล NAG_5 จับกับบริเวณ
จับด้วยโครงรูปแบบตรง ขณะที่โครงสร้างของ E315M-NAG_6 แสดงให้เห็นว่าน้ำตาล NAG_6 จับกับ
บริเวณจับด้วยโครงรูปแบบหัก การตรวจพบโครงรูปชั่วคราวจากแผนที่ความหนาแน่นอิเล็กตรอน
ของโครงสร้าง E315M-NAG_6 แสดงให้เห็นว่าน้ำตาลที่จับกับบริเวณเร่งมีการเปลี่ยนโครงรูปเพื่อทำ
ให้เกิดปฏิกิริยาการสลาย นอกจากนี้ยังพบว่ากรดอะมิโนวงแหวนหลายตัวที่ไม่เปลี่ยนแปลงจัดเรียง
เป็นแนวอยู่ที่บริเวณจับและทำหน้าที่จับกับน้ำตาลโดยการสร้างชั้นไฮโดรโฟบิกกับวงแหวนไพรา
โนสของน้ำตาล

การกลายพันธุ์เฉพาะตำแหน่งของกรดอะมิโน Trp168 Tyr171 Trp275 และ Trp570 ให้เป็น
ไกลซีน และ Trp397 ให้เป็นฟีนิลอะลานีน ส่งผลให้มีการเปลี่ยนแปลงรูปแบบการย่อยสลายของไค
โตโอลิโกแซคคาไรด์ ซึ่งบ่งชี้ว่ากรดอะมิโนเหล่านี้มีความสำคัญต่อการสลายของไคตินที่ละลายน้ำ
ได้

สาขาวิชาชีวเคมี   ลายมือชื่อนักศึกษา_____
ปีการศึกษา 2550   ลายมือชื่ออาจารย์ที่ปรึกษา_____
                                                    ลายมือชื่ออาจารย์ที่ปรึกษาร่วม_____

CHOMPHUNUCH SONGSIRIRITTHIGUL : STRUCTURAL AND FUNCTIONAL CHARACTERIZATION OF CHITINASE A FROM *Vibrio carchariae*. THESIS ADVISOR : ASST. PROF. WIPA SUGINTA, Ph.D. 236 PP.

CHITINASE A/CHITOOLIGOSACCHARIDES/ENDOCHITINASE/TIM BARREL DOMAIN/TRANSIENT CONFORMATION/*Vibrio carchariae*

Chitinase A from *Vibrio carchariae* is an endochitinase that degrades chitin, yielding $GlcNAc_2$ as the end product. To understand the mode of enzyme action, four crystal structures of wild-type chitinase A, mutant E315M without substrate and mutant E315M in complex with NAG_5 and NAG_6 were refined at 2.00 Å, 1.70 Å, 1.72 Å and 1.80 Å resolution. The overall structure of chitinase A comprises three separate domains; an *N*-terminal chitin-binding domain, a catalytic $(\beta/\alpha)_8$-TIM-barrel domain, and a small $(\alpha+\beta)$ insertion domain. The substrate binding cleft of the enzyme has a long, deep groove structure of 33 Å × 14 Å and comprises multiple binding sites extended from subsite -4 (at the non-reducing end) to subsite +2 (at the reducing end). The crystal structures of E315M-NAG_5 and E315M-NAG_6 revealed that the enzyme bound to the straight conformation of NAG_5, but to the bent conformation of NAG_6. The transient conformation of -1 NAG observed in the electron density map of E315M-NAG_6 complex strongly suggested that the interacting sugars adopted a conformational change to facilitate hydrolysis. Several conserved aromatic residues that lie along the substrate binding cleft are found to act as the binding residues, by forming hydrophobic stack against the pyranose rings of the bound sugars.

Point mutations of Trp168, Tyr171, Trp275 and Trp570 to glycine and Trp397 to phenylalanine significantly changed the cleavage patterns against chitooligosaccharides, indicating that these residues are important for the hydrolysis of soluble chitin.

School of Biochemistry   Student's Signature_____

Academic Year 2007   Advisor's Signature_____

                                    Co-adviser's Signature_____

ACKNOWLEDGEMENTS

CONTENTS

CONTENTS (Continued)

CONTENTS (Continued)

CONTENTS (Continued)

CONTENTS (Continued)

CONTENTS (Continued)

CONTENTS (Continued)

Page

LIST OF TABLES

LIST OF TABLES (Continued)

LIST OF FIGURES

LIST OF FIGURES (Continued)

LIST OF FIGURES (Continued)

LIST OF FIGURES (Continued)

LIST OF ABBREVIATIONS

A	Absorbance
BSA	Bovine serum albumin
$^{\circ}$C	Degree celsius
CD	Circular dichroism
CSA	Nonhygroscopic ammonium (+)-10-comphorsulfonate
dmole	Deci mole
g	Gravitational acceleration
(m, μ, n) g	(Milli, micro, nano) gram
h	Hour
IPTG	Isopropyl-β-D-thiogalactopyranoside
kDa	Kilo Dalton
min	Minute
(m, μ) M	(Milli, micro) molar
(m, μ) l	(Milli, micro) liter
MRE	Mean residue ellipticity
M_r	Relative molecular mass
OD	Optical density
PAGE	Polyacrylamide gel electrophoresis
SDS	Sodium dodecyl sulfate
s	Second

LIST OF ABBREVIATIONS (Continued)

TEMED	Tetramethylenediamine
Tris	Tris-(hydroxymethyl)-aminoethane
UV	Ultraviolet
v/v	Volume/volume
w/v	Weight/volume

CHAPTER I

INTRODUCTION

1.1 Chitin and applications

Chitin, the second most abundant biopolymer in nature, is composed of units of *N*-acetyl-D-glucosamine (GlcNAc, NAG or G1) linked by β-1→4-glycosidic bonds (Figure 1.1). This fibrous polysaccharide is widely distributed in the shells of crustaceans (such as lobsters, crabs, and shrimps), in the cuticles of insects in the shells and skeletons of mollusks and in the cell walls of fungi (Huber *et al.*, 1995).
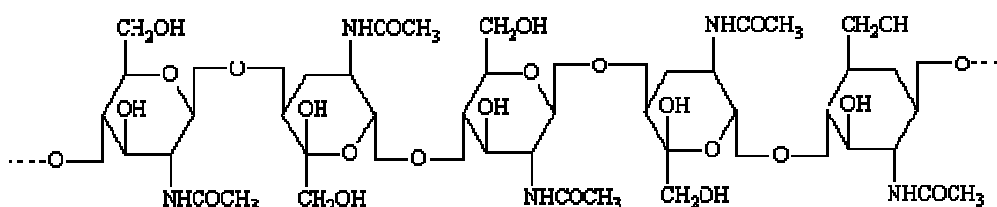
Figure 1.1 The chitin repeating unit (Cohen-Kupiec and Chet, 1998).

The abundance of chitin in both marine and terrestrial environments has attracted much attention in biomedical, pharmacological, agricultural and biotechnological applications (Li *et al.*, 1992; Muzzarelli, 1993; 1996). A serious pollution from chitin wastes released from seadfood industries leads to an interest to bioconvert chitin to utilizable carbohydrates (Brine, 1984). *N*-acetylchitooligosaccharides, which are of special interest in the fileds of agriculture and medicine, have been prepared by chemical and enzymatic methods. However, the

chemical hydrolysis usually occurs via a series of chemical reactions that generate unwanted by-products (Rupley, 1964; Chang *et al*., 1997; 2000). On the other hand, the enzymatic hydrolysis of chitin occurs under mild conditions, in which the selectivity of the end products depending on the substrate specificity of chitinolytic enzymes. Chitinases (EC 3.2.1.14) are major enzymes that primarily hydrolyze chitin into small oligosaccharide fragments. The enzymes are found in various organisms, including bacteria, fungi, plants and animals (Cohen-Kupiec and Chet, 1998). Bacteria produce chitinases to meet nutritional needs. They usually secrete several chitinases, probably to hydrolyze different types of chitin and convert them to carbon and nitrogen sources (Svitil *et al*., 1997). Fungal chitinases have multiple functions. They play a nutritional role as well as involve in fungal development and morphogenesis (Sahai and Manocha, 1993). Plants use chitinases as a defense against pathogenic fungi (Leah *et al*., 1991). In animals and some vertebrate species, chitinases are involved in dietary uptake processes (Spindler-Barth *et al*., 1993). For example, chitinases are found in the digestive tract of gold fish *Carassius auratus* (L.) (Jeuniaux, 1961; 1966), sea bass *Latelabrax japonicus* (Okutani, 1967; 1977) and dover sole *Solea solea* (L.) (Clark *et al*., 1988).

1.2 Classification of chitinases

Chitinases (EC 3.2.1.14) are classified in two major categories based on the mode of enzyme action (Cohen-Kupiec and Chet, 1998). Endochitinases cleave chitin randomly at internal sites, generating soluble chitooligo fragments, such as chitotetraose, chitotriose and chitobiose. On the other hand, exochitinases progressively remove *N*-acetylglucosamine residues from the non-reducing end of a

chitin chain. Other chitinolytic enzymes, such as chitobiases (EC 3.2.1.52 or formally EC 3.2.1.30) release $GlcNAc_2$ units in a stepwise mode, while N-acetyl-β-1,4-D-glucosaminidases (EC 3.2.1.52) cleave the oligomeric products released by endochitinases, generating monomeric GlcNAc.

Based on amino acid sequence and folding similaritity (Henrissat and Bairoch, 1993; Davies and Henrissat, 1995), chitinases are grouped into unrelated families 18 and 19 glycosyl hydrolases. Both families show little homology, differing in both structures and mechanisms (Davies and Henrissat, 1995). Family 18 chitinases are distributed in a wide range of organisms, including viruses, bacteria, fungi, plants, insects, mammals, whereas family 19 chitinases are mainly found in plants (Brameld and Goddard, 1998; Sasaki *et al*., 2002) and only found in a bacterium, *Streptomyces griseus* HUT 6037 (Mitsutomi *et al*., 1995).

The catalytic domain of family 18 chitinases has a deep substrate-binding cleft located at the top of the catalytic $(β/α)_8$ barrel domain. In contrast, the catalytic domain of family 19 chitinases (Hart *et al*., 1995) does not possess a TIM-barrel structure, but comprises of two lobes, each of which is rich in α-helical structure. The substrate binding cleft of family 19 chitinases is positioned between the two lobes (Figure 1.2).
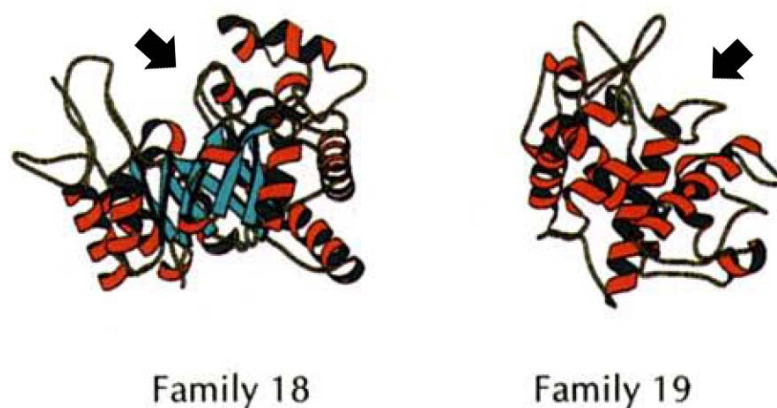
Family 18   Family 19

Figure 1.2 A ribbon representation of the main characteristics of the catalytic domains of the family 18 and 19 chitinases (modified from Davies and Henrissat, 1995). An arrow indicates the substrate-binding cleft.

The mode of enzyme action of family 18 chitinases has been proposed to be the anchimeric stabilization mechanism (Brameld and Goddard, 1998). To date, several experimental studies identified the β-anomeric form of the hydrolytic products, which confirmed that family 18 chitinases catalyze the hydrolytic reaction through a retaining mechanism (Armand *et al*., 1994; Hollis *et al*., 1997; Babiker *et al*., 1997; 2002; Fukamizo, *et al*., 2001; Aronson *et al*., 2003; 2006; Suginta *et al*., 2004; 2005). On the other hand, the mode of action of family 19 chitinases employs the concerted single displacement mechanism, which yields an inversion of anomeric configuration with a predominant α-anomeric product (Hollis *et al*., 1997).

Bacterial family 18 chitinases are further classified into four subclasses, which are chitinase A, B, C1 and D1 (Suzuki *et al*., 1999; 2002; Matsumoto *et al*., 1999). All of them contain the catalytic domain with two characteristic sequence motifs, SxGG and DxxDxDxE and found to possess a TIM-barrel structure. The distinct

characteristics of chitinase A are an N-terminal signal peptide and a small α+β insertion domain inserted between the two catalytic regions (Brurberg *et al.*, 1994; 1995). In addition, the chitin-binding domain of chitinase A locates at the N-terminal part, preceeding the catalytic domain. In contrast, the catalytic domain of chitinases B and C1 locates at the N-terminus lacking the signal peptide. The C-terminal end of chitinase C1 contains an additional fibronectin type III-like (FnIII-like) domain preceeding the chitin-binding domain. On the other hand, chitinase D1 of *Bacillus circulans* also possesses an N-terminal chitin-binding domain that is similar to chitinase A, but followed by FnIII-like domain (Matsumoto *et al.*, 1999).

The domain organization of chitinases A, B and C1 from *Serratia marcescens* 2170 and chitinase D1 from *B. circulans* is presented in Figure 1.3.
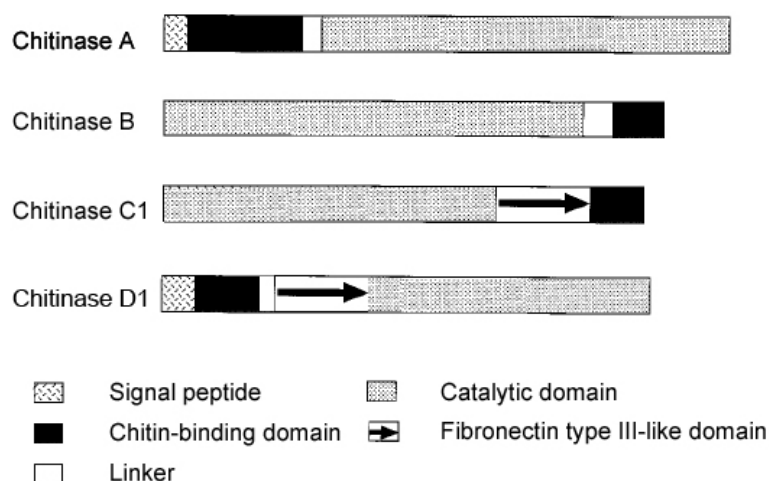
Figure 1.3 The domain organization of chitinase A, B and C1 from *S. marcescens* 2170 and chitinase D1 from *B. circulans* (modified from Suzuki *et al.*, 1999 and Brurberg *et al.*, 1994; 1995).

To date, only X-ray structures of chitinase A and chitinase B are available. Figure 1.4 shows the X-ray structure of *S. marcescens* chitinase A (Perrakis *et al.*,

1994) comprising three domains, an N-terminal chitin-binding domain, a catalytic ($\beta/\alpha)_8$-barrel domain, and a small (α +β) domain, which is inserted into the ($\beta/\alpha)_8$-barrel domain. The 3D-structure of *S. marcescens* chitinase B (van Aalten *et al*., 2000) reveals the N-terminal catalytic ($\beta/\alpha)_8$-barrel domain and a C-terminal putative chitin-binding domain. The support loop and the chitin-binding domain extend the substrate-binding cleft of chitinase B from the reducing side of the active site, whereas the chitin-binding domain of chitinase A extends the substrate-binding cleft from the non-reducing end of the catalytic domain.
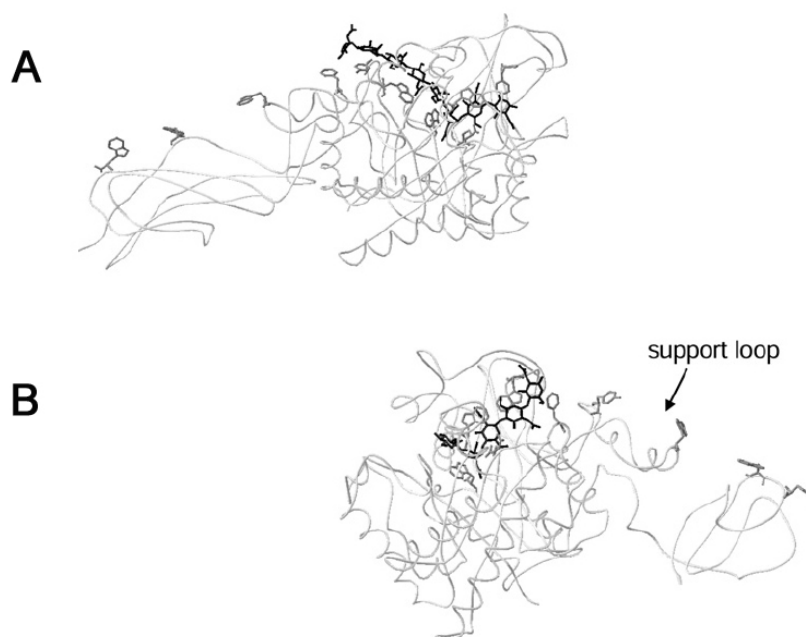
Figure 1.4 Crystallographic structures of (A) chitinase A (Papanikolau *et al*., 2001) and (B) chitinase B (van Aalten *et al*., 2001), showing the catalytic domains co-crystallized with oligosaccharide substrates.

Although chitinase A and other two *S. marcescens* chitinases (chitinases B and C1) have different orientations when bound to a polymeric chitin chain, the catalytic

domains of these three enzymes share the same overall fold of the $(\beta/\alpha)_8$-barrel. The catalytic domain of chitinase A contains a deep substrate binding groove, which is open at both sides. This structure is a characteristic of endochitinase (Perrakis *et al*., 1994; Aronson *et al*., 2003). In contrast, the substrate binding cleft of chitinase B is relatively closed (van Aalten *et al*., 2001), giving this cleft much of the tunnel character. This is a typical characteristic of exo-acting glycosyl hydrolases. Although, no availability of the 3D-structure of chitinase C1, a sequence comparison of chitinase C1 with other bacterial chitinases clearly indicates that the catalytic domain of chitinase C1 is smaller than that of chitinases A and B. The lack of the $\alpha+\beta$ insertion domain in chitinase C1 suggests that the substrate binding groove is much more open, which is also a characteristic of an endochitinase. In a synergistic effect of chitin degradation, it is likely that chitin degradation is initiated by the action of endo chitinase A and chitinase C1, followed by the exo-action of chitinase B (Suzuki *et al*., 1999; 2002).

1.3 Enzymatic properties of chitinases

The enzymatic activity of chitinases has been examined by a variety of methods, including a monitor of changes in the molecular size of substrates and determination of oligosaccharides, or *N*-acetyl-glucosamine liberated in the reaction. The colorimetric assay by detecting the amount of monomeric GlcNAc released from colloidal chitin could be achieved by the enzymatic hydrolysis of the reaction products, followed by derivatizing with dimethylaminobenzadehyde (DMAB) (Boller and Mauch, 1988) or ferriccyanide reagents (Imoto and Yagishita, 1971). The most widely used substrates for testing the chitinase activity are *p*-nitrophenyl-*N*-acetyl-

chitooligosaccharides (pNP-GlcNAc$_{(1-5)}$) (Xia *et al*., 2001; Aronson *et al*., 2003; 2006; Suginta *et al*., 2004; 2005) and 4-methylumbelliferyl-*N*-acetyl-chitooligosaccharides (4MU-(GlcNAc)$_{1-5}$) (Hollis *et al*., 1997; Tanaka *et al*., 1999; 2001; Fukamizo *et al*., 2001). Chromogenic measurements monitor the release of *p*-nitrophenol (*p*NP) or 4-methylumbelliferone (4MU) from the chromogenic substrates. Such method is convenient, rapid, and quantitative, but gives a limited explaination on the enzyme binding mode.

Viscosity measurements for chitinase activity monitor the changes in the molecular size of substrates (Jeuniaux, 1966), by measuring a significant reduction of the viscosity upon chitin degradation. Insoluble compounds, such as colloidal chitin and glycol chitin are used in this assay procedure. Although this method is somewhat troublesome and time consuming, it provides an insight in the endo, exo characteristics of the studied enzymes. Gel activity assay (Trudel and Asselin, 1989; Thamthiankul *et al*., 2001; Suginta *et al*., 2005) is also used to determine chitinase activity using glycol chitin as the substrate. The enzyme activity could be visualized on gel with Calcofluor White M2R, which is fluorescent and highly specific for glycol chitin. Alternatively, analyses of the degradation products obtained from the hydrolysis of colloidal chitin and soluble *N*-acetyl-chitooligosaccharides by chitinases can be carried out using HPLC and TLC (Table1.1).

Table 1.1 A summary of enzymatic methods of chitinase enzymes.

Source	Substrate	Methods of characterization	References
Aspergillus fumigatus YJ-407	pNP-GlcNAc$_2$, GlcNAc$_{2, 3, 6}$ and colloidal chitin	Qualitative TLC (study of time course reaction)	Xia *et al*., 2001
	Glycol chitin	Viscosimetric method	
B. thuringiensis subsp. *Pakistani*	Glycol chitin	Gel activity assay	Thamthiankul *et al*., 2001
	Colloidal chitin	Qualitative TLC (study of time course reaction)	
B. circulans WL-12	GlcNAc$_{3, 6}$	Quantitative HPLC (study of time course reaction)	Armand *et al*., 1994;
	GlcNAc$_4$H	^{1}H NMR (identification of anomeric products)	Watanabe *et al*., 2003
Barley	4MU-GlcNAc$_3$	Colorimetric method	Hollis *et al*., 1997
Coccidioides immitis	GlcNAc$_6$	Quantitative HPLC (identification of anomeric products)	Fukamizo *et al*., 2001
Hevea brasiliensis	GlcNAc$_{5, 6}$	Quantitative HPLC (study of hydrolytic pattern)	Bokma *et al*., 2000
Pyrococcus kodakaraensis KOD1	4MU-GlcNAc$_{(1-3)}$	Colorimetric method	Tanaka *et al*., 1999;
	pNP-GlcNAc$_{(1-5)}$, GlcNAc$_{1-6}$ and colloidal chitin	Qualitative TLC and quantitative HPLC (study of time course reaction)	2001

Table 1.1 (continued).

Source	Substrate	Methods of characterization	References
S. marcescens	pNP-GlcNAc$_{(2-4)}$	Qualitative TLC (study of time course reaction)	Aronson *et al*., 2003;
	GlcNAc$_5$	[1]FAB-MS (identification of anomeric products)	2006
	GlcNAc$_{3-6}$	Quantitative HPLC (study of time course reaction and identification of anomeric products)	
Vibrio carchariae	pNP-GlcNAc$_2$	Colorimetric method	Suginta *et al*., 2004;
	GlcNAc$_{3-6}$	Quantitative HPLC-MS (study of time course reaction)	2005; 2007
	Colloidal chitin	Quantitative HPLC-MS (identification of anomeric products)	
	Glycol chitin	Viscosimetric assay and gel activity assay	
Vibrio sp. 98CJ11027	Colloidal chitin	Qualitative TLC (study of time course reaction)	Park *et al*., 2000

[1]FAB-MS (fast atom bombardment-mass spectrometry)

1.4 The catalytic mechanism of family 18 chitinases

Since 1994, the 3D-structures of family 18 chitinases were solved using protein crystallography technique either in the absence or in the presence of substrates and inhibitors. These structures include *S. marcescens* chitinase A (Perrakis *et al*., 1994; Aronson *et al*., 2003; Papanikolau *et al*., 2001; 2003), *S. marcescens* chitinase B (van Aalten *et al*., 2001), *B. circulans* chitinase A1 (Matsumoto *et al*., 1999) and *C. immitis* chitinase (Hollis *et al*., 2000; Bortone *et al*., 2002). As mentioned earlier, the 3-D structures reveal that all the enzymes in this family share the catalytic domain consisting of a $(\beta/\alpha)_8$-barrel with a deep substrate-binding cleft formed by the loops following the C-termini of the eight parallel β-strands. The glutamic residue at the end of the DxxDxDxE motif is identified as the catalytic residue (Perrakis *et al*., 1994; Hollis *et al*., 2000).

In terms of the mode of enzyme action, there are two major general mechanistic pathways that describe the acid hydrolysis catalyzed by glycosyl hydrolases (Brameld and Goddard, 1998); i) the retention of the stereochemistry of the anomeric oxygen at C1' relative to the initial configuration (see Scheme 1 and 3); and ii) the inversion of the stereochemistry (see Scheme 2).

Scheme 1. Double-Displacement Hydrolysis Mechanism Which Requires Two Acidic Residues in the Active Site and Leads to Retention of the Anomeric Configuration
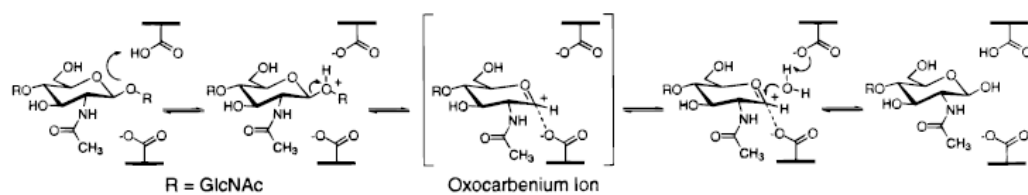
Scheme 2. Single-Displacement Mechanism Which Requires Only One Acidic Residue in the Active Site and Results in Inversion of the Anomeric Configuration
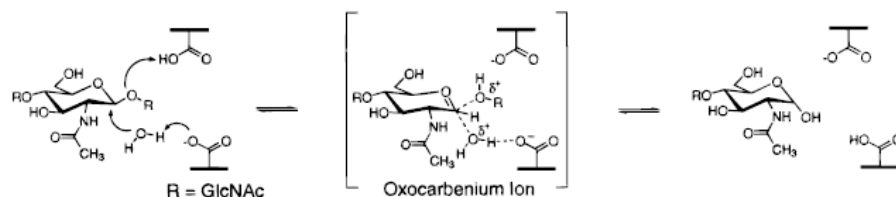
Scheme 3. Anchimeric Stabilization Hydrolysis Mechanism[24] of Family 18 Chitinases Where the Substrate Is Distorted to a Boat Conformation and the Oxazoline Ion Intermediate Is Stabilized through Anchimeric Assistance from the Neighboring C2′ N-Acetyl Group
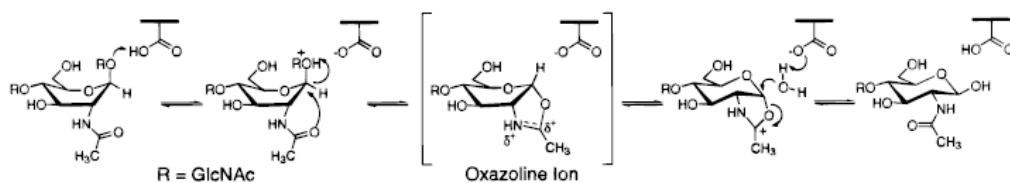
Two different models have been proposed for the retaining catalytic mechanism of family 18 glycosyl hydrolases (Perrakis *et al*., 1994; Terwisscha van Scheltinga *et al*., 1994). The first model is designateted as the double displacement hydrolysis mechanism (Scheme 1). An example of the double displacement mechanism is hen egg white lysozyme, HEWL (Blake *et al*., 1965), which requires two acidic residues, one of which is protonated. According to this mechanism, the *β*-(1,4)-glycosidic oxygen is protonated by the carboxylic group of Glu35, leading to an oxocarbenium ion intermediate that is stabilized by a second carboxylate group (Asp52). Subsequent nucleophilic attack by water yields the hydrolytic product, which retains the initial anomeric configuration.

The second model of the retaining mechanism is described as the substrate-assisted catalytic mechanism (see Scheme 3). This mechanism has been proposed

based on the X-ray structure of hevamine chitinase in complex with allosamidin inhibitor (Terwisscha van Scheltinga *et al*., 1995). With this mechanism, the catalytic residue (Glu127) plays a functional role in protonating the glycosidic oxygen that links between NAG units at subsites -1 and +1. The positive charge built up on -1 NAG led to the formation of an oxazolinium intermediate, which is stabilized by an interaction with its own *N*-acetyl group (Figure 1.5).

The molecular dynamics (MD) simulations investigated the substrate binding and the possible resulting hydrolytic intermediates of chitinase A from *S. marcescens* (Brameld and Goddard, 1998). It was found that the hexaNAG substrate was forced to distort to a boat geometry at subsite -1 prior to protonation, which then led to a spontaneous anomeric bond cleavage and a subsequent formation of an oxazolinium ion. X-ray diffraction analyses confirmed that the reaction mechanism of all the family 18 chitinases proceeds through the substrate-assisted catalytic mechanism (Terwisscha van Scheltinga *et al*., 1995; 1996; van Aalten *et al*., 2001; Papanikolau *et al*., 2001; 2003; Bortone *et al*., 2002; Aronson *et al*., 2003).

In contrast, the single displacement mechanism as shown in Scheme 2 is likely to be employed by family 19 chitinases. The hydrolytic products of family 19 chitinases showed an inversion of the anomeric configuration (Fukamizo *et al*., 1995; Iseli *et al*., 1996; Hollis *et al*., 1997; Ueda *et al*., 2003). The crystal structure of barley chitinase (Hart *et al*., 1995) suggested that the second catalytic carboxylate may be sufficiently close to make coordinations with a bound water molecule that acts as a nucleophile.
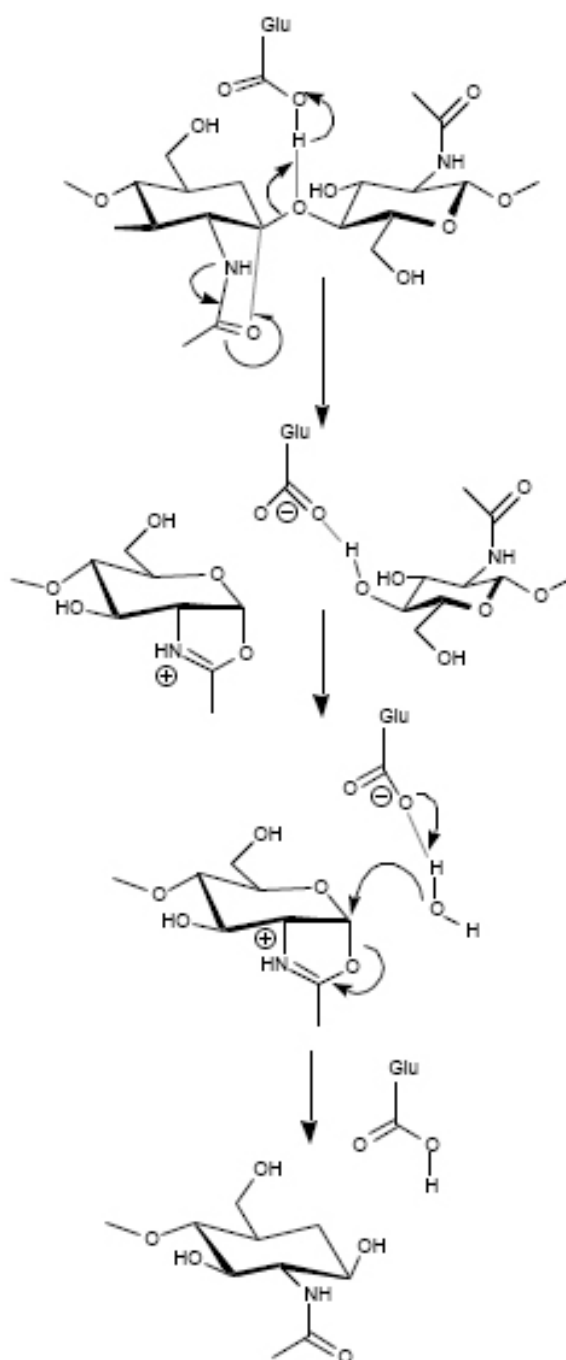
Figure 1.5 Substrate-assisted hydrolysis catalyzed by family 18 chitinases. The oxazolinium ion intermediate is stabilized by an anchimeric assistance of the sugar *N*-acetyl group after proton donation from the catalytic carboxylic acid (Fukamizo, 2000).

1.5 Structural analysis of family 18 chitinases

The first three-dimensional structure of bacterial chitinase A was determined from *S. marcescens* (Perrakis *et al*., 1994). The crystal structure of the native enzyme was solved and refined to a 2.3 Å resolution using the synchrotron radiation source. *S. marcescens* chitinase A consists of three domains: i) an all β-strand N-terminal chitin-binding domain (similar to FnIII-like domain), ii) a catalytic TIM-barrel, and iii) a small α+β-fold domain. It was suggested that the FnIII-like domain evolutionally evolved and has been found in several glycosyl hydrolases, such as cellulases and amylases (Bork & Doolittle, 1992; Prag *et al*., 1997). Although the FnIII-like (or the N-terminal chitin-binding) domain of chitinases is not directly responsible for chitin binding, several lines of experimental evidence indicated that this domain participates in directing the filamentous chtin substrate to the catalytic groove to facilitate efficient hydrolysis (Watanabe *et al*., 1992). In the case of *S. marcescens* chitinase A, the chitin-binding domain is linked with the catalytic domain through a small hinge as shown in Figure 1.6. The catalytic domain of chitinase A comprises two sequence motifs, namely CatI and CatII that are separated by the α+β small insertion domain. The two catalytic motifs typically form a $(\beta/\alpha)_8$-barrel structure with a deep substrate-binding cleft.
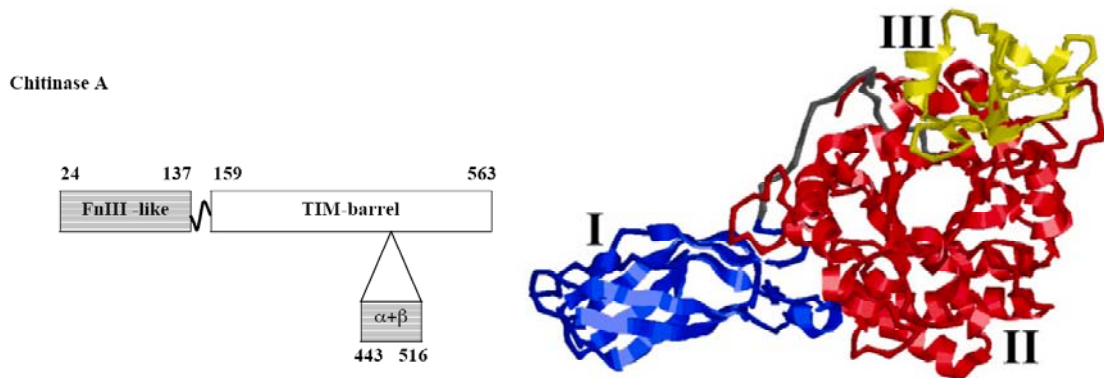
Figure 1.6 Domain structures of chitinase A from *S. marcescens* (Perrakis *et al*., 1994). I) The FnIII-like or N-terminal chitin-binding domain; II) The TIM-barrel catalytic domain; and III) The α+β small insertion domain

The crystal structures of hevamine chitinase (Terwisscha van Scheltinga *et al*., 1995), *C. immitis* chitinase (Bortone *et al*., 2002) and *S. marcescens* chitinase A (Papanikolau *et al.,* 2003) bound to allosamidin also provided the detailed hydrolytic mechanism of such enzymes. Allosamidin was found to strongly inhibit all family 18 chitinases. It consists of two β-1,4-linked *N*-acetylallosamine residues linked with an oxazolinium derivative, allosamizoline as shown in Figure 1.7. The strong inhibition by allosamidin suggested that the structure of allosamizolium residue was complementary to that of the catalytic center (Papanikolau *et al.,* 2003). Thus, the allosamizoline structure is most likely to reflect the transition state of the enzyme complex as described in Figure 1.5.
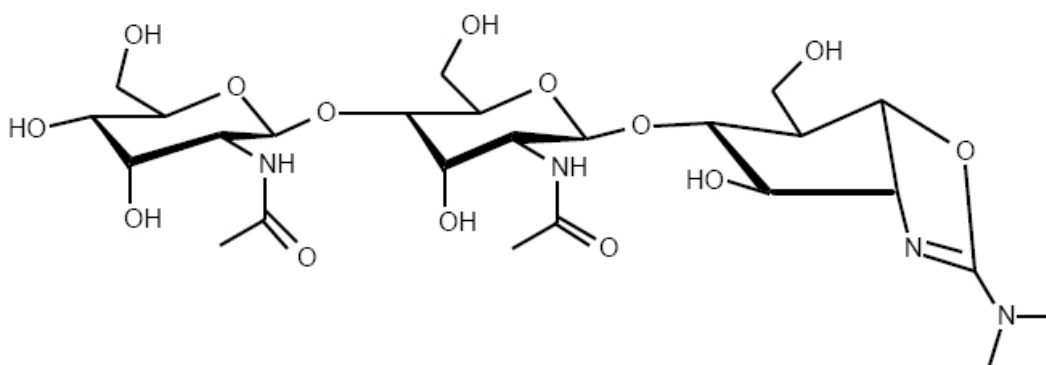
Figure 1.7 The structure of allosamidin (Bortone *et al.*, 2002).

The X-ray structure of hevamine complexed with allosamidin was determined at 1.85 Å resolution (Terwisscha van Scheltinga *et al.*, 1995). This structure suggested the role of Glu127 as a proton donor in the substrate-assisted mechanism. The allosamizoline group bound in the center of the active site, mimicking the reaction intermediate in which a positive charge at C1 was stabilized intramolecularly by the carbonyl oxygen of the N-acetyl group at C2. Structural analyses of *C. immitis* chitinase complexed with allosamidin revealed the catalytic role of Glu171 (Bortone *et al.*, 2002). After proton donating by Glu171, the positive charge built up on the sugar at subsite -1 was stabilized by interaction with its own *N*-acetyl group, forming an oxazolinium intermediate (Figure 1.8). Therefore, only one catalytic group is involved in this mechanism.
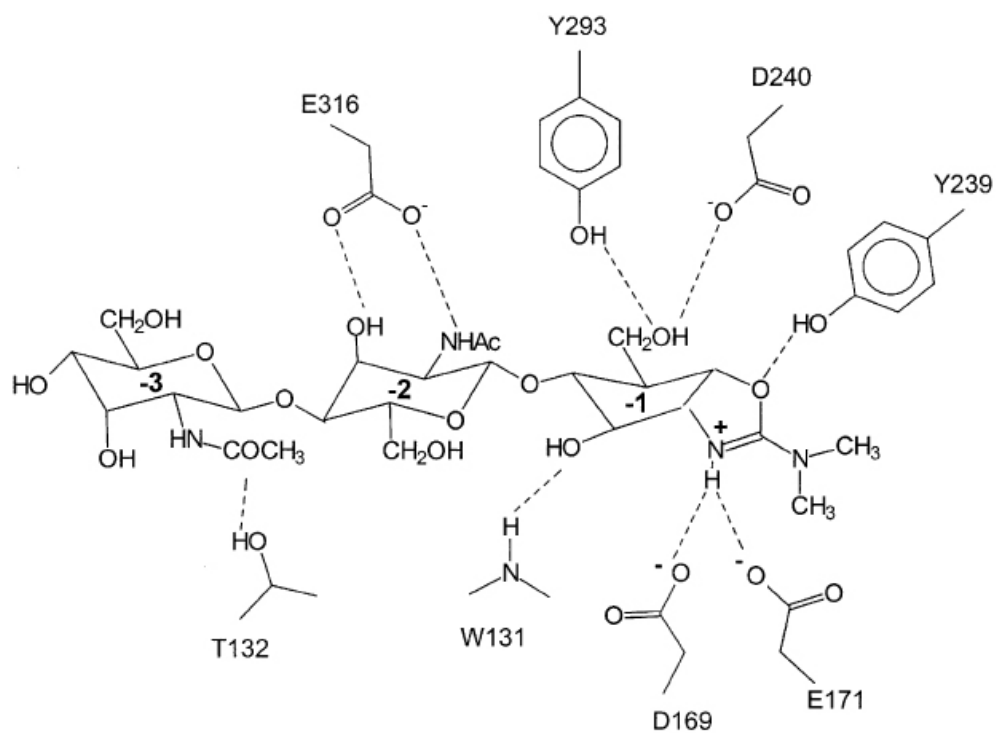
Figure 1.8 A schematic representation of polar interactions between allosamidin and the important residues located at the active site of *C. immitis* chitinase (Bortone *et al.*, 2002). Hydrogen bonds are shown as dashed lines.

The X-ray structure of the complexes between *S. marcescens* chitinase A mutants and hexaNAG and octaNAG substrates (Papanikolau *et al*., 2001; Aronson *et al*., 2003) demonstrated that the catalytic site of the enzyme contained a full occupancy of six substrate binding subsites extending from subsite -4 (non-reducing end) to subsite +2 (reducing end). The crystal structures of these complexes showed that the reducing-end disaccharide of a bound chitin oligosaccharide was in *β*-anomeric configuration and occupied subsites +1 and +2. GlcNAc at -1 was the glycosyl unit protonated by the catalytic Glu315. Thus, the disaccharide at positions +1 and +2 act as the leaving group. Additional subsites of the binding cleft (-5 to -13) were proposed to interact with the non-reducing end (NRE) of the glycone region of chitin polymer. These binding sites locate beyond in the catalytic cleft, and extended towards the chitin-binding domain of chitinase A. It was reported that substrate binding was controlled by a series of aromatic residues (Papanikolau *et al*., 2001; Aronson *et al*., 2003; Watanabe *et al*., 2003). Aronson *et al*. (2003) solved the structure of *S. marcescens* chitinase A mutant (E315L) with GlcNAc$_6$ and found that the aglycone disaccharide in the binding cleft interacted with three aromatic residues, including Tyr418 and Phe396 at the +2 site and Trp275 at the +1 site (Figure 1.9). Although Tyr418 appeared to mark the end of the cleft, this residue did not seem to interfere with the extension of the reducing end beyond the +2 site. In *S. marcescens* chitinase A, Trp275 and Phe396 formed the opposite sides of the cleft and stacked against the hydrophobic faces of the corresponding GlcNAcs. In contrast, the sugar ring of the glycone component of the substrate that lied flat in the cleft and every other GlcNAc in this region had its hydrophobic face aligned with an aromatic amino acid in the cleft floor [-1 (Trp539), -3 (Trp167), -5 (Trp170)].
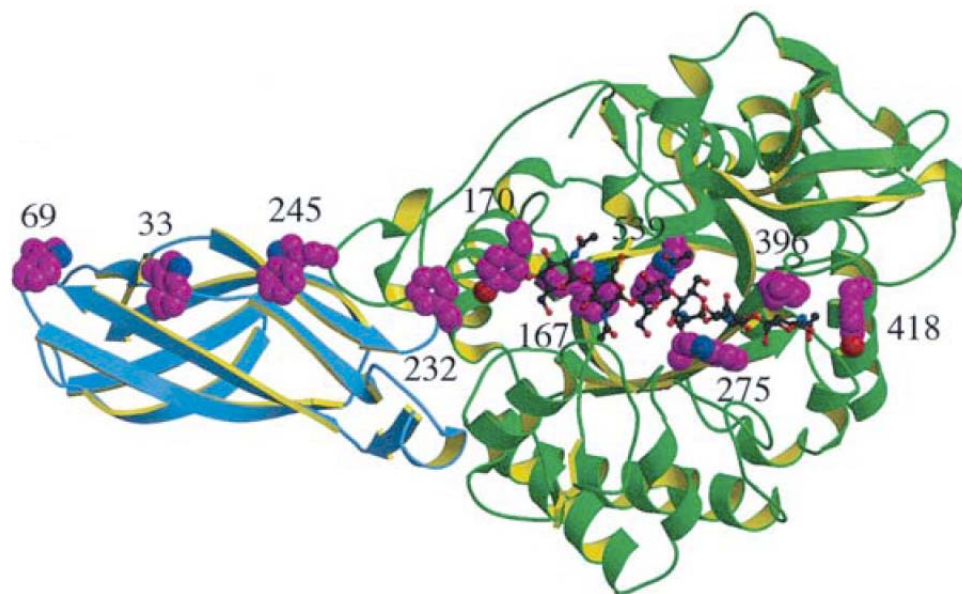
Figure 1.9 Three-dimensional structure and molecular surface of *S. marcescens* chitinase A mutant E315L with the hexasaccharide in the binding cleft (Aronson *et al.,* 2003). The N-terminal chitin-binding domain is shown in blue and the C-terminal catalytic domain in green. Aromatic residues that line along the substrate-binding cleft are shown in space-filling mode. GlcNAc$_6$ in the substrate-binding cleft is shown in ball-and-stick mode.

A plausible model by which family 18 chitinases degrade pure *β*-chitin was proposed previously by Uchiyama *et al*. (2001) and Watanabe *et al*. (2003). The model suggestsed that the chitin-binding domain maintains the enzyme binding to the insoluble substrate so that the reaction could be progressive. The chitin-binding domain of chitinase A is located at its N-terminus and has a FnIII fold (Perrakis *et al.,* 1994). The chitin-binding domain contains two surface exposed tryptophan residues (Trp33 and Trp69), along with two additional residues (Trp232 and Trp245) located at the edge of the catalytic domain beyond the −5 site of the cleft. All these residues

are positioned correctly and serve as additional binding sites for odd-numbered GlcNAcs (Aronson *et al.,* 2003). Point mutation study of Trp33 and Trp69 from *S. marcescens* chitinase A revealed that both residues were important for the degradation of crystalline *β*-chitin, but not for the degradation of oligosaccharides (Uchiyama *et al.,* 2001). Likewise, Trp232 and Trp245 on the catalytic domain of chitinase A were selective in helping to degrade only the natural polymer. The binding takes place with the reducing end of a chitin chain on the surface of the insoluble chitin matrix that is first located by the surface exposed residues like Trp33, Trp69, Trp232, and Trp245 (Figure 1.10). Subsequent hydrolysis led to the release of the reducing end disaccharide at positions +1 and +2, and then the enzyme moves symmetrically two GlcNAc residues towards the non-reducing end, allowing the chitin chain to be degraded processively.
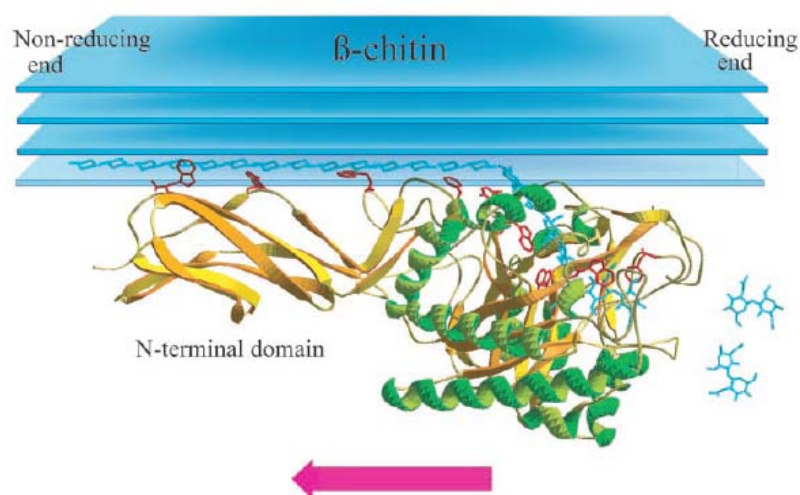
Figure 1.10 A model for crystalline β-chitin hydrolysis by chitinase A (Uchiyama *et al.,* 2001).

1.6 Background of chitinase A from *Vibrio carchariae*

V. carchariae (a synonym of *V. harveyi*) is a gram-negative marine bacterium that particularly expresses high level of chitinase A (Suginta *et al*., 2000). The mature enzyme is active as a monomer of M_r 63,000 as judged on SDS-PAGE.

On the basis of sequence and structural similarities, this monomeric enzyme is classified as a member of family 18 chitinases (Suginta *et al*., 2004). Like other family 18 microbial enzymes (Perrakis *et al*., 1994; Matsumoto *et al*., 1999; Bortone *et al*., 2002), the catalytic domain of *V. carchariae* chitinase A comprises two short sequence regions, which form an $(\beta/\alpha)_8$-TIM barrel active site. A completely conserved acidic amino acid (Glu315) located at the end of the conserved motif DxxDxDxE (in the loop connected to the strand β4) is identified to be the catalytic residue (Suginta *et al*., 2005). The action of native chitinase A on chitin initially released various lengths of small chitooligomeric fragments, which were further hydrolyzed to GlcNAc$_2$ as the end product, suggesting that the enzyme acts as an endochitinase (Suginta *et al*., 2005). The retention of the β over α anomer of all the products observed at initial time of reactions supports that the enzyme employed the substrate-assisted mechanism. The higher affinity of *V. carchariae* chitinase A toward higher M_r chitooligosaccharides suggested that the catalytic cleft of the enzyme comprises an array of most probably six binding subsites, comparable to that of *C. immitis* chitinase A (Bortone *et al*., 2002) and *S. marcescens* chitinase A (Perrakis *et al*., 1994).

This hydrolytic activity of *V. carchariae* chitinase A mutants, E315Q, E315M and D392N (Suginta *et al*., 2005) towars glycol chitin showed that the D392N mutant retained significant chitinase activity in the gel activity assay, while the E315M and

E314Q mutants had a complete loss of the hydrolytic activity, suggesting that E315M is the only essential residue in catalysis.

Since high-level expression of the recombinant chitinase A has been established in *E. coli* M15, the main aim of this study is to employ protein crystallization technique to determine the 3D-structure of *V. carchariae* chitinase A. A rapid screening for obtaining chitinase crystals was carried out using the microbatch method. Further optimization for crystallization conditions was performed using the hanging drop vapor diffusion technique. Under collaborative project with Dr. Jirundon Yuvaniyama, the diffraction data of the first wild-type crystal was collected using a Rigaku/MSC RU-H3R X-ray generator equipped with an R-AXIS IV^{++} detector (Rigaku Corporation, Sendagaya, Shibuya-Ku, Tokyo, JAPAN) located at Center for Protein Structure and Function, Faculty of Science, Mahidol University, Thailand. Preliminarily structural analysis of *V. carchariae* chitinase A was subsequently performed using *S. marcescens* chitinase A (PDB code; 1CTN) as a phasing model (Songsiriritthigul *et al*., 2005).

In the later stage of this research, several active site variants were generated to investigate the catalytic role of Glu315 and Asp392 residues using site directed mutagenesis technique. The first seven variants had changes of two acidic residues, namely D392N, D392K, E315Q, E315M, D392NE315Q, D392NE315M, D392KE315M. Additional eight variants were mutated from the highly conserved aromatic residues that were predicted to be important for substrate binding. These mutants included W168G, Y171G, W275G, W397F, W570G, a double mutant (W397F/W570G), a triple mutant (W397F/W570G/W275G), and a quadruple mutant (W397F/W570G/W275G/Y171G). The active wild-type chitinase A and all variants

were produced as recombinant proteins expressed in *E. coli* and were subjected to functional characterization using TLC and quantitative HPLC.

In collaboration with Dr. Robert C. Robinson, the Institute of Molecular and Cell Biology (IMCB), Singapore, extensive experiments on crystallization of chitinase A and chitinase E315 mutant with four structures of wild-type, E315M in the absence and in the presence of NAG_5 and NAG_6 being elucidated at high resolution. X-ray data collection was performed using a Rikagu/MSC FR-E SuperBright X-ray generator equipped with an R-AXIS IV^{++} imaging plate area detector (Rigaku Corporation, Sendagaya, Shibuya-Ku, Tokyo, JAPAN) located in IMCB, Singapore.

Together with functional, structural data from *V. carchariae* chitinase A and sequence comparison among chitinase A from *V. carchariae* and chitinases from other organisms, the knowledge gained finally provided an insight into the detailed mechanism of *V. carchariae* chitinase A in chitin hydrolysis.

1.7 Objectives

The objectives of this thesis include:

1. To functionally express and purify *V. carchariae* chitinase A expressed in *E. coli* M15 cells.

2. To solve the 3D-structures of chitinase A/inactive chitinase A E315M mutant in complex with chitooligosaccharides.

3. To gain an insight into the detailed mechanism of chitinase A in chitin hydrolysis.

CHAPTER II

MATERIALS AND METHODS

2.1 Chemicals and reagents

Chemicals and reagents used for protein expression, purification, characterization, and crystallization of *V. carchariae* chitinase A were of analytical grade unless stated otherwise. Acrylamide, aniline, ammonium sulphate, ammonium persulphate, bromophenol blue, bis-N, N"-methylenebisacrylamide, calcofluor white M2R, calcium chloride 2-hydrate, chitin flake, coomassie blue R250, coomassie blue G250, aniline-diphenylamine, ethylenediamine tetra-acetic acid (EDTA), isopropyl β-D-thiogalactoside (IPTG), 2-mercaptoethanol, magnesium chloride, glycerol, glycine, sodium azide, sodium dodecyl sulphate (SDS) and tris (hydroxymethylamine), *N, N', N", N'''*-tetramethylethylenediamine (TEMED) were purchased from Sigma-Aldrich (St.Louis, MO, USA).

Acetone, acetonitrile (HPLC grade), ammonium hydroxide, glacial acetic acid, hydrochloric acid, methanol, n-butanol, phosphoric acid, potassium chloride, potassium hydroxide, sodium acetate, sodium bicarbonate, sodium chloride, sodium hydroxide, sodium dihydrogen phosphate, sodium hydrogen phosphate and water (HPLC grade) were purchased from Carlo ERBA (Rodano, Milano, Italy).

Ampicillin, phenyl methylsulfonyl fluoride (PMSF), imidazole, isopropyl β-D-thiogalactoside (IPTG), hen egg white lysozyme, *p*-nitrophenol sodium salt, MES [2-(N-morpholino) ethanesulfonic acid)], MOPS [3-(N-morpholino) ethanesulfonic

acid], PIPES (piperazine-1,4-bis(2-ethanesulfonic acid), HEPES [N-(2-hydroxyethyl)piperazine-N-(2-ethanesulfonic acid], CAPS [(3-(cyclohexylamino)-1-propanesulfonic acid)], triton X-100, PEG 4000 and PEG 8000 were purchased from USB Corporation (Cleaveland, OH, USA).

Nanosep membrane centrifugal filter (10 kDa molecular-weight cut-off) was a product of PALL Life Sciences, Michigan, USA. Vivaspin-20 ultrafiltration membrane concentrators (10 kDa molecular-weight cut-off) were obtained from Vivascience AG, Hanover, Germany). Surfactant-free cellulose acetate (SFCA) membrane, polystyrene housing, 0.2 μm pore size was bought from Nalgene, Rochester NY, USA. MF-Millipore Membrane Filters (0.22 μm and 0.45 μm pore size) were purchased from Millipore Corporation (Bedford, U.S.A.).

N-acetyl-chitooligosaccharides (di-N-acetyl-chitobiose, tri-N-acetyl-chitotriose, tetra-N-acetyl-chitotetraose, penta-N-acetyl-chitopentaose, hexa-N-acetyl-chitohexaose) and p-nitrophenyl-di-N-acetyl-chitobioside [pNP-(GlcNAc)$_2$], were purchased from Seikagaku Corporation (Tokyo, Japan). Silica gel 60 F_{254} aluminium sheet (0.2 mm) was purchased from Merck (Damsladt, Germany).

A CARBOSep CHO-411 Oligosaccharide column (7.8 mm ID × 300 mm, 20 μm particle size) and a CARBOSep CHO-611/C Guard Cartridge (4.0 mm ID × 20 mm, 20 μm particle size) were purchased from Transgenomic (Omaha, NE USA). A Zorbax Carbohydrate Analysis column (4.6 mm ID × 250 mm, 5 μm particle size) and a Zorbax NH$_2$ Guard Cartridge (4.6 mm ID × 12.5 mm, 5 μm particle size) were purchased from Agilent Technologies (Englewood, CO, USA).

Ni-nitrilotriacetic acid (Ni-NTA) agarose resin was a product of Qiagen (Qiagen, Valencia, CA, USA). Chromatographic media and prepacked columns for

automated protein purification were products of Amersham Pharmacia Biotech (Amersham Biosciences, Piscataway, NJ, USA). These prepacked columns included HisTrap HP 1-ml, Superdex 200 10/300 GL (1.0 × 30 cm) and HiLoad 16/60 Superdex 200 prep grade (1.6 × 60 cm) gel filtration columns.

JB Screen HTS I and HTS II were purchased from Jena Bioscience GmbH (Jena, Germany). Micro-Bridge, Imp@ct Plate, Cryschem Plate^{TM}, Linbro Plate$^{®}$, VDX Plate Greased^{TM}, 20 mm Siliconized glass cover, Crystal Screen HT, SaltRx HT, Index HT, 2,4-dimethyl-5-pentanediol (MPD), glycerol, Al's oil and Crystal Clear sealing tape were purchased from Hampton Research (Aliso Viejo, CA, USA). 96 well CrystalQuick™, microbatch sitting drop plates were purchased from Greiner bio-one (Frickenhausen, Germany). Bacto tryptone, yeast extract, bacto agar were purchased from Scharlau Chemie (Barcelona, Spain). Luria-Bertani broth (LB) was obtained from USB Corporation (Cleaveland, OH, USA).

2.2 Bacterial strains

Escherichia coli type strain M15 (Qiagen, Valencia, CA, USA) and the pQE 60 expression vector harboring *chitinase A* gene fragments were used for high-level expression of recombinant chitinases. *E. coli* type strain DH5α and XL1Blue were used for routine cloning, subcloning, and plasmid preparations.

2.3 Instrumentation

All instrument required for protein expression, purification, characterization and preliminary crystallization are located at the Center for Scientific and Technology Equipment at Suranaree University of Technology, Nakhon Ratchasima, Thailand.

These instrument included a Sonopuls Ultrasonic homogenizer with a 6 mm diameter probe (Sigma-Aldrich, St.Louis, MO, USA), an HP Series 1100 HPLC system (Hewlett Packard, Waldbronn, Germany), a Mini-PROTEAN® 3 Cell (BioRAD, Hercules, CA, USA), a microtiter plate reader (Applied Biosystems, Foster City, CA, USA), a Genway UV-VIS spectrophotometer (Feisted, Dunmow, Essex, UK), an ÄKTA purifier system (Amersham Biosciences, Piscataway, NJ, USA), a Stereo Microscope (Stemi 2000-C Zeiss, Germany) mounted with a color video camera (Sony, SSC-DC398P, Sony Corporation, Tokyo, Japan).

A Jasco J-715 spectropolarimeter (Japan Spectroscopic Co., Japan) was located at the Institute of Molecular Biology and Genetics, Mahidol University, Salaya, Nakhon Pathom, Thailand. A Rigaku/MSC RU-H3R X-ray generator equipped with an R-AXIS IV^{++} detector (Rigaku Corporation, Sendagaya, Shibuya-Ku, Tokyo, JAPAN) was located at the Center for Protein Structure and Function, Faculty of Science, Mahidol University, Bangkok, Thailand.

Instrument used for protein purification and crystallization work that located at the Institute of Molecular and Cell Biology, Proteo, Singapore were the Screenmaker 96+8™ (Innovadyne Technologies, Inc.'s, Santa Rosa, CA, USA), Rikagu/MSC FR-E SuperBright X-ray generator equipped with an R-AXIS IV^{++} imaging plate area detector (Rigaku Corporation, Sendagaya, Shibuya-Ku, Tokyo, JAPAN).

2.4 General methods

2.4.1 Transformation of recombinant plasmid into *E. coli* M15 cells

The DNA fragment that encodes wild-type chitinase A was cloned into the pQE60 expression vector and expressed in *E. coli* M15 cells as the 576-amino acid

fragment with a C-terminal (His)$_6$ sequence (Suginta *et al.*, 2004). Point mutations were introduced to the wild-type *chitinase A* DNA by PCR technique (Suginta *et al.*, 2005; 2007) using the QuickChange Site-Directed Mutagenesis Kit according to the Manufacturer's protocols. Active-site chitinase A variants were generated using oligonucleotides synthesized from Proligo Pte Ltd. (Helios, Singapore) and Bio Service Unit (BSU) (Bangkok, Thailand). Single mutants (W168G, Y171G, W275G, W397F, W570G and D392N) were constructed using the DNA fragment encoding wild-type chitinase A as template. A double mutant (W397F/W570G), a triple mutant (W397F/W570G/W275G), and a quadruple mutant (W397F/W570G/W275G/Y171G) were produced using mutants W570G, W397F/W570G, and W397F/W570G/W275G, respectively, as DNA templates. The success of newly-generated mutations was confirmed by automated DNA sequencing (BSU, Thailand). The programs used for nucleotide sequence analyses were obtained from the DNASTAR package (DNASTAR, Inc., Madison, USA).

The recombinant pQE60 harboring the *chitinase A* gene fragments was transformed into *E. coli* M15 cells (Qiagen) as described by Sambrook *et al.* (1989). The competent cells of *E. coli* M15 host strain were prepared as described in Appendix A. About 100 ng of plasmids was transformed into a 50-µl aliquot of the competent cells, and spread on LB agar plates containing 100 µg/ml of ampicillin. The transformed *E. coli* cells were further expressed as described in section 2.4.2.

2.4.2 Expression of recombinant chitinase A in *E. coli* M15 cells

For chitinase expression, the ampicillin resistant colonies were picked and grown overnight at 37°C in 10 ml of LB medium containing 100 µg/ml ampicillin.

The freshly inoculated culture was diluted to a ratio of 1:100 with LB broth containing the same concentration of ampicillin, and then continued to grow at 37°C until OD_{600} reached 0.5-0.6. The culture was cooled down to 25°C, then IPTG was added to a final concentration of 0.5 mM and the culture was shaken at 200 rpm at 25°C for an additional 18 h. The IPTG-induced cells were harvested by centrifugation at 5,000 rpm at 4°C for 30 min, and the cell pellet kept at -30°C for 30 min or longer until used. To obtain highest level of protein expression, optimal IPTG concentrations, temperatures, various times for chitinase induction were optimized. During chitinase induction, concentrations of IPTG were varied from 0-2.0 mM. Three induction temperatures of 20°C, 25°C and 37°C were tested with induction times of 0, 2, 5, 8 and 18 h. The condition that gave highest level of wild-type expression was chosen for further studies and for expression of the chitinase mutants.

To determine protein expression level, total protein profiles of *E. coli* M15 cells containing the pQE60 plasmid with and without DNA insert were compared. After IPTG induction, the cells were pelleted from a 100-µl liquid culture in a microtube and the pellets resuspended in 50 µl of 1× SDS sample buffer (50 mM Tris pH 6.8, 1.6% of 2-mercaptoethanol, 2% SDS, 10% glycerol and 0.03% bromophenol blue). The suspension was boiled for 5 min, then centrifuged and a 10-15 µl aliquot was analyzed on 12% SDS-PAGE as described in method 2.4.7.

2.4.3 Preparation of crude extract of recombinant chitinase A from *E. coli* M15 cells

The cell pellet prepared from section 2.4.2 was thawed, resuspended in 40 ml lysis buffer (20 mM Tris-HCl pH 8.0 containing 150 mM NaCl, 1 mM

phenylmethylsulfonylfluoride (PMSF) and 1 mg/ml lysozyme), and then incubated on ice for 30 min. The cell suspension was sonicated on ice using a Sonopuls Ultrasonic homogenizer with a 6 mm diameter probe (50% duty cycle, amplitude setting, 20%, total time, 30 s, 6-8 cycles, Sigma-Aldrich). Unbroken cells and cell debris were removed by centrifugation at 12,000 rpm at 4°C for 30 min.

2.4.4 Purification of recombinant chitinase A by Ni-NTA agarose resin

Purification of recombinant chitinases was carried out using Ni-NTA agarose resin (Qiagen) at 4°C. For condition optimization trials, a small scale purification was initially tried using the modified protocol from Qiagen (http://www1.qiagen.com/literature/handbooks/INT/ProteinPurification.aspx). For a large scale purification, crude supernatant prepared as described in section 2.4.3 was gravitationally applied onto a Ni-NTA agarose affinity column (1.0 × 10 cm) equilibrated with 100 ml of the equilibration buffer (20 mM Tris-HCl pH 8.0 and 150 mM NaCl). After sample loading, the column was washed with 100 ml of 20 mM Tris-HCl buffer pH 8.0 containing 5 mM imidazole, followed by 50 ml of the same buffer containing 20 mM imidazole. The recombinant protein was eluted with 20 ml of the elution buffer (250 mM imidazole in the equilibration buffer). Then, the eluted fraction was concentrated to 1 ml using Vivaspin-20 ultrafiltration membrane concentrator (M_r 10 000 cut-off, Vivascience AG). Purification of other chitinase variants was also carried out following the same protocol as described for wild-type chitinase A.

To determine the protein purity, each protein fraction was loaded onto 12% SDS and electrophoresed as described in method section 2.4.7.

2.4.5 A complete purification of the recombinant chitinase A for

  crystallization studies

  2.4.5.1 Protocol I

  The protein fraction obtained from Ni-NTA agarose step was concentrated, then further purified using an ÄKTA purifier system (Amersham Biosciences) on a Superdex 200 10/300 GL (1.0 × 30 cm) gel filtration column (Amersham Biosciences). The running buffer was 20 mM Tris-HCl buffer pH 8.0 containing 150 mM NaCl. A flow rate of 0.25 ml/min was maintained and fractions of 0.5 ml were collected and assayed for chitinase activity. The chitinase-containing fractions were pooled, then exchanged into 20 mM Tris-HCl buffer pH 8.0 and concentrated using the same type of Vivaspin membrane concentrator.

  2.4.5.2 Protocol II

  Alternatively, recombinant chitinase A was purified using the HisTrap HP 1-ml affinity column (Amersham Biosciences). The crude supernatant obtained from section 2.4.3 was filtered through SFCA membrane, 0.22 µm (Nalgene). Then, the filtrate was applied to two columns of HisTrap HP 1-ml connected in series using an ÄKTA purifier system (Amersham Biosciences). The equilibration buffer was 20 mM Tris-HCl buffer pH 8.0 containing 150 mM NaCl and a flow rate of 2.8 ml/min was maintained. After sample loading, the columns were washed with 20 ml of 20 mM Tris-HCl buffer pH 8.0 containing 5 mM imidazole, followed by another 10 ml of the same buffer containing 20 mM imidazole. Fractions of 2.0 ml were collected and protein fractions eluted with 250 mM imidazole were concentrated using Vivaspin-20 ultrafiltration membrane concentrator. The concentrated enzyme obtained from Ni-

elution was further purified by gel filtration chromatoghraphy on a HiLoad 16/60 Superdex 200 prep grade (1.6 × 60 cm, Amersham Biosciences) connected to an ÄKTA purifier system (Amersham Biosciences). The running buffer was 20 mM Tris-HCl buffer pH 8.0 containing 150 mM NaCl. A flow rate of 1.2 ml/min was maintained and fractions of 2.0 ml were collected and pooled. Then, the pooled fraction was exchanged into 10 mM Tris-HCl buffer pH 8.0 and concentrated using Vivaspin membrane concentrator.

2.4.6 Determination of protein concentration by Bradford's method

Protein concentration was estimated by the method of Bradford (1976) using bovine serum albumin (BSA) as standard (0-10 μg) (see Appendix A and B). A diluted sample (100 μl) was mixed with 1 ml of dye reagent (see Appendix A) and 50 μl of 1 M NaOH solution. The solution was mixed and allowed to stand at room temperature for 10 min. The absorbance at 595 nm was measured using a Genway UV-VIS spectrophotometer.

2.4.7 Denaturing polyacrylamide gel electrophoresis (SDS-PAGE)

SDS-PAGE was performed according to the method of Laemmli (Laemmli, 1970). One part of protein solutions was mixed with 2 parts of 3× sample buffer (150 mM Tris-HCl pH 6.8, 5% of 2-mercaptoethanol, 6% SDS, 30% glycerol, 0.03% bromophenol blue). The suspension was boiled for 5 min, a 10-15 μl aliquot was loaded onto 12% SDS-PAGE gel set in a Mini-PROTEAN® 3 Cell (BioRAD), and then electrophoresed using Tris-glycine pH 8.3 as a running buffer (see Appendix A)

at a constant 120 V for 1 h from a cathodic (-) end to an anodic (+) end. After electrophoresis, the gel was stained with coomassie brilliant blue R250 (Appendix D) for 30 min, and then destained with a destaining solution (Appendix D) until the background was clear. The size of protein bands was estimated by comparing with the low molecular weight protein marker (Amersham Biosciences) comprising phosphorylase b (97 kDa), bovine serum albumin (66 kDa), ovalbumin (45 kDa), bovine carbonic anhydrase (30 kDa), trypsin inhibitor (20.1 kDa) and bovine α-lactalbumin (14.4 kDa).

2.4.8 Circular Dichroism (CD) spectroscopy

The purified chitinases were diluted to 0.40 to 1.40 mg/ml in 20 mM Tris-HCl buffer, pH 8.0. CD spectra over 3 scans were measured using a Jasco J-715 spectropolarimeter at near UV (190 to 250 nm) regions. CD measurements were performed at 25$^\text{o}$C with a scan speed of 20 nm/min, 2 nm bandwidth, 100 mdeg sensitivity, an average response time of 2 s and an optical path length of 0.2 mm. The baseline buffer for all the proteins was 20 mM Tris-HCl buffer, pH 8.0. The baseline was measured and subtracted from each spectrum before the raw data were transformed to mean residue ellipticity (MRE) using the following equation:

$$[\Theta] = (73.33 \ m^{o}) / ([\text{prot}]_{mM} \cdot l_{cm} \cdot n)$$

Where $[\Theta]$ is the MRE in deg$\cdot$cm$^{2}\cdot$d/mol, n is the number of amino acids in the polypeptide chain, m$^\text{o}$ is the measured ellipticity, and l is the path length of cuvette used in centrimeter. The intensity of JASCO standard CSA (nonhygroscopic ammonium (+)-10-camphorsulfonate at wavelength 290 nm was around 45 units. Therefore, the conversion factor was calculated to be 3,300/CSA intensity at 290 nm

or 73.33 using the equation above. The molecular weight of each protein was calculated corresponding to the number of amino acids. After noise reduction and concentration adjustment, the measured ellipticity was converted to the molar ellipticity, which was plotted versus wavelength.

2.5 Sequence comparison and modeled structural topology

An amino acid sequence alignment of bacterial chitinases was constructed using "CLUSTALW" algorithm in a GCG package (Thompson *et al.*, 1994) and displayed in Genedoc (http://www.psc.edu/biomed/genedoc/). The putative *V. carchariae* chitinase A sequence was compared with seven bacterial chitinase A sequences available in the Swiss-Prot or TrEMBL databases (http://us.expasy.org/). These chitinase sequences are from *V. parahaemolyticus* (accession number Q8VTN2), *S. marcescens* (accession number Q54275), *S. liquefaciens* (accession number Q9ALZ0), *Aeromonas hydrophila* (accession number Q9L5D5), *Altermonas* sp. strain O-7 (accession number P32823), *Enterobacter* sp. G-1 (accession number O54328), and *Pantoea agglomerans* (accession number P97034). The putative chitinase A amino acid sequence was subsequently subjected to the program PHD (http://cubic.bioc.columbia.edu/predictprotein/ and Burkhard and Chris, 1993; 1994) for the secondary structure prediction. A modeled topology of the catalytic domain of *V. carchariae* chitinase A was built based on the X-ray structure of *S. marcescens* chitinase A (PDB code; 1CTN).

2.6 Structural determination of *V. carchariae* chitinase A

2.6.1 Initial crystallization

For initial crystallization screening, the microbatch under oil, hanging drop and sitting drop vapor diffusion methods were employed to obtain suitable conditions for reproducing single crystals for X-ray diffraction experiments. Initial crystallization experiments were carried out manually by the microbatch under oil method (Figure 2.1A) using an Imp@ct Plate (Hampton Research) filled with 10 µl Al's oil (Hampton Research). For each crystallization drop, 1 µl of wild-type chitinase A (10 mg/ml in 20 mM Tris-HCl buffer pH 8.0) was added to 1 µl of each precipitant from Crystal Screen (Hampton Research), JB Screen HTS I and HTS II (Jena Bioscience GmbH) without mixing. Under oil crystallization was performed at two different temperatures of 4ºC and 16ºC. After setting up the screen, the protein drop was immediately examined under a Stemi 2000-C stereomicroscope (Zeiss), mounted with a color video camera (Sony). The crystal growth was examined daily for one week, then continued once a week afterwards. Results were recorded by indicating whether the protein drop was clear, or contained precipitates or crystals (see Appendix C).

In the later stage, robotic screening crystallization using a Screenmaker 96+8™ (Innovadyne Technologies) was used for the microbatch sitting drop technique (Figure 2.1B). A series of crystallization trials was setup using Crystal Screen HT, SaltRx HT, Index HT (Hampton Research), JB Screen HTS I and HTS II (Jena Bioscience GmbH) and a CrystalQuick™ (Greiner bio-one). For each crystallization drop, 20 nl of chitinase A (20 mg/ml in 10 mM Tris-HCl buffer pH 8.0) was added to 20 nl of each commercial precipitant, and 50 µl of the same precipitant was applied into the well as reservoir. The crystallization plates were

incubated under free of vibration at three different temperatures of 4ºC, 15ºC and 22ºC. The protein drops that were equilibrated over the reservoir of the precipitating agent were examined under a stereomicroscope periodically as mentioned for the microbatch under oil method.
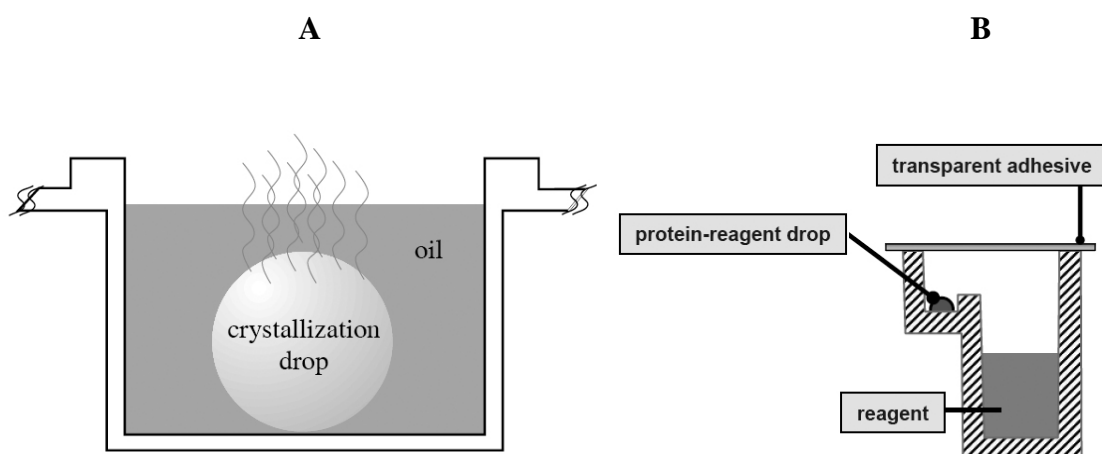
Figure 2.1 A schematic representation of microbatch techniques. (A) Microbatch under oil technique (http://www.hamptonresearch.com/products/ProductSearch.aspx? q=CRYSTAL) and (B) Microbatch sitting drop technique (http://www.greinerbioone. com/en/germany/articles/news/26/informations/99/).

2.6.2 Optimization of crystal growth conditions

Either the hanging drop (Figure 2.2A) or the sitting drop vapor diffusion techniques (Figure 2.2B) were used for further optimization of the crystal growth of wild-type chitinase A and its inactive mutant E315M.

For the hanging drop technique (Figure 2.2A), the crystallization experiments were setup using a Linbro Plate® and a VDX Plate Greased™ (Hampton Research). Different conditions including types of precipitant, salt and buffer at various

concentrations were tested. A grid of various 24 conditions was made (see Results 3.1.6). A crystallization droplet of 2 µl was prepared on a 20 mm siliconized glass cover slip by pipeting 1 µl of chitinase A into the center of the cover slide, and then mixed with an equal volume of the reservoir solution. The prepared cover slide with droplet was subsequently inverted and placed over an 1-ml buffer reagent added into reservoir, then the edge of the reservoir was sealed by applying high vacuum grease along the top edge of the wells. The procedure was repeated with other buffer systems using a clean pipette tip for each reagent to avoid cross contamination of reagents. Crystallization was carried out at 4ºC, 15ºC, 16ºC and 22ºC.

For sitting drop experiments, Cryschem Plate™ (Hampton Research) was used as shown in Figure 2.2B. A droplet of chitinase A was mixed with the crystallization reagent by pipeting 1 µl of chitinase and an equal volume of the buffer reagent. The protein droplet was placed on a platform in vapor equilibration with the reservoir reagent, and then sealed with plain cover slides using vacuum grease or clear sealing tape.

A   **B**
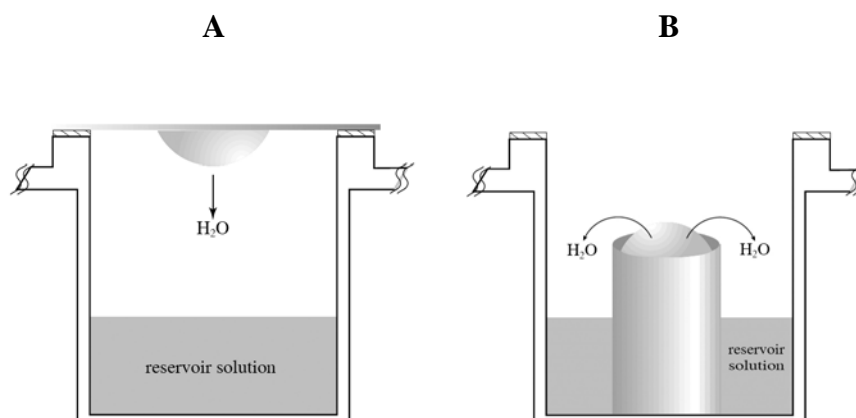
Figure 2.2 A schematic representation of vapor diffusion technique (A) Hanging drop vapor diffusion technique, (B) Sitting drop vapor diffusion technique (http://www.hamptonresearch.com/products/ProductSearch.aspx?q=CRYSTAL).

When the vapor diffusion method was chosen for crystallization optimization, small crystals were observed in the crystallization plates. These small crystals were used as seeds to grow larger crystals. Two seeding methods are employed; microseeding (Figure 2.3A) and macroseeding (Figure 2.3B). To obtain microseeds, a small, single crystal was transferred to a microcentrifuge tube and resuspended in 1 ml of non-dissolving precipitant solution (usually the reservoir precipitant contains 10% glycerol). The microseeds were produced after a repeated step of spinning and vortexing in the initial stock solution. The protein sample was then diluted with the non-dissolving precipitant solution to obtain a serial dilution of 1/100-1/1,000,000 in a final volume of 1 ml, then stored at 4ºC. The protein drops were pre-equilibrated against a 1-ml reservoir of the precipitant solution using the same method as described for the vapor diffusion technique. The pre-equilibrated growth drops were streaked from less to higher dilutions in order to obtain an optimal dilution that yielded a few crystals per drop.

A   B
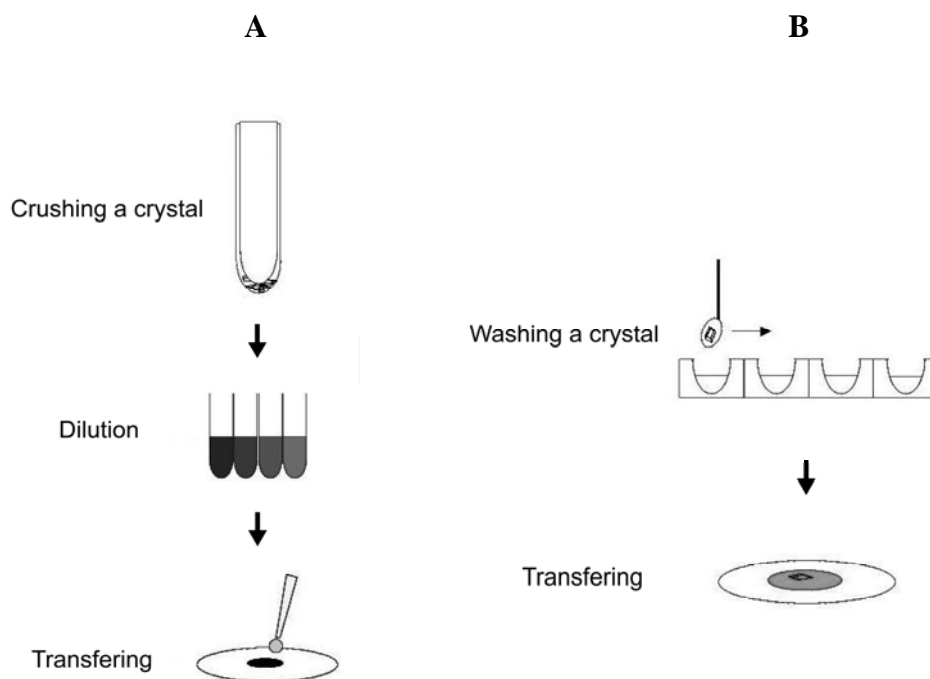
Figure 2.3 A schematic representation of microseeding and macroseeding techniques (A) Microseeding technique (http://www.douglas.co.uk/rep1.htm), (B) Macroseeding technique (http://www.structmed.cimr.cam.ac.uk/Course/Crystals/).

With macroseeding technique, a small single crystal was picked by a cryoloop and transferred to a freshly precipitant solution, in which the crystal was slowly dissolved on the surface by gently crushing. Washing steps were repeated several times until a fresh growth surface was seen on the crystal and dissolved any microcrystals. Then, the crystal was transferred to a protein drop pre-equilibrated to the growth conditions with a minimal amount of solution.

2.6.3 Soaking of inactive mutant E315M chitinase A crystals with penta-*N*-acetyl-chitopentaose (NAG$_5$) and hexa-*N*-acetyl-chitohexaose (NAG$_6$)

Crystals of E315M were grown under the optimized hanging drop vapor

diffusion method (see Method 2.6.2). For preliminary crystallization of E315M-NAG$_5$ and E315M-NAG$_6$ complexes, X-ray quality crystals of inactive E315M mutant were further transferred to a 1-µl mother liquor containing 5 or 10 mM of NAG$_5$ and NAG$_6$ in cryoprotectant solutions, containing 2-4% higher concentrations of PEG 4000 and 10% of glycerol. The survival of the soaked crystals was periodically observed under a stereomicroscope as described in section 2.6.1.

2.6.4 Cryocrystallization

To protect chitinase A crystals from the damaging effect of ice formation, the obtained crystals were treated with varied concentrations of 5-20% glycerol that serves as a cryoprotectant. It was found that both wild-type and E314M crystals survived when 10% glycerol was used. The wild-type and inactive mutant crystals were picked by a cryoloop, then flash-cooled in a nitrogen stream before X-ray diffraction was performed. On the other hand, the crystals of E315M-NAG$_5$ and E315M-NAG$_6$ complexes were directly flash cryocooled without the addition of glycerol, since their precipitants already contained 10% glycerol.

2.6.5 Data collection and processing

All the diffraction data of wild-type, E315M and E315M-substrate complexes were collected at 100K by the Rikagu/MSC FR-E SuperBright, X-ray generator equipped with R-AXIS IV^{++} imaging plate area detector (Rigaku) that located at the Institute of Molecular and Cell Biology, Proteos, Singapore using an incident wavelength of 1.5418 Å. A crystal-to-detector distance was varied from 120 mm to 150 mm in order to maximize the resolution of diffracted spots. The exposure time

was set between 0.5 to 1 min to give a few overloads in the resolution range of interest and a reasonably low background. The first step of data collection was to mount a crystal and to take a diffraction pattern. Once a satisfactory image was visualized, this first image was preliminarily analyzed by indexing to check the crystal quality and its space group using program MOSFLM (Leslie, 1991). A lattice type, unit cell parameters and crystal orientation were determined using a single oscillation image. The overall scanning range of the Φ angle comprised 360° for the lowest symmetry of wild-type crystal. Four data sets were recorded with 0.5° per image oscillation around the omega axis. The final steps were refinement and integration of the diffraction data sets using the same program as for indexing. The integrated data were then converted into an *mtz* format. Scaling, merging and statistical analysis of all the data sets were further examined using program Scala from the CCP4 suite (CCP4, 1994). The maximum resolution to which a crystal diffracted was determined by analyzing the ratio of the measured intensity to its standard deviation, *I/σ(I)*. All the four data sets were scaled using the maximum resolution range of 2.00 to 1.70 Å (see Table 3.8). Another criterian to assess the quality of the measured data was the completeness of the dataset, the redundancy of the data, and the merging *R*-factor (R_{merge}) (equation 1) (Rhodes, 2000). R_{merge} is dependent on the redundancy of the measured data and increasing the more often a given reflection is measured. Therefore, it is a measure of how well multiple observations of the same reflection and its symmetry related reflections merge.

$$R_{\text{merge}} = \sum_{hkl} \sum_{i} \left| I_i(hkl) - \langle I(hkl) \rangle \right| \Big/ \sum_{hkl} \sum_{i} I_i(hkl) \qquad \{1\}$$

Where I_i is the intensity for the *i*th measurement of an equivalent reflection with indices *hkl*.

2.6.6 Phase determination by molecular replacement method

In this study, the molecular replacement method (Navaza, 1994) was employed using program *AmoRe* from the CCP4 suite to obtain phase information. In order to obtain the molecular replacement solution, the first data set of inactive E315M mutant was solved using the crystal structure of chitinase A from *S. marcescens* (PDB code 1CTN; 47% identical to chitinase A from *V. carchariae*) as a search model. Subsequently, the final model of inactive E315M mutant from *Vibrio* enzyme was further used as a template for other three data sets obtained from E315M-NAG$_5$, E315M-NAG$_6$ complexes and the wild-type chitinase A as summarized in Table 2.1.

Table 2.1 A summary of the search model used in the molecular replacement method using program *AmoRe* for phase determination.

V. carchariae chitinase A crystals	Search model
E315M	*S. marcescens* chitinase A (PDB code; 1CTN)
E315M-NAG$_5$ complex	E315M mutant from *V. carchariae* chitinase A
E315M-NAG$_6$ complex	E315M mutant from *V. carchariae* chitinase A
Wild-type	E315M mutant from *V. carchariae* chitinase A

2.6.7 Model rebuilding

Once the search model was placed in the new unit cell, an electron density map was calculated using model phases and the observed structure factor amplitudes (Rhodes, 2000). The electron density ρ is calculated at each point *(x, y, z)* of the

crystal from the structure factor amplitude *F (h, k, l)*, which is proportional to the square root of the measured intensity *I* for the reflection *(h, k, l)*, the phase α *(h, k, l)*, and the volume V of the unit cell (equation 2).

$$\rho(x, y, z) = \frac{1}{V} \sum_h \sum_k \sum_l |F_{hkl}| e^{-2\pi i(hx + ky + lz - \alpha'_{hkl})}. \qquad \{2\}$$

Subsequently, program *O* (Jones *et al.*, 1991) was used to manually rebuild the structural model. The Fourier difference maps (F_o-F_c and $2F_o$-F_c maps) were generated from the observed structure-factor amplitudes ($|F_{obs}|$) and the calculated amplitudes ($|F_{calc}|$. Whereas each $|F_{obs}|$ is derived from a measured reflection intensity and each $|F_{calc}|$ is the amplitude of the corresponding structure factor calculated from the current model.

The resultant electron density map showed the regions of disagreement between the search model and the new structure, which was further determined through rebuilding and refinement processes.

2.6.8 Structure refinement

After a reasonable model was obtained from a molecular replacement experiment, the positional parameters and the temperature factor of each atom have to be refined in order to adjust the protein model to fit the observed data. To judge convergence and assess the model quality, there is the possibility to overfit data, especially at moderate resolution. To obtain the correct structure, the measured structure-factor amplitudes $|F_{obs}|$ and the calculated structure-factor amplitudes $|F_{calc}|$ should converge. Therefore, structure validation using the residual index or

crystallographic *R*-value (equation 3) was the most widely used to measure the structural convergence (Rhodes, 2000).

$$R = \frac{\sum \left\| F_{obs} \right| - \left| F_{calc} \right\|}{\sum \left| F_{obs} \right|} \qquad \{3\}$$

The crystallographic *R*-value measures for the agreement between the structure factors calculated for the existing model and the observed structure factors. The *R*-factor obtained when a set of measured amplitudes is compared with a set of random amplitudes. A more demanding and revealing criterion of model quality and of improvements during refinement is the free *R*-factor, R_{free}. To compute R_{free}, data were divided into a working set and a test set. The test set comprised a random selection of 5% of the observed reflections. Only the working set was used to refine the model. The free *R*-value was computed from the test set, which was not included in the refinement process using the same equation. If a structure was improved during refinement, both the *R*-value and R_{free} should decrease.

Throughout this work, refinements were performed under restraint conditions using programs REFMAC (Murshudov *et al.*, 1997) and *ARP/wARP* (Lamzin *et al.*, 1993) in the CCP4 suite until the convergence of the indices R_{factor} and R_{free} was reached. Fourier maps with coefficients of $2F_{obs}-F_{calc}$ and $F_{obs}-F_{calc}$ were calculated. Alternate sessions of model building using program *O* and refinements were carried out until well-fit statistics of each final model were obtained as shown in Table 3.8.

2.6.9 Validation of model quality

To examine the stereochemistry of the polypeptide chain, a Ramachandran plot (Ramachandran and Sasisekharan, 1968) was constructed for the final structure

using program PROCHECK (Laskowski *et al*., 1993). The dihedral angles Φ and Ψ for each residue were plotted in a square matrix. For all the four structures, the majority of the Φ/Ψ values lied within the allowed regions, as judged from the corresponding Ramachandran plots (see section 2.6.10-2.6.13). This indicated that the conformationally reasonable models were finally built. The root-mean-square (R.M.S.) deviations from ideality of bond length and angles were also determined with PROCHECK as shown in Table 3.8. The criteria of a well-refined model exhibits R.M.S. deviations of no more than 0.02 Å for bond lengths and 4° for bond angles.

2.6.10 Structural determination of inactive E315M mutant

The E315M mutant in the absence of substrate was the first structure that was successfully solved. A single crystal prepared by the hanging drop method under the precipitant containing 20% (w/v) PEG 4000, 0.1 M ammonium sulfate and 0.1 M Tris-HCl pH 7.5, diffracted to a maximum resolution of 1.70 Å. Using MOSFLM as the data processing software, the crystal was assigned to the orthorhombic $P2_12_12_1$ space group.

The phase of the E315M X-ray diffraction pattern was further determined by the molecular replacement method using the crystal structure of chitinase A from *S. marcescens* as a search model (PDB code; 1CTN). The rotation, translation and subsequent fitting functions were executed by appropriate software available in the CCP4 suite. The final fitting solution performed in the $P2_12_12_1$ space group gave an *R*-factor of 47.25%. The number of molecules was determined to be one protein monomer (63 kDa) per asymmetric unit, corresponding to a Matthew's coefficient (Matthews, 1968) of 2.27 Å^3/Da and a solvent content of 44.4%. The first round of

restraint refinement led to a significant decrease of an *R*-factor to 37.40% and a free *R*-factor to 41.70%. At the second round of refinement, approx. 120 amino acid residues were deleted from the model, yielding a decrease of an *R*-factor to 33.50% and a free *R*-factor to 36.00%. Restraint refinements done in REFMAC were thoroughly carried out, followed by iterative cycles of model building in *O*. At the first three cycles of model rebuilding, the six histidine residues tagged at the C-terminal region were not located in the E315M model because of their labile behavior.

After three alternating sessions of the model rebuilding and refinement, a new map called an omitted (unbiased) map showed an improved map of $2F_o$-F_c and a clear positive map of F_o-F_c in the active cleft (data not shown). At this point, the six histidine residues were built in the model that matched the omitted density. The restraint refinement was further employed, giving a slight decrease of the *R*-factor and the free *R*-factor by 1.40% and 2.00%, respectively. After the sixth round of consecutive rebuilding, the C-terminal region starting from residues 598-605 revealed a perfect match with the density map and suggested a blockage of the catalytic cleft of the inactive E315M mutant by the C-terminal six histidine residues. Renumbering and rebuilding residues was done after the seventh round of refinement and the final model of the inactive E315M mutant comprised 581 amino acid residues.

The final round of the refinement was complete with the *R*-factor and free *R*-factor converged to 18.90% and 21.90%, respectively. The R.M.S. deviations of 0.006 Å for bond distances and of 0.932° for bond angles indicated the correct geometry of almost all the residues. The final model gave good fit with the electron density map with an average B-factor value of 15.10 $Å^2$ for protein atoms. The refined model contained 740 water molecules with an average B-factor of 25.69 $Å^2$. The geometry

of the model was well verified by program PROCHECK, which indicated most of the residues (91.1%) in the polypeptide chain in the most favored regions, 8.7% in the additionally allowed regions and 0.2% in the generously allowed regions. No residues lied in disallowed Ramachandran regions.

2.6.11 Structural determination of inactive E315M-NAG$_5$ complex

The crystals of inactive E315M mutant soaked with NAG$_5$ and NAG$_6$ were diffracted and the data were processed the same way as described for the E315M structure. The diffraction data gave a maximum resolution of 1.72 Å and 1.80 Å, respectively. These crystals also contained one monomer per asymmetric unit, which corresponded to the same Matthew's coefficient (V_M) of 2.2 Å^3/Da. A solvent content of 43.2% and 44.1% was calculated for E315M-NAG$_5$ and for E315M-NAG$_6$ complexes. Although different crystal growth conditions were required for the inactive mutant and its two complexes, the crystals were assigned as the same orthorhombic $P2_12_12_1$ space group.

For E315M-NAG$_5$ complex, the first rigid body refinement by REFMAC yielded an R-factor of 35.10% and a free R-factor of 35.50%. With sugar residues being omitted, $2F_o$-F_c and F_o-F_c electron density maps obviously showed differences between the model and the calculated maps. When four rings of NAG coordinates taken from the data bank, 1NH6 (Papanikolau et al., 2001) were rebuilt in the clear density, giving an improvement of an R-factor and a free R-factor to 34.60% and 35.20%. During rebuilding process, the last non-reducing sugar (-3 NAG) was missing because of the poor electron density map found in this region. The refined structure of inactive E315M complexed with NAG$_5$ showed that the protein comprised

567 residues. Upon completion of the refinement, the *R*-factor and free *R*-factor had converged to 18.80% and 21.50% with the R.M.S. deviations of 0.006 Å and 0.994°, indicating an ideal geometry of almost all the residues. The protein atoms exhibited good fit with the electron density map with an average B-factor of 14.24 Å^2. The refined structure contains 665 water molecules with an average B-factor of 24.92 Å^2 and the four sugar residues (from subsites -2 to +2) were modeled with an average B-factor of 19.82 Å^2. The overall geometry of the model was well verified by program PROCHECK. Most of the residues (90.9%) in the polypeptide chain were found within the most favored regions, 8.9% was found within the additionally allowed regions, 0.2% was found within the generously allowed regions and no residues lied in disallowed Ramachandran regions.

2.6.12 Structural determination of inactive E315M-NAG$_6$ complex

For E315M-NAG$_6$ complex, the first rigid body refinement resulted in an *R*-factor of 29.20% and a free *R*-factor to 30.90%. Subsequent rebuilding and refinement were carried out and significantly lowered the *R*-factor to 25.60% and a free *R*-factor to 27.90%. The omitted maps (2F$_o$-F$_c$ and F$_o$-F$_c$) were generated by excluding the coordinates of NAG$_6$ residues from the refinement process. The F$_o$-F$_c$ omitted map that showed obvious differences between the model map and the calculated map allowed the sugar coordinates to be located and led to an improvement of an *R*-factor and a free *R*-factor to 0.70% and 0.20%. The final model of E315M-NAG$_6$ complex showed that the protein consists of 567 amino acid residues. Tight restraint refinement was performed, yielding a final *R*-factor and free *R*-factor converged to 18.10% and 20.90%, respectively. The R.M.S. deviations of 0.006 Å and of 0.992°, respectively

indicated an ideal geometry for almost all the residues. The final model gave good fit with the electron density map with an average B-factor value of protein atoms of 13.74 Å^2. All six sugar residues were modeled with an average B-factor of 21.79 Å^2. The refined model contains 740 water molecules with an average B-factor of 25.42 Å^2. The geometry of the model was validated by PROCHECK with the same values of the residues within the most favored regions, the additionally allowed regions and the generously allowed regions as for E315M-NAG$_5$ complex and no residues lie in disallowed Ramachandran regions.

Later, a thorough inspection of the refined structure of E315M-NAG$_6$ showed that the electron density of the sugar +1 extend to -1 was ambiguous. Therefore, the omitted map was further refined with the coordinates of the -4 to +2 NAG residues being omitted from the refinement process. This led to a slight increase of R-factor of 18.90% and free R-factor of 21.70%, (comparing with the final structure of E315M-NAG$_6$, which gave the R-factor of 18.10% and the free R-factor of 20.90%). The sugar conformation obtained from E315M-NAG$_5$ was remodeled and refined corresponding to the diffraction data of E315M-NAG$_6$ complex and finally gave an R-factor of 18.40% and a free R-factor of 21.40%.

2.6.13 Structural determination of wild-type chitinase A

As earlier mentioned in section 1.6, the preliminarily crystallographic analysis of the wild-type crystal was studied (Songsiriritthigul *et al*., 2005). The diffraction data provided an initial molecular replacement solution. The later stage of this research under the collaboration with Dr. Robert C. Robinson's guidance (IMCB, Singapore), model rebuilding and refinement of such data set were attempted without

success, as indicated by the high value of R-factor (42%). Therefore, new conditions for crystal growth to obtain single crystals of wild-type chitinase were tried.

The diffraction data of wild-type chitinase A were processed and gave a maximum resolution of 2.0 Å. After autoindexing and integrating the data, the crystal was assigned to the triclinic space group P1. The crystal contains two protein monomers per asymmetric unit, which corresponded to a matthews coefficient of 2.3 Å^3/Da and a solvent content of 46.9%. The structure of the wild-type enzyme was determined by the molecular replacement methods using the crystal structure of E315M mutant as the model. The first round of restraint refinement gave an R-factor of 29.50% and a free R-factor of 32.00%. For further refinement, noncrystallographic symmetry (NCS) restraint was introduced to keep tight restraints of the main-chain atoms and the side-chain atoms. By doing so, the obtained electron density map appeared to match well with the model of molecule A, with some regions only agreed with that of molecule B. For molecule B, the N-terminal region showed substantial disagreements between the model map and the electron density map. The improvement of the model was done by superimposing molecule A onto molecule B. Therefore, the resulting model comprised two copies of molecule A designated as molecule A and B. The rigid body refinement allowed the three domains of the two molecules, domain 1 (A22-A589), domain 2 (B40-B60) and (B130-B589) and domain 3 (B22-B39) and (B61-B129) move independently, while keeping tight NCS restraints. The restraint refinement lowered the R-factor to 26.50% and a free R-factor to 28.80%. For subsequent refinement, tight NCS restraint was still defined, which resulted in a slight decrease of the R-factor and the free R-factor to 24.50% and 26.40%. On the other hand, an R-factor of 22.70% and a free R-factor of 25.00% were

obtained when no NCS restraint was tried. This indicated an improvement in both *R*-factor and free *R*-factor by releasing the NCS restraint refinement for the wild-type structure. Program *ARP/wARP* was used to iteratively search for potential water molecules. Subsequently, water molecules were manually removed from the model if their respective $2F_o$-F_c density was less than 0.7 σ. At the end of the refinement, the *R*-factor and free *R*-factor had converged to 16.80% and 20.50% with the final refined structure consisted of 1,134 amino acid residues and 1,091 water molecules. The R.M.S. deviations of bond length and angles were calculated to be 0.007 Å and 0.968° respectively. The final model gave good fit with the electron density map with an average value of atomic temperature factor (B-factor) of 15.15 Å^2. The higher B-factor value of molecule B (15.85 Å^2) than that of molecule A (14.45 Å^2) suggested that molecule B contained more mobility parts than molecule A. The refined model reveals water molecules with an average B-factor of 24.46 Å^2. The geometry of the final model was assessed by PROCHECK with most of the residues (91.4%) in the polypeptide chain found within the most favored regions, 8.4% of the residues found within the additionally allowed regions, and 0.2% found within the generously allowed regions. No residues lied in disallowed Ramachandran regions.

With all the four structures, only three residues of 590, 591 and 592 could not be modeled due to their poor electron density maps. In addition, the C-terminal region starting from residues 598 to 605 could only fit in the density of the inactive E315M mutant, whilst these residues were too labile to be seen in the structures of wild-type, E315M-NAG$_5$ and E315M-NAG$_6$.

After the final models were constructed, the four enzyme structures were compared using program Superpose available in the CCP4 suite. Direct contacts were

determined by program Contact in the CCP4 suite. All the structures and electron density maps were created and displayed with Pymol (www.pymol.org).

2.7 Biochemical characterization

2.7.1 Chitinase activity assay using pNP-(GlcNAc)$_2$

Chitinase activity was determined in a 96-well microtiter plate. A 100-μl assay mixture contained protein sample (10 μl), 1 mM pNP-(GlcNAc)$_2$ (25 μl), and 0.1 M sodium acetate buffer, pH 5.0 (65 μl). The reaction mixture was incubated at 37°C for 10 min with constant agitating, then the enzymatic reaction was terminated by the addition of 50 μl 1.0 M Na$_2$CO$_3$. The amount of p-nitrophenol (pNP) released was determined spectrophotometrically at 405 nm in a microtiter plate reader (Applied Biosystems). The molar quantity of the liberated pNP was calculated from a calibration curve constructed with pNP standard varying from 0-30 nmol (see Appendix B).

One unit of chitinase activity is defined as the amount of enzyme, which produces 1 μmol of pNP per min at 37°C.

2.7.2 TLC analysis of the hydrolytic products of wild-type chitinase A and mutants

Hydrolysis of chitooligosaccharides (G2-G6) by chitinase A and its mutants were carried out in a 80-μl reaction mixture, containing 0.1 M sodium acetate buffer, pH 5.0, 2.5 mM substrate and 800 ng purified enzyme. Chitooligosaccharides hydrolyzed by wild-type chitinase A was incubated at various times of 2, 5, 10, 30, 60

min and 18 h (overnight) at 30°C with shaking at 70 rpm. Then, the reaction was terminated by boiling for 5 min. For product analysis, each reaction mixture was applied five times (one μl each) to a silica TLC plate (7.0 × 10.0 cm), then chromatographed three times (1 h each) in a mobile phase containing n-butanol: methanol: 28% ammonia solution: H$_2$O (10:8:4:2) (v/v) (modified from Tanaka *et al.,* 1999), followed by spraying with aniline-diphenylamine reagent and baking at 180°C for 3 min. Hydrolysis of chitooligosaccharides by mutants, D392N, W168G, Y171G, W275G and W397F were further studied under the same condition with two varied time points of 10 min and 1 h.

Hydrolytic products of wild-type chitinase A against colloidal chitin at various time points was studied. A reaction mixture (150 μl) containing 20 mg of colloidal chitin suspended in 0.1 M sodium acetate buffer pH 5.0 was incubated with wild-type chitinase A (4 μg) at 30°C with shaking at 100 rpm for 2, 5, 10, 30 min, 1 h and 18 h. Hydrolysis of colloidal chitin by mutants D392N, D392K, E315M, E315Q, D392NE315Q, D392NE315M, D392KE315M, W168G, Y171G, W275G, W397F, W570G, a double mutant, a triple mutant, and a quadruple mutant were also investigated. A 150 μl-reaction mixture containing 20 mg of colloidal chitin in 0.1 M sodium acetate buffer pH 5.0 was incubated with enzyme (80 μg) at 30°C for 18 h. The reaction products of all chitinase A mutants were relatively analyzed with that of wild-type enzyme. The products were analyzed by TLC under the same condition as described for the oligosaccharides.

2.7.3 HPLC analysis of the hydrolytic products of wild-type chitinase A and mutants

Initially, HPLC was operated on a CARBOSep CHO-411 Oligosaccharide column using a CARBOSep CHO-611/C Guard Cartridge (Transgenomic) connected to an HP Series 1100 HPLC system (Hewlett Packard). The temperature was set at 70^oC, and the column was eluted with HPLC water at a constant flow rate 0.4 ml/min with 205 nm UV detection. Various mobile phases were tried to separate G1-G6 standard but it was unsuccessful. Finally, HPLC analysis of the hydrolytic products was carried out using a Zorbax Carbohydrate Analysis column with a Zorbax NH_2 Guard Cartridge (Agilent Technologies) connected to an HP series 1100 automated HPLC system (Hewlett Packard).

G3-G6 hydrolysis by wild-type chitinase A was investigated using quantitative HPLC with the same set of reaction times as described for TLC experiments, whereas the hydrolyse of G3-G6 by mutants D392N, W168G, Y171G, W275G and W397F were studied under the same condition with 10 min of incubation. For all the variants, a reaction mixture (80 μl) containing 2.5 mM G3-G6 in 0.1 M sodium acetate buffer pH 5.0 and 800 ng chitinase A, was incubated at 30^oC with a constant shaking. After a specified period of incubation, the reaction mixture was boiled at 100^oC for 5 min, then the enzyme was removed from the reaction mixture by a Nanosep membrane centrifugal filter (M_r 10 000 cut-off). The reaction mixture was subsequently diluted 2.5 times with pure HPLC water, then 20 μl of the diluted reaction was analyzed on a Zorbax Carbohydrate Analysis column. The column was operated with an HP Series 1100 HPLC system at 40^oC at a constant flow rate of 1.0 ml/min, under an isocratic condition using acetonitrile:H_2O (65:35, v/v) as a mobile phase (see Appendix A).

After four minutes of sample injection, the resultant products were eluted under a run time set to 20 min with sugar peaks detected at A_{205}. The peak areas of the resolved sugars were then converted to nmol quantities using the standard calibration curve constructed individually from G1-G6 (see Appendix B). Twenty microliters of a standard mixture G1-G6 (1-25 nmol) were resolved under the same condition. The estimated values represent mean values from the three separate datasets, using the reactions containing sugars without enzyme as a reaction control.

Hydrolytic products obtained from colloidal chitin hydrolysis by wild-type were analyzed by HPLC following the same protocol as described for G3-G6 hydrolysis, with the reaction mixture diluted two times before HPLC injection.

CHAPTER III

RESULTS

3.1 Structural determination

3.1.1 Optimization of recombinant chitinase A expression from *E. coli* M15 cells

The DNA fragment that encodes wild-type chitinase A (amino acid residues 22-597, without the 598-850 C-terminal fragment) was cloned into the pQE60 expression vector and highly expressed in *E. coli* M15 cells as the 576-amino acid fragment with a C-terminal $(His)_6$ sequence (Suginta *et al*., 2004). To achieve a high level of expression of soluble chitinase, IPTG concentrations, temperatures and times required for chitinase induction were determined. When the cells were grown at $37^{o}C$ to an OD_{600} of about 1.0, then the chitinase expression was induced by the addition of varied concentrations of IPTG (0-2 mM) at 25°C for 8 h. The induced cells were harvested, lysed and analyzed by SDS-PAGE. The concentration of 0.5 mM IPTG was found to produce highest level of soluble enzyme. Further optimization was carried out at a fix concentration of 0.5 mM IPTG for 8 h with various temperatures ($20^{o}C$, $25^{o}C$, $30^{o}C$ and $37^{o}C$). SDS-PAGE analysis of total proteins obtained in cell pellet and crude supernatant displayed highest amount of the soluble protein with an induction temperature of $25^{o}C$. For further optimization, chitinase induction was performed at $25^{o}C$ with 0.5 mM IPTG concentration. The expression level of chitinase was tested at various induction times (0, 2, 5, 8 and 18 h). SDS-PAGE

analysis showed no protein band of expected size (63 kDa) at 0 h of incubation. However, this band gradually appeared when the time of induction increased from 2 to 18 h (overnight). For the convenience of experimental handling, an overnight incubation was chosen for chitinase expression.

In conclusion, the expression level of the soluble chitinase was dependent on IPTG concentration, temperature and time course, with the optimal condition established with 0.5 mM IPTG concentration at 25°C for 18 h. This condition was further used for obtaining the high-level expression of all the chitinase variants for functional and structural studies.

3.1.2 Purification of the recombinant chitinase A

3.1.2.1 A small scale purification of the recombinant chitinase A using Ni-NTA agarose affinity chromatography

The recombinant chitinase A was expressed in *E. coli* M15 cells under the optimized condition as mentioned earlier. Crude supernatant was prepared, then further purified by Ni-NTA agarose affinity chromatography using a modified Qiagen's protocol (http:///www1.qiagen.com/literature/handbooks/INT/ProteinPurifi-ation.aspx). Briefly, the Ni-NTA slurry was transferred to a microcentrifuge tube, equilibrated, and washed by centrifugation. To prevent non-specific binding, different concentrations of imidazole (5, 10, 15 and 20 mM) were tested as a single step wash protocol before the bound protein was eluted with 250 mM imidazole. The purification profiles of chitinase A obtained from Ni-NTA chromatography after being washed with the specified concentrations of imidazole were compared (data not shown). As judged by SDS-PAGE, the imidazole concentrations of 10-20 mM used in

the washing step remove unwanted protein bands, yielding a major band of chitinase A.

3.1.2.2 A large scale purification of the recombinant chitinase A for functional studies

Since a relatively high concentration of a highly purified protein (10 mg/ml) is generally required for crystallization experiments, one litre of the bacterial culture was set up as described in section 2.4.2 and 2.4.3. The results obtained from the small scale purification with the single step protocol still displayed nonspecific binding of a 97 kDa protein. To improve the purity of the eluted protein, a two-step wash (5 mM, followed by 20 mM imidazole) was applied prior to elution with 250 mM imidazole.
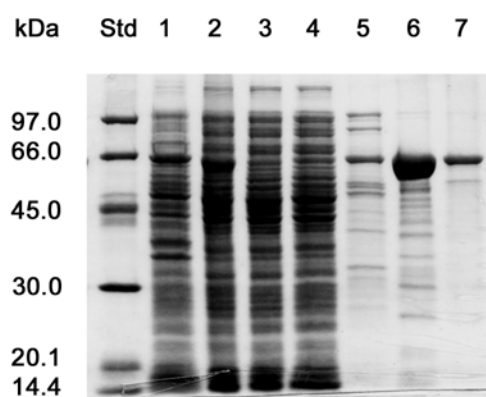
Figure 3.1 A large scale purification of the recombinant chitinase A using Ni-NTA affinity chromatography with the two-step wash protocol.

Cell pellet and crude supernatant were prepared as described in Sections 2.4.2 and 2.4.3. Lanes: Std, low molecular weight protein markers; 1, cells induced with 0.5 mM IPTG; 2, crude supernatant; 3, flow through; 4, 5 mM imidazole wash fraction; 5, 20 mM imidazole wash fraction; 6, the first fraction eluted with 250 mM imidazole; 7, the second fraction eluted with 250 mM imidazole.

Figure 3.1 demonstrates an improvement of the purity of the 63 kDa band when the two-step wash protocol was applied. The overall yield obtained from one litre of bacterial culture was approx. 15 mg of the purified chitinase A. For further purification, the eluted protein obtained from the first fraction (lane 6) was concentrated and subjected to gel filtration chromatography.

A purification of other chitinase variants (D392N, D392K, E315Q, E315M, D392NE315Q, D392NE315M, D392KE315M, W168G, Y171G, W275G, W397F, W570G, a double mutant (W397F/W570G), a triple mutant (W397F/W570G/W275G) and a quadruple mutant (W397F/W570G/W275G/Y171G) were also carried out using Ni-affinity chromatography with a two-step wash without additional purification by gel filtration chromatography with similar yields of approximately 10-15 mg of highly purified protein per liter of bacterial culture.

3.1.3 A complete purification of the recombinant chitinase A for crystallization studies

For initial crystallization set up, the first eluted fraction obtained from the Ni-NTA affinity step was concentrated using Vivaspin-20 ultrafiltration membrane concentrator, and then further purified using a Superdex 200 10/300 GL connected with an ÄKTA purifier system (see Protocol I, section 2.4.5.1). The running buffer was 20 mM Tris-HCl buffer pH 8.0, containing 150 mM NaCl. A flow rate of 0.25 ml/min was maintained and 0.5 ml fractions were collected and assayed for chitinase activity.
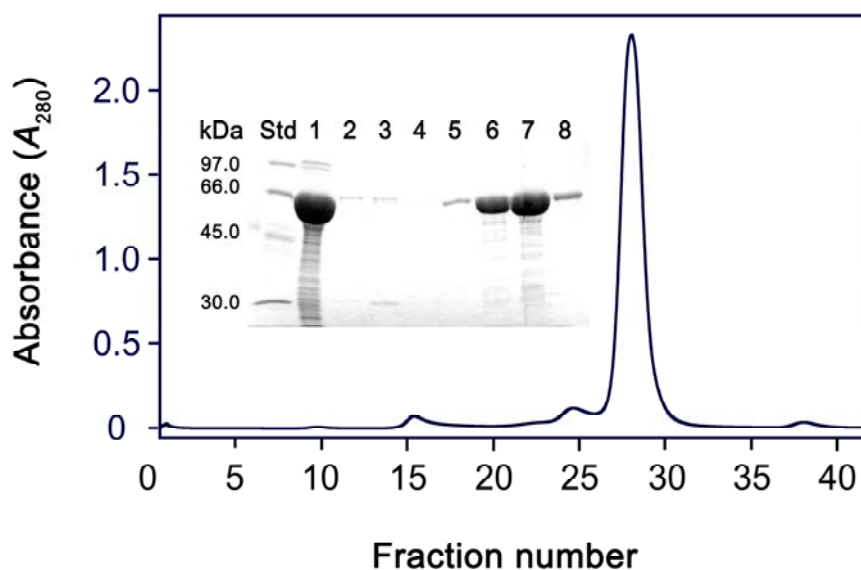
Figure 3.2 An elution profile of the recombinant wild-type chitinase A obtained from an ÄKTA purifier system with a Superdex 200 10/300 GL gel filtration column.

The protein sample obtained from the Ni-affinity step was applied on to Superdex 200 10/300 GL gel filtration column under the condition given in Section 2.4.5.1. Lanes: Std, low molecular weight protein markers; 1, the eluted fraction with 250 mM imidazole from Ni-NTA affinity column; 2-8, the eluted fractions 24, 25, 26, 27, 28, 29 and 30 from Superdex 200 10/300 GL gel filtration column, respectively.

Figure 3.2 shows an elution profile of the protein fractions eluted from Superdex 200 10/300 GL gel filtration column. As seen on SDS-PAGE gel, a major band of 63 kDa was observed in fractions 27-30. These eluted fractions were then pooled and concentrated. The purity of the protein obtained from this step was found to be sufficient for crystallization purpose.

Chitinase activity of the eluted fractions was also determined by colorimetric assay using pNP-GlcNAc$_2$ as the substrate. A summary of the complete purification procedure is described in Table 3.1.

Table 3.1 A complete purification of the recombinant wild-type chitinase A

Purification step	Total protein (mg)	Total activity (Units[a])	Specific activity (U mg^{-1})	Purification fold	Activity yield (%)
Crude supernatant	102.4	11.3	0.11	1	100
Ni-affinity	14.3	7.54	0.53	4.8	66.8
Superdex 200 10/300 GL	7.3	4.1	0.57	5.2	36.6

[a] The release of *p*-nitrophenol was recorded at 405 nm. One unit of chitinase activity is defined as the amount of enzyme that produces 1 µmol of *p*-nitrophenol per min at 37°C.

Table 3.1 shows that the purification fold of the recombinant wild-type chitinase A increased to 4.8 after Ni-affinity chromatography with the activity yield of 66.8%. After gel filtration chromatography, the purity of the enzyme increased to 5.2 fold with the overall yield of 36.6%. From one litre of bacterial culture, 7.3 mg of the purified chitinase A was obtained.

In collaboration with Dr. Robert C. Robinson, the Institute of Molecular and Cell Biology (IMCB), Singapore, crystallization experiments of both wild-type and inactive mutant E315M chitinase A were carried out based on the initial screening trial done at SUT. To obtain a large scale production of the enzymes, one litre of bacterial culture was grown, and crude enzyme was then purified using the modified protocol of the two-step wash Ni-affinity chromatography, followed by two HisTrap HP 1-ml columns connected in series with an ÄKTA purifier system (see Protocol II, section 2.4.5.2). The Ni-affinity columns were first washed with 20 ml of 5 mM imidazole, then an additional wash with 10 ml of 20 mM imidazole. The fractions

eluted with 250 mM imidazole were pooled, concentrated, and then applied on a Hiload 16/60 Superdex 200 prep grade gel filtration column. Figure 3.3 shows an elution profile obtained from a Hiload 16/60 Superdex 200 prep grade gel filtration column. SDS-PAGE analysis indicates a major band of the 63 kDa protein in the A_{280}-containing fractions, suggesting the high purity of the enzyme. The enzyme obtained from this step was used for crystallization experiments.
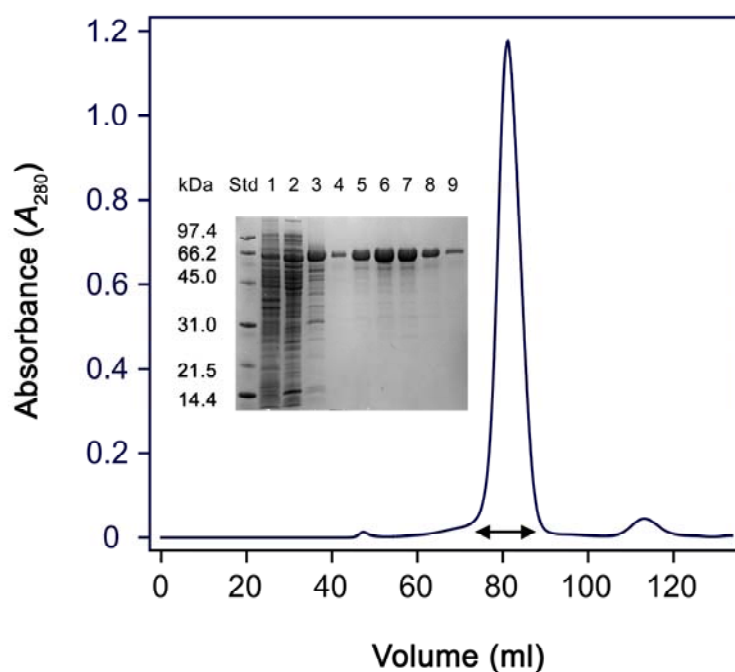
Figure 3.3 An elution profile of the recombinant wild-type chitinase A obtained from an ÄKTA purifier system with a Hiload 16/60 Superdex 200 prep grade gel filtration column.

Cell pellet and crude supernatant were prepared as described in Section 2.4.2 and 2.4.3. Lanes: Std, low molecular weight of protein markers; 1, cells induced with 0.5 mM IPTG; 2, crude supernatant; 3, the pooled fraction eluted with 250 mM imidazole by HisTrap HP 1-ml columns; 4-9, the A_{280}-containing fractions obtained from a Hiload 16/60 Superdex 200 prep grade column.

Expression and purification of E315M mutant was carried out following the purification protocol of the wild-type enzyme with a similar yield of approximately 8 mg per litre of bacterial culture.

3.1.4 Circular Dichroism (CD) spectroscopy

Circular dichroism was employed to investigate the folding states of the *E. coli* expressed enzymes. CD measurements of the highly purified variants were carried out as mentioned in section 2.4.8. The CD spectra of the mutated proteins were compared with that of the wild-type chitinase.

Figure 3.4 shows the CD spectra of the chitinase variants acquired from the wavelength scan between 250 and 190 nm. The overall characteristic of the spectra of the mutated proteins were similar to the spectrum of the native chitinase. This gives an indication that mutations of the studied amino acid residues did not affect the overall structure of the enzymes. The spectra exhibited the minimum absorbance at 220 and 208 nm implied that the protein contained a mixture of α-helices and β-sheets. This spectral characteristic was expected for a $(\beta/\alpha)_8$-barrel containing enzyme (Davies and Henrissat, 1995).
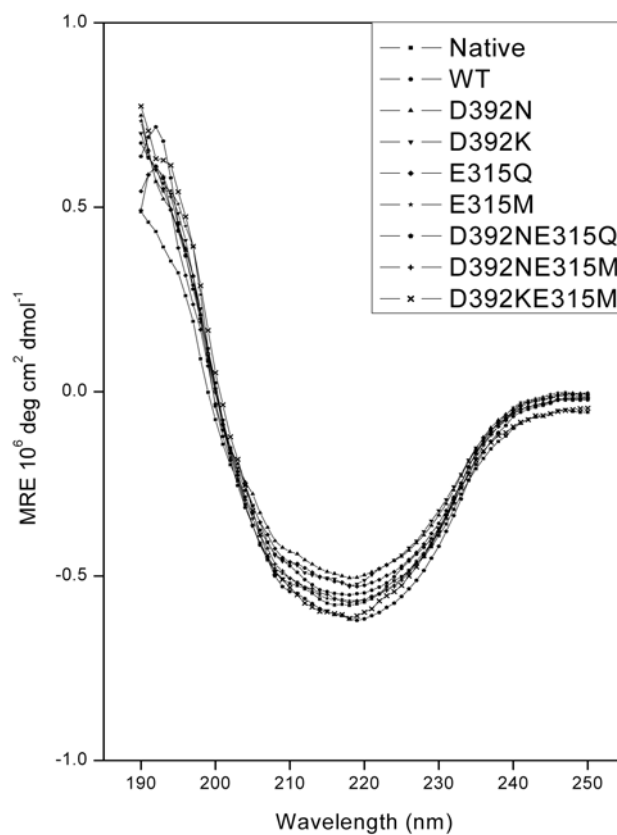
A

Figure 3.4 Determination of the folding states of chitinase A and its mutants.

A) The CD spectra of wild-type, Glu315 and Asp392 mutants; B) The CD spectra of wild-type and its active-site aromatic side chain mutants. The enzymes were prepared by a single-step purification using Ni-NTA agarose affinity chromatography, then dialyzed extensively to remove imidazole. The proteins were solubilized in 20 mM Tris-HCl buffer pH 8.0 to final concentrations of 0.40 to 1.40 mg/ml. The CD spectra of chitinase proteins were obtained with a Jasco J-715 spectropolarimeter. A buffer solution containing 20 mM Tris-HCl pH 8.0 was used for background subtraction.

B
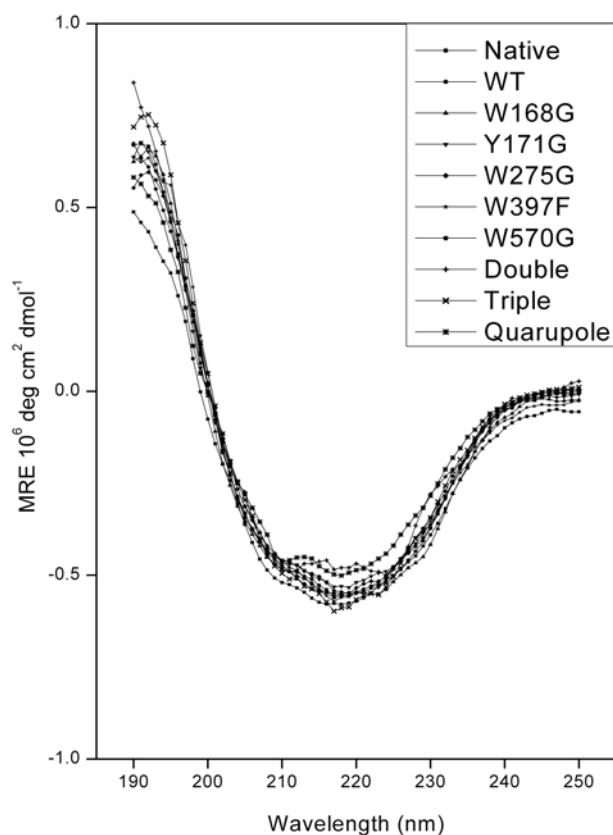
Figure 3.4 Determination of the folding states of chitinase A and its mutants.

A) The CD spectra of wild-type, Glu315 and Asp392 mutants; B) The CD spectra of wild-type and its active-site aromatic side chain mutants. The enzymes were prepared by a single-step purification using Ni-NTA agarose affinity chromatography, then dialyzed extensively to remove imidazole. The proteins were solubilized in 20 mM Tris-HCl buffer pH 8.0 to final concentrations of 0.40 to 1.40 mg/ml. The CD spectra of chitinase proteins were obtained with a Jasco J-715 spectropolarimeter. A buffer solution containing 20 mM Tris-HCl pH 8.0 was used for background subtraction.

3.1.5 Sequence comparison and modeled structural topology

The cDNA encoded a M_r 95 kDa chitinase A precursor was previously isolated from a marine bacterium *V. carchariae* (Suginta *et al.*, 2004). MALDI-TOF measurement of the isolated chitinase A yielded a peak of M_r 63 kDa, indicating that the mature enzyme was proteolytic cleaved, most likely at the C-terminus with the cleavage site predicted to be between Arg597 and Lys598.

The deduced amino acid sequence of a full-length *V. carchariae* chitinase A was compared with other bacterial chitinase sequences. The putative chitinase A showed highest identity with ChiA from *V. parahaemolyticus* (94%), followed by ChiA from *S. liquefaciens* (48%), ChiA from *Alteromonas* sp. (47%) and ChiA from *Enterobacter* sp. (47%), ChiA from *S. marcescens* (47%), and ChiA from *Pantoea agglomerans* (44%). On the other hand, *V. carchariae* chitinase A aligned with chitinase A1 from *B. circulans* with low identity (18%).

Figure 3.5 shows the amino acid sequence comparison of *V. carchariae* chitinaseA with three selected sequences from *Alteromonas* sp ChiA, *P. agglomerans* ChiA and *S. marcescens* ChiA.
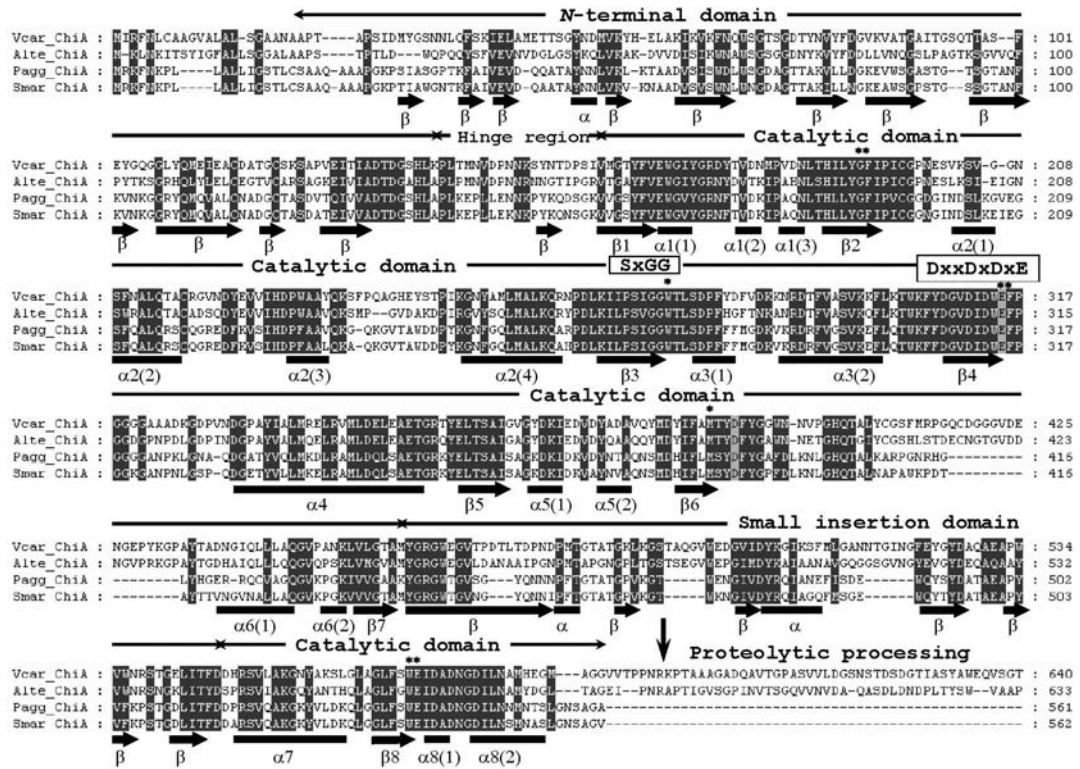
Figure 3.5 An amino acid sequence alignment of *V. carchariae* chitinase A with other bacterial chitinase A sequences.

Completely conserved regions are shaded in black and the catalytic residues in grey. The amino acid residues that are suggested to form three *cis* peptide bonds or to provide hydrophobic environments in the active site of *S. marcescens* ChiA are indicated (asterisks). Key: Vcar_ChiA: chitinase A from *V. carchariae* (*harveyi*) (Q9AMP1); Alte_ChiA: ChiA from *Alteromonas* sp. strain O-7 (P32823); Pagg_ChiA: ChiA from *Pantoea* (*Enterobacter*) *agglomerans* (P97034); and Smar_ChiA: ChiA from *S. marcescens* (P07254, Q54275). ➤: β-strand; ▬: α-helix.

The predicted secondary structure of *V. carchariae* chitinase A using *S. marcescens* ChiA as a template indicated that the polypeptide comprises the N-terminal domain connected with a small hinge region, a typical $(\alpha/\beta)_8$-TIM barrel catalytic domain, and a small $\alpha+\beta$ insertion domain. As shown in the sequence comparison, the catalytic domain of all the bacterial chitinases A is found to be extensively identical, with two completely conserved motifs SxGG and DxxDxDxE located at strand β3 and at the end of strand β4, respectively. These motifs are found in all family 18 chitinases (Davies and Henrissat 1995). The glutamic acid (Glu315) at the end of the DxxDxDxE motif is identified as the most important residue in the catalysis. Amino acid residues that are suggested to form three *cis* peptide bonds (equivalent to residues Gly191-Phe192, Glu315-Phe316, and Trp570-Glu571) or to provide hydrophobic environments (equivalent to residues Phe192, Trp275, Phe316, and Met389) in the active site of *V. carchariae* ChiA are also completely conserved in all the aligned sequences.

It is noticeable that the C-terminal proteolytic fragment in the sequence of full-length of *V. carchariae* chitinase A is predicted to be cleaved off to generate the active 63-kDa enzyme with the proteolytic site located between Arg597 and Lys598. The prediction of the proteolytic cleavage site corresponds well with the molecular weight (62,698 Da) of the native chitinase as determined by MALDI-TOF mass spectrometry (Suginta *et al.*, 2004).

3.1.6 Crystallization of inactive mutant E315M chitinase A

Initial screening experiments for crystallization of wild-type enzyme and E315M mutant were carried out in parallel. However, the crystals of E315M mutant

were obtained earlier. Therefore, further screening to obtain high quality crystal will be described first with E315M mutant.

Initial crystallization of E315M mutant was screened by the Screenmaker 96+8™ located at IMCB, Singapore (see Method 2.6.1). A protein concentration of 20 mg/ml was freshly prepared in 10 mM Tris-HCl buffer pH 8.0. Initial microbatch crystallization experiments were carried out by the sitting drop technique with Crystal Screen HT, SaltRx HT, JB Screen HTS I and HTS II. Positive conditions, which produced crystalline samples, were obtained in many conditions as summarized in Table 3.2.

Table 3.2 A summary of positive conditions obtained from the commercial screening kits for crystallization of E315M.

Commercial screening kit	Condition	Precipitant composition	Temperature (°C)	Days of incubation	Crystal morphology
Crystal Screen HT	C2	30% (w/v) MPD, 0.2 M ammonium acetate,	15	6	Needle cluster
(Hampton		0.1 M tri-sodium citrate dihydrate pH 4.0			
SaltRx HT	H3	0.6 M potassium sodium tartrate tetrahydrate,	22	4	Needle cluster
(Hampton		0.1 M Tris pH 8.5			
Research)	H5	0.5 M potassium thiocyanate,	22	4	Needle cluster
		0.1 M sodium acetate pH 4.6			
JB Screen HTS I	B11	10%(w/v) PEG 4000, 0.2 M magnesium chloride,	15	6	Rod cluster [a]
(Jena Bioscience		0.1 M MES sodium salt pH 6.5			
GmbH)	D10	20%(w/v) PEG 4000, 0.2 M ammonium sulfate	15	6	Plate [a]
	E3	22%(w/v) PEG 4000, 0.2 M ammonium sulfate,	15	6	Needle cluster
		0.1 M sodium acetate			
JB Screen HTS II	A9	2%(w/v) PEG 1000, 1.6 M ammonium sulfate,	4	6	Needle cluster
(Jena Bioscience		0.1 M HEPES sodium salt pH 7.5			
GmbH)	D2	47%(w/v) MPD, 2%(w/v) *tert*-butanol	15	5	Needle cluster

[a] The conditions used for further optimization.

Of all the conditions tested, only conditions B11 and D10 from JBScreen HTS I gave rod cluster and plate types of crystals and were used for further screening by the hanging drop vapor diffusion method. For further optimization, two major parameters were considered simultaneously and were refined as two-dimensional (2D) optimization or "grid screening" (Table 3.3). For condition D10 optimization, concentrations of PEG 4000 and ammonium sulfate were varied in the hanging drop trays. It was found that the effective concentrations of PEG 4000 were in a range of 6-20%. Ammonium sulfate concentrations were varied with 0.05 M increment (0 M to 0.1 M). In addition, a grid screen of PEG 4000 and ammonium sulfate concentrations (Table 3.3A) was performed with a discrete range of pH from 5.0 to 8.0. With all the conditions used, crystals appeared in 20% PEG 4000, 0.1 M ammonium sulfate in 0.1 M Tris-HCl pH 7.5 and pH 8.0 (not shown) and these two conditions were further refined (as shown in Table 3.3B), in which a combination of PEG 4000 and ammonium sulfate was tried under 0.1 M Tris-HCl pH 7.5 or pH 8.0.

Table 3.3 A grid screening of PEG 4000, ammonium sulfate concentrations and various pH for crystallization of E315M chitinase A.

A A coarse screening under 4 different pH values [a] obtained from condition D10.

%PEG 4000	Concentration of ammonium sulfate (M)		
(w/v)	0	0.05	0.1
6	6%	6%	6%
	0 M	0.05 M	0.1 M
10	10%	10%	10%
	0 M	0.05 M	0.1 M
14	14%	14%	14%
	0 M	0.05 M	0.1 M
20	20%	20%	**20% [b]**
	0 M	0.05 M	**0.1 M**

[a] 0.1 M sodium acetate pH 5.0, 0.1 M HEPES pH 7.0, 0.1 M Tris-HCl pH 7.5 and 0.1 M Tris-HCl pH 8.0.

[b] The condition used for a refined screening.

B A refined screening of the condition containing 20% (w/v) PEG 4000, 0.1 M ammonium sulfate obtained from Table 3.3A under two pH values [c].

Concentration of ammonium sulfate (M)	%PEG 4000 (w/v)					
	12	14	16	18	20	22
0.05	12%	14%	16%	18%	20%	22%
	0.05 M	0.05 M	0.05 M	0.05 M	0.05 M	0.05 M
0.08	12%	14%	16%	18%	20%	22%
	0.08 M	0.08 M	0.08 M	0.08 M	0.08 M	0.08 M
0.10	12%	14%	16%	18%	**20% [d]**	22%
	0.10 M	0.10 M	0.10 M	0.10 M	**0.10 M**	0.10 M
0.13	12%	14%	16%	18%	20%	22%
	0.13 M	0.13 M	0.13 M	0.13 M	0.13 M	0.13 M

[c] 0.1 M Tris-HCl pH 7.5 and 0.1 M Tris-HCl pH 8.0

[d] The condition produced single crystals.

From the two sets of screening experiment, the best condition in which single crystals were observed was 20% (w/v) PEG 4000 and 0.1 M ammonium sulfate in 0.1 M Tris-HCl pH 7.5 as shown in Figure 3.6A. An average size of the crystal obtained at Day 6 at 15°C was measured as $100 \times 30 \times 50$ μm^3. A single crystal of E315M was then transferred to a cryoprotectant composed of a reservoir solution with 10% glycerol, then subjected to X-ray diffraction analysis. The diffraction data was collected by a Rikagu/MSC FR-E SuperBright X-ray generator equipped with R-AXIS IV^{++} imaging plate area detector located at IMCB, Singapore (see Methods 2.6.5). After completing data collection, the crystal was transferred from the cryoloop, dissolved in gel loading buffer, and then analyzed on SDS-PAGE (Figure 3.6B). Another positive condition was also found in the grid screen of PEG 4000 and ammonium sulfate concentration with a pH of 7.5. The E315M protein was crystallized as thin needles in the condition of 18% (w/v) PEG 4000, 0.13 M ammonium sulfate and 22% (w/v) PEG 4000, 0.08 M ammonium sulfate.
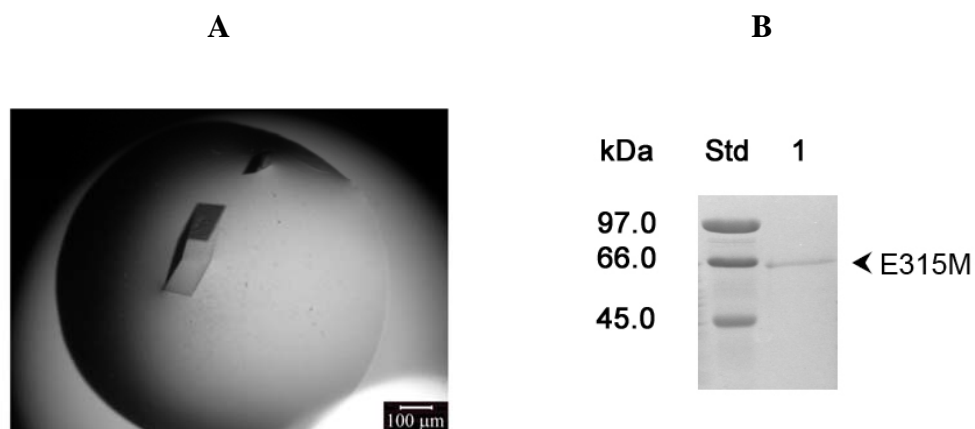
Figure 3.6 Crystallization of E315M inactive mutant.

(A) A crystal of inactive mutant E315M chitinase A obtained from the hanging drop technique using 20% (w/v) PEG 4000, 0.1 M ammonium sulfate and 0.1 M Tris-HCl pH 7.50. (B) The diffracted crystal was analyzed by SDS-PAGE. Lanes; Std, low molecular weight protein markers; 1, a diffracted crystal of E315M obtained from (A).

The data analysis processed by MOSFLM gave a representative diffraction image with orthorhombic space group, and the crystal diffracted to 1.70 Å resolution (Figure 3.7).
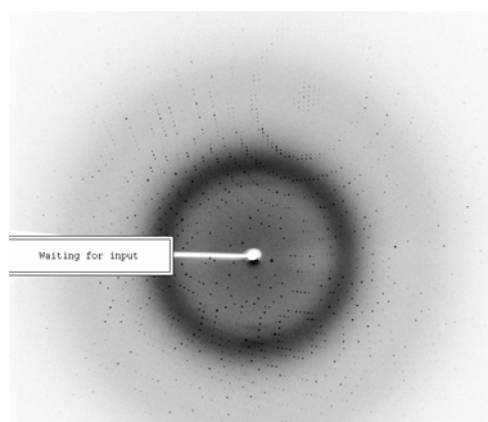
Figure 3.7 A diffraction image of mutant E315M diffracted to 1.70 Å resolution.

The crystal-to-detector distance was set to 150 mm, with all frames collected at 100 K and the exposed time of 0.5 min per image. Total diffraction images collected were 515 images with a width of 0.5° per image. The processed data suggested that the crystals belong to space group $P2_12_12_1$ with cell parameters $a = 63.96$ Å (1 Å = 0.1 nm), $b = 83.11$ Å and $c = 106.98$ Å (Table 3.8).

This data led to the structural determination of E315M by the molecular replacement method based on the crystallographic data of chitinase A from *S. marcescens* (PDB code; 1CTN). *S. marcescens* chitinase A comprises 540 amino acids and exhibits a molecular weight of 58.7 kDa (Perrakis *et al*., 1994), which is similar to the size of *V. carchariae* chitinase A. The two enzymes share 47% sequence identity (Results 3.1.5), and the 3D-structure modeling suggested that *V. carchariae* chitinase A has a similar fold with *S. marcescens* chitinase A (Suginta *et al*., 2007).

3.1.7 Crystallization of E315M-NAG$_5$ and E315M-NAG$_6$ complexes

In the case of the inactive mutant complexed with chitooligosaccharides, various soaking experiments were tried. Initially, the X-ray quality crystals of E315M mutant obtained under 20% (w/v) PEG 4000, 0.1 M ammonium sulfate and 0.1 M Tris-HCl pH 7.5 using the hanging drop method were further transferred to a mother liquor containing a series of 5 mM and 10 mM NAG$_5$ or NAG$_6$ in the cryoprotectant solution [22% (w/v) PEG 4000, 10% glycerol, 0.1 M ammonium sulfate in 0.1 M Tris-HCl pH 7.5]. Under this condition, the crystals were successfully soaked for only 1 day, then damaged after 2 days of soaking time.

Therefore, different conditions of crystal growth were tested to improve the stability of the crystals. Condition B11 from JBScreen HTS II (see Table 3.4) was

then selected for further optimization using the hanging drop method with various concentrations of precipitants PEG 4000 and magnesium chloride in 0.1 M HEPES pH 7.0. A protein concentration of 10 mg/ml was prepared in 10 mM Tris-HCl buffer pH 8.0. A coarse optimization was performed by varying concentrations of PEG 4000 (2-20%) and magnesium chloride (0-0.2 M). A grid screening with varied PEG 4000 and magnesium chloride concentrations is shown in Table 3.4.

Table 3.4 A grid screening of PEG 4000 and ammonium sulfate concentrations for crystallization of E315M-NAG$_5$/NAG$_6$ complexes.

A A coarse screening obtained from condition B11.

Concentration of magnesium chloride (M)	%PEG 4000 (w/v)					
	2	6	8	10	14	20
0.0	0 M	0 M	0 M	0 M	0 M	0 M
	2%	6%	8%	10%	14%	20%
0.05	0.05 M	0.05 M	0.05 M	0.05 M	0.05 M	0.05 M
	2%	6%	8%	10%	14%	20%
0.1	0.1 M	0.1 M	0.1 M	0.1 M	**0.1 M** [a]	0.1 M
	2%	6%	8%	10%	**14%**	20%
0.2	0.2 M	0.2 M	0.2 M	0.2 M	0.2 M	0.2 M
	2%	6%	8%	10%	14%	20%

[a] The condition used for a refined screening.

B A refined screening of the condition 14% (w/v) PEG 4000, 0.1 M ammonium sulfate in 0.1 M HEPES pH 7.0 obtained from Table 3.4A.

%PEG 4000 (w/v)	Concentration of magnesium chloride (M)					
	0.05	0.08	0.1	0.16	0.2	0.24
12	12%	12%	12%	12%	12%	12%
	0.05 M	0.08 M	0.1 M	0.16 M	0.2 M	0.24 M
14	14%	14%	14%	14%	14%	14%
	0.05 M	0.08 M	0.1 M	0.16 M	0.2 M	0.24 M
16	16%	16%	**16%** [b]	16%	16%	16%
	0.05 M	0.08 M	**0.1 M**	0.16 M	0.2 M	0.24 M
18	18%	18%	18%	18%	18%	18%
	0.05 M	0.08 M	0.1 M	0.16 M	0.2 M	0.24 M

[b] The condition produced single crystals.

Of all the conditions tested (Table 3.4A), small single crystals were obtained from 14% (w/v) PEG 4000, 0.1 M magnesium chloride in 0.1 M HEPES pH 7.0 within 10 days. Therefore, this condition was further refined under HEPES buffer pH 7.0 using the hanging drop method. The refined grid screening of PEG 4000 and magnesium chloride concentrations is shown in Table 3.4B. High quality crystals for E315M mutant was observed within 12 days at 15°C in the condition containing 16% (w/v) PEG 4000, 0.1 M magnesium chloride in 0.1 M HEPES pH 7.0. Another condition of 14% (w/v) PEG 4000, 0.08 M magnesium chloride in 0.1 M HEPES pH 7.0 also gave single crystals, but with smaller sizes. The average size of the crystals obtained from the best condition was $50 \times 30 \times 15$ μm^3 as shown in Figure 3.8.
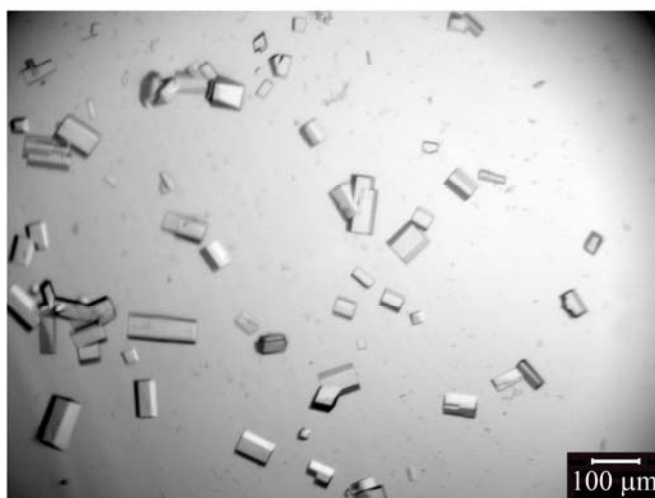
Figure 3.8 Crystals of inactive E315M mutant in the absence of substrate.

The crystals of inactive E315M mutant were obtained from the hanging drop technique using 16% (w/v) PEG 4000, 0.1 M magnesium chloride and 0.1 M HEPES pH 7.0.

Therefore, the crystals obtained under the condition consisting 16% (w/v) PEG 4000, 0.1 M magnesium chloride in 0.1 M HEPES pH 7.0 was chosen for soaking experiments. The inactive mutant crystals were transferred to the cryoprotectant solutions [20% (w/v) PEG 4000, 10% (v/v) glycerol, 0.1 M magnesium chloride in 0.1 M HEPES pH 7.0] containing 5 mM and 10 mM NAG_5 or NAG_6. The crystals were successfully soaked after 2 days at $15^{o}C$ at both concentrations of the substrates.

For X-ray data collection of E315M-complex crystals, two single crystals were picked directly from the hanging drop without any cryoprotectant solution since 10% glycerol present in the precipitant solution already served as a cryoprotectant. The diffraction X-ray data were collected by the same X-ray generator with crystal-to-detector distance set to 120 mm and all frames collected at 100 K for both data set to Diffraction of 360 and 430 images with a width of 0.5^{o} per image for NAG_5 and NAG_6 were collected. The processed data revealed that the crystals belong to space group $P2_12_12_1$ with cell parameters $a = 63.96$ Å, $b = 83.11$ Å and $c = 106.98$ Å for E315M-NAG_5 complex and $a = 63.70$ Å, $b = 83.32$ Å and $c = 106.56$ Å for E315M-NAG_6 complex (Table 3.8). The structure was subsequently determined by the rigid body refinement using the crystal structure of inactive E315M mutant as the structural model as described in Methods 2.6.11 and 2.6.12.

3.1.8 Crystallization of wild-type chitinase A

The purified chitinase A (20 mg/ml) was kept in the storage buffer (20 mM Tris-HCl buffer pH 8.0 and 150 mM NaCl) at $4^{o}C$ before crystallization setup. The buffer was later exchanged to 10 mM Tris-HCl buffer pH 8.0 in order to effectively

maintain the lowest possible ionic strength of the protein solution (Papanikolau and Petratos, 2002). The crystallization experiments were carried out by the microbatch method using commercially available screening kits; Crystal Screen HT, JB Screen HTS I and HTS II (see Methods 2.6.1). Under all the tested solutions, a number of positive conditions that produced micro crystals were obtained as summarized in Table 3.5. The hanging drop, sitting drop vapor diffusion, microseeding and macroseeding techniques were tried for all the conditions listed in Table 3.5.

Table 3.5 A summary of positive conditions obtained from the commercial screening kits for crystallization of wild-type.

Commercial screening kit	Condition	Precipitant composition	Temperature (^{o}C)	Days of incubation	Crystal morphology
Crystal Screen HT (Hampton Research)	B10	30%(w/v) PEG 4000, 0.2 M sodium acetate, 0.1 M Tris-HCl pH 8.5	15	5	Rod cluster [a]
JB Screen HTS I (Jena Bioscience GmbH)	C10	30%(w/v) PEG 4000, 0.1 M magnesium chloride, 0.1 M sodium acetate pH 4.6	15	2	Needle cluster
	D9	16%(w/v) PEG 4000, 10%(w/v) 2-propanol, 0.1 M HEPES sodium salt pH 7.5	4	4	Needle cluster
	D10	20%(w/v) PEG 4000, 0.2 M ammonium sulfate	15	4	Needle cluster
	E2	22%(w/v) PEG 4000, 10%(w/v) 2-propanol, 0.1 M HEPES sodium salt pH 7.5	22	4	Needle cluster
	E3	22%(w/v) PEG 4000, 0.2 M ammonium sulfate, 0.1 M sodium acetate	15	5	Needle cluster
JB Screen HTS II (Jena Bioscience GmbH)	A4	1 M ammonium sulfate, 0.1 M Tris-HCl pH 8.5	15, 22	1	Needle cluster [a]
	A9	2%(w/v) PEG 1000, 1.6 M ammonium sulfate, 0.1 M HEPES sodium salt pH 7.5	4	21	Plate
	B1	5%(v/v) PEG 400, 2 M ammonium sulfate, 0.1 M MES sodium salt pH 6.5	15	8	Plate
			22	4	Needle cluster
	C6	30%(w/v) MPD, 0.2 M ammonium acetate,	15	8	Needle cluster

[a] The conditions used for further optimization.

With all the conditions tested, condition B10 from Crystal Screen HT [30% (w/v) PEG 4000, 0.2 M sodium acetate trihydrate and 0.1 M Tris-HCl pH 8.5] provided starting crystals that could be further optimized by the hanging drop, sitting drop or microseeding techniques at 15°C. For each of the 2D grid screening, two major factors were optimized simultaneously. Concentrations of PEG 4000 and pH values were screened, while fixing 0.1 M sodium acetate trihydrate as shown in Table 3.6.

Table 3.6 A grid screening of PEG 4000 concentrations and various pH[a] for crystallization of wild-type chitinase A.

A A coarse screening under 4 different pH values [a] obtained from condition B10.

%PEG 4000	pH [a]			
(w/v)	7.5	8.0	8.5	9.0
14	14%	14%	14%	14%
	7.5	8.0	8.5	9.0
16	16%	16%	16%	16%
	7.5	8.0	8.5	9.0
18	18%	18%	18%	18%
	7.5	8.0	8.5	9.0
20	20%	20%	20%	20%
	7.5	8.0	8.5	9.0

B Another coarse screening under 4 different pH values [a] obtained from condition B10 (continued).

%PEG 4000	pH [a]			
(w/v)	7.5	8.0	8.5	9.0
22	22%	22%	22%	22%
	7.5	8.0	8.5	9.0
26	26%	26%	26%	**26% [b]**
	7.5	8.0	8.5	**9.0**
30	30%	30%	30%	30%
	7.5	8.0	8.5	9.0
34	34%	34%	34%	34%
	7.5	8.0	8.5	9.0

[a] 0.1 M Tris-HCl pH 7.5, 0.1 M Tris-HCl pH 8.0, 0.1 M Tris-HCl pH 8.5 and 0.1 M Tris-HCl pH 9.0.
[b] The condition produced crystals.

Under the condition comprising 26% (w/v) PEG 4000, 0.1 M sodium acetate and 0.1 M Tris-HCl pH 9.0, single crystals were found in the hanging drop well after 7 days of incubation at 15°C. A well-formed crystal was picked, flash-cooled in

liquid-nitrogen stream using a cryoprotectant solution [26% (w/v) PEG 4000, 10% (v/v) glycerol, 0.1 M sodium acetate, 0.1 M Tris-HCl pH 9.0], and subjected to the same X-ray generator. A diffraction image of the wild-type crystal diffracted to 2.36 Å resolution. The crystal-to-detector distance was set to 190 mm, with exposure time of 1 min per image. After autoindexing and integrating some of the diffraction data, the crystal was assigned to the triclinic space group $P1$. However, due to the twinning problem that arose from so many layers of crystals, the data set obtained from this condition could not be further processed.

To obtain other crystal growth conditions, all the conditions listed from the commercial screening kits (Table 3.5) were re-screened with various types of PEG, salts, buffers and a wide range of pH. All the optimized conditions tested from those commercially available screen kits failed to generate X-ray quality crystals for structural analysis, except for condition A4 from JB Screen HTS II [1 M ammonium sulfate and 0.1 M Tris-HCl pH 8.5]. Therefore, this condition was further optimized under a pH range of 6.5-9.0 and different concentrations of 0.8-1.4 M ammonium sulfate at varied temperatures of 4°C, 15°C and 22°C (Table 3.7).

Table 3.7 A coarse screening of condition A4 for crystallization of wild-type chitinase A.

Concentration of ammonium sulfate (M)	pH [a]					
	6.5	7.0	7.5	8.0	8.5	9.0
0.8	0.8 M 6.5	0.8 M 7.0	0.8 M 7.5	0.8 M 8.0	0.8 M 8.5	0.8 M 9.0
1.0	1.0 M 6.5	1.0 M 7.0	1.0 M 7.5	1.0 M 8.0	1.0 M 8.5	1.0 M 9.0
1.2	1.2 M 6.5	1.2 M 7.0	1.2 M 7.5	**1.2 M [b] 8.0**	1.2 M 8.5	1.2 M 9.0
1.4	1.4 M 6.5	1.4 M 7.0	1.4 M 7.5	1.4 M 8.0	1.4 M 8.5	1.4 M 9.0

[a] 0.1 M MES pH 6.5, 0.1 M HEPES pH 7.0, 0.1 M Tris-HCl pH 7.5, 0.1 M Tris-HCl pH 8.0, 0.1 M Tris-HCl pH 8.5 and 0.1 M Tris-HCl pH 9.0.

[b] The condition used for further macroseeding optimization.

The crystallization results obtained from the hanging drop method indicated many plates and needle clusters obtained under the optimized conditions shown in Table 3.7. Some plates were seen in the hanging drops at 15°C and 22°C with buffer pH 8.0 containing 1.2 M ammonium sulfate as shown in Figure 3.9A. Single crystals were only obtained after 2 days of incubation at 15°C using the macroseeding technique. With varied protein concentrations of 5, 10 and 20 mg/ml, only a drop of 5 mg/ml of protein concentration pre-equilibrated in 0.1 M Tris-HCl pH 8.0 containing 1.2 M ammonium sulfate provided large crystals with an average dimension of 230 × 100 × 15 µm^3 (Figure 3.9B).

A   B

Figure 3.9 Crystals of wild-type chitinase A.

(A) Plates and needle clusters of wild-type chitinase A obtained from the hanging drops using 1.2 M ammonium sulfate in 0.1 M Tris-HCl pH 8.0 (B) Crystals of wild-type chitinase A obtained from the macroseeding technique under 1.2 M ammonium sulfate and 0.1 M Tris-HCl pH 8.0.

A single crystal obtained from Figure 3.9B was transferred to a cryoprotectant composed of a reservoir solution containing 10% glycerol. X-ray diffraction data were measured using the same X-ray machine located at IMCB as described for E315M mutant. The crystal-to-detector distance was set to 120 mm, with all frames collected at 100 K. The diffraction data of 720 images with a width of 0.5° per image were collected and processed. The crystal belongs to space group $P1$ with cell parameters $a = 60.27$ Å, $b = 64.28$ Å and $c = 83.52$ Å (Table 3.8). All four data sets from single crystals of wild-type, inactive E315M mutant, E315M-NAG$_5$ and E315M-NAG$_6$ complexes were further scaled and merged as described in Methods 2.6.10-2.6.13. The structure of wild-type enzyme was determined by the molecular replacement methods with program *AmoRe* (Navaza, 1994), using the crystal structure of refined E315M mutant as the model. Crystallographic data collection and refinement statistics obtained from the final models is shown in Table 3.8.

Table 3.8 Crystallographic data collection and refinement statistics of the four chitinase structures.

Crystal	Wild-type	E315M	E315M-NAG$_5$	E315M-NAG$_6$
Space group	$P1$	$P2_12_12_1$	$P2_12_12_1$	$P2_12_12_1$
Unit-cell parameters	a = 60.27 Å	a = 63. 96 Å	a = 63.51 Å	a = 63. 70 Å
	b = 64.28 Å	b = 83.11 Å	b = 83.08 Å	b = 83.32 Å
	c = 83.52 Å	c = 106.98 Å	c = 105.59 Å	c = 106.56 Å
	α = 91.74°	α = β = γ = 90°	α = β = γ = 90°	α = β = γ = 90°
	β = 91.17°			
	γ = 112.91°			
Solvent content (%)	46.9	44.4	43.2	44.1
Unique reflections	73693 (10404)	61563 (7880)	59561(8247)	53131 (7564)
Observed reflections	292719 (41321)	607216 (59894)	406849 (45783)	452556 (63380)
Multiplicity	4.0 (4.0)	9.9 (7.6)	6.8 (5.6)	8.5 (8.4)
Resolution limits [a] (Å)	24.60-2.10 (2.00)	24.70-1.80 (1.70)	21.50-1.80 (1.72)	30-1.90 (1.80)
Completeness (%)	94.6 (91.9)	97.2 (87.2)	99.2 (95.6)	99.7 (99.0)
R_{merge} [a, b] (%)	6.60 (22.80)	7.10 (36.10)	7.10 (12.30)	7.00 (31.20)
$<I/sigmaI>$	19.5 (5.5)	26.9 (4.5)	26.3 (9.9)	26.3 (6.1)
R_{factor} [c] (%)	16.80	18.90	18.80	18.10
R_{free} [d] (%)	20.50	21.90	21.50	20.90
No. of protein residues	1134	581	567	567
No. of protein atoms	8708	4474	4353	4353
No. of carbohydrate atoms	-	-	57	85
No. of ordered waters	1091	740	665	691
R.M.S. deviation				
Bond length	0.007	0.006	0.006	0.006
Bond angle	0.968	0.932	0.994	0.992
Mean atomic B values				
Protein atoms	14.45	15.10	14.24	13.74
Substrate	-	-	19.82	21.79
Waters	24.46	25.69	24.92	25.42
Overall	16.19	16.60	15.70	15.45

[a] Values in parentheses refer to the corresponding values of the highest resolution shell.

[b] $R_{merge} = \sum_{hkl} \sum_i \left| I_i(hkl) - \langle I(hkl) \rangle \right| / \sum_{hkl} \sum_i I_i(hkl)$ where I_i is the intensity for the ith measurement of an equivalent reflection with indices hkl.

[c] $R_{factor} = \dfrac{\sum \left| |F_{obs}| - |F_{calc}| \right|}{\sum |F_{obs}|}$ where F_{obs} and F_{calc} are the observed and calculated structure-factors.

[d] $R_{free} = \dfrac{\sum \left| |F_{obs}| - |F_{calc}| \right|}{\sum |F_{obs}|}$ calculated from 5% of the reflections selected randomly and omitted from the refinement process.

3.1.9 The structure elucidation of *V. carchariae* chitinase A

The structures of E315M, E315M-NAG$_5$ and E315M-NAG$_6$ consist of one monomer per asymmetric unit and comprise 576 amino acid residues, whilst the structure of the wild-type enzyme consists of two monomers per asymmetric unit and comprises 1,134 amino acid residues. The overall structure of the *Vibrio* enzyme contains three domains (Figure 3.10).

The amino terminal domain

The amino terminal domain has a fold comprising mostly β-strands with residues 22-138.

The hinge region

The hinge region comprises 21 amino acid residues, connected between the amino-terminal domain and the main α/β-barrel domain. The formed coil consisting of residues 139-159.

The β/α-barrel domain

The eight stranded β/α-barrel is the catalytic domain of the enzyme comprising two separate regions designated Cat I and Cat II. Cat I is formed by residues 160-460, while Cat II is formed by residues 548-588. It has the TIM characteristic, which is referred as the (β/α)$_8$-barrel fold comprising of eight β-strands tethered to eight α-helices by loops.

The small α+β insertion domain

The small α+β fold is inserted between strand B7 of Cat I and helix A7 of the Cat II. It comprises three α-helices and five β-strands. These strands make up all antiparallel β strands, which are connected by β turns.
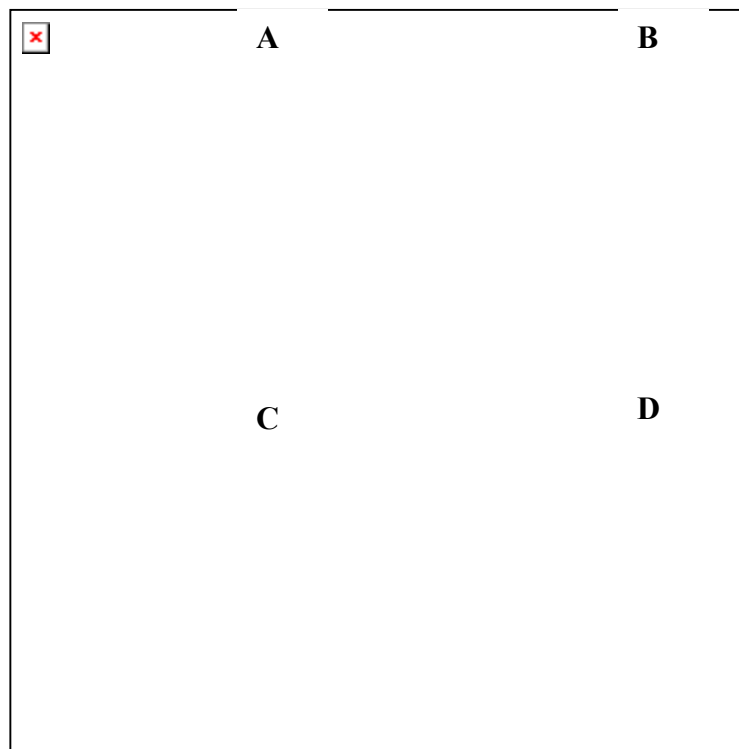
Figure 3.10 A ribbon representation of the overall structure of *V. carchariae* chitinase A.

The N-terminal domain is depicted in blue, the catalytic TIM-barrel domain is in red for (A) wild-type structure; in salmon for (B) inactive E315M mutant; in orange for (C) E315M-NAG$_5$ complex and in yellow for (D) E315M-NAG$_6$ complex. The small insertion domain is in green. Molecule A is only presented for the wild-type structure. Stick models represent His$_6$ residues, NAG$_5$, and NAG$_6$ from inactive E315M mutant, E315M-NAG$_5$ and E315M-NAG$_6$ complex, respectively.

Overall, the chitinase structures exhibit three additional common features as follows; i) Tyr171 is detected in generously disallowed region in Ramachandran plot; ii) three *cis* peptide bonds are formed between residues Gly191-Phe192, Glu315-Phe316, and Trp570-Glu571 located at the catalytic cleft (see Discussion 4.4); iii) there are three disulfide bonds, one of which (Cys116-Cys121) located at the end of the N-terminal region and two of which (Cys196-Cys217 and Cys409-Cys418) located at the catalytic domain (Figure 3.11).
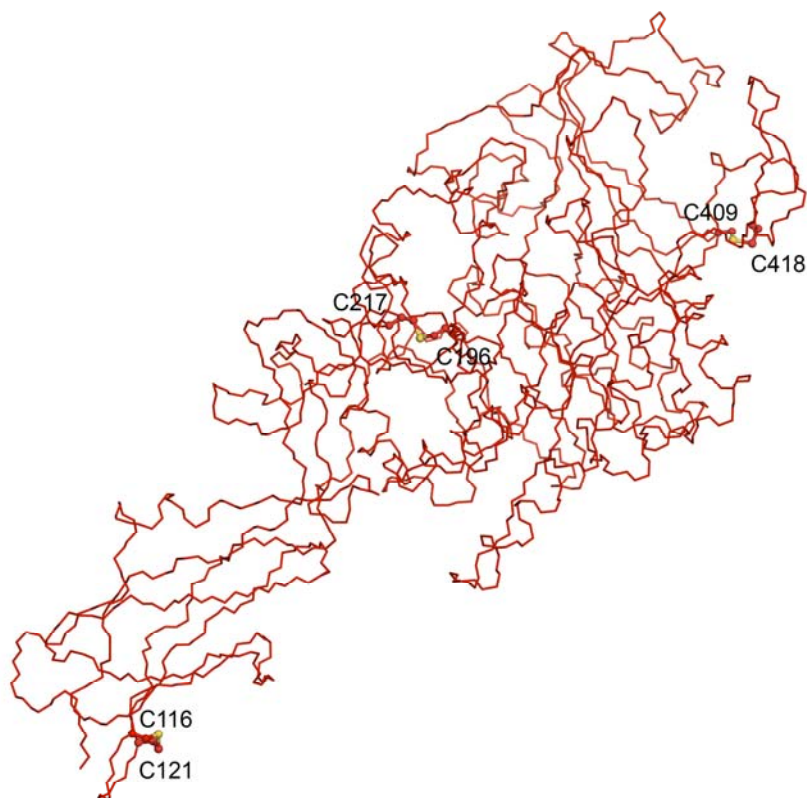
Figure 3.11 A representation of three disulfide bonds of *V. carchariae* chitinase A. The backbone structure is shown in red. Ball-and-stick model represents Cys residues. Sulfur is labeled in orange yellow.

The structure of inactive mutant without substrate (Figure 3.10B) reveals that the histidine tagged residues, which were added to aid purification, buries in the catalytic cleft of the enzyme. These histidine residues apparently mimic the substrate structure by interacting with all the important binding residues that lie within the substrate binding cleft. The overall structure of the complex E315M-NAG$_5$ (Figure 3.10C) shows that the substrate NAG$_5$ is bound within the long deep groove (about 30 Å in width and about 14 Å in depth). The structure of the complex E315M-NAG$_6$ (Figure 3.10D) indicates that the NAG$_6$ substrate is firmly embedded within the groove extended to 33 Å in width with the same dept of 14 Å as for NAG$_5$. The substrate-binding groove appears to be long and open at both ends, which allows sugar substrates to extend either directions beyond subsites -4 or +2 (see Figure 3.13B for subsite identification).

A structural comparison of *V. carchariae* and *S. marcescens* chitinase A

The putative sequence of chitinase A from *V. carchariae* shows 47% identity to that of the template sequence (*S. marcescens* chitinase A) (see Results 3.1.5). The superposition of 459 residues of the *Vibrio* enzyme with the equivalent residues of the *Serratia* enzyme using program Superpose available in the CCP4 suit (CCP4, 1994) gave an R.M.S. of 6.221 Å (Figure 3.12A), which indicates a high similarity of the overall fold of the two enzymes. Figure 3.12B-C presents the secondary structural arrangement between *Serratia and Vibrio* chitinase A.
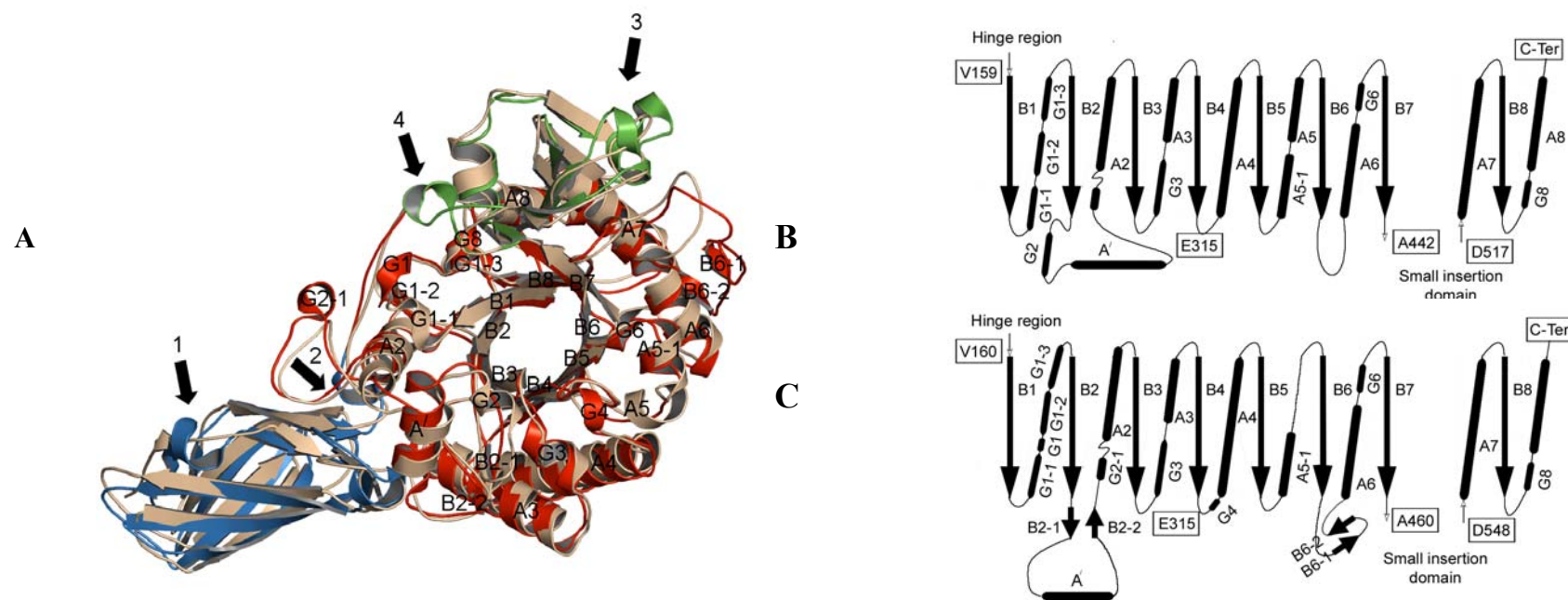
Figure 3.12 A comparison of *V. carchariae* and *S. marcescens* chitinase A structures.

(A) A ribbon representation of superposition of *V. carchariae* and *S. marcescens* chitinase A. The N-terminal domain of *V. carchariae* is depicted in blue, the catalytic TIM-barrel domains is in red and the small insertion domain is in green. The overall structure of *S. marcescens* is shown in wheat color. Arrow indicates the helix that is not present in *S. marcescens* structure. (B) and (C) Topology diagrams of the catalytic domains of *S. marcescens* and of *V. carchariae* chitinase A. Symbols and nomenclatures of strands and helices used are given based on the topology of the secondary structure of *S. marcescens* chitinase A (Perrakis *et al.*, 1994). Eight β-strands that form the core of the enzyme are referred as B1 to B8, whereas eight α-helices connected between β-strands are referred as A1 to A8.

The structural comparison shows that both *S. marcescens* and *V. carchariae* chitinase A have a distinct N-terminal β-sandwich domain that presumably acts as a chitin anchor. Essentially, both structures are identical (Figure 3.12) with only a few minor differences. Considering the differences at N-terminal domain, the first two parallel strands are interrupted with a helix, which was absent in *S. marcescens* chitinase A (indicated by an arrow 1 in Figure 3.12A). In addition, the N-terminal domain of *Vibrio* enzyme contains an interchain disulfide bond between residues 116 and 121 (see Figure 3.11) but in the *Serratia* enzyme this bond formed between residues 115 and 120. Furthermore, the hinge region of the *Vibrio* structure is preceded by a short helix (as indicated by an arrow 2 in Figure 3.12A). This helix is not found the *Serratia* structure.

Additional discrepancies are found in their catalytic domains. Topology of the catalytic domain reveals that strand B1 connects four short α-helices (G1-1, G1, G1-2 and G1-3) together in the *Vibrio* enzyme (Figure 3.12C), while only three helices (G1-1, G1-2 and G1-3) are found in the *Serratia* enzyme (Figure 3.12B). In contrast, there are four α-helices connected between B2 and B3 in the *Serratia* domain, but only three (Á, G2-1 and A2) are found in the *Vibrio* domain, with two extra short antiparallel strands namely B2-1 and B2-2 are found in *Vibrio*. Both structures have two α-helices (G3 and A3) connected between B3 and A4 and contain two conserved motifs; the SxGG motif located within strand B3 and the DxxDxDxE motif consisting Glu315 located at the end of strand B4. In *V. carchariae* chitinase A, two helices (G4 and A4) are found between strands B4 and B5, while only helix A4 is found in the *S. marcescens* domain. Although, two α-helices (A6 and G6) that connect between

strands B6 and B7 are the same for both enzymes, the two extra antiparallel β-sheets, B6-1 and B6-2, are only formed in the *V. carchariae* domain.

In the *Vibrio* catalytic domain, two intrachain disulfide bonds are found between Cys196-Cys217 and Cys409-Cys418 (see Figure 3.11), while only Cys195-Cys218 was found in the *Serratia* catalytic domain. In the *Vibrio* structure, the first intrachain disulfide bond joins between B2-1 and Á, while the second bond connects the loop of B6 and B6-1 together. These cystine bridges appear to restrict the flexibility of the connected strands. The amino acid residues that form three *cis* peptide bonds are located between Gly191-Phe192, Glu315-Phe316, and Trp570-Glu571 (as discussed in section 4.4).

Both enzymes have the small α+β insertion domain positioned between strands B7 and A7. The overall fold of this domain is very similar between the two enzymes. There are three conserved residues from this domain that participate in binding with substrate. Two of which (Tyr461 and Arg463 in *Vibrio* or Tyr444 and Arg446 in *Serratia*) are found in both enzymes, while only Trp497 is found in *Vibrio* chitinase A. Additional differences are; i) the α+β fold of *V. carchariae* chitinase A comprises five α-helices instead of two helices as found in *S. marcescens*. Arrow 3 (Figure 3.12A) indicates three extra connected helices found in *Vibrio* domain, while only one helix found in *Serratia* domain; and ii) the two short parallel stands are interrupted with an extra helix (as indicated by an arrow 4 in Figure 3.12A). This is only found in the *Vibrio* domain.

3.1.10 A comparison of wild-type and mutant structures

The overall structures of wild-type, E315M mutant and complexes of E315M mutant with NAG_5 and NAG_6 are identical (Figure 3.10A-D). Superimposition of wild-type with E315M-NAG_6 complex gave an R.M.S. of 0.655 Å (Figure 3.13A), while superimposition of the free E315M mutant and its complex with NAG_6 resulted a less R.M.S. value of 0.234 Å (not shown) and superimposition of E315M-NAG_5 and E315M-NAG_6 complexes gave the least R.M.S. value of 0.161 Å (see section 4.4.1). The higher R.M.S. value of wild-type structure aligned with the E315M structure than the value of E315M-NAG_5 aligned with E315M-NAG_6 could potentially reflect the structural movement upon substrate binding.

The structure of E315M-NAG_6 complex shows that NAG_6 units extend over the substrate binding cleft of the *Vibrio* chitinase (Figure 3.13A).
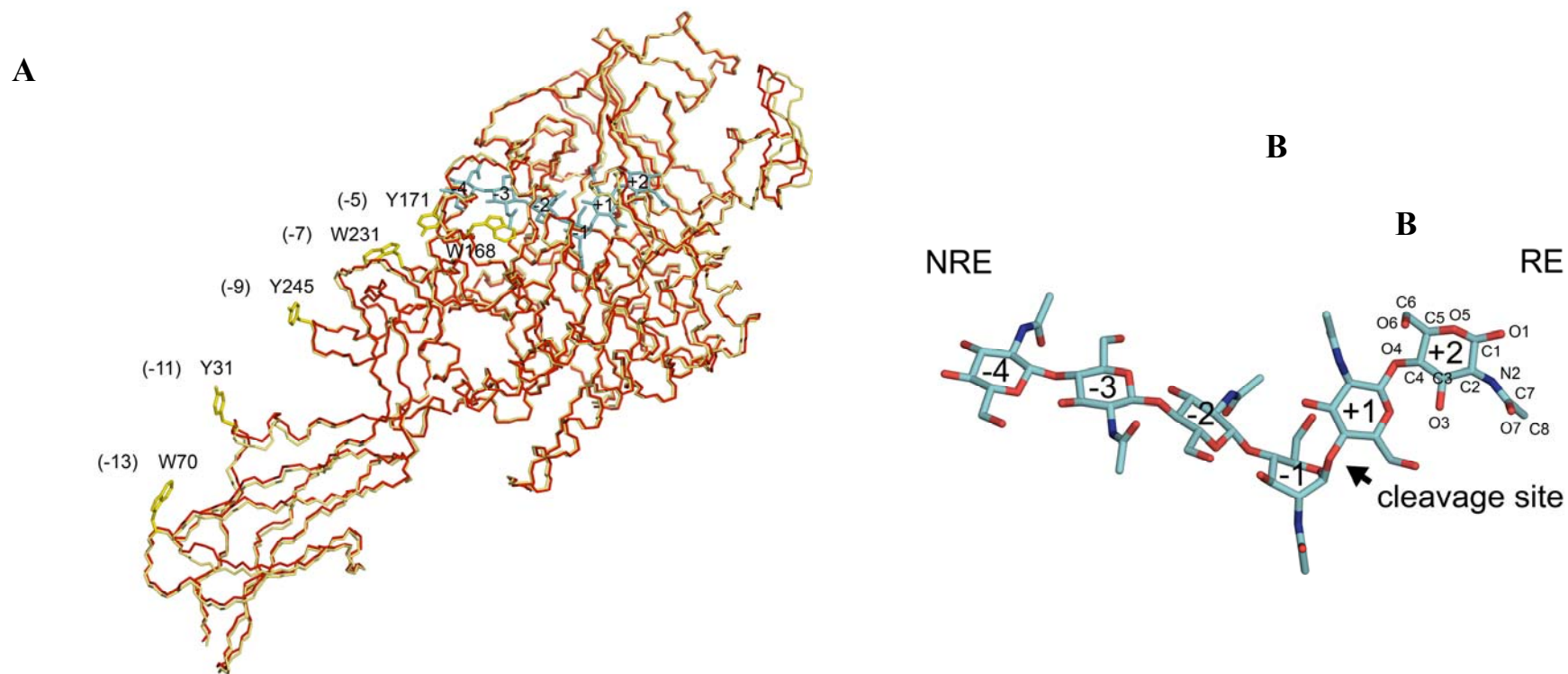
Figure 3.13 Structural superimposition of wild-type and E315M-NAG$_6$ complex.

(A) The backbone structure of *V. carchariae* chitinase A. Wild-type is depicted in red and E315M-NAG$_6$ complex in yellow. The six sugar units are shown as sticks in cyan. (B) The NAG$_6$ structure obtained from E315M-NAG$_6$ complex. Designation of carbon (cyan), oxygen (red) and nitrogen (blue) atoms are indicated at the reducing end sugar. NRE: the non-reducing end sugar; RE: the reducing end sugar.

Based on subsite nomenclature assigned by Davies and Henrissat (1995), the sugar unit located at the non-reducing end is assigned as subsite -4. The following subsites located towards the reducing end are assigned as subsites -3, -2, -1, +1 and +2, respectively (Figure 3.13B). Based on this subsite assignment, the scissile bond or the cleavage site is placed between -1 NAG and +1 NAG. The subsequent cleavage will mainly release the reducing end NAG_2 (+1 NAG and +2 NAG units) as the end products. This binding topology agrees well with the functional study as described previously that the *Vibrio* chitinase degrades chitin substrates, releasing $GlcNAc_2$ as the end product (Suginta *et al*., 2005).

As shown in Figure 3.13A, many conserved aromatic residues (W168, Y171, W231, Y245, Y31 and W70) are found to be surface exposed. The role of these residues will be discussed in section 4.4.

3.1.11 The structure of E315M mutant structure

The sequence alignment (see Figure 3.5) shows that Glu315 is completely aligned with the catalytic residue of *S. marcescens* chitinase A (Glu315). Mutation of Glu315 to Met and Gln led to a complete lack of chitinase activity towards chitin substrates, suggesting that Glu315 is essential in catalysis of *Vibrio* chitinase (Suginta *et al*., 2005). The structure of inactive mutant in the absence of substrate reveals that the C-terminal hexahistidine residues, which were genetically engineered to aid purification, were completely buried in the catalytic cleft of the enzyme (Figure 3.10B). The electron density map of the hexahistidine tag is clearly shown in Figure 3.14. These His_6 residues appear to mimic the structure of NAG_6 substrate and fully

occupied all the six binding subsites by interacting with all the residues which were later found to be important for binding to NAG_5 and NAG_6.
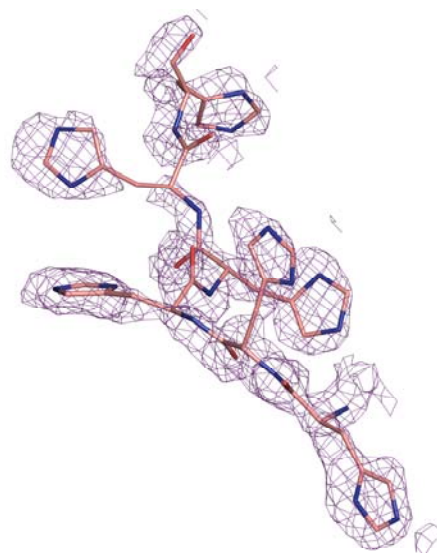
Figure 3.14 The electron density map of hexahistidine residues in the inactive E315M structure in the absence of substrate.

A $2F_o$-F_c map was calculated from the final refined model and contoured at 1.0 σ. The histidine residues are shown in stick models. Salmon for carbon; blue for nitrogen and red for oxygen atoms.

To prove that the C-terminal attached $(His)_6$ tag specifically occupied the active site of E315M, direct contacts between the His_6 residues and their interacting residues were calculated using program Contact in the CCP4 suite. The maximal contact distance between the six histidine residues and their interacting residues are given as ≤ 4Å (Table 3.9). This contact distance is in accordance with the distances formed by hydrogen bonds or hydrophobic interactions (Figure 3.15). The interaction of the His_6 residues and the binding residues are summarized in Table 3.10.

Table 3.9 Direct contacts between $(His)_6$ tag residues and the substrate binding residues of inactive E315M mutant.

His residue number and atoms [a]	Binding residues and atoms [a]	Distance (Å)	Hydrogen bond	Hydrophobic interaction
600	Y164	3.19	-	+
ND1 [a]	Y164 OH	3.56	+	-
	F192	3.27	-	+
	G274	3.29	-	+
	W275	3.72	-	+
O	W275 N	2.82	+	-
	D313	3.75	-	+
ND1 [a]	D313 OD2	3.15	+	-
	E315M	3.83	-	+
	A363	3.77	-	+
	M389	3.42	-	+
601	W168	3.31	-	+
	F192	3.57	-	+
	W275	3.49	-	+
	T276	3.57	-	+
	E498	3.50	-	+
NE2 [a]	E498 OE1	3.74	+	-
602	W168	3.30	-	+
	V205	3.76	-	+
603	R173	3.72	-	+
O	R173 NH2	2.80	+	-
	E498	3.54	-	+
ND1 [a]	E498 OE1	2.84	+	-
	V501	3.87	-	+

Table 3.9 (continued).

His residue number and atoms [a]	Binding residues and atoms [a]	Distance (Å)	Hydrogen bond	Hydrophobic interaction
604	V205	3.18	-	+
NE2 [a]	G207 N	3.78	+	-
	W497	3.58	-	+
N	W497 O	3.78	+	-
	E498	3.45	-	+
605	V496 O	3.84	+	-
NE2 [a]	W497	3.43	-	+
N	W497 O	3.44	+	-
	E498	3.83	-	+
	D499	3.19	-	+

[a] Atom designation of amino acid residues is defined in Appendix D.
Interactions involved at least one atom of each amino acid residue at a distance ≤ 4Å from an atom of the corresponding His residue.
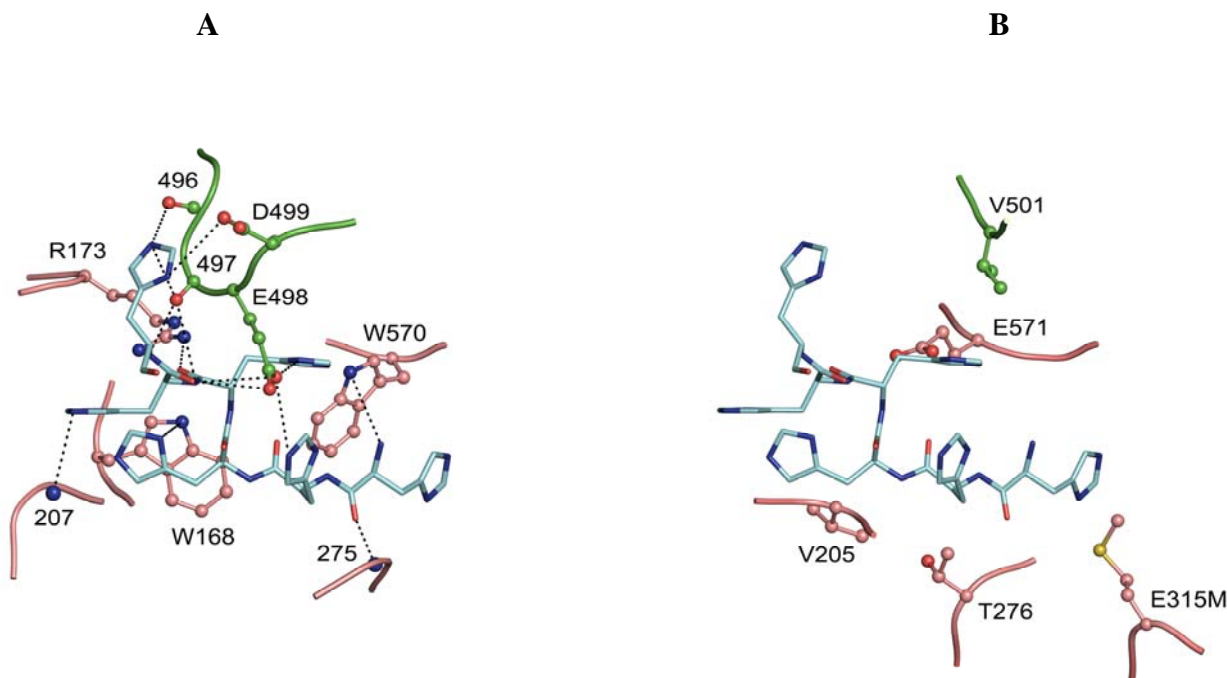
Figure 3.15 The interactions of the binding residues of E315M with hexahistidine tag in the active cleft.

(A) Hydrogen bonds and (B) hydrophobic interactions. The aromatic and hydrophilic residues that interact with the hexahistidine tag are shown as ball-and-stick models, the hexahistidine tag are in stick models. Hydrogen bond is shown in dash line (⋯). The binding residues are colored; salmon for carbon in the catalytic domain; green for carbon in the small insertion domain and orange yellow for sulfur. Six histidine residues are colored; cyan for carbon, blue for nitrogen and red for oxygen.

As will be shown later, the aromatic and charged residues (i.e. Y164, W168, R173, F192, V205, G274, W275, D313, E315M, A363, M389, Y391 and W570) that interacted with His_6 also involved in substrate binding in E315M-NAG_5 and E315M-NAG_6 complexes (see section 3.1.12 and 3.1.13). As summarized in Table 3.10, the histidine residue 600 particularly makes most contact with the active site residues and is completely buried within the $(\beta/\alpha)_8$-TIM barrel in the catalytic pocket as illustrated in Figure 3.16.

Table 3.10 A summary of the interactions between the C-terminal attached $(His)_6$ tag residues and the binding residues of inactive E315M mutant.

$(His)_6$ tag residues	Binding residues
600	Y164, F192, G274, W275, D313, E315M, A363, M389, Y391, W570
601	W168, F192, W275, T276, E498, W570
602	W168, V205
603	R173, E498, V501, E571
604	V205, W497, E498
605	V496, W497, E498, D499
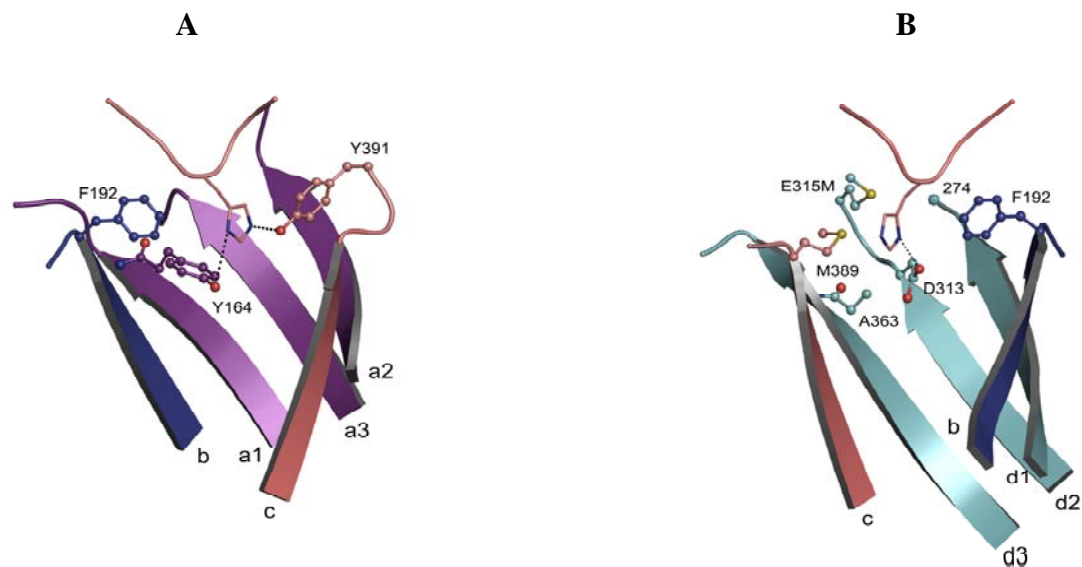
Figure 3.16 A close representation of the residue His600 in the TIM-barrel of the inactive E315M structure.

The interactions of binding residues with His600 are formed by hydrogen bonds and hydrophobic interactions. Hydrogen bond is shown in dash line (⋯⋯). The eight β-strands are defined; a1 (residues 160-165); a2 (residues 455-460); a3 (residues 566-571); b (residues186-192); c (residues 384-389); d1 (residues 267-273); d2 (residues 308-313) and d3 (residues 358-366). Carbon atoms of the labeled amino acids are colored; violet for strands a1, a2 and a3; blue for strand b; deep salmon for strand c; pale cyan for strands d1, d2 and d3. The binding residues are depicted as ball-and-stick models and orange yellow for sulfur. A stick model is shown for His600 residue. Blue for nitrogen and red for oxygen. (B) is a 180° rotation of (A).

3.1.12 The structure of E315M-NAG$_5$

The structure elucidation of inactive mutant E315M crystals soaked with NAG$_5$ and NAG$_6$ provides an insight into the important function of several conserved residues located at the active site. The overall structure of the E315M-NAG$_5$ complex was previously presented in Figure 3.10C. The electron density map of the refined structure of E315M-NAG$_5$ complex only reveals four sugar moieties instead of five moieties occupied subsites -2 to +2 as shown in Figure 3.17.
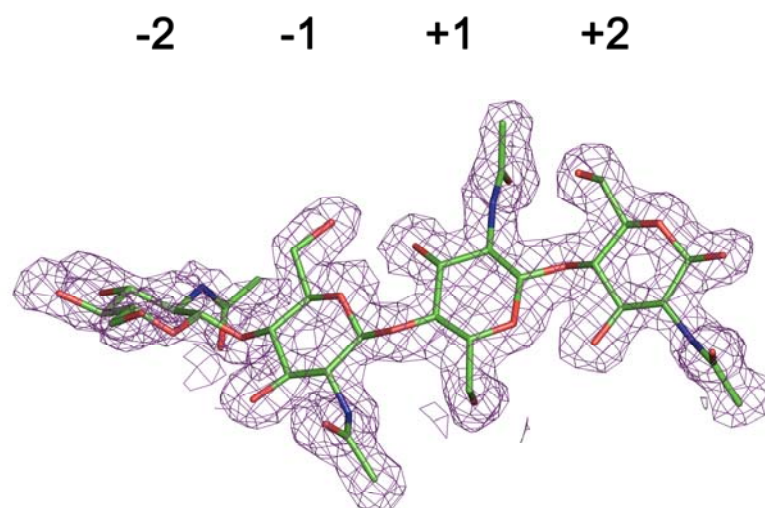
Figure 3.17 The electron density map of NAG$_5$ in the structure of E315M-NAG$_5$ complex.

A 2F$_o$-F$_c$ map was calculated from the final model and contoured at 1.0 σ. The sugar residues are shown in stick models. Green for carbon; blue for nitrogen and red for oxygen.

While the electron density map allowed the coordinates of the sugar moieties at subsites -2 to +2 to be located, the electron density corresponded to the -3 sugar

was clearly missing. This reflects low affinity of binding between the -3 sugar ring with the corresponding binding residues. As a result, the sugar moiety is allowed to be freely moved. The electron density map also suggests that the NAG moiety at subsite -2 is tilted and lies perpendicular from the plane of other NAG units. Under this situation, the -1 NAG still maintains 'chair configuration' instead of 'boat conformation' as observed in the structure of E315M-NAG$_6$. The structure of the E315M-NAG$_5$ complex provides important evidence how NAG$_5$ oriented in the catalytic cleft. An estimation of direct contacts between the interacting residues and their corresponding sugars exhibits that the interactions are mainly mediated by hydrophobic interactions between the aromatic or hydrophobic side chain residues and the cyclic faces of NAG units and by hydrogen bonds between charge residues that lie within the substrate binding residues and the ionizable groups of the sugar units (i.e. OH, CO and NH groups) as shown in Table 3.11. The maximal contact distance between NAG$_5$ and amino acid residues are estimated to be ≤ 4 Å. Figure 3.18 illustrates the interactions of the binding residues with the sugar units via hydrogen bonds and hydrophobic interactions.

Table 3.11 Direct contacts between the bound substrate NAG_5 and the substrate binding residues in the inactive E315M active site.

Sugar subsites and atoms [a]	Binding residues and atoms [b]	Distance (Å)	Hydrogen bond	Hydrophobic interaction
+2 NAG	W275	3.31	-	+
	K370	3.43	-	+
O7	K370 NZ	2.85	+	-
	D392	3.65	-	+
N2	D392 O	2.88	+	-
	W397	3.54	-	+
+1 NAG	W275	3.05	-	+
	E315M	3.77	-	+
	D392	3.23	-	+
O6	D392 OD2	2.61	+	-
-1 NAG	F192	3.53	-	+
	G274	3.74	-	+
O7	W275	3.39	-	+
	W275 N	2.85	+	-
O6	E498	3.38	-	+
	E498 OE1	2.87	+	-
-2 NAG	W168	3.61	-	+
	R173	3.19	-	+
O7	R173 NH2	2.25	+	-
	V205	3.18	-	+
	T276	3.52	-	+
O6	T276 OG1	2.53	-	+

[a] Nomenclature for sugar subsites is proposed in section 3.1.10 (Figure 3.13B).
[b] Atom designation of amino acid residues is defined in Appendix D.
Interactions involved at least one atom of each amino acid residue at a distance ≤ 4Å from an atom of the corresponding sugar ring.
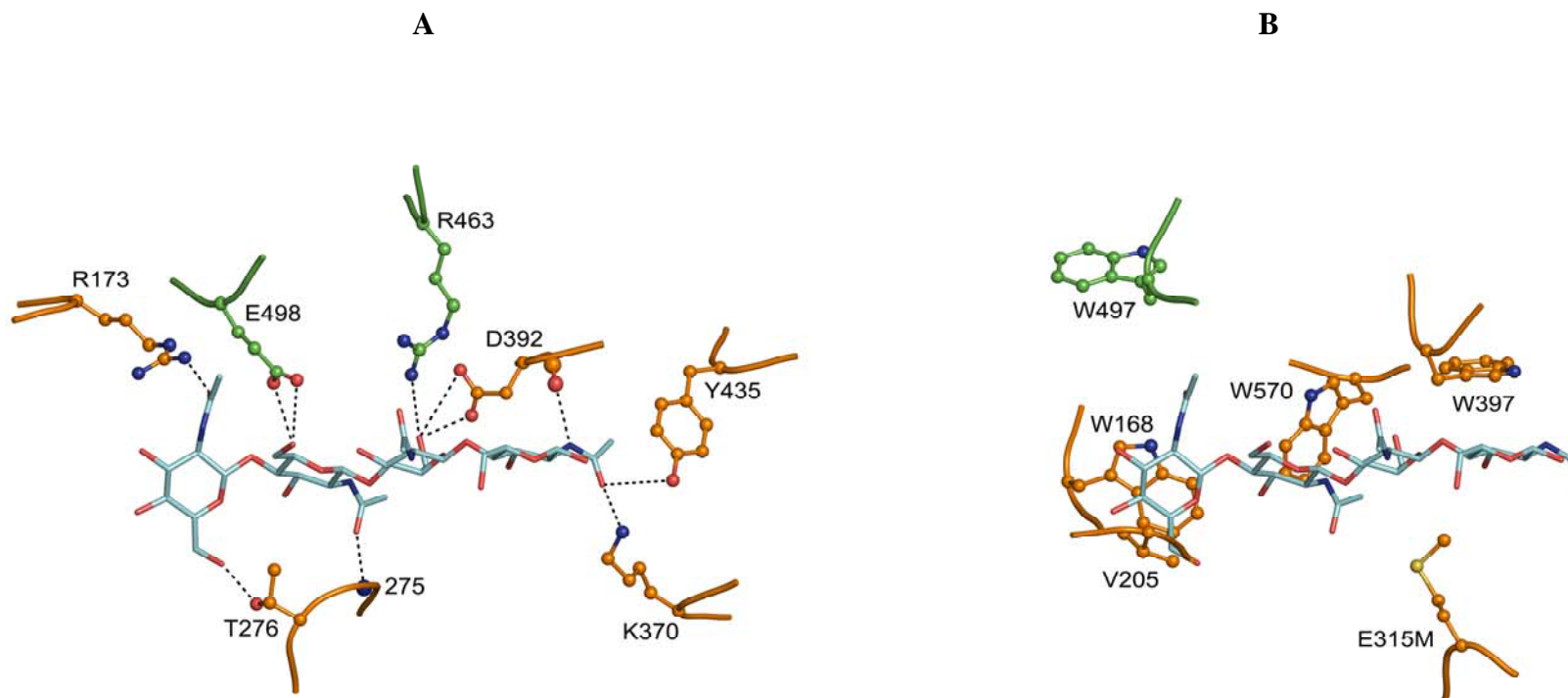
Figure 3.18 The interactions of the binding residues of E315M with NAG$_5$ in the active cleft.

(A) Hydrogen bonds and (B) hydrophobic interactions. The aromatic and hydrophilic residues that interact with NAG$_5$ are depicted as ball-and-stick models with four sugar residues in stick models. Hydrogen bond is shown in dash line (·····). The binding residues are colored; orange for carbon in the catalytic domain; green for carbon in the small insertion domain and orange yellow for sulfur. NAG$_5$ are colored; cyan for carbon; blue for nitrogen and red for oxygen.

Figure 3.18 shows that the interactions of the binding residues with each subsite occur via hydrogen bonds or hydrophobic interactions, in which five amino acid residues (W275, K370, D392, W397 and Y435) contribute to the binding of +2 NAG (see also Table 3.12). The +1 NAG bound to four amino acid residues, W275, E315M, D392 and R463, while the -1 NAG interacted with five amino acid residues including, F192, G274, W275, E498 and W570. There are six amino acid residues participating in substrate binding at subsite -2. These residues are W168, R173, V205, T276, W497 and E498.

Table 3.12 A summary of the interactions between NAG_5 and the binding residues in the inactive E315M active site.

Sugar subsites	Binding residues
+2	W275, K370, D392, W397, Y435
+1	W275, E315M, D392, R463
-1	F192, G274, W275, E498, W570
-2	W168, R173, V205, T276, W497, E498
-3	Non observable

3.1.13 The structure of E315M-NAG$_6$

The overall structure of the E315M-NAG$_6$ complex is shown in Figure 3.10D. Investigation of the electron density maps (Figure 3.19) clearly reveals a different conformation of the six sugar moieties that lied along the binding groove from the conformation of the sugar units in the structure of E315M-NAG$_5$.
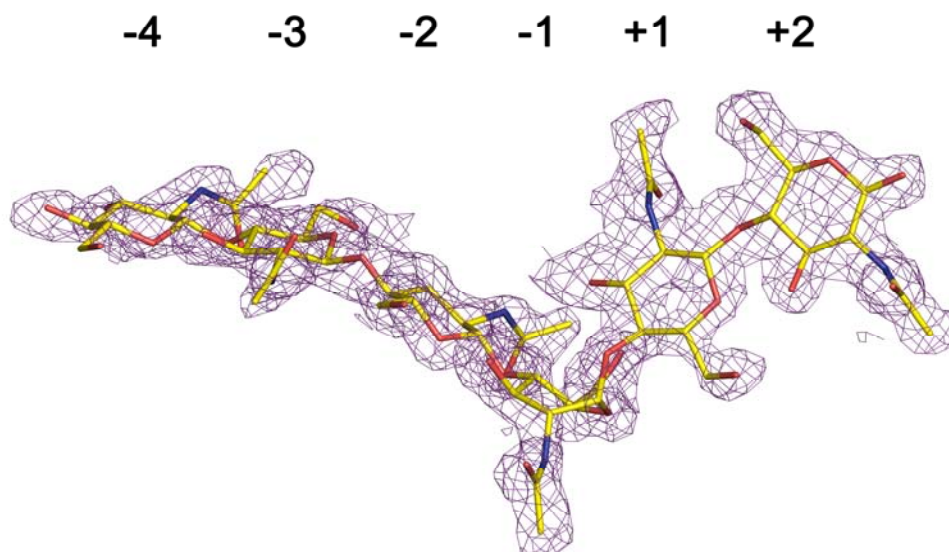
Figure 3.19 The electron density map of NAG$_6$ in the structure of E315M-NAG$_6$ complex.

A 2F$_o$-F$_c$ map was calculated from the final model and contoured at 1.0 σ. The sugar residues are shown in stick models. They are colored; yellow for carbon; blue for nitrogen and red for oxygen.

Unlike NAG$_5$ in the structure of E315M-NAG$_5$ complex, all six sugar rings of the E315M-NAG$_6$ structure fully occupied subsites -4 (at the non-reducing end) through subsite +2 (at the reducing end). However, the plane of the NAG units bound to subsites -4 to -1 lies perpendicular with the plane of the +1 and +2 sugars, indicating the geometric constraint of the scissile bond joining between -1 and +1 sugars. This observation is different from NAG$_5$ bound to E315M binding residues, by which a 'straight plane' of -1 NAG to +2 NAG and the tilt of -2 NAG is found in NAG$_5$ substrate instead (see Figure 3.17). The most striking finding is that the sugar unit in boat conformation at subsite -1 is sunk downward together with the twist of the scissile bond between subsites -1 and +1, yielding the 'bent conformation' of NAG$_6$.

On the other hand, the sugar units found for NAG_5 orientated in the binding site is in a 'straight chair conformation'. The observed conformation of NAG_6 is expected to be energetically favored for bond cleavage.

In addition, the electron density map of the +1 to -1 NAG units of NAG_6 displays somewhat ambiguity, by which the electron density map revealed patches of the extended map around +1 NAG. In contrast, the electron density of the -1 NAG residue was partially broken and incomplete. Together with findings that the -1 NAG and the predicted scissile bond were distorted, yielding the plane of the sugars at product sites (+1 and +2) to be perpendicular with the plane of the rest of the sugar oligomer. It has been assumed that the -1 sugar adopts a conformation change upon binding with the substrate to facilitate efficient cleavage of the scissile bond.

The complex of chitinase A E315M with NAG_6 provides detailed structural analysis of the enzyme-substrate interactions. Similar to observations made with the E315M-NAG_5 complex, direct contacts are mainly mediated via aromatic and charged residues as shown in Table 3.13. Figure 3.20 illustrates the interactions of these binding residues with the sugar residues via hydrogen bonds and hydrophobic interactions.

Table 3.13 Direct contacts between the bound substrate NAG$_6$ and the substrate binding residues in the inactive E315M active site.

Sugar subsites and atoms [a]	Binding residues and atoms [b]	Distance (Å)	Hydrogen bond	Hydrophobic interaction
+2 NAG	W275	3.63	-	+
	F316	3.98	-	+
	G367	3.86	-	+
	K370	3.43	-	+
O7	K370 NZ	2.82	+	-
	D392	3.33	-	+
N2	D392 O	3.09	+	-
	W397	3.71	-	+
+1 NAG	W275	3.58	-	+
	E315M	3.23	-	+
	F316	3.72	-	+
	M389	3.69	-	+
	D392	3.19	-	+
O5	D392 OD2	3.22	+	-
-1 NAG	Y164	3.21	-	+
	F192	3.67	-	+
O3	W275 N	3.05	+	-
	D313	3.42	-	+
O7	D313 OD2	3.49	+	-
	E315M	3.67	-	+
	A363	3.53	-	+
	M389	3.48	-	+
	Y391	3.58	-	+
	D392	3.57	-	+
O6	D392 OD2	2.88	+	-
	Y461	3.71	-	+

Table 3.13 (continued).

Sugar subsite and atoms [a]	Binding residues and atoms [b]	Distance (Å)	Hydrogen bond	Hydrophobic interaction
-2 NAG	F192	3.71	-	+
	W275	3.70	-	+
O6	W275 N	3.28	+	-
	T276	3.65	-	+
O6	T276 OG1	3.34	+	-
	W570	3.55	-	+
-3 NAG	W168	3.57	-	+
	R173	3.89	-	+
O6	R173 NH$_2$	2.91	+	-
	T276	3.60	-	+
O7	T276 OG1	2.74	+	-
-4 NAG	Y171	4.14	-	+
	R173	3.79	-	+
O6	R173 NH1	2.79	+	-

[a] Nomenclature for sugar subsites is proposed in section 3.10 (Figure 3.11B).
[b] Atom designation of amino acid residues is defined in Appendix D.
Interactions involved at least one atom of each amino acid residue at a distance ≤ 4Å from an atom of the corresponding sugar ring (with the exception for Y171 which is contacted with the distance of 4.14 Å).

Considering specific interactions among the E315M-NAG$_6$ complex, the binding of NAG$_6$ to the enzyme involves a number of aromatic residues that extend over the catalytic cleft. Figure 3.20 reveals that Y435 located at the end of the reducing end of the sugar forms hydrophobic interaction with +2 sugar and its -OH group also hydrogen-bonds with the oxygen atom of the acetamido group of +2 NAG, while W275 and F397 from opposite sides of the cleft stack against the hydrophobic faces of +1 NAG and +2 NAG. In addition, the nitrogen atom of W275 forms two critical hydrogen bonds with the O3 and O6 hydroxyl groups of the -1 NAG and -2 NAG. Subsite -3 contains W168 that stacks against the hydrophobic face of the corresponding sugar. The carbonyl oxygen in the main chain of W497 residue forms a hydrogen bond with subsite -3 for which its two aromatic rings making hydrophobic interaction with subsite -4 NAG. At the edge of subsite -4, Y171 is positioned to form hydrophobic interaction with -4 NAG.

Considering the most important subsite (-1 site), hydrophobic interactions are mediated by many residues, including Y164, F192, W275, E315M, A363, M389, Y391 and W570. Both D313 and D392 seem to play a binding role through hydrogen bonds, by which the carboxylic side chain of Asp313 makes a direct contact with the O7 of the acetamido group of the -1 NAG (Table 3.13), and the acidic side chains of D392 forms a hydrogen bond with O6 of the hydroxyl group of the -1 NAG. In addition, the carbonyl oxygen from the main chain of D392 also contacts via a hydrogen bond with N2 of the acetamido group of the +2 NAG, whereas its acidic side chains forms a hydrogen bond with the cyclic O5 of the +1 NAG. As also shown in Table 3.13, the mutated methionine (E315M) is found to strongly interact with both the +1 and -1 NAG in the structure of E315M-NAG$_6$. The sulfur atom of its side chain

forms hydrophobic interactions to +1 and -1 NAG with the contact distance of 3.23 Å and 3.67 Å, respectively. These interactions are probably responsible for forcing the substrate into the non-favored conformation. In the substrate-assisted mechanism, Glu315 residue acts as a proton donor, while the terminal oxygen (O7) of the acetamido group of the -1 NAG acts as a nucleophile. It may be hypothesized that the formation of a hydrogen bond between O7 of the acetamido and Asp313 stabilizes the transition state by maintaining the constraint 'boat conformation' of -1 NAG. Further discussion in the bending of the -1 NAG will be made in section 4.4.1.
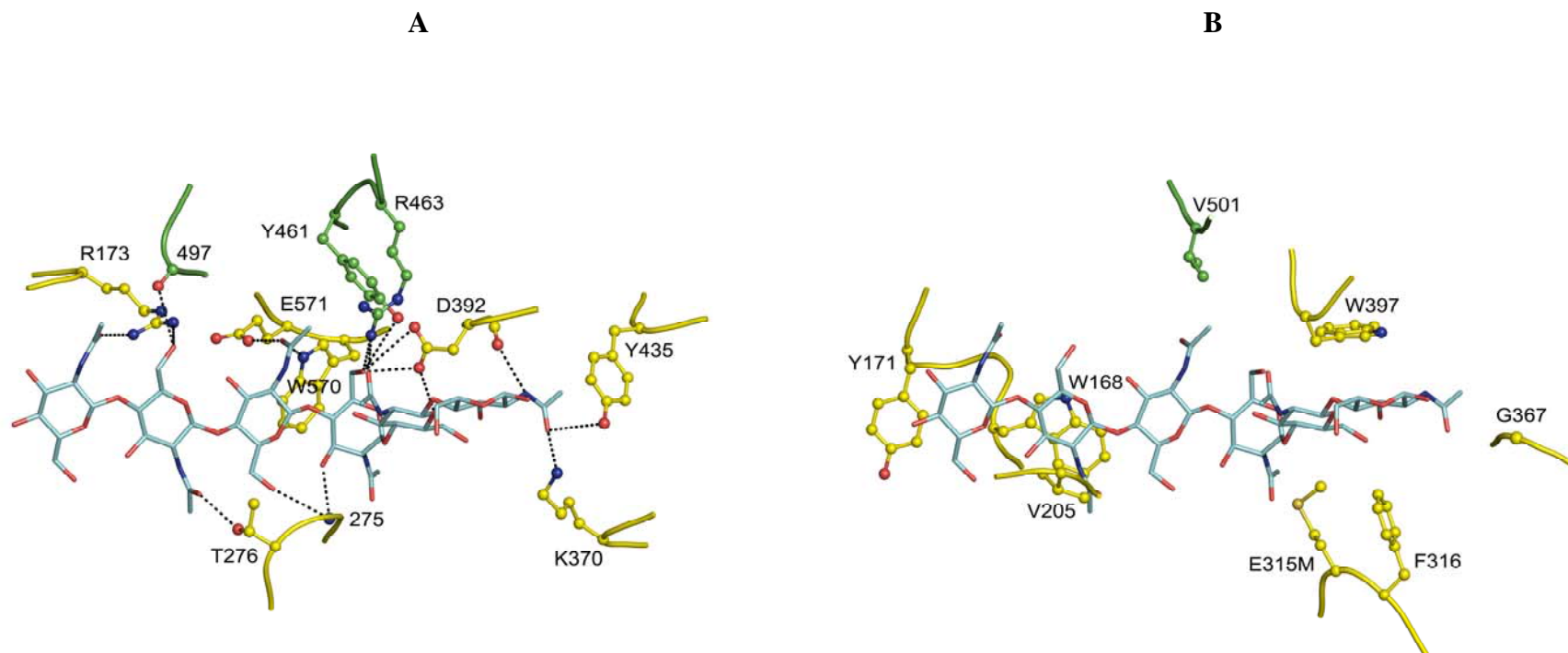
Figure 3.20 The interactions of the binding residues of E315M with NAG_6 in the active cleft.

(A) Hydrogen bonds and (B) hydrophobic interaction. The aromatic and hydrophilic residues that interact with NAG_6 are depicted as ball-and-stick models with six sugar residues in stick models. Hydrogen bond is shown in dash line (·····). The binding residues are colored; yellow for carbon in the catalytic domain; green for carbon in the small insertion domain and orange yellow for sulfur. NAG_6 are colored; cyan for carbon, blue for nitrogen and red for oxygen.

In summary, there are many conserved residues play interactions with NAG_6 units (Table 3.14).

Table 3.14 A summary of the interactions between NAG_6 and the binding residues in the inactive E315M active site.

Sugar subsites	Binding residues
+2	W275, F316, G367, K370, D392, W397, Y435
+1	W275, E315M, F316, M389, D392, R463
-1	Y164, F192, W275, D313, E315M, A363, M389, Y391, D392, Y461, R463, W570
-2	F192, W275, T276, W570, E571
-3	W168, R173, T276, W497
-4	Y171, R173, W497

There are six amino acid residues contributing to the binding of +2 NAG (the reducing end); W275, F316, G367, K370, D392, W397 and Y435 (Table 3.14). All of these residues except for G367 and F316 were found to interact with the +2 NAG in the E315M-NAG_5 complex (Table 3.12). These binding residues are found to bind to the same geometry of +2 NAG located in both E315M-NAG_5 and E315M-NAG_6 complexes (Figure 3.18 and Figure 3.20).

With regard to the +1 NAG, this sugar interacts with six amino acid residues including W275, E315M, F316, M389, D392 and R463. Most of the interacting residues also contribute to the binding of +1 NAG in E315M-NAG_5 complex, with the

exception of F316 and M389. This reflects minor differences between the binding preference of E315M bound to NAG_5 and to NAG_6.

The -1 NAG is found to interact with a large number of amino acid residues including Y164, F192, W275, D313, E315M, A363, M389, Y391, D392, Y461, R463 and W570 in E315M-NAG_6 complex, indicating the strong binding at this subsite. On the other hand, the -1 NAG in E315M-NAG_5 complex interacted with only five amino acid residues (F192, G274, W275, E498 and W570). A dramatic drop in a number of the interacting residues when comparing with E315M-NAG_6 complex probably reflects the unfavorable geometry of the -1 NAG in the E315M-NAG_5 complex.

There are five amino acid residues that participate in the binding at subsite -2. These residues included F192, W275, T276, W570 and E571 in E315M-NAG_6 complex. It is noticeable that most of these residues do not bind to -2 NAG in E315M-NAG_5 complex with the exception of T276. This clearly indicates that the binding of the sugar at subsite -2 take place in a different manner between NAG_5 and NAG_6.

The -3 NAG in E315M-NAG_6 complex are found to interact with four amino acid residues including W168, R173, T276 and W497. All these residues are found to bind with -2 NAG in E315M-NAG_5 complex, with other two additional interacting residues (V205 and E498). This implies the overlapping geometries between the -2 NAG in E315M-NAG_5 complex (Figure 3.17) and the -3 NAG in E315M-NAG_6 complex (Figure 3.19).

There are only three amino acid residues that contribute to the binding of -4 NAG (the non reducing end). These amino acids are Y171, R173 and W497. It is noticeable that a small number of the interactions at the -3 sugar (four binding

residues) and -4 sugar (three binding residues) accounts for weaker interactions towards the non-reducing end subsites. This feature is also seen in the structure of E315M-NAG$_5$ complex, particularly subsite -3 has so low affinity of binding towards the corresponding sugars that the electron density map was not seen. Therefore, the direct contact of both enzyme complexes reveals the tendency of stronger interactions from the reducing end (+2) to weaker interaction towards the non-reducing end (-4). A comparison between direct contacts from E315M-NAG$_6$ and E315M-NAG$_5$ complexes shows a higher number of the binding residues that simultaneously interact with the longer chain oligomers (NAG$_6$) than the shorter one (NAG$_5$). This observation agrees well with the previous finding that *V. carchariae* chitinase A has higher affinity toward longer substrates (Suginta *et al*., 2005).

3.2 Functional characterization

3.2.1 Optimization of TLC conditions for determination of the hydrolytic activity of chitinase A

Previous reports employed TLC to analyze the hydrolytic products obtained as a result of family 18 chitinase action (Park *et al*., 2000; Tanaka *et al*., 1999; 2001; Thamthiankul *et al*., 2001). TLC technique can be used to separate mixtures of different sugar components contained in the hydrolytic products. The rate of migration of the components depends on the partition between polar matrices and the mobile phase, and allows individual chitooligosaccharide to be identified. In this study, the composition of mobile phase and the separation condition was used following the modified method of Tanaka (Tanaka *et al*., 1999). For preliminary studies, a standard mixture containing 5 nmol of G1-G6 was applied on a silica TLC

plate (4.0 × 7.0 cm), then chromatographed three times in a mobile phase containing n-butanol: methanol: 25% ammonia solution: H_2O (v/v) in various solvent compositions (10:8:4:2, 10:8:4:3 and 10:8:4:4). Various heights of TLC (7 cm and 10 cm) and different rounds of chromatography were also tried to maximize the resolution of the separated sugars. Of all the trial conditions (see Methods 2.7.2), the G1-G6 mixture was best resolved when the reaction mixture was applied on a silica TLC plate of 4.0 × 10.0 cm, and chromatographed three times using a mobile phase containing 28% ammonia (Figure 3.21).
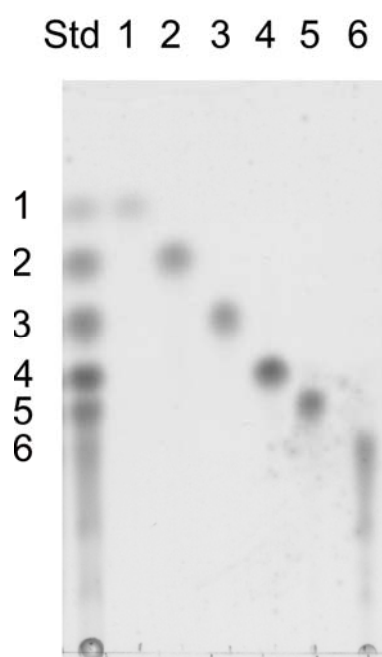
Figure 3.21 A TLC chromatogram of a standard G1-G6.

A sample mixture (5 μl) was applied on a silica TLC plate (4.0 × 10.0 cm), and chromatographed three times (1 h each) using the mobile phase containing n-butanol: methanol: 28% ammonia solution: H_2O (10:8:4:2) (v/v). Sugar signals were detected with aniline-diphenylamine reagent by baking at $120^{\circ}C$ for 5 min. Lanes: Std, a standard mixture of G1-G6 (5 nmol each); 1-6, standard G1-G6.

3.2.2 Optimization of HPLC conditions for determination of the hydrolytic activity of chitinase A

Identification of the various reaction products released by the chitinase variants were assessed by quantitative HPLC technique. Previous research reported the determination of degradation products of chitinases as a function of time using various types of HPLC systems i.e. gel filtration on a TSK-GEL G2000PW column (Fukamizo *et al*., 2001), an Ultron-NH$_2$ column (Watanabe *et al*., 2003), a TSKgel Amide-80 column (Tanaka *et al*., 2001), and a Toso-Haas Amide-80 column (Aronson *et al*., 2003). In addition, the anomeric configuration of the hydrolytic products were also investigated using a reversed C18 Nucleosil column (Armand *et al*., 1994; Terwisscha van Scheltinga *et al*., 1995), a TSKgel Amide-80 amino column (Fukamizo *et al*., 2001), or a Hypercarb hydrophobic column (Suginta *et al*., 2005).

In this study, a separation of the standard G1-G6 was initially tested with CARBOSep CHO-411 HPLC column with various mobile phases. However, the separation efficiency obtained from this size exclusion column found to be relatively poor (data not shown). Therefore, a different HPLC condition was tried using a Zorbax Carbohydrate Analysis column. The column was operated with an isocratic elution using varied ratios of acetonitrile: H$_2$O (75:25 (v/v), 70:30 (v/v), 65:35 (v/v) and 60:40 (v/v)) at a constant flow rate of 1.0 ml/min and room temperature. Sugar signals were detected at various wavelengths including 205, 210, 215, 220 and 260 nm, with the best signals being seen at 205 nm (data not shown). The effects of mobile phase compositions on retention times of standard sugars were also studied. Peak identification of each oligosaccharide was carried out by spiking with the corresponding *N*-acetyl-chitooligosaccharide standard. The results showed that the

ratio of 75:25 (v/v) of ACN to H_2O gave the separation time longer than 80 min to complete the elution of all the sugars, whereas lower ratios of ACN to H_2O, 70:30, 65:35 and 60:40 (v/v) eluted the last sugar peak within 35.44 min, 16.27 min and 9.06 min, respectively. The separation basis of a Zorbax Carbohydrate Analysis column, depends on the ability of the separated molecules to be partitioned on the stationary phase, allowing the smaller sugar to be eluted earlier. The results showed that the higher ratios of ACN to H_2O (75:25 and 70:30 (v/v)) resulted in good resolution but broad peaks. On the other hand, the overlapping peaks occurred when a ratio of ACN: H_2O was 60:40 (v/v) was used. Under all the conditions tested, the ratio of 65:35 ACN to H_2O provided the best resolution. Therefore, this condition was further optimized by investigating the effect of column-operating temperatures on peak separation. The results displayed the best quality of the peak with good separation when the HPLC was operated at $40^{o}C$, comparing to $30^{o}C$ and $35^{o}C$ (data not shown). The separation of standard G1-G6 mixture obtained under the optimized HPLC conditions was shown in Figure 3.22.
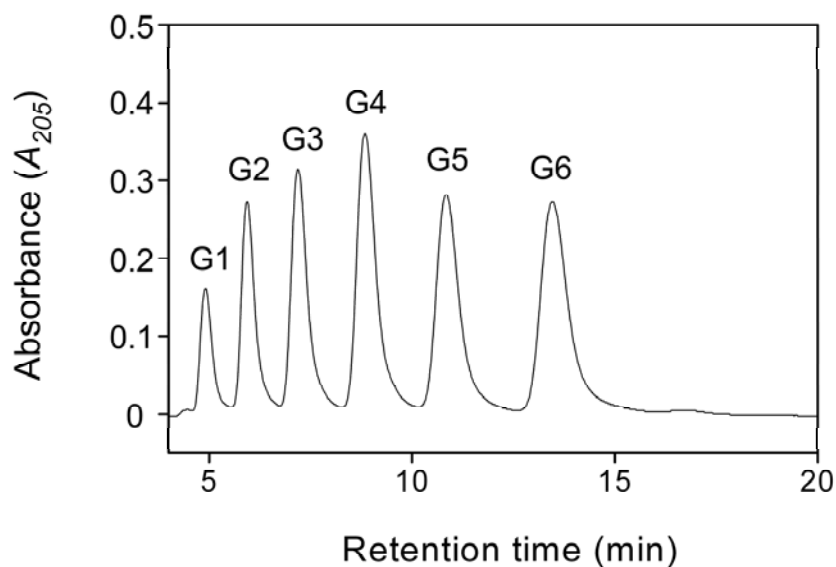
Figure 3.22 An HPLC chromatogram of a standard mixture G1-G6 (20 nmol) using a Zorbax Carbohydrate Analysis column.

Mobile phase composition was acetonitrile: H_2O 65:35 (v/v). An applied flow rate was 1.0 ml/min at temperature 40°C with 205 nm UV detection.

3.2.3 Time course of chitooligosaccharide hydrolysis of wild-type chitinase A

3.2.3.1 TLC analysis of the hydrolytic products of wild-type chitinase A

The hydrolytic activity of chitinase A towards short chitooligosaccharides (G2 to G6) and colloidal chitin was examined at various time points using TLC (Figure 3.23), while quantification of the reaction products was simultaneously investigated by means of calibrated HPLC.
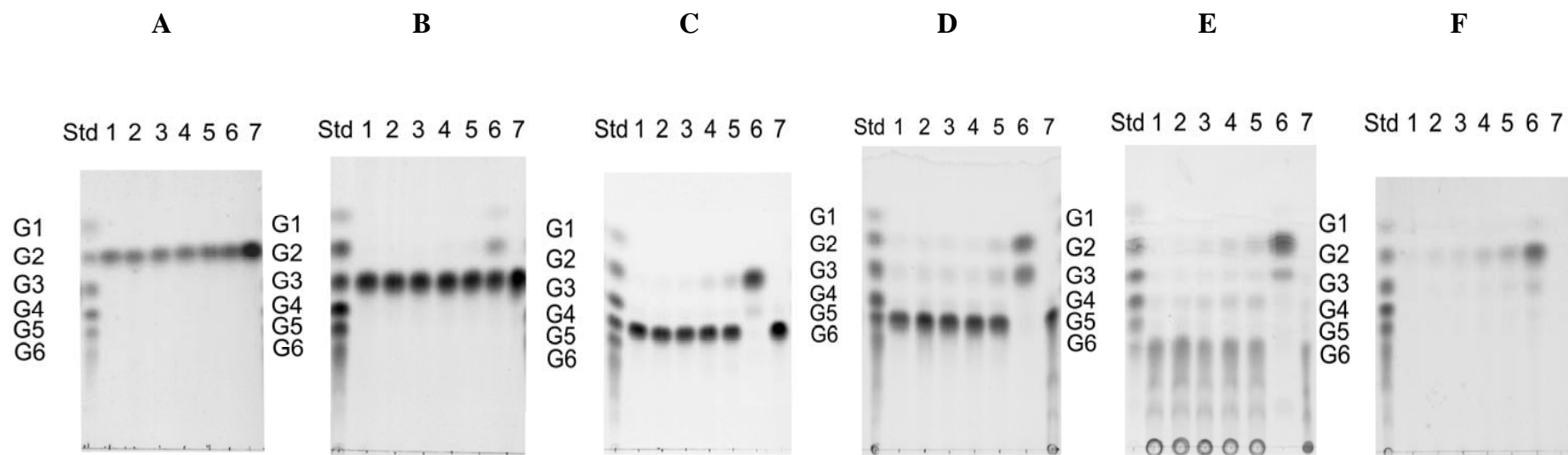
Figure 3.23 Time course of G2-G6 hydrolysis by wild-type chitinase A as analyzed by TLC.

The reaction mixture (80 µL), containing 800 ng chitinase and 2.5 mM substrate (G2-G6) in 100 mM sodium acetate buffer pH 5.0, was incubated at various times at 30^0C (A-E). The reaction mixtures (120 µL), containing 4 µg chitinase and 20 mg colloidal chitin in 100 mM sodium acetate buffer pH 5.0, was incubated at various times at 30^0C (F). After boiling, the reaction solution (5 µl) was analyzed on TLC and sugar products detected with aniline-diphenylamine reagent. (A) G2 hydrolysis; (B) G3 hydrolysis; (C) G4 hydrolysis; (D) G5 hydrolysis; (E) G6 hydrolysis and (F) Colloidal chitin hydrolysis. Lanes: Std, a standard mixture of G1-G6; 1-6, the reaction products at 2, 5, 10, 30, 60 min and 18 h, respectively; 7, substrate blank.

When chitinase A was incubated with G2, the TLC results showed no detectable products observed even after 18 h of incubation (Figure 3.23A). The obtained result suggested G2 does not at all act as the substrate of this enzyme. With G3 substrate, only pale spots of G1 and G2 were detected only 18 h of incubation, indicating that G3 was poorly hydrolyzed by the enzyme (Figure 3.23B). With G4 substrate (Figure 3.23C), the enzyme mainly recognized the middle glycosidic bond of the tetrameric chain, releasing G2 as the major product. As expected, the enzyme degraded G5, releasing G2 and G3 end products (Figure 3.23D). On the other hand, the hydrolysis of G6 initially yielded G2, G3 and G4 (Figure 3.23E). At the end of the reaction, G3 and G4 were further hydrolyzed to G1 and G2 with G2 being produced as the major products. The hydrolytic activity of chitinase A against colloidal chitin was also studied at various incubation times (Figure 3.23F). The TLC result showed that the dimer (G2) was significantly formed only after 2 min of the incubation time. Other reaction intermediates (G1, G3 and G4) were observed only when the reaction was proceeded up to 18 h. Again at the end of the reaction, G2 was observed as the major product.

To quantify how much these transient products were generated from the degradation reactions of G3-G6, the remaining reaction mixtures from TLC were subjected to HPLC analysis as shown in Figures 3.24-3.27.

3.2.3.2 HPLC analysis of G3 hydrolysis by wild-type chitinase A.

The reaction products of G3 hydrolysis by wild-type chitinase A were resolved by HPLC under the conditions described in section 3.2.2 (Figure 3.24).

A

B

Figure 3.24 HPLC analysis of G3 hydrolysis by wild-type chitinase A at various times.

The reaction mixture (80 µL), containing 800 ng chitinase and 2.5 mM G3 in 100 mM sodium acetate buffer pH 5.0, was incubated at various times (2, 5, 10, 30, 60 min and 18 h) at 30°C. After boiling, the reaction mixture (20 µl) was resolved on HPLC using a Zorbax Carbohydrate Analysis column and sugar peaks detected by UV absorption at A_{205} nm. (A) HPLC chromatogram of G3 hydrolysis (B) Quantification of G3 hydrolysis by wild-type chitinase A at various times. SB, substrate blank.

The G1 and G2 products were converted to nmol quantity by estimating their peak area, using a standard curve of each corresponding sugar. A plot of mole quantity of the reaction products and G3 substrate versus reaction times is shown in Figure 3.24B.

Figure 3.24 shows that G2 products (1.29 nmol) was detected within the first 10 min, while no G1 was detectable at very early stage of reaction. Even as longer time of incubation as 18 h, G3 could only be partially hydrolyzed, giving 16.04 nmol of G1 and 22.08 nmol of G2. These amounts of G1 and G2 products were calculated to be only ~10% and ~13% of the starting substrate. Once again, the HPLC result confirmed that G3 is a poor substrate for *Vibrio* chitinase A.

3.2.3.3 HPLC analysis of G4 hydrolysis by wild-type chitinase A.

The hydrolysis of G4 substrate as a function of time is shown in Figure 3.25. It can be seen that the enzyme recognized the middle bond of G4 so that G2 was mainly formed. An increased signal of G2 (6.02 min) was already seen even at the 2 min of incubation (Figure 3.25A). On the other hand, G3 (7.58 min) was measured only in trace amount upon incubation upto 18 h. G3 intermediate was further degraded to G2 and G1 (5.08 min) towards the completion of the hydrolysis. Quantitative analysis of the hydrolytic products (Figure 3.25B) indicated that 4.9 nmol of G1 was produced, which was only 2% of G2 after the end of the reaction, while 265.94 nmol and 34.09 nmol of G2 and G3 were calculated from 142.69 nmol of the starting material (G4).

A

B
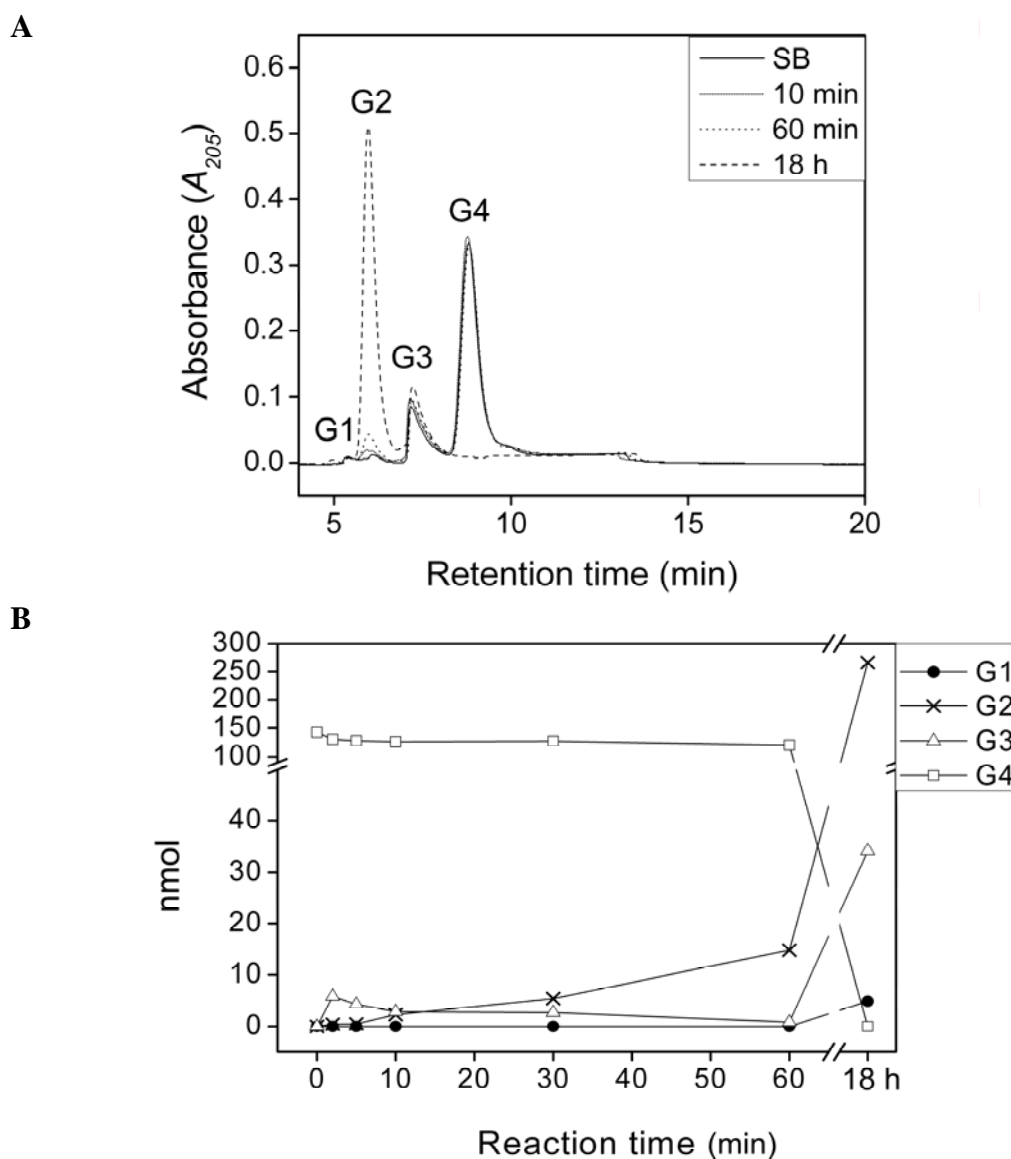
Figure 3.25 HPLC analysis of G4 hydrolysis by wild-type chitinase A at various times.

The reaction mixture (80 µL), containing 800 ng chitinase and 2.5 mM G4 in 100 mM sodium acetate buffer pH 5.0, was incubated at various times (2, 5, 10, 30, 60 min and 18 h) at 30°C. After boiling, the reaction mixture (20 µl) was resolved on HPLC using a Zorbax Carbohydrate Analysis column and the sugar peaks detected by UV absorption at A_{205} nm. (A) HPLC chromatogram of G4 hydrolysis (B) Quantification of G4 hydrolysis at various times. SB, substrate blank.

3.2.3.4 HPLC analysis of G5 hydrolysis by wild-type chitinase A

The hydrolysis of G5 is shown in Figure 3.26. Two major peaks corresponded to the retention times of G2 (6.02 min) and G3 (7.58 min) were observed upon the incubation time of 18 h (Figure 3.26A). Figure 3.26B shows that both G2 and G3 were formed in relatively equal amounts since 2 min of reaction. The amounts of both products were steadily increased at longer times of incubation. At the end of the reaction, 160.24 nmol and 91.28 nmol of G2 and G3 were detected. Again, only very small amount of G1 (9.21 nmol) was observed even as long as 18 h of incubation. The yield of G1 was only ~6% of the dimer. This is because G1 could be only produced from the subsequent degradation of G3 intermediate.

A

B
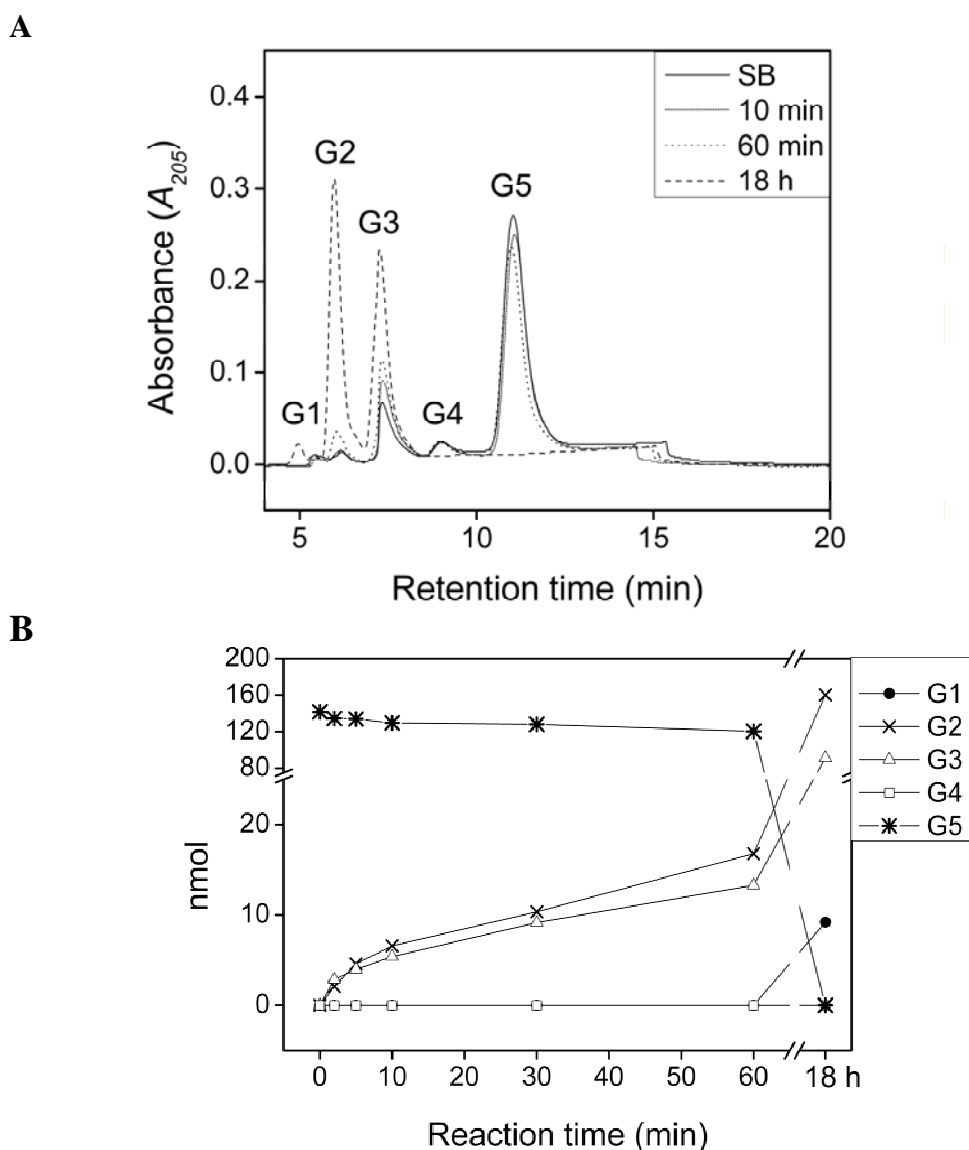
Figure 3.26 HPLC analysis of G5 hydrolysis by wild-type chitinase A at various times.

The reaction mixture (80 µL), containing 800 ng chitinase and 2.5 mM G5 in 100 mM sodium acetate buffer pH 5.0, was incubated at various times (2, 5, 10, 30, 60 min and 18 h) at 30°C. After boiling, the reaction mixture (20 µl) was resolved on HPLC using a Zorbax Carbohydrate Analysis column and the sugar peaks detected by UV absorption at A_{205} nm. (A) HPLC chromatogram of G5 hydrolysis (B) Quantification of G5 hydrolysis at various times. SB, substrate blank.

3.2.3.5 HPLC analysis of G6 hydrolysis by wild-type chitinase A.

Figure 3.27A shows an HPLC elution profile of the reaction products at various incubation times. The retention times of 5.08, 6.02, 7.58, 9.40, 11.60 and 14.50 min corresponded to G1, G2, G3, G4, G5 and G6, respectively.

For G6 hydrolysis, G2 and G4 were produced as the primary products. The production of G2 major product most likely occurred directly from the degradation of G6. The cleavage of G4 intermediate to G2 seemed to take place to a lessen extent as judged from the relative amount of G4 being released at early time of reaction. On the other hand, the production of G3 proceeded by a single step action of the enzyme indicated the enzyme also recognized the middle bond of G6. At 10 min of reaction, the rate of G3 formation detected was approx one-fifth slower than that of G2 formation. This exhibits the preference of the enzyme towards the second bond of the sugar chain. At 1 h of reaction time, the yields of the trimer was 3.16 nmol, the tetramer was 12.05 nmol and the dimer was 29.72 nmol. The amounts of the trimer and the tetramer were calculated to be 10% and 40% of the yield of dimer. In addition, the G3 intermediate was also further hydrolyzed, giving G1 (5.65 nmol) as the end product with 2% of that of dimer.

A

B
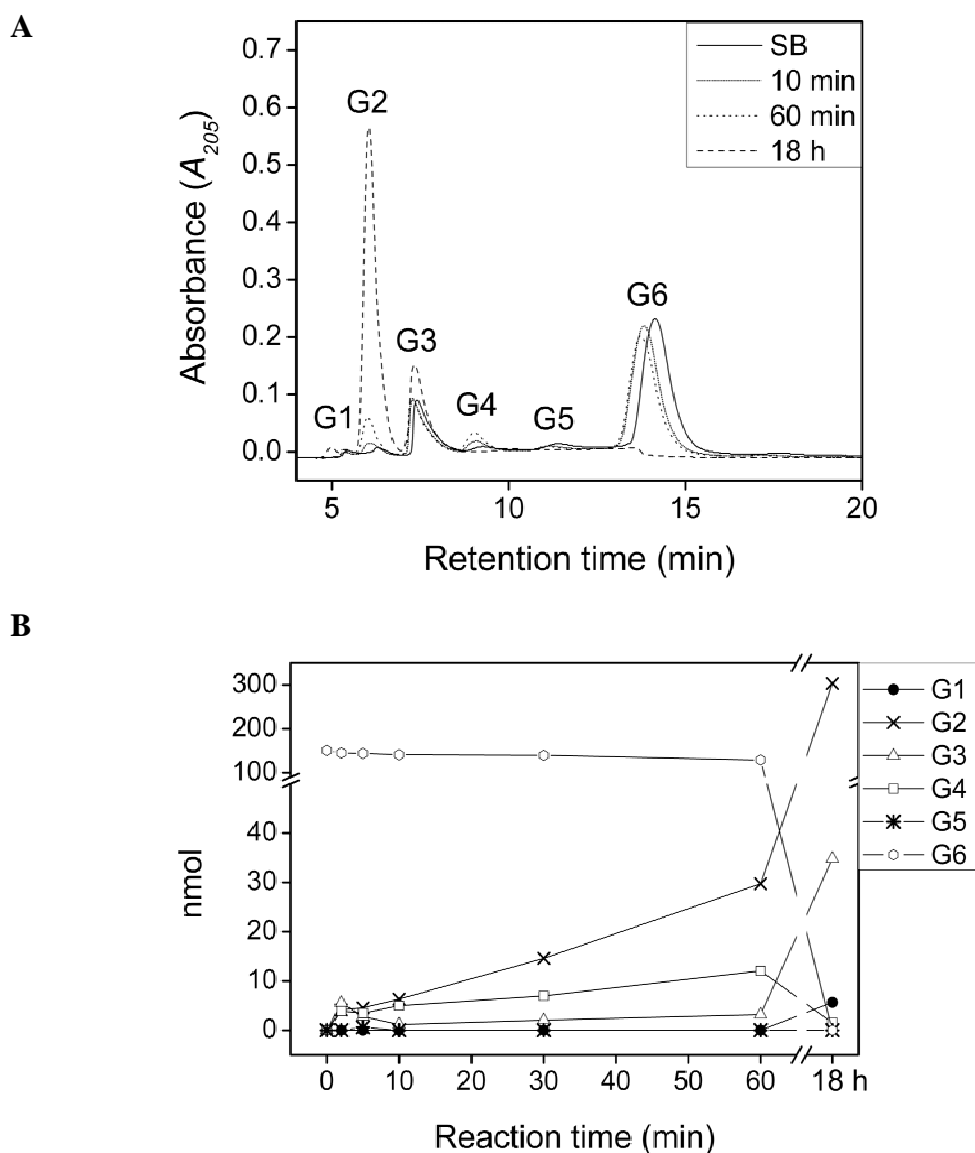
Figure 3.27 HPLC analysis of G6 hydrolysis by wild-type chitinase A at various times.

The reaction mixture (80 µL), containing 800 ng chitinase and 2.5 mM substrate of G6 in 100 mM sodium acetate buffer pH 5.0, was incubated at various times (2, 5, 10, 30, 60 min and 18 h) at 30°C. After boiling, the reaction solution (20 µl) was resolved on HPLC using a Zorbax Carbohydrate Analysis column and the sugar peaks detected by UV absorption at A_{205} nm. (A) HPLC chromatogram of G6 hydrolysis. (B) Quantification of G6 hydrolysis at various times. SB, substrate blank.

3.2.3.6 HPLC analysis of chitin hydrolysis by wild-type chitinase A.

Hydrolytic patterns of colloidal chitin by chitinase A were also analyzed by quantitative HPLC. Figure 3.28A shows an HPLC chromatogram of chitooligosaccharide products at various incubation times. Quantitation of the hydrolytic products obtained from colloidal chitin hydrolysis is shown in Figure 3.28B.

When colloidal chitin was the substrate, only chitooligosaccharides, G1, G2 and G3 were observed with G2 being predominantly formed. Like other substrates, G3 intermediate was gradually released in the course of the reaction and simultaneously hydrolyzed, giving G1 end product. For quantitative analysis (Figure 3.28B), G2 formation was 207.23 nmol, while G1 and G3 formation were 12.08 nmol and 43.49 nmol.
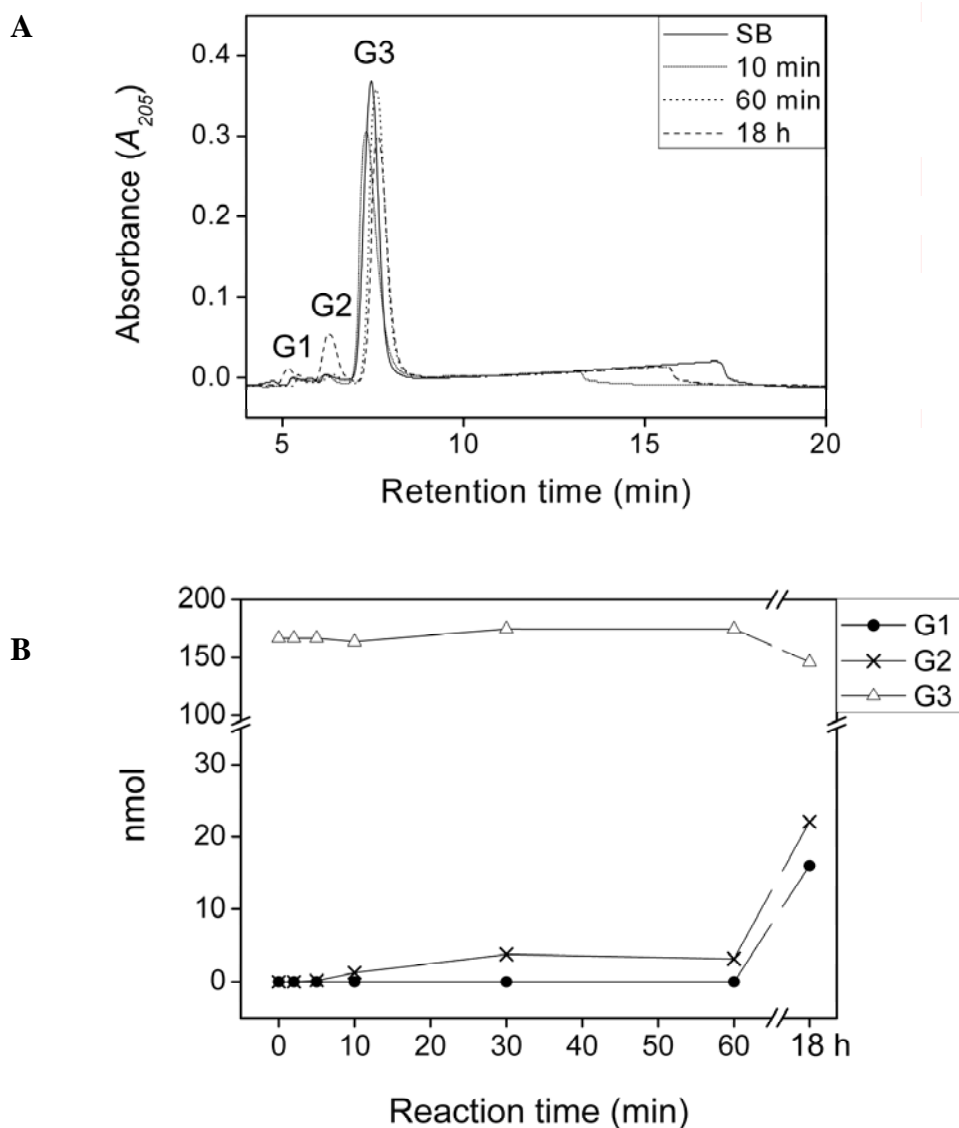
A

B
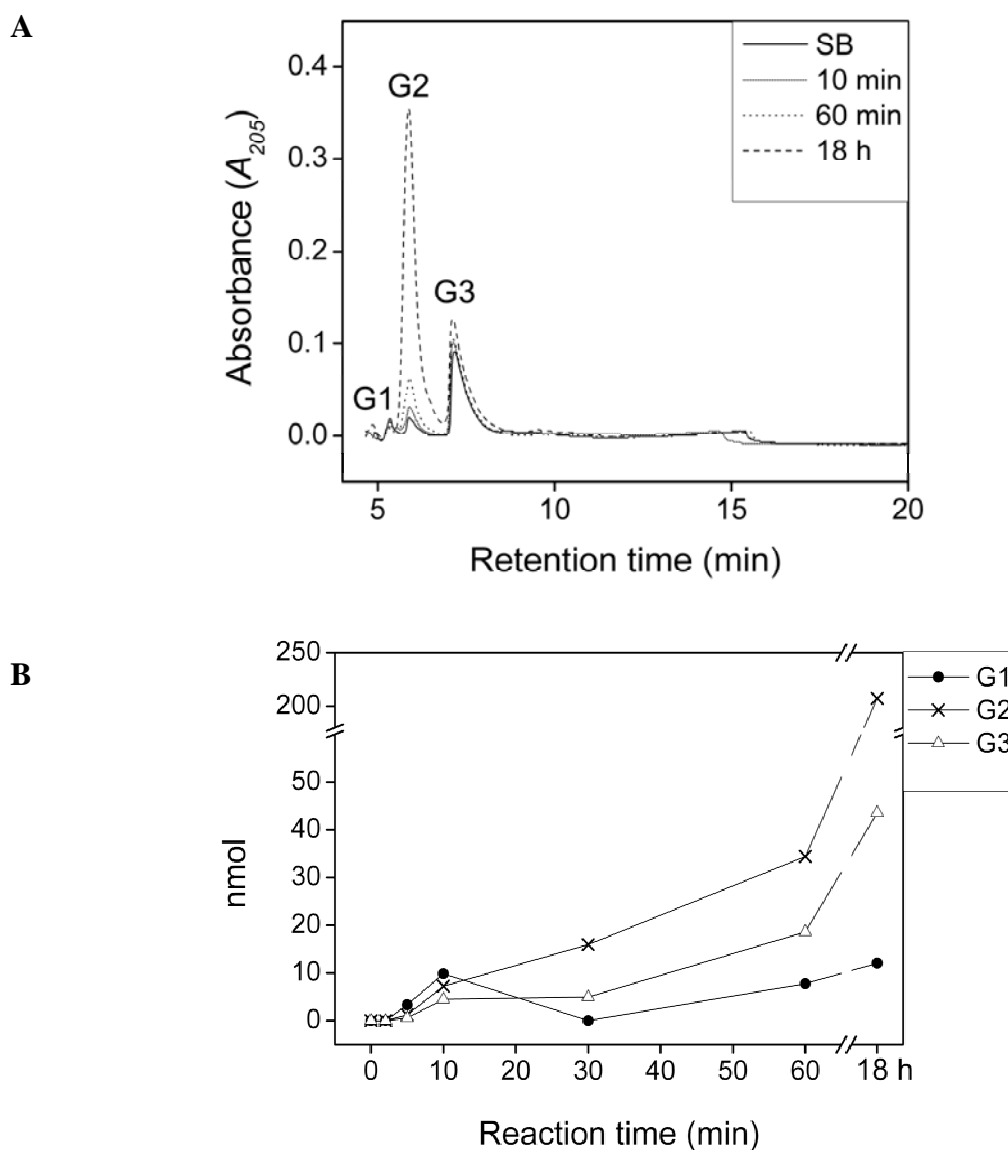
Figure 3.28 HPLC analysis of chitin hydrolysis by wild-type chitinase A at various times.

The reaction mixture (120 µL), containing 4 µg chitinase and 20 mg colloidal chitin in 100 mM sodium acetate buffer pH 5.0, was incubated at various times (2, 5, 10, 30, 60 min and 18 h) at 30°C. After boiling, the reaction solution (20 µl) was resolved on HPLC using a Zorbax Carbohydrate Analysis column and the sugar peaks detected by UV absorption at A_{205} nm. (A) HPLC chromatogram of colloidal chitin hydrolysis. (B) Quantification of colloidal chitin hydrolysis at various times. SB, substrate blank.

3.2.4 TLC and HPLC analyses of the hydrolytic products of chitinase A mutants

3.2.4.1 Screening the hydrolytic activity of chitinase A mutants

The hydrolytic activity of all chitinase A variants were initially tested with colloidal chitin by adjusting concentrations of the enzymes to yield detectable activity. The products of chitin hydrolysis generated by chitinase wild-type and mutants were analyzed at overnight reaction using TLC as shown in Figure 3.29.

From Figure 3.29A, all the E315 mutants did not hydrolyze colloidal chitin at all even with the enzyme was as high as 80 µg. Only D392N mutant was able to hydrolyze chitin with lessen activity than the wild-type activity. On the other hand, the aromatic mutants (W168G, Y171G, W275G and W397F) still remained hydrolytic activity with various degrees, while W275G and W397F retained most significant activity (Figure 3.29B). Mutant W570G displayed most severe effect by abolishing the hydrolyzing activity against colloidal chitin. No activity was detected with triple and quadruple mutants, giving an indication of an accumulative effect of multiple point mutations on the hydrolyzing activity of *Vibrio* chitinase A.

A **B**

Std 1 2 3 4 5 6 7 8 9   Std 1 2 3 4 5 6 7 8 9 10

G1
G2
G3
G4
G5
G6
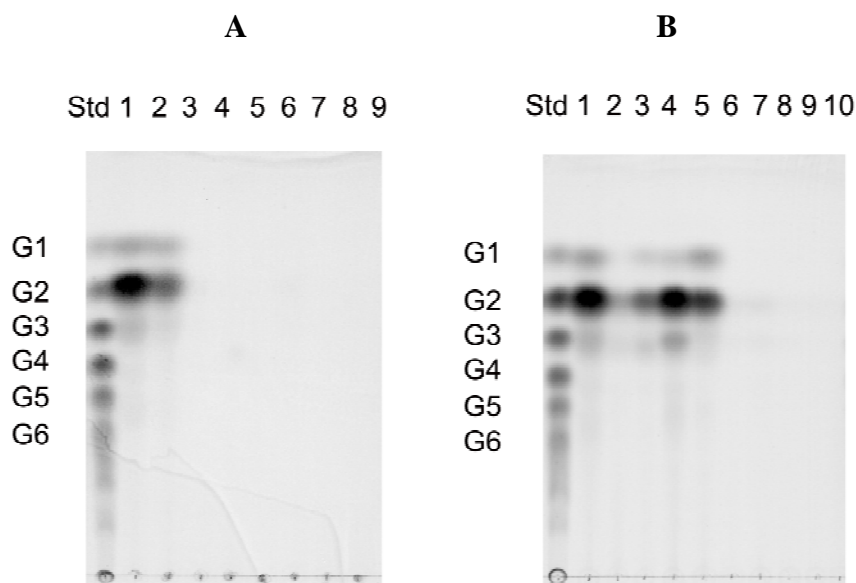
Figure 3.29 TLC analysis of chitin hydrolysis by chitinase A and its mutants.

The reaction mixture (150 µL), containing chitinase A (80 µg) and colloidal chitin (20 mg) in 100 mM sodium acetate buffer pH 5.0, was incubated for 18 h at 30°C. After boiling, the reaction solution (5 µl) was analyzed on TLC and sugar products detected with aniline-diphenylamine reagent. (A) Hydrolysis by wild-type chitinase A, Asp392 and Glu315 mutants. Lanes: Std, a standard mixture of G1-G6; 1, wild-type; 2, D392N; 3, D392K; 4, E315Q; 5, E315M; 6, D392NE315Q; 7, D392NE315M; 8; D392KE315M and 9, substrate blank. (B) Hydrolysis by wild-type chitinase A and aromatic-residue mutants. Lanes: Std, a standard mixture of G1-G6; 1, wild-type; 2, W168G; 3, Y171G; 4, W275G; 5, W397F; 6, W570G; 7, double; 8, triple; 9, quadrupole and 10, substrate blank.

3.2.4.2 TLC analysis of G2-G6 hydrolysis by chitinase A mutants

As noted above, mutations of the active site residues (Asp392→Asn, Trp168→Gly, Tyr171→Gly, Trp275→Gly and Trp397→Phe) led to a significant modification of the chitinase hydrolytic activity towards colloidal chitin. The ability of the enzymes to hydrolyze chitooligosaccharides (G2-G6) was further investigated. The discriminations in the cleavage patterns of each mutant were observed at 10 min (data not shown) and 60 min of the reaction (Figure 3.30A-E).
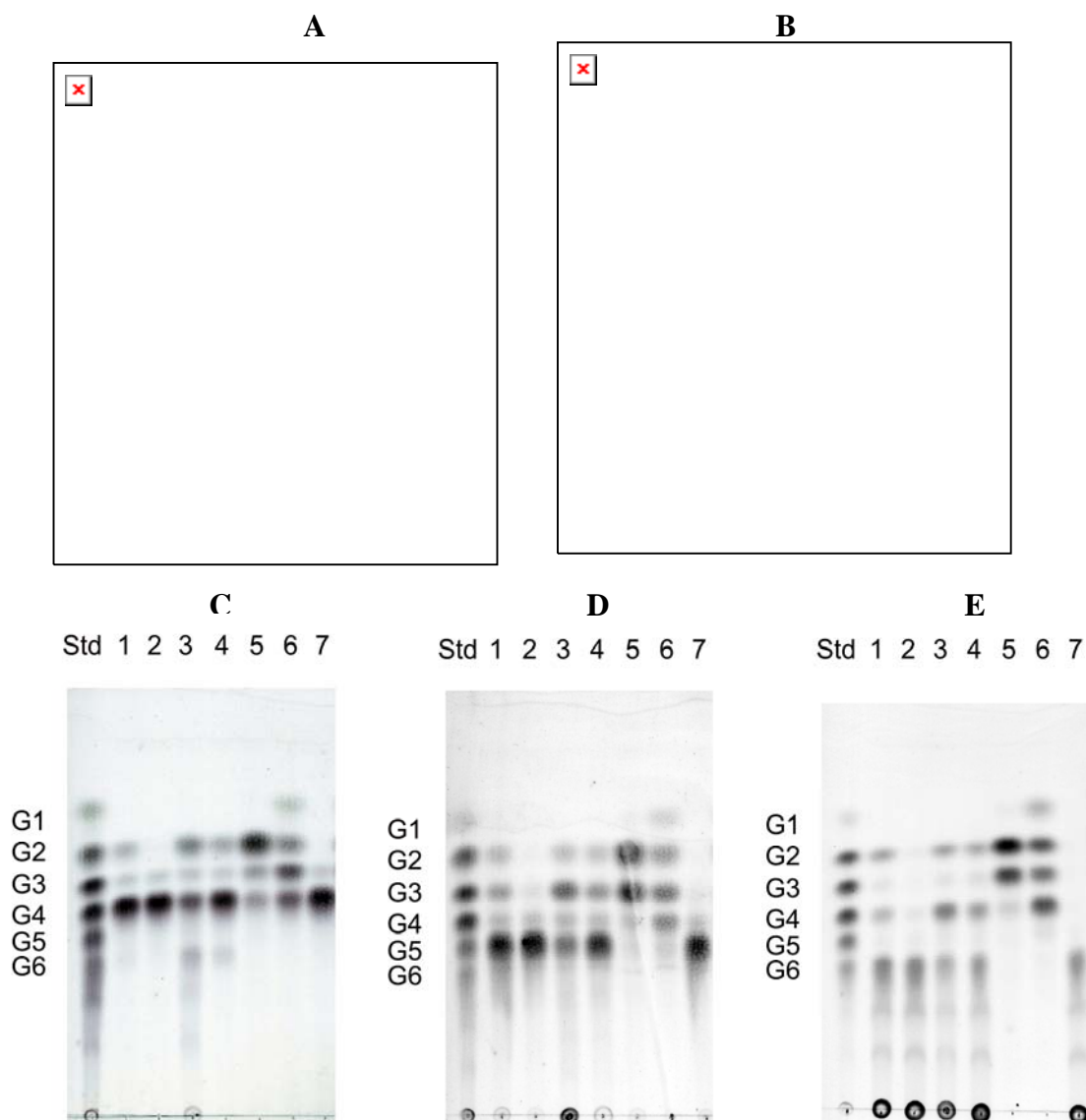
Figure 3.30 TLC analysis of G2-G6 hydrolysis by chitinase A mutants.

A reaction mixture (80 µL), containing 800 ng chitinase and 2.5 mM substrate (G2-G6) in 100 mM sodium acetate buffer pH 5.0, was incubated for 1 h at 30°C. After boiling, the reaction solution (5 l) was analyzed on TLC and sugar products detected with aniline-diphenylamine reagent. (A) G2 hydrolysis, (B) G3 hydrolysis, (C) G4 hydrolysis, (D) G5 hydrolysis, and (E) G6 hydrolysis. Lanes: Std, a standard mixture of G1-G6; 1, wild-type; 2, D392N; 3, W168G; 4, Y171G; 5, W275G; 6, W397F; and 7, substrate blank.

As expected, none of the mutants hydrolyzed G2 (Figure 3.30A). After 60 min of incubation, only W397F clearly displayed the hydrolytic activity by cleaving G3 to G1 and G2, whereas wild-type and other mutants were unable to utilize G3 at all (Figure 3.30B). The pale spots corresponding to G1 and G2 products were a result of G3 hydrolysis by W397F, indicating that this mutant had a greater efficiency in the utilization of G3 than the non-mutated enzyme. A notable difference in the patterns of product formation by mutants W275G and W397F was particularly observed with longer-chain chitooligomers, G4-G6, (Figure 3.30C-E). With G4 hydrolysis, greater amounts of the G2 product were generated by mutants W168G, Y171G, W275G and W397F, with W275G having the most prominent signal (Figure 3.30C). Two pale spots corresponding to G6 that were additionally seen in the reaction mixture containing G4 and W168G and Y171G gave evidence that transglycosylation was concurrently taking place during the hydrolytic reactions of these two mutants (Figure 3.30C). The elongated oligomer, G6 was predominately generated as early as 10 min after the initiation by mutant W168G (data not shown). A complete degradation of G5 and G6 was reached when the reactions containing W275G and W397F (Figure 3.30D-E) were incubated at 30°C for 60 min, whilst substantial amounts of the substrates remained present in the reaction mixtures containing wild-type chitinase A. These results clearly indicated enhanced hydrolytic activity of the two mutants towards G5-G6. In summary, the hydrolytic activity towards G4, G5 and G6 (Figure 3.30C-E), generating the G2 product, was best achieved by W275G. Further analysis showed a series of chitooligosaccharide fragments (G1, G2, G3, G4 and G5) were produced from G6 hydrolysis by W397F (Figure 3.30E). It was found that mutation of

Trp397 to Phe led to a distinct cleavage mode from wild-type enzyme and resulted in the enhanced hydrolytic activity.

3.2.4.3 HPLC analysis of G3 hydrolysis by chitinase A mutants.

In the previous section, TLC analysis of hydrolytic products revealed differences in the ability of mutants W168G, Y171G, W275G and W397F to utilize chitooligomers. In this section, the reaction intermediates of the hydrolysis of these substrates with the chitinase variants were quantitated at the early stage of the reaction (10 min) by HPLC under the conditions described in Methods 2.7.3. The calculated amounts of the products were shown as relative values compared to those obtained from wild-type. Table 3.15 shows the amounts of hydrolytic products of chitinase A and mutants with G3 substrate, the products G1 and G2 were calculated from triplicate injection according to the HPLC experimental data.

Table 3.15 Quantification of G3 hydrolysis by chitinase A mutants.

Chitinase A variant	nmol of products released	
	G1	G2
Wild-type	n.d. [a]	1.53 (1) [b]
D392N	0	0
W168G	0.21	3.17 (2.09)
Y171G	n.d.	2.67 (1.75)
W275G	25.83	2.55 (1.68)
W397F	31.32	2.66 (1.75)

[a] n.d. represents non-detectable activity.
[b] Values in brackets represent relative amount comparing to that of wild-type (set to 1).

The results showed that D392N was unable to hydrolyze G3 substrate. The increased signals of G1 and G2 products as a result of G3 hydrolysis by the W168G, W275G and W397F mutants indicated that these mutants had greater efficiency in G3 utilization than the wild-type enzyme. The amounts of G1 products released from G3 hydrolysis by mutant W275G and W397F were estimated to be 25.83 nmol and 31.32 nmol, which were most significantly higher than G1 produced by wild-type.

3.2.4.4 HPLC analysis of G4 hydrolysis by chitinase A mutants.

Table 3.16 shows the quantitative HPLC analysis of the relative amounts of the oligomers produced by the selected mutants as specified in section 3.2.4.3.

Table 3.16 Quantification of G4 hydrolysis by chitinase A mutants.

Chitinase A variant	nmol of products released		
	G1	G2	G3
Wild-type	n.d. [a]	3.10 (1) [b]	n.d.
D392N	0	0	1.74
W168G	0.26	12.04 (3.89)	3.91
Y171G	14.16	7.40 (2.39)	5.06
W275G	n.d.	93.37 (30.19)	4.84
W397F	2.66	10.56 (3.41)	8.94

[a] n.d. represents non-detectable activity.
[b] Values in brackets represent relative amount comparing to that of wild-type (set to 1).

With the exception for D392N, all the selected variants gave a significant increase in G2 product, especially W275G with the 30.19-fold of the yield obtained from wild-type enzyme. In addition, Y171G and W397F mutants displayed differences in the hydrolytic patterns compared to wild-type. With G4 substrate, Y171G and W397F cleaved G4 to G1 with the amount of G1 products released by Y171G and W397F estimated to be 14.16 nmol and 2.66 nmol, while G1 was non-detectable at all from wild-type protein. It is obvious that mutant W275G most often recognized the middle glycosidic bond of G4 as G2 product was the most prominent compared to other mutants.

3.2.4.5 HPLC analysis of G5 hydrolysis by chitinase A mutants.

The detectable signals of G1-G4 products as a result of G5 hydrolysis by all the variants at 10 min of reaction is shown in Table 3.17.

Table 3.17 Quantification of G5 hydrolysis by chitinase A mutants.

Chitinase A variant	nmol of products released			
	G1	G2	G3	G4
Wild-type	n.d. [a]	9.86 (1) [b]	3.57 (1)	5.61 (1)
D392N	n.d.	n.d.	n.d.	2.13 (0.38)
W168G	5.83	6.28 (0.64)	18.89 (5.31)	5.24 (0.94)
Y171G	3.73	4.13 (0.42)	4.46 (1.25)	n.d.
W275G	7.10	61.79 (6.27)	50.57 (14.21)	7.57 (1.35)
W397F	19.15	15.92 (1.62)	6.45 (1.81)	10.78 (1.93)

[a] n.d. represents non-detectable activity.
[b] Values in brackets represent relative amount comparing to that of wild-type (set to 1).

With G5 as the substrate, G2 and G3 were formed as the primary products of wild-type with the hydrolytic rate of the D392N mutant being much slower than that of other variants. Although the cleavage patterns of W168G and Try171G were similar to the wild-type analogue, both enzymes released greater amounts of G3 with the 5.31-fold and 1.25-fold of the yield obtained from the wild-type enzyme. Mutant W275G degraded G5 to main products of G2 and G3 with 6.27-fold of G2 and 14.21-fold of G3 compared to the value obtained by wild-type. The levels of G2-G4 products generated from G5 by mutant W397F were 2-fold greater as compared to the levels obtained from the wild-type enzyme. W397F also released highest amount of G1 (19.15 nmol), whereas it was non-detectable from wild-type enzyme. Noticeably, both W275G and W397F mutant hydrolyzed G5 much more efficiently, as well as displayed significantly distinct cleavage patterns from the wild-type enzyme.

3.2.4.6 HPLC analysis of G6 hydrolysis by chitinase A mutants.

Hydrolysis of G6 by the same mutants is presented in Table 3.18.

Table 3.18 Quantification of G6 hydrolysis by chitinase A mutants.

Chitinase A variant	nmol of product released				
	G1	G2	G3	G4	G5
Wild-type	n.d. [a]	10.29 (1) [b]	0.96 (1)	3.31 (1)	n.d.
D392N	n.d.	n.d.	2.22 (2.31)	n.d.	n.d.
W168G	n.d.	9.42 (0.92)	3.77 (3.92)	14.34 (4.33)	n.d.
Y171G	n.d.	7.85 (0.76)	3.58 (3.72)	3.49 (1.06)	n.d.
W275G	1.68	76.36	30.51 (31.78)	14.53 (4.39)	5.45
W397F	15.31	24.94	4.68 (4.88)	10.37 (3.13)	8.69

[a] n.d. represents non-detectable activity.

[b] Values in brackets represent relative amount comparing to that of wild-type (set to 1)

Table 3.18 shows that wild-type enzyme asymmetrically cleaved G6 to G2 and G4 products. Thus G3 was much less produced by wild-type enzyme compared to the mutated enzyme. After 10 min of reaction time, D392N failed to generate G2 and G4 products, but the yield of the trimer was 2.31-fold higher than the value of wild-type. Both W168G and Y171G hydrolyzed G6, giving the asymmetric products of G2 and G4. W168G released higher amounts of G3 and G4 (about 4-fold), comparing to the values obtained from wild-type. On the other hand, Y171G released comparable of G2 and G4 and greater amount of G3 (3.72-fold higher than that obtained from wild-type). Mutant W275G particularly enhanced the hydrolytic activity, producing G2, G3 and G4 with 7.42, 31.78 and 4.39 fold, respectively, higher yields than wild-type. The break down of G6 substrate to G2 and G3 was best achieved by W275G. W397F enhanced the hydrolytic activity by generating G2-G4 products with the range 5-fold

higher than that value obtained from wild-type. Table 3.18 shows that the G1 product was best produced by W397F compared to G1 produced by other mutants.

In conclusion, HPLC provided greater sensitivity for oligosaccharide hydrolysis and the construction of the sugar standard curve allowed the hydrolytic products to be quantitated. Under the given conditions, the reaction intermediates of the hydrolytic reactions were detected as early as 10 min of incubation. The hydrolysis of G2 was unnoticeable at this time point, whereas the highest amounts of G1 products were released from G3 hydrolysis by mutants W275G and W397F (Table 3.15). Similar results were observed with higher-M_r substrates, by which the cleavage patterns of G4-G6 notably exhibited enhanced-hydrolytic activity of mutants W275G and W397F over the wild-type enzyme. Mutant W275G preferably cleaved G4 to G2 (Figure 3.30C), whilst mutant W397F degraded G4 to G1-G3. By TLC technique, the transglycosylation was clearly seen in the reaction mixture containing G4 and W168G or Y171G. In addition, W168G displayed greater transglycosylation than Y171G, as higher M_r sugar could be observed as early as 10 min reaction, whilst Y171G showed the spot corresponding to larger sugar only at 1 h of incubation. With G5 and G6 substrates (Figure 3.30D-E), the highest amount of G3 product was generated by W275G higher than the G3 product obtained from the non-mutated enzyme. On the other hand, mutant W397F hydrolyzed G5 (Figure 3.30D), and G6 (Figure 3.30E), produced a series of smaller fragments ranging from G1-G4 for G5 substrate and G1-G5 for G6 substrate. The G1 product, which was a result of the hydrolysis of G3 intermediate was most seen by mutant W397F (with the highest amount of 19.15 nmol from G5 hydrolysis). The levels of G2-G5 products generated from G6 by the same enzyme were 2-5 fold greater than the wild-type enzyme. The most

distinguishable cleavage patterns found for W275G and W397F mutants suggested that these two residues are particularly important for primary binding of the soluble substrates.

CHAPTER IV

DISCUSSION

4.1 Recombinant expression and purification of chitinase A from

E. coli M15 cells

The *chitinase A* gene isolated from *V. carchariae* genome encodes 850 amino acids, expressing 95 kDa precursor. However, the molecular weight of the native chitinase A was determined to be 63 kDa, suggesting that the functional enzyme was proteolytically processed, most likely at the C-terminus with the cleavage site predicted to locate between Arg597 and Lys598 (Suginta *et al.*, 2004). The *chitinase A* gene, lacking 254-amino acid C-terminal fragment was subsequently cloned into the pQE60 expression vector and expressed in *E. coli* M15 cells.

In this study, conditions for high expression level of recombinant chitinase A was established with the attempt to obtain sufficient amounts of highly purified enzyme for functional and structural determination. Varied IPTG concentrations, temperatures and times required for maximal production of the wild-type enzyme were tested. The results showed highest level of the protein expression when the cells were induced with 0.5 mM IPTG at 25°C for 18 h. Under this condition, the major band of ~63 kDa obtained from crude enzyme was clearly detected on SDS-PAGE gel. The recombinant chitinase A was expressed with six histidine residues tagged at the C-terminus, so that the enzyme could be further purified by Ni-affinity chromatography. Other chitinase mutants produced from the

same expression vector and host cells were also expressed and purified under the same condition as for the wild-type enzyme.

Ni-affinity chromatography was carried out using the two-step wash protocol, in which 5 mM, followed by 20 mM imidazole were used in the washing step prior to chitinase elution with 250 mM imidazole. A single step purification was employed for functional characterization. However, further purification by gel filtration chromatography was applied if the enzymes were subjected for crystallization experiments. A complete purification of wild-type and inactive E315M yielded approx. 8-10 mg of purified enzyme per litre of bacterial culture. Other chitinase variants (D392N, D392K, E315Q, E315M, D392NE315Q, D392NE315M, D392KE315M, W168G, Y171G, W275G, W397F, W570G, a double mutant, a triple mutant and a quadruple mutant) were purified using a single step of Ni-affinity purification with slightly higher yields of approximately 10-15 mg of the purified proteins per liter of bacterial culture.

4.2 Secondary structural analysis of *V. carchariae* chitinase A
by CD spectroscopy

The effects of point mutations of the active-site residues on the hydrolytic activity towards chitin and chitooligosaccharide substrates were studied (Results 3.2.4). Mutations of some of those mutants resulted in significant changes in the catalytic activity of the enzyme. To verify that the functional modifications were not caused by the structural disruption, the folding states of the native and expressed chitinase A variants from *E. coli* were investigated by means of CD spectroscopy.

The CD spectra of the mutated proteins were compared with the spectrum of the non-mutated enzyme. The spectra of the mutated enzymes were found to be nearly superimposed as shown in Figure 3.4, which indicated that all the expressed proteins folded into native conformations. The CD spectra displayed a mixture of α-helices and β-sheets with a minimum absorbance of 220 and 208 nm. This spectral characteristic is expected for the $(\beta/\alpha)_8$-TIM barrel containing structures.

4.3 Sequence analysis of *V. carchariae* chitinase A

When the amino acid sequence of the full-length *V. carchariae* chitinase A was compared with other bacterial chitinases, the *V. carchariae* chitinase A was found to align well with all the family 18 chitinases (Figure 3.5) with the overall sequence identity of 47%. It is well studied that bacterial chitinase A has the highly conserved catalytic region, with two typical conserved motifs SxGG and DxxDxDxE located at strands B3 and B4 of the TIM-barrel catalytic domain (Henrissat and Bairoch, 1993). The glutamic residue located at the end of DxxDxDxE motif (equivalent to Glu315 of the *Vibrio* sequence) is identified as the most important residue in catalysis (Watanabe *et al.*, 1993; Terwisscha van Scheltinga *et al.*, 1995; 1996; Matsumoto *et al.*, 1999; Hollis *et al.*, 2000; Bortone *et al.*, 2002; Suginta *et al.*, 2005).

4.4 Three-dimensional structure of *V. carchariae* chitinase A

For crystallization experiments, various types of crystallization techniques were used, such as microbatch under oil, microbatch sitting drop, sitting drop and hanging drop vapor diffusion methods. Microseeding and macroseeding were also employed in the later steps of the crystal growth optimization. Although the first

crystal was obtained from wild-type protein, it was later found to be twin crystal that gave the non-identificable X-ray diffraction pattern. Later, the high quality crystals of E315M mutant (without substrate) were obtained. The crystals of E315M complexed with two chitooligosaccharide substrates were originally grown under the same conditions using the hanging drop technique. Further optimization was carried out until the X-ray quality crystal of wild-type was obtained by macroseeding technique.

The X-ray structures of *V. carchariae* chitinase A wild-type and its E315M mutant were solved by the molecular replacement method (see Methods 2.6.6). In general, the structure of the *Vibrio* enzyme is similar to the structures of *S. marcescens* chitinase A (Perrakis *et al.*, 1994; Papanikolau *et al.*, 2001; 2003; Aronson *et al.*, 2003), hevamine chitinase (Terwisscha van Scheltinga *et al.*, 1995; 1996), *B. circulans* chitinase A1 (Matsumoto *et al.*, 1999) and *C. immitis* chitinase (Hollis *et al.*, 2000; Bortone *et al.*, 2002).

The overall structure of *V. carchariae* chitinase A comprises three major domains as shown in Figure 3.10. The N-terminal chitin-binding domain (residues 22-138), which consists mostly of β-strands, connects through a hinge region (residues 139-159) to the main $(\beta/\alpha)_8$-barrel catalytic domain. The TIM-barrel domain has two regions (Cat I contains residues 160-460 and Cat II contains residues 548-588). These two regions are separated by the third domain (residues 461-547), which has an α+β fold. This domain is referred as a small α+β domain.

The superimposition between *Vibrio* and *Serratia* structures gave an R.M.S. of 6.221 Å, suggesting a high similarity of the overall fold of the two enzymes with a few minor differences over the three domains.

A difference between the two structures was found in the N-terminal chitin-binding domain. The first two parallel strands are interrupted with a helix in the chitin-binding domain of the *Vibrio* enzyme. This strand interruption was not found in the *Serratia* domain. In addition, the *Vibrio* structure has an extra helix preceeding the hinge region, which was also absent in *Serratia* structure (see Figure 3.12A).

The superimposition between wild-type with E315M-NAG$_6$ reveals a complete identity of the two structures. The active site of the enzyme has a long deep cleft characteristic with a dimension of ~33 × 14 Å. The structure of E315M-NAG$_6$ complex reveals a full occupancy of the six NAG units along the substrate binding cleft (Figure 3.13A). The nomenclature for sugar subsites was designated from E315M-NAG$_6$ structure (Figure 3.13B). Based on Devies and Henrissat (1995), the sugar unit at subsite +2 is at the reducing end, while the sugar unit at subsite -4 is at the non-reducing end. The bond located between subsites -1 and +1 is identified as the scissile bond.

Several conserved aromatic residues, including Trp168, Tyr171, Trp231 and Tyr245 appear to position along the substrate binding site (Figure 3.13A). Other two additional conserved residues (Tyr31 and Trp70) are found to extend over the surface beyond the substrate binding site towards the N-terminal chitin-binding domain of the *Vibrio* structure. The positions of Trp168 and Tyr171 are alternately placed at the substrate binding sites -3 and -5, while Trp231, Tyr245, Tyr31 and Trp70 are placed at the predicted sites -7, -9, -11 and -13, respectively. The binding at subsite -3 and -5 was strongly confirmed by the direct contact from E315M-NAG$_6$ structure that will be later described in section 4.4.2. Two of these conserved residues (Trp122 and Trp134) were well studied in chitinase A1 from *B. circulans* (Watanabe *et al.*, 2001).

The residue Trp122 is equivalent with Trp168 and Trp134 equivalent with Tyr171 of the *Vibrio* enzyme. Both residues are surface exposed and found to be aligned on the extension of the oligomer chain bound to the binding cleft. These two aromatic residues have been shown to be particularly essential for hydrolysis of crystalline chitin. The N-terminal chitin-binding domain was suggested to be partially flexible and to work cooperatively with a connecting hinge in order to direct a chitin chain into the recognition site for a subsequent hydrolysis (Watanabe *et al*., 2001).

The TIM-barrel catalytic domain of *V. carchariae* chitinase A is located at the C-terminal and made of strands B1-B8 and helices A1-A8 alternately connected between each β-strand as shown in Figure 3.12. Some differences that are found between the TIM-barrel domain of *V. carchariae* and of *S. marcescens* are; i) strand B1 is connected by four short α-helices in *V. carchariae* (G1-1, G1, G1-2 and G1-3), but by only three helices (G1-1, G1-2 and G1-3) in *S. marcescens*, ii) there are three helices connected between B2 and B3 (Á, G2-1 and A2) with two extra short antiparallel strands (B2-1 and B2-2) in *V. carchariae*, but there are four α-helices in *S. marcescens* without two β-strands connected to the helix Á, iii) in *V. carchariae* chitinase A, two helices (G4 and A4) are found between B4 and B5, while only one (A4) found in *S. marcescens*, and iv) the two extra antiparallel β-sheets (B6-1 and B6-2) connected between B6 and B7 are formed in *V. carchariae*. These two strands are absent in *S. marcescens*.

The most important characteristic of the TIM-barrel domain of the *Vibrio* chitinase is the completely conserved motif SxGG located at strand B3, and the DxxDxDxE motif at the end of strand B4. The latter motif contains Glu315 that is known to be the most important residue in catalysis (Perrakis *et al*., 1994; Terwisscha

van Scheltinga *et al*., 1995; 1996; Matsumoto *et al*., 1999; Hollis *et al*., 2000; Papanikolau *et al*., 2001; 2003; Bortone *et al*., 2002; Aronson *et al*., 2003; Suginta *et al*., 2005).

Like other family 18 chitinases, the catalytic cleft of *V. carchariae* chitinase A contains a number of *cis* peptide bonds (Figure 4.1). There are three non-Pro *cis* bonds (Gly191-Phe192, Glu315-Phe316 and Trp570-Glu571). These *cis* bonds are also found in *S. marcescens* (Perrakis *et al*., 1994) and in hevamine (Terwisscha van Scheltinga *et al*., 1996). In the case of *C. immitis* chitinase (Hollis *et al*., 2000), the enzyme contains four *cis* peptide bonds. One involves a *cis* Pro, the other three are non-Pro *cis* bonds. The locations of these *cis* peptide bonds that surround the active site strongly suggested that they are involved in the overall architecture of the catalytic cleft of *V. carchariae* chitinase A.
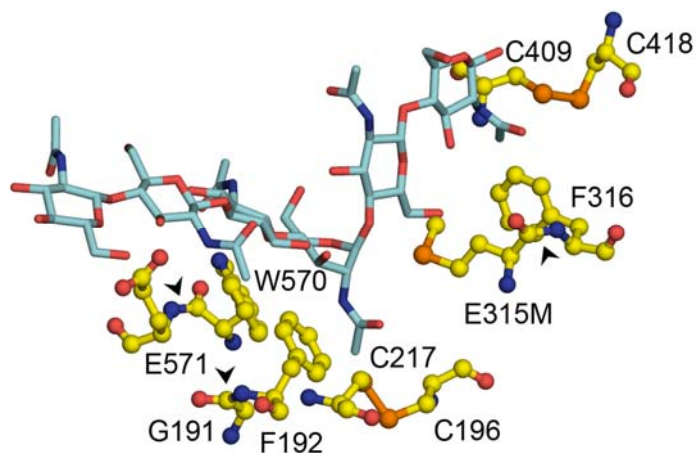
Figure 4.1 A representation of non-Proline *cis* bonds and disulfide bonds found in E315M-NAG$_6$ complex.

The amino acid residues are depicted as ball-and-stick model. NAG$_6$ comprising six sugar residues are in stick model. Amino acid residues are colored; yellow for carbon; blue for nitrogen; red for oxygen and orange for sulfur atoms. NAG$_6$ are colored; cyan for carbon; blue for nitrogen and red for oxygen. Non-Proline *cis* bonds are indicated by arrow (▲). Disulfide bonds are shown in orange.

The structure of E315M-NAG$_6$ revealed that -1 sugar interacts with the side chains of Phe192, Glu315→Met and Trp570. All these residues are involved in *cis* peptide bond formation as mentioned earlier. In the structure of *C. immitis* chitinase, these residues are presumed to be crucial for preserving the correct peptide geometry for substrate binding and for catalysis (Hollis *et al*., 2000). It was assumed that they are often associated with the active sites of enzymes in order to achieve essential constraints (Perrakis *et al*., 1994). In the case of two intrachain disulfide bonds found between Cys217-Cys196 and Cys418-Cys409 located at the catalytic cleft (Figure

4.1), the first bond near subsite -1 and the latter one near the reducing end of the sugar chain. These cystine bridges were suggested to restrict the flexibility of binding of the NAG units at these two subsites (Perrakis *et al*., 1994).

The small insertion domain of *Vibrio* enzyme is located between strands B7 and A7 (Figure 3.12A). Although, function of this domain is still unknown, direct contacts from the structure of E315M-NAG$_6$ suggests that the conserved residues Tyr461, Arg463 and Trp497 of this domain participate in substrate binding by interacting with -1, -3 and -4 NAG. In contrast, the insertion residues in *C. immitis* chitinase (Hollis *et al*., 2000) did not at all play a role in substrate binding as their positions were further away from the catalytic site.

As seen in Figure 3.10, the overall structures of wild-type, E315M mutant and complexes of E315M mutant with NAG$_5$ and NAG$_6$ are identical. The only difference is that the structure of chitinase A E315M either in the presence or absence of NAG substrates consists of one monomer per asymmetric unit, while the structure of wild-type consists of two monomers per asymmetric unit. Figure 3.10B shows the structure of inactive mutant in the absence of substrate. It is clearly seen that the engineered six histidine tagged residues completely buried in the catalytic cleft of the enzyme. These tagged residues mimicked the sugar structures by interacting with all the residues that are important for the bindings of NAG$_5$ and NAG$_6$ (i.e. Tyr164, Trp168, Arg173, Phe192, Val205, Trp275, Asp313, Glu315→Met, Ala363, Met389, Tyr391 and Trp570).

The overall structure of the complex E315M-NAG$_5$ is shown in Figure 3.10C. The substrate NAG$_5$ was bound within a long deep groove (about 30 Å in width and about 14 Å in dept) of the substrate binding cleft. On the other hand, the structure of

E315M-NAG$_6$ complex (Figure 3.10D) demonstrates that NAG$_6$ was firmly embedded within the longer groove (about 33 Å in width and about 14 Å in depth) of the enzyme. In both cases, the groove appeares to be open at both ends, which is a characteristic of an endo chitinase.

The crystal structure of inactive mutant-NAG$_5$ complex reveals an occupancy of subsites (-2) to (+2) with the 'straight chair conformation' of NAG$_5$. The last sugar ring at subsite (-3) that was supposed to be seen in the structure could not be modeled due to its poor density (Figure 3.17). This observation suggests that the binding affinity between the sugar and the binding residues at subsite -3 was relatively weak, thus allowing the sugar residue to be freely moved.

The structure of the inactive mutant E315M complexed with NAG$_6$ clearly reveals a higher number of interactions between several conserved residues in the E315M-NAG$_6$ complex than in the E315M-NAG$_5$ complex. This supports the previous finding on the preference of *V. carchariae* chitinase A upon an increase in the chain length of chitooligomer (Suginta *et al*., 2005). As found also for other chitinases, *Vibrio* chitinase contains multiple binding sites (Figure 3.20), in which the hexasaccharide moieties fully occupied subsites (-4), (-3), (-2), (-1), (+1) and (+2) with the particular 'bent conformation' of -1 sugar. The scissile bond located between -1 NAG and +1 NAG is in the twist conformation, giving the plane of +1 and +2 NAG lie perpendicular to the plane of the sugar units at the preceeding subsites. Direct contacts between NAG$_6$ and the binding sites as shown in Table 3.13 are mainly mediated by several aromatic and charged residues. As judged by a number of contacts at each subsite, it can be concluded that the NAG units formed stronger interactions at the reducing end subsites (+2, +1 and -1), but weaker interactions at the

non-reducing end subsites (-3 and -4). This observation somehow reflects the binding preference of the incoming chitooligosaccharide towards the reducing end subsites. Another word, the binding of the incoming substrate would probably take place at the reducing end subsites prior to bindings at the non-reducing end subites. This assumption agrees well with the non observable sugar at subsites -3 (non-reducing end) in the structure of E315M-NAG$_5$ complex.

4.4.1 The proposed catalytic mechanism of *V. carchariae* chitinase A

The availability of the structures of E315M mutant in the presence of NAG$_5$ and NAG$_6$ is found to be a key solution to the catalytic mechanism of the enzyme. When the overall structures of E315M-NAG$_5$ and E315M-NAG$_6$ complexes are superimposed using program Superpose available in CCP4 suite, the low R.M.S. value of 0.161 Å suggests the complete identity of the two structures. The overlaid structures of NAG$_5$ and NAG$_6$ are shown in Figure 4.2.

A　　　　　　　　　　　　　　　　　　　　　**B**
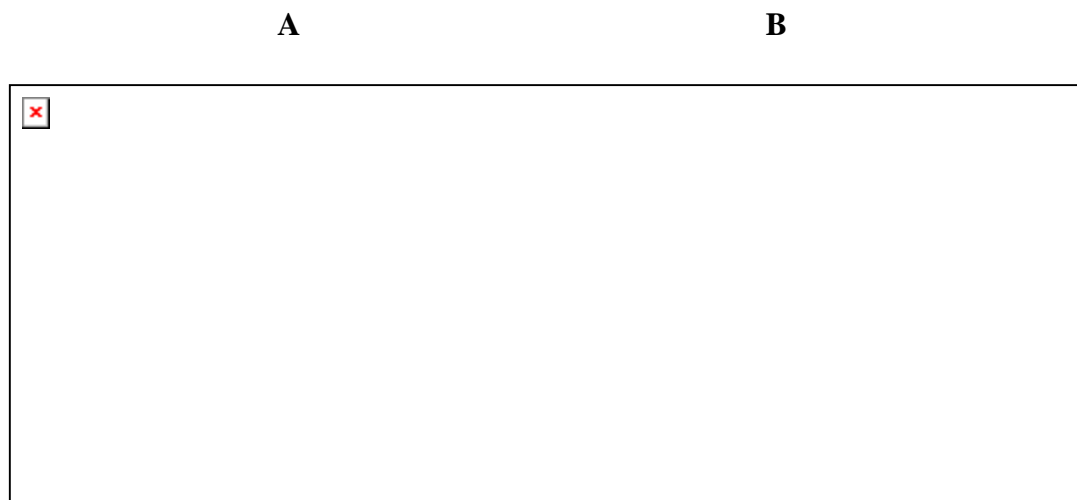
Figure 4.2 A structural comparison of NAG$_5$ and NAG$_6$ in TIM-barrel of E315M-NAG$_6$ complex.

The interactions of binding residues with sugar residues are formed by hydrogen bonds and hydrophobic interactions. Hydrogen bond is shown in dash line (·····). The eight β-strands are defined; a1 (residues 160-165); a2 (residues 455-460); a3 (residues 566-571); b (residues 186-192); c (residues 384-389); d1 (residues 267-273); d2 (residues 308-313) and d3 (residues 358-366). Carbon atoms of the labeled amino acids are colored; purple for strands a1, a2 and a3; blue for strand b; deep salmon for strand c; pale cyan for strands d1, d2 and d3. The binding residues are depicted as ball-and-stick models and orange yellow for sulfur. A stick model is shown for sugar residues. NAG$_5$ units are colored green for carbon. NAG$_6$ units are colored yellow for carbon; blue for nitrogen and red for oxygen. (B) a 180° rotation of (A).

Considering a cluster of amino acid residues contributing to the bindings of +2 and +1 NAG, obvious differences of the interactions between NAG_5 and NAG_6 are seen at subsite -1. The -1 sugar in NAG_6 makes contact with Tyr164, Asp313, Ala363, Met389 Tyr391, Asp392, Tyr461 and Arg463 via its boat conformation (Table 3.13), whereas these residues did not interact with the chair conformation of -1 sugar in NAG_5. The residues Asp313 and Asp392 that especially hydrogen bonded with -1 NAG in NAG_6 are not seen in NAG_5. The observation suggests that both residues probably play an important role in introducing -1 NAG into the binding cleft by changing the geometry from the 'straight chair conformation' to the 'bent boat conformation'. The presence of Glu315→Met near the scissile bond between subsites -1 and +1 in NAG_6 supports the catalytic role of this residue towards the bent conformation but not towards the straight conformation.

Most importantly, the area where +1 NAG gave a patch of the electron density map in the final model of E315M-NAG_6 complex that does not correspond to any particular conformation of NAG. It has been assumed that the electron density in that area may adopt a transient conformation of the sugars lying within these two subsites. Therefore, the omitted map of E315M-NAG_6 was further calculated with the coordinates of the -4 to +2 NAG moieties being omitted in the refinement process. The NAG_5 conformation obtained from E315M-NAG_5 was then remodeled into the electron density of E315M-NAG_6, then refined. It has been shown that the coordinates of NAG_5 at positions, +2, +1, -1 and -2 could be reasonably modeled in the refined map of E315M-NAG_6 as shown in Figure 4.3.
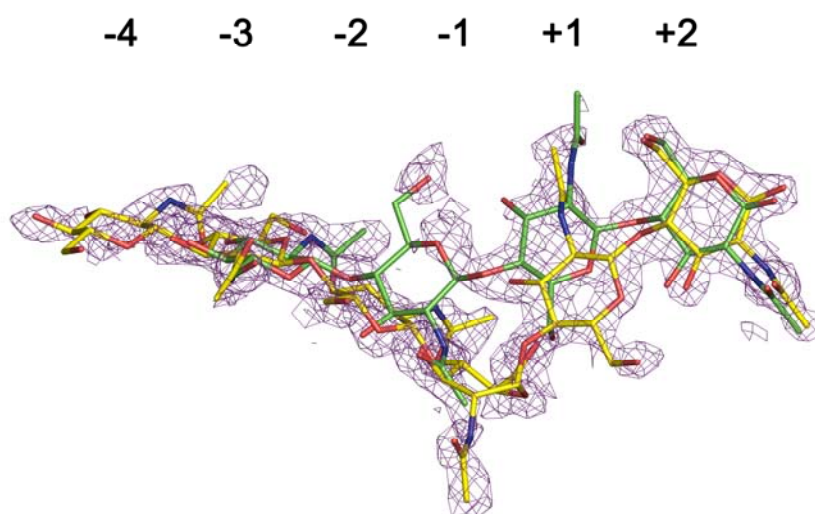
Figure 4.3 The omitted electron density map of NAG_5 and NAG_6 bound to E315M mutant.

A $2F_o$-F_c map was calculated by the omitting sugar residues and contoured at 1.0 σ. Stick model is shown for sugar residues. Carbon atoms of two sugar conformations are colored as follows: yellow for NAG_6 major conformation; green for NAG_5 minor conformation. Blue for nitrogen and red for oxygen atom.

The direct contact studies (Table 3.13) demonstrates that the coordinates of +2 NAG is similar between the refined structures of E315M-NAG_5 and E315M-NAG_6. As shown in Figure 4.3, the electron density at subsites +2, +1 and -3 NAG of E315M-NAG_6 could be modeled relatively well with their corresponding sugars from NAG_5. The only sugar that could not be modeled is -1 NAG. The broken electron density at -1 NAG could be explained that the sugar at this subsite has adopted more than one conformation, most likely from 'straight' to 'bent' conformation to facilitate bond cleavage. It has been hypothesized that the bending process takes place to allow

the scissile bond to be accessed by the catalytic residue (Glu315). Based on the E315M-NAG$_5$ structure, the cleavage can not take place with a 'straight conformation' as the -1 sugar is positioned too far away from the catalytic residue.

Taken all the data together, the catalytic mechanism of *V. carchariae* chitinase is proposed as depicted in Figure 4.4.
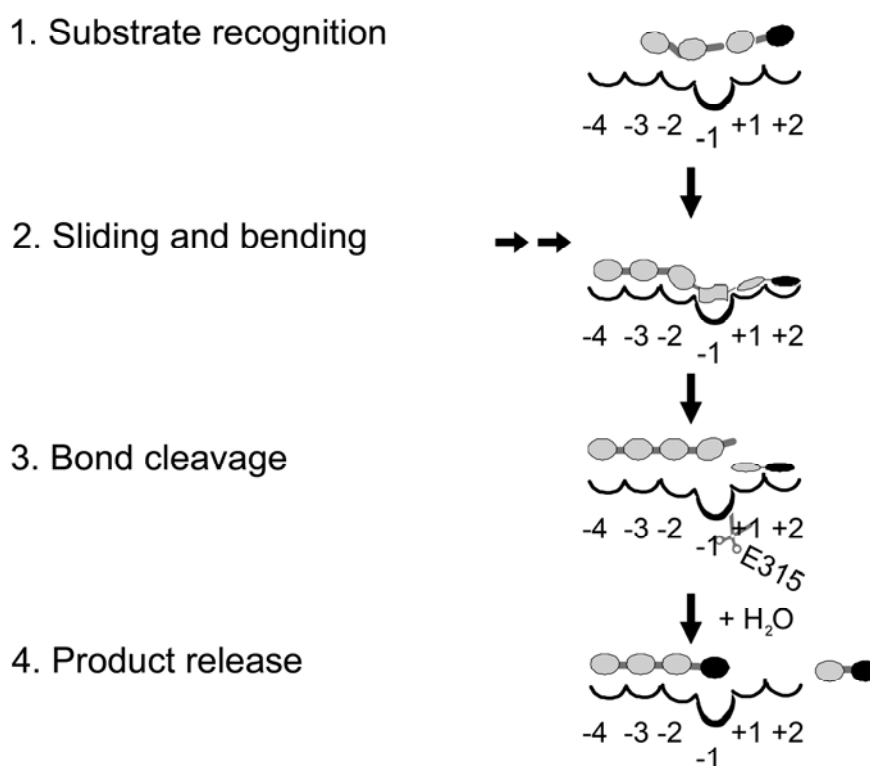
Figure 4.4 The proposed catalytic mechanism of *V. carchariae* chitinase A

From Figure 4.4, four major steps are thought to involve in the hydrolysis of chitooligosaccharide substrate of the *Vibrio* chitinase A.

Step 1: Substrate recognition

The incoming substrate binds to the substrate binding site in the 'straight conformation' with -1 sugar in 'chair conformation' joining with the straight plane of other sugar moieties. The structure of E315M-NAG$_5$ complex suggested a weak binding affinity at subsite -3 NAG (see Results 3.1.12).

Step 2: Sliding and bending

Subsequent binding of NAG units at subsites -3 and -4 may provide enough energy for the sugar chain to slide forward towards the reducing end, thus creating the most unstable sugar (-1 NAG) to bend as seen in Figure 4.3. This process concurrently takes place with the twist of the bond between subsites -1 and +1. The change of the geometry of the plane of the sugars has brought the -1 NAG closed to Glu315 that locates at the bottom of subsite -1.

Step 3: Bond cleavage

The protonated Glu315 now acts as a general acid catalyst by donating a proton to the glycosidic oxygen, which leads to a subsequent cleavage of the bond.

Step 4: Product release

After bond cleavage, the constraint of the sugar chain is then released. A nucleophilic attack by a neighboring water yields the final form of the products. The dimeric product (G2) at subsites +1 and +2 diffuses away.

4.4.2 Assumption of the roles of the active-site aromatic residues on substrate hydrolysis of *V. carchariae* chitinase A

The refined structure of E315M-NAG$_6$ complex reveals that the substrate binding site of *V. carchariae* comprises several conserved aromatic residues in the

cleft floor [-4 (Tyr171 and Trp497), -3 (Trp168 and Trp497), -2 (Phe192, Trp275 and Trp570), -1 (Tyr164, Phe192, Trp275, Tyr391, Tyr461 and Trp570), +1 (Trp275 and Phe316) and +2 (Trp275, Trp397 and Tyr435)] as shown in Figure 4.5.
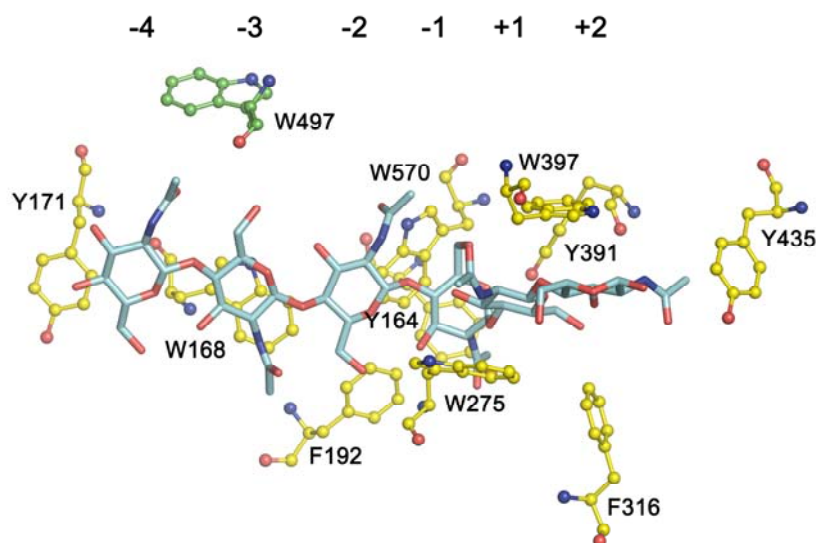
Figure 4.5 A representation of substrate stabilizing via hydrophobic stack of E315M-NAG$_6$ complex.

The aromatic residues that interact with the substrate are depicted as ball-and-stick model. NAG$_6$ comprising six sugar residues are in stick model. The aromatic residues are colored; yellow for carbon in the catalytic domain; green for carbon in the small insertion domain. NAG$_6$ are colored; cyan for carbon; blue for nitrogen and red for oxygen.

To clarify the roles of these aromatic residues, they were mutated as mentioned in section 1.6. The effects of point mutations (mutants W168G, Y171G, W275G, W397F and W570G) on the hydrolytic activity of *V. carchariae* chitinase were also studied by TLC and quantitative HPLC (Results 3.2.4).

As revealed by both chromatographic methods, the hydrolytic products generated from the degradation of G4-G6 and colloidal chitin by wild-type *Vibrio* (see Figure 3.25-3.28) showed that G2 was the main product of the hydrolytic reactions against all the substrates. G5 hydrolysis by wild-type enzyme initially produced G2 and G3 in equal amounts (Section 3.2.3.4), assuming that G5 occupied subsites -3 to +2 in the substrate binding cleft. A time course study of the wild-type reaction showed that the enzyme initially hydrolyzed G6 to G4 and G2 (Section 3.2.3.5). According to the occupation of the primary subsites (-4 to +2), the G2 product will occupy subsites +1 and +2. The G6 hydrolysis also results in the formation of G3 product. It indicates that the enzyme recognize both second and third bonds of the hexamer.

The structure of E315M-NAG$_6$ complex clearly shows that Tyr435 is located at the end of the substrate-binding cleft with its aromatic ring facing to the methyl acetamido group of the sugar at site +2 (Figure 4.5). However, this residue does not seem to hinder the sugar chain to extend beyond subsite +2. This supports the endo characteristic of the enzyme.

Product analysis by TLC and quantitative HPLC showed higher efficiency of W275G and W397F in G4-G6 hydrolysis over the wild-type enzyme. In addition, the distinct hydrolytic patterns between wild-type and mutants W275G and W397F revealed differences in the cleavage behavior of the chitinase variants.

The discriminations in the cleavage patterns of each mutant were analyzed at 10 min of incubation. W275G significantly created G2-G5 intermediates. In contrast, W397F initially produced G1-G5 with G6 substrate. With G5 and G6 substrates, the higher amount of G3 product was generated by W275G with ~14-fold and ~32-fold

higher than the product obtained from the non-mutated enzyme. The results suggest that the hydrolytic pattern by W275G was distinct from the wild-type enzyme. Further hydrolysis of G5 and G6 by W397F released G1 product, which accounts for the break down of the sugar intermediates with a higher rate than the rate produced by the wild-type enzyme.

The structure of E315M-NAG$_6$ complex shows that Trp275 and Phe397 lie on the opposite side of the cleft and stack against the hydrophobic faces of +1 and +2 NAG (Figure 4.5). Mutations of the two residues to a less steric hindrance, by which Trp275→Gly and Trp397→Phe certainly caused a loss in their ability to form hydrophobic interaction with the +1 and +2 sugars due to the absence of the two aromatic rings. This may enhance the turn over of the enzyme due to the fact that the cleaved product could diffuse away relatively quickly compared to when it is bound to Trp275 and Trp397 residues.

In addition, the loss of hydrophobic interaction with the +2 subsite by the Trp397→Phe mutant appeared to shift the binding site of the substrate from the primary subsites (at -4 to +2) to the secondary subsites (-3 to +2). It could be explained that the incoming oligosaccharide has more freedom to assemble itself in the binding cleft, thus permitting various bonds to be exposed to the cleavage site. This observation is strongly confirmed by a time course study of G6 and colloidal chitin hydrolyse (Suginta *et al.*, 2007).

Mutation of W275 to glycine residue seemed to affect the binding preference around the cleavage site, by allowing the second and the third bonds of G6 to be equally accessed. The production of a high amount of G2 and G3 products by W275G than by produced by the wild-type supports this idea.

Y171G and W168G mutants remained hydrolytic activity against colloidal chitin by giving lower yields of products compared to those obtained from wild-type (see Results 3.2.4.1). In contrast, both enzymes released G3 with higher yields than that of the wild-type at 10 min of incubation with G6 substrate (see Table 3.18). The assumption based on the loss of hydrophobicity is the same as discussed for W397F. In *B. circulans*, the effect of mutation of Tyr56 at subsite -5 and Trp53 at subsite -3 (corresponding to Tyr171 and Trp168 in *V. carchariae*) against crystalline chitin and reduced NAG_5 were analyzed. The results clearly demonstrated that two mutants, Y56A and W53A did not cause the loss of the binding activity towards reduced NAG_5. In contrast, Y56 and W53 seem to be required only for the hydrolysis of crystalline chitin but not for soluble substrates. This is inconsistency with our results that two mutants, Y171G and W168G had a dramatic lessen catalytic efficiency towards colloidal chitin but not much on chitooligosaccharides (Table 3.15-3.18).

Higher M_r intermediates occurring in the course of hydrolysis of W168G and Y171G were identified. Transglycosylation evidence has been clearly seen from TLC analysis at 10 min and 1 h incubation of G4 hydrolysis (Figure 3.30C). A recent report (Aronson *et al.*, 2006) showed that the mutation of W167A in *S. marcescens* (corresponding to W168G in *V. carchariae*) favored transglycosylation.

Of all aromatic-residue mutants, W570G mutant seemed to completely abolish the chitinolytic activity against colloidal chitin after the prolonged reaction of 18 h (Figure 3.29). The effects of mutation of the equivalent residue was also studied by chitinase A1 from *B. circulans* (Watanabe *et al.*, 2003). It was found that the mutation of W433 in *Bacillus* enzyme drastically reduced the hydrolyzing activity against all substrates tested. The structure of E315M-NAG_6 reveals that W570 interacts with the

most important -1 sugar through hydrophobic interaction, as well as hydrogen bonding (see Table 3.13). The hydrogen bond is formed between its nitrogen atoms of aromatic ring and the cyclic O4 of the -1 NAG. Like Trp539 in the *Serratia* structure (Papanikolu *et al.*, 2001), this residue would likely be responsible for holding the GlcNAc ring in place so that the glycosidic cleavage between subsites -1 and +1 could take place.

The triple and quadruple mutants yielded non-detectable activity against colloidal chitin. It is assumed that the cluster of the aromatic residues in the catalytic cleft were important in a cooperative binding and in directing the substrate through the binding cleft than by particular residues.

CHAPTER V

CONCLUSION

This research describes structural studies of *Vibrio* chitinase A and its hydrolytic function in order to understand the mode of action of the enzyme.

For functional characterization, wild-type and active site mutants of chitinase A from *V. carchariae* chitinase A were overexpressed and purified using a single step Ni-affinity chromatography. However, wild-type and inactive E315M mutant were further purified by gel filtration chromatography for crystallization purpose. The purified wild-type and active site mutants reveal similar folding as analyzed by CD measurement and suggested that point mutations did not affect their overall structures.

For crystallization of chitinase A, initial screenings were performed with the microbatch technique using various commercially available screening kits. The conditions that produced crystalline samples were further optimized by the hanging drop and the sitting drop vapor diffusion techniques. Two-dimensional optimization by the hanging drop vapor diffusion technique provided the first single crystals of free inactive E315M. Later, the soaking experiments were achieved, giving the crystals of E315M-NAG$_5$ and E315M-NAG$_6$ complexes, while the crystals of wild-type enzyme were obtained by macroseeding technique.

After the completion of X-ray diffraction data, the first model was built from a molecular replacement technique using *Serratia* chitinase A as the search model. On the other hand, the structural models of E315M-NAG$_5$, E315M-NAG$_6$ and wild-type

chitinase A were built based on the structure of E315M. Alternate sessions of model building and refinement were carried out in order to improve the quality of the structural models. The final models of the four structures gave good fit with their electron density maps with an average B-factor value of protein atoms of 15.10, 14.24, 13.74 and 15.15 Å^2 for E315M protein, E315M-NAG$_5$ complex, E315M-NAG$_6$ complex and wild-type. The refinement of the four structures was completed with an R-factor of 16.80% to 18.90% and free R-factor of 20.50% to 21.90%, which show the well refined structures. The R.M.S. deviations of 0.006-0.007 Å for bond distances and 0.932°-0.994° for bond angles indicated the correct geometry of almost all the residues of the final models. The geometry of the final models were well verified and indicated most of the residues (90.9-91.4%) in the polypeptide chain in the most favored regions, 8.4-8.9% in the additionally allowed regions and 0.2% in the generously allowed regions. No residues lied in the disallowed Ramachandran regions.

The X-ray structure of *V. carchariae* chitinase A is similar to the known X-ray structures of family 18 chitinases (Perrakis *et al.*, 1994; Terwisscha van Scheltinga *et al.*, 1996; Hollis *et al.*, 2000). The overall structure of *V. carchariae* chitinase A comprises three domains, i) the N-terminal chitin-binding domain (residues 22-138), which consists mostly of β-strands and connects through a hinge region (residues 139-159), ii) the main β/α barrel catalytic domain (residues 160-460 and 548-588), iii) the α+β small insertion domain (residues 461-547). The catalytic domain contains two completely conserved motifs; SxGG located in the strand B3; and DxxDxDxE consisting of the catalytic Glu315 residue in loop that connects with strand B4.

The overall structures of wild-type, E315M mutant and complexes of E315M mutant with NAG_5 and NAG_6 are identical. In the absence of substrate, the engineered six histidine tagged residues are found to bury within the catalytic cleft found in the structure of inactive E315M mutant and interact with all the important binding residues. The structures of E315M-NAG_5 and E315M-NAG_6 show that the sugar substrates are firmly embedded within the long, deep substrate binding groove of the enzyme. The refined structure of E315M-NAG_6 complex reveals that the substrate binding site of *V. carchariae* comprises many conserved aromatic residues in the cleft floor [-4 (Tyr171 and Trp497), -3 (Trp168 and Trp497), -2 (Phe192, Trp275 and Trp570), -1 (Tyr164, Phe192, Trp275, Tyr391, Tyr461 and Trp570), +1 (Trp275 and Phe316) and +2 (Trp275, Trp397 and Tyr435)].

The crystal structure of inactive mutant-NAG_5 complex shows that NAG_5 substrate occupied subsites (-2) to (+2) with the 'straight conformation', while the non-reducing end sugar at subsite -3 is missing. Whilst NAG_6 fully occupies subsites (-4) to (+2) with the particular 'bent conformation' of the sugar at subsite (-1). The twist of scissile bond is also found between -1 NAG and +1 NAG in the structure of E315M-NAG_6 complex but not in the structure of E315M-NAG_5 complex. Further refinement of the omitted map generated from E315M-NAG_6 diffraction data provides a key evidence of the transient conformation of the -1 sugar between the 'straight' and 'bent' conformations. Presumably, the -1 sugar of a 'straight conformation' of the NAG_5 structure was unable to proceed the bond cleavage as its position is too far away from the catalytic residue (Glu315). On the other hand, the 'bent conformation' of NAG_6 allows the scissile bond to be favorably accessed by the catalytic residue so that the scissile bond can be further cleaved. This finding suggests that the -1 sugar

adopts a conformational change to facilitate the bond cleavage. Based on this assumption, the proposed mechanism of *V. carchariae* chitinase A is suggested to involve four major steps; i) the substrate recognition process is initiated via the 'straight conformation'; ii) the sliding-bending process thermodynamically forces the substrate to adopt the 'bent conformation'; iii) the bond cleavage process that is proceeded via the 'bent conformation' of -1 NAG and the twist of the scissile bond; and iv) the release of the cleaved products from the subsites +1 and +2 (the reducing end).

Several conserved residues lie along the substrate binding cleft that comprises of Trp168, Tyr171, Trp275, Trp397 and Trp570. Point mutations were carried out using site-directed mutagenesis. Mutation of these residues resulted in the change of cleavage patterns towards G3-G6 substrates, by which mutation of Trp168 to Gly enhanced the transglycosylation of the enzyme. Mutation of Tyr171 caused less effect on the hydrolytic activity as its location near to the edge of binding cleft, which give less binding effect to the bound sugar. Mutation of Trp570 caused a severe loss in the hydrolytic activity, since this residue interacts with the most crucial NAG (-1 NAG). Mutation of Trp275 to Gly led to an equal access of the second and the third bonds of G6, indicating that this residue is important for the binding selectivity around the cleavage site. Mutation of Trp397 to Phe entirely changed the cleavage pattern by releasing a series of smaller chitooligosaccharide intermediates from particularly G5 and G6 substrates, indicating that Trp397 plays a role in defining the primary binding subsite for the incoming sugar. The improvement of the efficiency in product formation maybe caused by the weaker affinity of the binding at subsite +2 due to less hydrophobicity of the mutated residue.

REFERENCES

REFERENCES

Armand, S., Tomita, H., Heyraud, A., Gey, C., Watanabe, T., and Henrissat, B. (1994). Stereochemical course of the hydrolysis reaction catalyzed by chitinases A1 and D from *Bacillus circulans* WL-12. **FEBS Lett.** 343: 177-180.

Aronson, N. N. Jr., Halloran, B. A., Alexyev, M. F., Amable, L., Madura, J. D., Pasupulati, L., Worth, C., and Van Roey, P. (2003). Family 18 chitinase-oligosaccharide substrate interaction: subsite preference and anomer selectivity of *Serratia marcescens* chitinase A. **Biochem. J.** 376: 87-95.

Aronson, N. N. Jr., Halloran, B. A., Alexyev, M. F., Zhou, X. E., Wang, Y, Meehan, E. J., and Chen, L. (2006). Mutation of a conserved tryptophan in the chitin-binding cleft of *Serratia marcescens* chitinase A enhances transglycosylation. **Biosci**. **Biotechnol. Biochem.** 70: 243-251.

Babiker, M. A., Banat, A, Kameyama, Y., Yoshioka, T., and Koga, D. (1999). Purification and characterization of a 54 kDa chitinase from *Bombyx mori*. **Ins. Biochem. Mol. Biol.** 29: 537-547.

Babiker, M. A., Banat, A., Zhou, W., Karasuda, S., and Koga, D. (2002). Analysis of Hydrolytic Activity of a 65-kDa Chitinase from the Silkworm, *Bombyx mori* **Biosci. Biotechnol. Biochem.** 66: 1119-1122.

Blake, C. C. F., Koenig, D. F., Mair, G. A., North, A. C. T., Phillips, D. C., and Sarma, V. R. (1965). Structure of hen egg-white lysozyme. A three-dimensional Fourier synthesis at 2 Å resolution. **Nature.** 206: 757-761.

Bokma, E., Barends, T., Terwisscha van Scheltinga, A.C., Dijkstra, B.W., and Beintema, J. J. (2000). Enzyme kinetics of hevamine, a chitinase from the rubber tree *Hevea brasiliensis*. **FEBS Lett.** 478: 119-122.

Boller, T., and Mauch, F. (1988). Colorimetric assay for chitinase. **Method. Enzymol.** 161(50): 430-435.

Bork, P., and Doolittle, R. F. (1992). Proposed acquisition of an animal protein domain by bacteria. **Proc. Natl. Acad. Sci.** 89: 8990-8994.

Bortone, K., Monzingo, A. F., Ernst, S., Cox, R., and Robertus, J.D. (2002). The structure of an allosamidin complex with the *Coccidioides immitis* chitinase defines a role for a second acid residue in substrate-assisted mechanism. **J. Mol. Biol.** 320: 293-302.

Bradford, M. M, (1976). A rapid and sensitive method for the quantitation of microgram quantities of protein utilizing the principle of protein-dye binding, **Anal. Biochem.** 72: 248-254.

Brameld, K. A., and Goddard, III. W.A. (1998). Substrate distortion to a boat conformation at subsite -1 is critical in the mechanism of family 18 chitinases. **J. Am. Chem**. **Soc.**120: 3571-3580.

Brine, C. J. (1984). **Chitin: Accomplishments and perspectives. In Chitin, Chitosan, and Related enzymes.** (Zakikas, J. P. (ed)). xxii-xxiv. New York: Academic Press.

Brurberg, M. B., Eijsink, V. G., and Nes, I. F. (1994). Characterization of a chitinase gene (*chiA*) from *Serratia marcescens* BJL200 and one-step purification of the gene product. **FEMS Microbiol. Lett.** 124: 399-404.

Brurberg, M. B., Eijsink, V. G., Haandrikman, A. J., Venema, G. and Nes, I. F. (1995). Chitinase B from *Serratia marcescens* BJL200 is exported to the periplasm without processing. **Microbiol.** 141: 123-131.

Brurberg, M.B., Nes, I.F., and Eijsink, V.G.H. (1996). Comparative studies of chitinases A and B from Serratia marcescens. **Microbiol.** 142: 1581-1589.

Burkhard, R., and Sander, C. (1993). Improved prediction of protein secondary structure by use of sequence profiles and neural networks. **Proc. Natl. Acad. Sci.** 90: 7558-7562.

Burkhard, R., and Sander, C. (1993). Prediction of protein structure at better than 70% accuracy. **J. Mol. Biol.** 232: 584-599.

Burkhard, R., and Sander, C. (1994). Conservation and prediction of solvent accessibility in protein families. **Proteins.** 20: 216-226.

Chang, K. L. B., Tsai, G., Lee, J. and Fu, W. R. (1997). Heterogeneous *N*-deacetylation of chitin in alkaline solution. **Carbohydr. Res.** 303: 327-332.

Chang, K. L. B., Lee, J., and Fu, W. R. (2000). HPLC Analysis of *N*-acetyl-chito-oligosaccharides during the acid hydrolysis of chitin. **J. Food and Drug Analysis.** 8(2): 72-85.

Clark, J., Quayle, K. A., Macdonald, N. L., and Stark, J. R. (1988). Metabolism in marine flatfish –V. chitinolytic activities in dover sole, *Solea Solea* (L.). **Comp. Biochem. Physiol.** 90B(2): 379-384.

Cohen-Kupiec, R., and Chet, I. (1998) The molecular biology of chitin digestion. **Curr. Opin. Biotechnol.** 9: 270-277.

Collaborative Computational Project, Number 4. (1994). The CCP4 suit: Programs for Protein Crystallography. **Acta Cryst.** D50: 760-763.

Davies, G., and Henrissat B. (1995). Structures and mechanisms of glycosyl hydrolases. **Structure.** 3: 853-859.

DeLano, W. L. (2002). **The PyMOL Molecular Graphics System** [On-line]. Available: http://www.pymol.org. html

Fukamizo, T., Goto, S., Torikata, T., and Araki, T. (1989). Enhancement of transglycosylation activity of lysozyme by chemical modification. **Agric. Biol. Chem.** 53: 2641-2651.

Fukamizo, T. (2000). Chitinolytic enzymes: Catalysis, substrate binding, and their application. **Current Protein and Peptide Science.** 1: 105-124.

Fukamizo, T., Sasaki, C., Schelp, E., Bortone, K., and Robertus, J.D. (2001). Kinetic properties of chitinase-1 from the fungal pathogen *Coccidioides immitis*. **Biochemistry.** 40: 2448-2454.

Hart, P. J., Pfluger, H. D., Monzingo, A. F., Hollis, T., and Robertus, J.D. (1995). The refined crystal structure of an endochitinase from *Hordeum vulgare* L. seeds at 1.8 Å resolution. **J. Mol. Biol.** 248: 402-413.

Henrissat, B. (1991). A classification of glycosyl hydrolases based on amino acid sequence similarities. **Biochem. J.** 280: 309-316.

Henrissat, B., and Bairoch, A. (1993). New families in the classification of glycosyl hydrolases based on amino acid sequence similarities. **Biochem. J.** 293: 781-788.

Hollis, T., Honda, Y., Fukamizo, T., Marcotte, E., Day, P., J., and Robertus, J. D. (1997). Kinetic analysis of barley chitinase. **Arch. Biochem. Biophys.** 344: 335-342.

Hollis, T., Monzingo, A. F., Bortone, K., Ernst, S., Cox, R., and Robertus, J.D. (2000). The X-ray structure of a chitinase from the pathogenic fungus *Coccidioides immitis*. **Protein Science.** 9: 544-551.

Huber, R., Stöhr, J., Hohenhaus, S., Rachel, R., Burggraf, S., Jannasch, H. W., and Stetter, K. O. (1995). *Thermococcus chitonophagus* sp. nov., a novel, chitin-degrading, hyperthermophilic archaeum from a deep-sea hydrothermal vent environment. **Arch. Microbiol.** 164: 255-264.

Hult, Eva-Lena, Katouno, F., Uchiyama, T., Watanabe, T., and Sugiyama, J. (2005). Molecular directionality in crystalline β-chitin: hydrolysis by chitinase A and B from Serratia marcescens 2170. **Biochem. J**. 388: 851-856.

Imoto, T., and Yagishita, K. (1971). A simple activity measurement of lysozyme. **Agric. Biol. Chem.** 35: 1154-1156.

Iseli, B., Armand, S., Boller, T., Neuhaus, Jean-Marc and Henrissat, B. Plant chitinases use two different hydrolytic mechanisms. **FEBS Lett.** 382: 186-188.

Jeuniaux, C. (1961). Chitinase an addition to the list of hydrolases in the digestive tract of verterbrates. **Nature.** 192: 135-136.

Jeuniaux, C. (1966). Chitinase. **Methods Enzymol.** 8: 644-650.

Jones, T. A., Zou, J. Y., Cowan, S. W. and Kjeldgaard, M. (1991). Improved methods for building models in electron density maps and the location of errors in these models. **Acta Cryst.** A47: 110-119.

Laemmli, U. K. (1970). Cleavage of structural proteins during assembly of head of bacteriophage-T$_4$. **Nature.** 227: 680-685.

Lamzin, V. S, Wilson, K. S. (1993). Automated refinement of protein models. **Acta Cryst.** D49: 129-147.

Laskowski, R. A., MacArthur, M. W., Moss, D. S. and Thornton, J. M. (1993). PROCHECK: a program to check the stereochemical quality of protein structures. **J. Appl. Crystallog.** 26: 283-291.

Leah, R., Tommerup, H., Svendsen, I. and Mundy, J. (1991). Biochemical and molecular characterization of three anti-fungal proteins from barley seed. **J. Biol. Chem.** 266: 1564-573.

Leslie, A. G. W. (1991). Recent changes to the MOSFLM package for processing film and image plate data. **Newsletters on Protein Crystallography**. SERC Laboratory, Daresbury, UK.

Li, Q., Dunn, E. T., Grandmaison, E. W. and Goosen, M. F. A. (1992). Applications and properties of chitosan. **J. Bioact. Compat. Polym.**7: 370-397.

Matsumoto, T., Nonaka, T., Hashimoto, M., Watanabe, T. and Mitsui, Y. (1999). Three-dimensional structure of the catalytic domain of chitinase A1 from *Bacillus circulans* WL-12 at a very high resolution. **Proc. Japan Acad.** 75: 269-274.

Matthews, B.W. (1968). Solvent content of protein crystals. **J. Mol. Biol.** 33: 491-497.

Mitsutomi, M., Hata, T. and Kuwahara, T. (1995). Purification and characterization of novel chitinase from *Streptomyces griseus* HUT 6037. **J. Ferment. Bioeng.** 80: 153-158.

Murshudov, G. N., Vagin, A. A., and Dodson, E. J. (1997). Refinement of macromolecular structures by the maximum-likelihood method. **Acta Cryst.** D53: 240-255.

Muzzarelli, R. A. A. (1993). Biochemical significance of exogenous chitins and chitosans in animals and patients. **Carbohydr. Polym.** 20: 7-16.

Muzzarelli, R. A. A. (1996). Chitosan-based dietary foods. **Carbohydr. Polym.** 29: 309-316.

Navaza, J. (1994). Amore - an automated package for molecular replacement. **Acta Cryst.** A50: 157-163.

Okutani, K. (1967). Studies of chitinolytic systems in the digestive tract of Latelabrax japonicus. Bull. Misaki Mar. **Biol. Inst.** 10: 1-47.

Okutani, K., (1977). Chitin digestion in the digestive tract of fish. **Proc. First Int. Confer. Chitin/Chitosan** (pp. 554-562). Boston MA (USA).

Papanikolau, Y., Prag, G., Tavlas, G., Vorgias, C.E., Oppenheim, A.B. and Petratos, K. (2001). High resolution structural analyses of mutant chitinase A complexes with substrates provide new insight into the mechanism of catalysis. **Biochemistry.** 40: 11338-11343.

Papanikolau, Y. and Petratos, K. (2002). Application of the effects of ionic strength reducing agents in the purification and crystallization of chitinase A. **Acta Cryst.** D58: 1593-1596.

Papanikolau, Y., Prag, G., Tavlas, G., Vorgias, C.E. and Petratos, K. (2003). De *novo* purification scheme and crystallization conditions yield high-resolution structures of chitinase A and its complex with the inhibitor allosamidin. **Acta Cryst.** D59: 400-403.

Park, S. H., Lee, J-H, and Lee, H. K. (2000). Purification and characterization of chitinase from a marine bacterium, *Vibrio* sp. 98CJ11027. **J. Microbiol.** 38: 224-229.

Patil, R.S., Ghormade, V. V., and Deshpande, M.V. (2000). Chitinolytic enzymes: an exploration. **Enz. Microb. Technol.** 26: 473-483.

Perrakis, A., Tews, I., Dauter, Z., Oppenheim, A. B., Chet, I., Wilson, K.S., and Vorgias, C.E. (1994). Crystal structure of a bacterial chitinase at 2.3 A resolution. **Structure.** 2: 1169-1180.

Prag, G., Greenberg, S., and Oppenheim, A. B. (1997). Structural principles of prokaryotic gene regulatory proteins and the evolution of repressors and gene activators. **Mol Microbiol.** 26: 619-620.

Ramachandran, G. N., and Sasisekharan, V. (1968). Conformation of polypeptides and proteins. **Adv. Protein Chem.** 23: 283-438.

Rhodes, G. (2000). **Crystallography made crystal clear. A guide for users of macromolecular models** (2nd ed.). New York: Academic Press.

Robertus, J. D., Hart, P. J., Monzingo, A. F., Marcotte, E., and Hollis, T. (1995). The structure of chitinases and prospects for structure-based drug design. **Can. J. Bot.** 73 (Suppl. 1): S1142-S1146.

Rupley, J. A. (1964). The hydrolysis of chitin by concentrated hydrochloric acid and the preparation of low-molecular-weight substrates for lysozyme. **Biochim. Biophys. Acta.** 83: 245-255.

Sahai, A. S., and Manocha, M. S. (1993). Chitinases of fungi and plants: their involvement in morphogenesis and host-parasite interaction. **FEMS Microbiol. Rev.** 11: 317-338.

Sambrook, J., Fritsch, E. F., and Maniatis, T. (1989). **Molecular cloning: a laboratory manual** (2nd ed.). New York: Cold Spring Harbor Laboratory Press.

Sasaki, C., Yokoyama, A., Itoh, Y., Hashimoto, M., Watanabe, T. and Fukamizo, T. (2002). Comparative study of the reaction mechanism of family 18 chitinases from plants and microbes. **J. Biochem.** (Tokyo). 131: 557-564.

Songsiriritthigul, C., Yuvaniyama, J., Robinson, R.C., Vongsuwan, A., Prinz, H., and Suginta, W. (2005). Expression, purification, crystallization and preliminary crystallographic analysis of chitinase A from *Vibrio carchariae*. **Acta Cryst.** F61: 895-898.

Spindler-Barth, M. (1993). **Hormonal regulation of chitin metabolism in insect cell lines. In Chitin Enzymology** (Muzzarelli, R. A. A. ed.). Italy: Plenum Press.

Suginta, W., Robertson, P. A., Austin, B., Fry, S. C., and Fothergill-Gilmore, L. A. (2000). Chitinases from *Vibrio*: activity screening and purification of chiA from *Vibrio carchariae*. **J. Appl. Microbiol.** 89: 76-84.

Suginta, W., Vongsuwan, A., Songsiriritthigul, C., Prinz, H., Estibeiro, P., Duncan, R.R., Svasti, J., Fothergill-Gilmore, L. A. (2004). An endochitinase A from *Vibrio carchariae*: cloning, expression, mass and sequence analyses, and chitin hydrolysis. **Arch. Biochem. Biophys.** 424: 171-180.

Suginta, W., Vongsuwan, A., Songsiriritthigul, C., Svasti, J., and Prinz, H. (2005). Enzymatic properties of wild-type and active site mutants of chitinase A from *Vibrio carchariae*, as revealed by HPLC-MS. **FEBS J.** 272: 3376-386.

Suginta, W., Songsiriritthigul, C., Kobdaj, A., Opassiri, R., and Svasti, J. (2007). Mutations of Trp275 and Trp397 altered the binding selectivity of *Vibrio carchariae* chitinase A. **BBA-General Subjects.** In press.

Sugiyama, J., Boisset, C., Hashimoto, M., and Watanabe, T. (1999). Molecular directionality of β-chitin biosynthesis. **J. Mol. Biol.** 286: 247-255.

Suzuki, K., Taiyoji, M., Sugawara, N., Nikaidou, N., Henrissat, B., and Watanabe, T. (1999). The third chitinase gene (chiC) of *Serratia marcescens* 2170 and the relationship of its product to other bacterial chitinases. **Biochem J.** 343: 587-596.

Suzuki, K., Sugawara, N., Suzuki, M., Uchiyama, T., Katouno, F., Nikaidou, N., and Watanabe, T. (2002). Chitinase A, B and C1 of *Serratia marcescens* produced by recombinant *Escerichia coli*: Enzymatic properties and synergism on chitin degradation. **Biosci. Biotechnol. Biochem.** 66 (5): 1075-1083.

Svitil, A. L, Chadhain, S. M. N., Moore, J. A., and Kirchman, D. L. (1997). Chitin degradation proteins produced by the marine bacterium *Vibrio Harveyi* growing on different forms of chitin. **Appl. Environ. Microbiol.** 63: 408-413.

Tanaka, T., Fujiwara, S., Nishikori, S., Fukui, T., Takagi, M., and Imanaka, T. (1999). A unique chitinase with dual active sites and triple substrate binding sites from the hyperthermophilic Archaeon *Pyrococcus kodakaraensis* KOD1. **Appl. Environ. Microbiol.** 15: 5338–5344.

Tanaka, T., Fukui, T., and Imanaka, T. (2001). Different cleavage specificities of the dual catalytic domains in chitinase from the hyperthermophilic Archaeon *Thermococcus kodakaraensis* KOD1. **J. Biol. Chem.** 276: 35629-35635.

Terwisscha van Scheltinga, A. C., Armand, S., Kalk, K. H., Isogai, A., Henrissat, B., and Dijkstra, B. W. (1995). Stereochemistry of chitin hydrolysis by a plant chitinase/lysozyme and X-ray structure of a complex with allosamidin: evidence for substrate assisted catalysis. **Biochemistry.** 34: 15619-15623.

Terwisscha van Scheltinga, A. C., Hennig, M., and Dijkstra, B. W. (1996). The 1.8 Å resolution structure of hevamine, a plant chitinase/lysozyme, and analysis of the

conserved sequence and structure motifs of glycosyl hydrolase family 18. **J Mol Biol.** 262, 243-257.

Thamthiankul, S., Suan-Ngay, S., Tantimavanich, S., and Panbangred, W. (2001). Chitinase from *Baccillus thuringiensis* subsp. *pakistani*. **Appl. Microbiol. Biotechnol.** 56: 395-401.

Thompson, J. D., Higgins, D. G, and Gibson, T. G. (1994). CLUSTAL W: improving the sensitivity of progressive multiple sequence alignment through sequence weighting, position specific gap penalties and weight matrix choice. **Nucleic Acids Res.** 22, 4673-4680.

Trudel, J. and Asselin, A. (1989). Detection of chitinase activity after polyacrylamide gel electrophoresis. **Anal. Biochem.** 178: 362–366.

Uchiyama, T., Katouno, F., Nikaidou, N., Nonaka, T., Sugiyama, J., and Watanabe, T. (2001). Roles of the exposed aromatic residues in crystalline chitin hydrolysis by chitinase A from *Serratia marcescens* 2170. **J. Biol. Chem.** 276: 41343-41349.

Ueda, M., Kojima, M., Yoshikawa, T., Mitsuda, N., Araki, K. and Kawaguchi, T., Miyatake, K., Arai, M., and Fukamizo, T. (2003). A novel type of family 19 chitinase from *Aeromonas* sp. No. 10S-24. Cloning, sequence, expression, and the enzymatic properties. **Eur. J. Biochem.** 270: 2513-2520.

van Aalten, D. M., Synstad, B., Brurberg, M. B., Hough, E., Riise, B. W., Eijsink, V. G. H., and Wierenga, R. K. (2000). Structure of a two-domain chitotriosidase from *Serratia marcescens* at 1.9 Å resolution. **Proc. Natl. Acad. Sci.** U.S.A. 97: 5842-5847.

van Aalten, D. M., Komander, D., Synstad, B., Gaseidnes, S., Peter, M. G., and Eijsink, V. G. (2001). Structural insights into the catalytic mechanism of a family 18 exo-chitinase. **Proc. Natl. Acad. Sci. U.S.A**. 98: 8979-8984.

Watanabe, T., Oyanagi, W., Suzuki, K., Ohnishi, K., and Tanaka, H. (1992). Structure of the gene encoding chitinase D of *Bacillus circulans* WL-12 and possible homology of the enzyme to other prokaryotic chitinases and class III plant chitinases. **J. Bacteriol**. 174: 408-414.

Watanabe, T., Kobori, K., Miyashita, K., Fujii, T., Sakai, H., Uchida, M., and Tanaka, H. (1993). Identification of glutamic acid 204 and aspartic acid 200 in chitinase A1 of *Bacillus circulans*WL-12 as essential residues for chitinase activity. **J. Biol. Chem.** 268: 18567-18572.

Watanabe, T., Ishibashi, A., Ariga, Y., Hashimoto, M., Nikaidou, N., Sugiyama, J., Matsumoto, T., and Nonaka, T. (2001). Trp122 and Trp134 on the surface of the catalytic domain are essential for crystalline chitin hydrolysis by *Bacillus circulans* chitinase A1. **FEBS Lett.** 494: 74-78.

Watanabe, T., Ariga, Y., Sato, U., Toratani, T., Hashimoto, M., Nikaidou, N., Kezuka, Y., Nonaka, T., and Sugiyama, J. (2003). Aromatic residues within the substrate-binding cleft of *Bacillus circulans* chitinase A1 are essential for hydrolysis of crystalline chitin. **Biochem. J.** 376: 237-244.

Xia, G., Jin, C., Zhou, J., Yang, S., Zhang, S. and Jin, C. (2001). A novel chitinase having a unique mode of action from *Aspergillus fumigatus* YJ-407. **Eur. J. Biochem.** 268: 4079-4085.

APPENDICES

APPENDIX A
SOLUTIONS AND REAGENTS PREPARATIONS

1. Reagents for bacterial culture and competent cell transformation

1.1 LB broth containing 100 μg/ml of ampicillin (1 L)

Dissolve 10 g Bacto Tryptone, 5 g Bacto Yeast Extract and 5 g NaCl in 950 ml distilled water. Stir until the solutes have been dissolved. Adjust the volume of the solution to 1 litre with distilled water. Sterilize by autoclaving the solution at 121°C for 15 min. Allow the medium to cool to 50°C before adding antibiotics, ampicillin to a final concentration 100 μg/ml and store at 4°C.

1.2 LB plate containing 100 μg/ml of ampicillin (1 L)

Dissolve 10 g Bacto Tryptone, 5 g Bacto Yeast Extract, 5 g NaCl and 15 g Bacto agar in 950 ml distilled water. Stir until the solutes have been dissolved. Adjust the volume of the solution to 1 litre with distilled water. Sterilize by autoclaving the solution at 121°C for 15 min. Allow the medium to cool to 50°C before adding antibiotics, ampicillin to a final concentration 100 μg/ml. Pour medium into Petri-dishes. Allow the agar to harden, and keep at 4°C.

1.3 Ampicillin stock solution (100 mg/ml)

Dissolve 1 g ampicillin in 10 ml sterile distilled water, then aliquot and store at -30°C.

1.4 IPTG stock solution (1.0 M)

Dissolve 2.38 g IPTG (isopropyl thio-β-D-galactoside) in distilled water and make to 10 ml final volume. Sterilize by filter sterilize, aliquot and store at -30°C.

1.5 Reagents for competent cell preparation

CaCl$_2$ solution (60 mM CaCl$_2$, 10 mM PIPES pH 7.0, 15% glycerol)

To prepare 100 ml solution, mix the stock solution as follow:

-   6 ml of 1 M CaCl$_2$ (14.7 g/100 ml, filter sterile)

-   10 ml of 100 mM PIPES (piperazine-1,4-bis(2-ethanesulfonic acid)) pH 7.0 (3.02 g/100 ml adjust pH with KOH, filter sterile)

-   15 ml of 100% glycerol (autoclave at 121°C, 15 min)

Add sterile distilled water to bring a volume up to 100 ml. Store the solution at 4°C.

2. Solutions for protein expression and purification

2.1 20 mM Tris pH 8.0 (1 L)

Dissolve 2.42 g Tris Base in 800 ml distilled water. Adjust pH to 8.0 with 6 M HCl and the volume to 1 L with distilled water. Store at 4°C.

2.2 20 mM Tris pH 8.0 containing 150 mM NaCl (Equilibration buffer, 1 L)

Dissolve 8.77 g NaCl in 1 L of 20 mM Tris pH 8.0. Store at 4°C.

2.3 20 mM Tris pH 8.0 containing 150 mM NaCl and 5 mM imidazole (Wash buffer I, 1 L)

Dissolve 0.3404 g imidazole in 1 L of Equilibration buffer. Store at 4°C.

2.4 20 mM Tris pH 8.0 containing 150 mM NaCl and 20 mM imidazole (Wash buffer II, 1 L)

Dissolve 1.3616 g imidazole in 1 L of Equilibration buffer. Store at 4°C.

2.5 20 mM Tris pH 8.0 containing 150 mM NaCl and 250 mM imidazole (Elution buffer, 100 ml)

Dissolve 1.7020 g imidazole in 100 of Equilibration buffer. Store at 4°C.

2.6 SDS-gel loading buffer (3× stock) (0.15 M Tris pH 6.8, 6% SDS, 0.1% bromophenol blue, 30% glycerol)

Dissolve 6 g SDS, 0.1 g bromophenol blue, 30 ml glycerol and add 0.15 M Tris pH 6.8 to bring a volume up to 100 ml. Store the solution at -30°C. Before use add 20 μl of 2-mercapthoethanol to 40 μl of solution mixture.

2.7 1.5 M Tris pH 8.8 (100 ml)

Dissolve 18.17 g Tris Base in 80 ml distilled water. Adjust pH to 8.8 with 6 M HCl and bring the volume up to 100 ml with distilled water. Store at 4°C.

2.8 1.0 M Tris pH 6.8 (100 ml)

Dissolve 12.10 g Tris Base in 80 ml distilled water. Adjust pH to 6.8 with 6 M HCl and bring the volume up to 100 ml with distilled water. Store at 4°C.

2.9 30% Acrylamide solution (100 ml)

Dissolve 29 g acrylamide and 1 g *N, N′*-methylene-bis-acrylamide in distilled water to a volume 100 ml. Mix the solution by stirring for 1 h to be homogeneous and filter through Whatman membrane No. 1. Store in the dark bottle at 4°C.

2.10 Tris-Glycine electrode buffer (5× stock) (1 L)

Dissolve 30.29 g Tris Base, 144 g glycine, 5 g SDS in distilled water. Adjust pH to 8.3 with HCl and bring the volume up to 1 L with distilled water.

2.11 Staining solution with coomassie brillant blue for protein (1L)

Mix 1 g Coomassie brilliant blue R-250, 400 ml methanol, 500 ml distilled water and 100 ml glacial acetic acid and filter through a Whatman No. 1.

2.12 Destaining solution for coomassie Stain (1L)

Mix 400 ml methanol, 100 ml glacial acetic acid, and add distilled water to a final volume of 1000 ml.

2.13 10% (w/v) Ammonium persulfate (1 ml)

Dissolve 100 mg ammonium persulfate in 1 ml distilled water. Store at -30°C.

2.14 12% Separating gel SDS-PAGE (10 ml)

Mix the solution as follow:

1.5 M Tris (pH 8.8)	2.5 ml
Distilled water	3.3 ml
10% (w/v) SDS	0.1 ml
30% acrylamide solution	4.0 ml
10% (w/v) ammonium persulfate	0.1 ml
TEMED	0.004 ml

2.15 5% Stacking gel SDS-PAGE (10 ml)

Mix the solution as follow:

1.0 M Tris (pH 6.8)	1.25 ml
Distilled water	3.0 ml
10% (w/v) SDS	0.05 ml
30% acrylamide solution	0.655 ml
10% (w/v) ammonium persulfate	0.025 ml
TEMED	0.005 ml

2.16 Bradford's reagent

Dissolve 0.01 g coumassie blue in 10 ml of 85% phosphoric acid and 5 ml of ethanol and add distilled water to a final volume of 100 ml. Mix well and filtered through a Whatman No. 1. Store at 4°C.

3. Buffers and reagents for enzymatic studies

3.1 10 mM *p*-nitrophenol (10 ml)

Dissolve 0.0139 *p*-nitrophenol in 100 mM NaOAc pH 5.0 buffer and make to 10 ml final volume.

3.2 100 mM NaOAc pH 5.0 buffer (100 ml)

Dissolve 0.81 g NaOAc in 80 ml distilled water, and adjust pH to 5.0 with glacial acetic acid and bring the volume up to 100 ml with distilled water.

3.3 1 M Na$_2$CO$_3$ (50 ml)

Dissolve 5.30 g Na$_2$CO$_3$ in distilled water, and adjust the volume to 50 ml with distilled water.

3.4 Stock solutions of substrates

N-acetyl-chitooligosaccharides (Di-*N*-acetyl-chitobiose, Tri-*N*-acetyl-chitotriose, Tetra-*N*-acetyl-chitotetraose, Penta-*N*-acetyl-chitopentaose, Hexa-*N*-acetyl-chitohexaose) and *p*-nitrophenyl-Di-*N*-acetyl-chitobioside [pNP-(GlcNAc)$_2$], (Seikagaku Corporation) were prepared for the stock solutions.

Dissolve 0.2212 mg of *N*-acetyl-glucosamine in 10 ml of distilled water, giving a final concentration of 100 mM *N*-acetyl-glucosamine.

Dissolve 50 mg of Di-*N*-acetyl-chitobiose in 1,180 µl of distilled water, giving a final concentration of 100 mM Di-*N*-acetyl-chitobiose.

Dissolve 50 mg of Tri-*N*-acetyl-chitotriose in 1,590 µl of distilled water, giving a final concentration of 50 mM Tri-*N*-acetyl-chitotriose.

Dissolve 50 mg of Tetra-*N*-acetyl-chitotetraose in 1,200 µl of distilled water, giving a final concentration of 50 mM Tetra-*N*-acetyl-chitotetraose.

Dissolve 50 mg of Penta-*N*-acetyl-chitopentaose in 1,930 µl of distilled water, giving a final concentration of 25 mM Penta-*N*-acetyl-chitopentaose.

Dissolve 50 mg of Hexa-*N*-acetyl-chitohexaose in 2,000 µl of distilled water, giving a final concentration of 20 mM Hexa-*N*-acetyl-chitohexaose.

A mixture of oligosaccharide containing $(GlcNAc)_n$, n =1–6 was prepared by dilution in range of 0–25 nmol.

Dissolve 50 mg of *p*-nitrophenyl-Di-*N*-acetyl-chitobioside in 2,000 µl of distilled water, giving a final concentration of 20 mM *p*-nitrophenyl-Di-*N*-acetyl-chitobioside.

3.5 Preparation of colloidal chitin

Colloidal chitin was prepared according to the modified method of Shimahara and Takiguchi (1988). Chitin flakes (10 g) were added into 200 ml of concentrated hydrochloric acid on ice. The suspension was vigorously stirred for 2 h on ice and kept overnight at 4^oC. The suspension was filtered through cheesecloth and the filtrate was poured into 600 ml of 50% ethanol on ice with stirring. After 1 h., the suspension was filtered with suction through Whatman No. 1 filter paper. The residue was washed with water until the washing become neutral. The acid-free residue was weighted out to calculate dry weight. Then store it in a dark place at 4^oC.

3.6 Preparation of HPLC mobile phase

HPLC mobile phase consisted of acetonitrile:H_2O (65:35, v/v) was prepared by mixing 650.0 ml of acetonitrile and 350.0 ml of deionized water in a flask.

4. Buffers and reagents for protein crystallization studies

The stock solutions of polyethylene glycol (PEG) with a range of molecular weight (PEG1000, PEG4000 and PEG8000), were prepared by dissolving 40 g of PEG in ~20 ml of distilled ultra-pure water, then heat and the volume was brought to 100 ml with a final concentration of 40% (w/v). In addition to PEG 400, 40 ml of PEG 400 were diluted in HPLC water and were finally made volume to 100 ml leading to final concentration of 40% (v/v). All of these solutions were filtered using 0.45 μm MF-Millipore Membrane Filters with a vacuum pump. Various types of salts and buffers were employed in the crystallization solutions. The pH of each buffer was titrated using 6 M HCl or 5 M NaOH to obtain the desire pH ranging from 4.6 to 10.5 for initial screening and optimizing. All of the stock solutions for crystallization were summarized below.

A summary of stock solutions used for crystallization experiments.

Crystallizing agents	Stock concentrations
Precipitants	
PEG 400	40% (v/v)
PEG 1000	40% (w/v)
PEG 4000	40% (w/v)
PEG 8000	40% (w/v)
Salts	
Ammonium acetate	1 M
Ammonium sulfate	3.2 M
Calcium chloride	1 M
Magnesium acetate	1 M
Magnesium chloride	1 M
Sodium acetate	2 M
Buffers	
Sodium acetate pH 4.0, 4.6, 5.0, 5.5 and 6.0	1.0 M
MES pH 6.0 and 6.5	1.0 M
MOPS pH 7.0	1.0 M
HEPES pH 7.0 and 7.5	1.0 M
Tris-HCl pH 7.5, 8.0, 8.5 and 9.0	1.0 M
CHES pH 9.0	1.0 M
CAPSO pH 9.5	1.0 M
CAPS pH 10.5	1.0 M
Substrates	
Penta-*N*-acetyl-chitopentaose	25 mM
Hexa-*N*-acetyl-chitohexaose	20 mM

APPENDIX B

STANDARD CURVES

1. Stand curve of BSA by Bradford's method

$$y = 0.0373x + 0.0088$$
$$R^2 = 0.9949$$
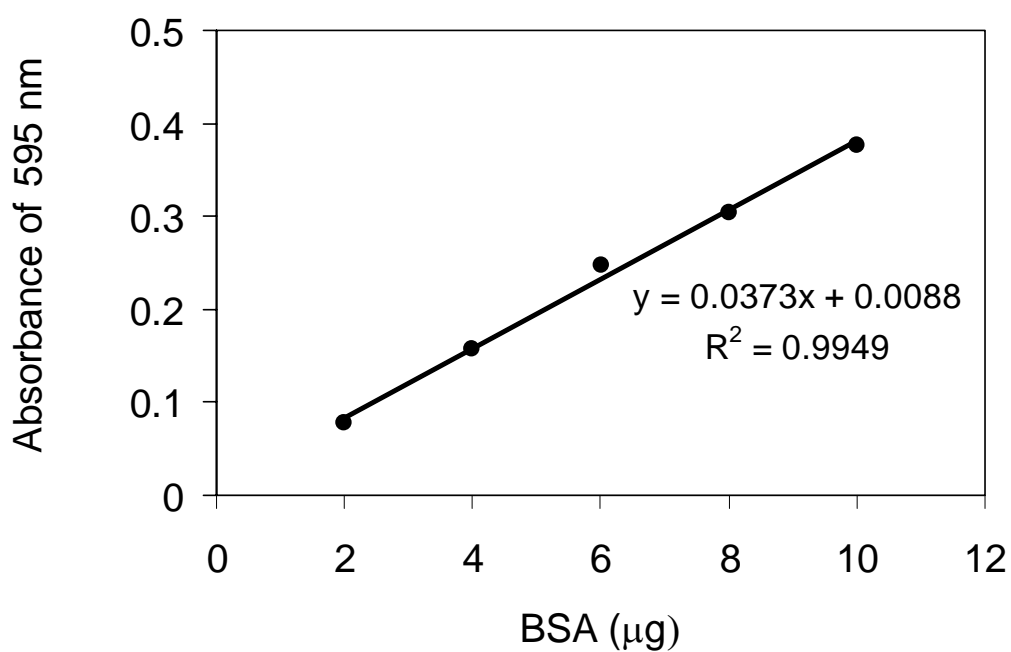
2. Standard curve of *p*-nitrophenol
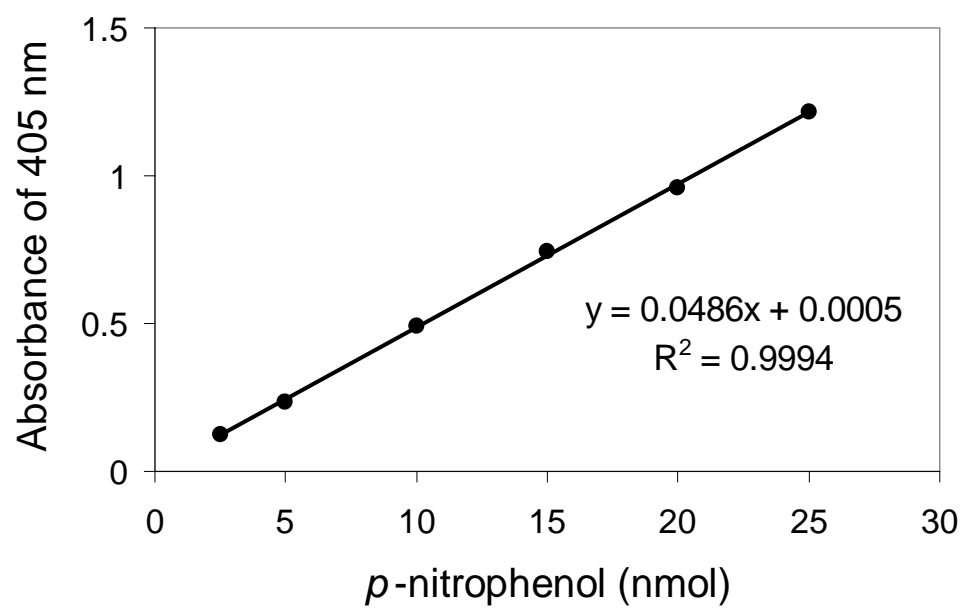
3. Standard curve of chitooligosaccharides (G1-G6)
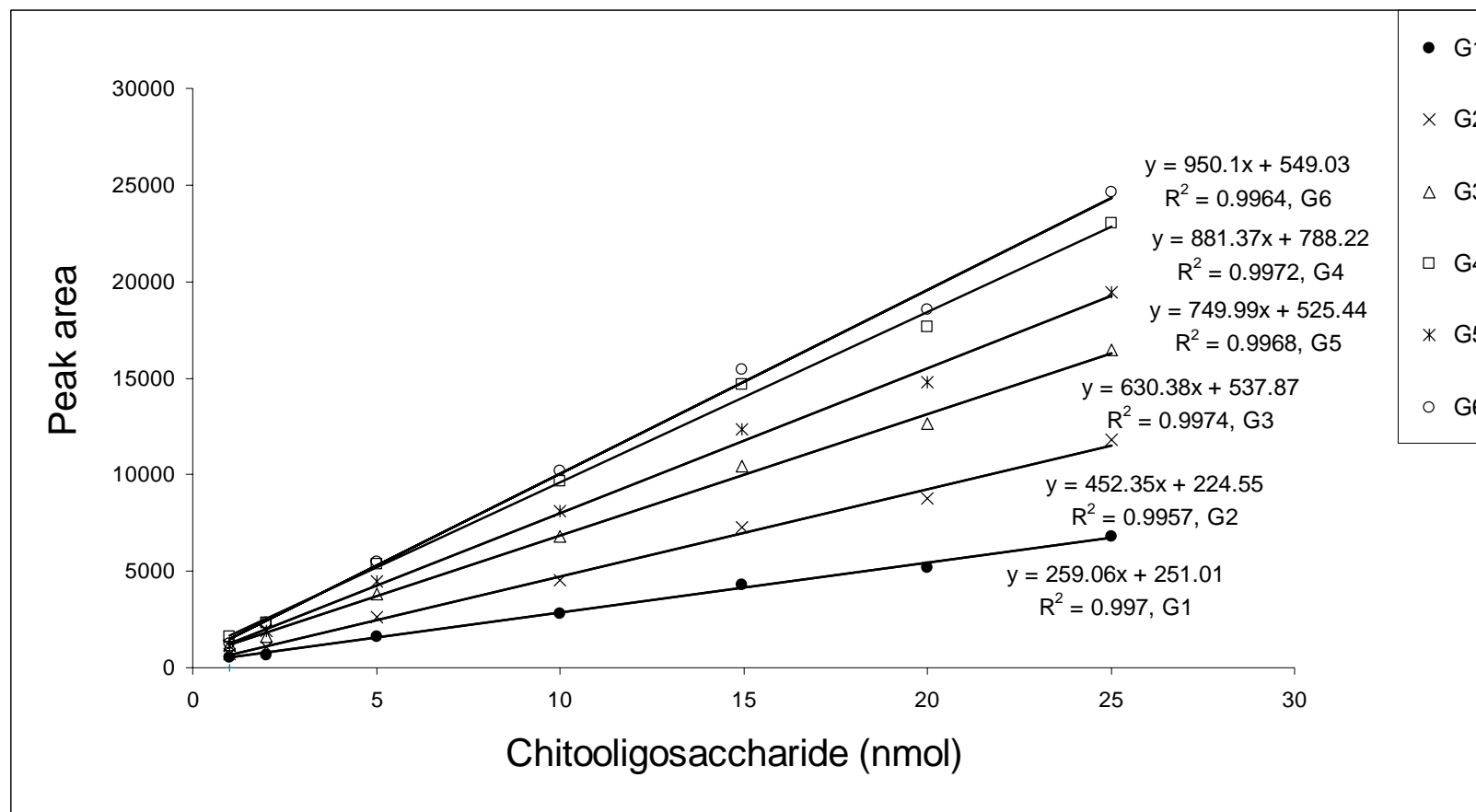
APPENDIX C

TYPICAL OBSERVATION IN A CRYSTALLIZATION

EXPERIMENT

Clear Drop

Skin/Precipitate

Precipitate

Precipitate/Phase

Quasi Crystals

Microcrystals

Needle Cluster

Plates

Rod Cluster

Single Crystal

APPENDIX D

STRUCTURES OF THE AMINO ACID SIDE CHAINS

AND ATOM DESIGNATION
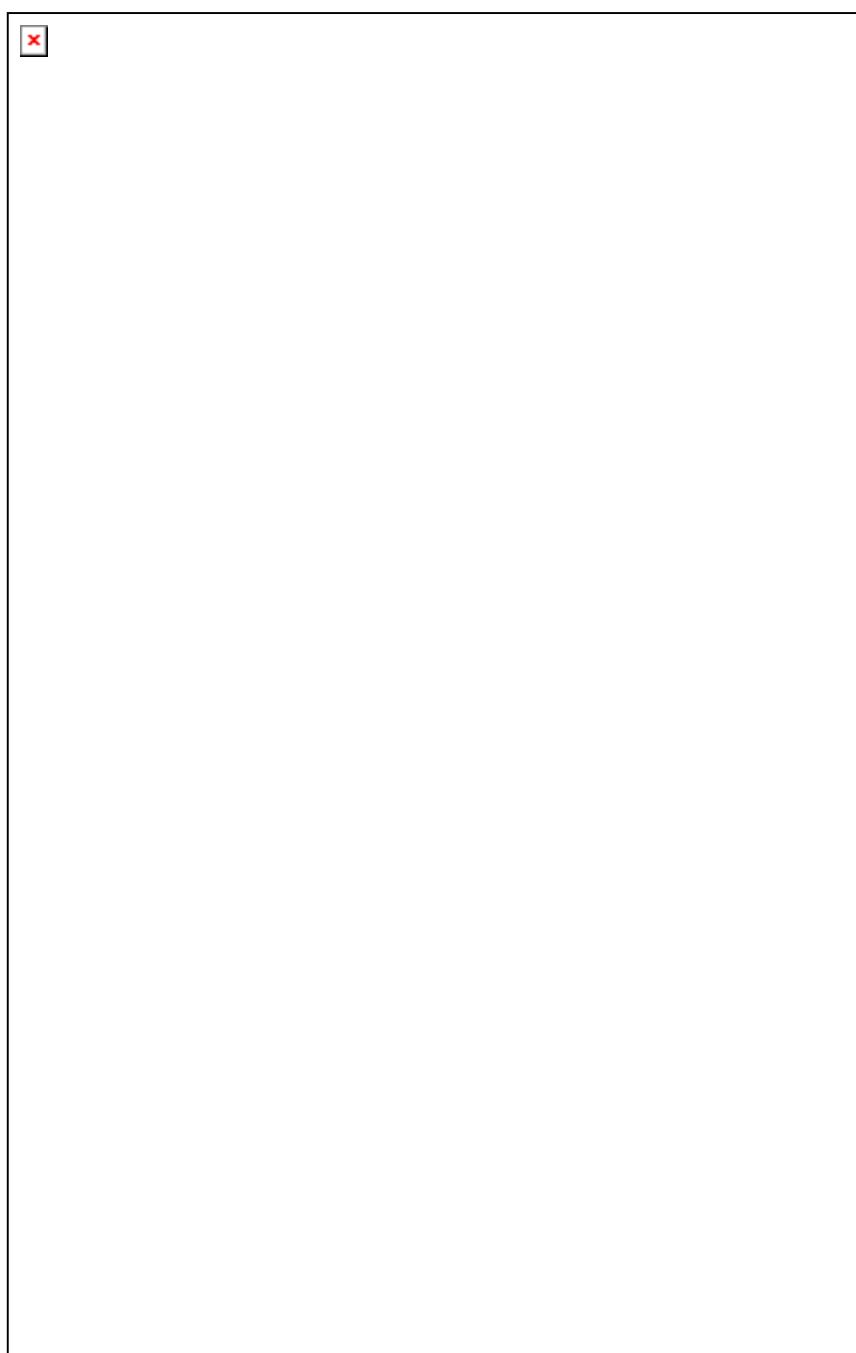
STRUCTURES OF THE AMINO ACID SIDE CHAINS

AND ATOM DESIGNATION (Continued)
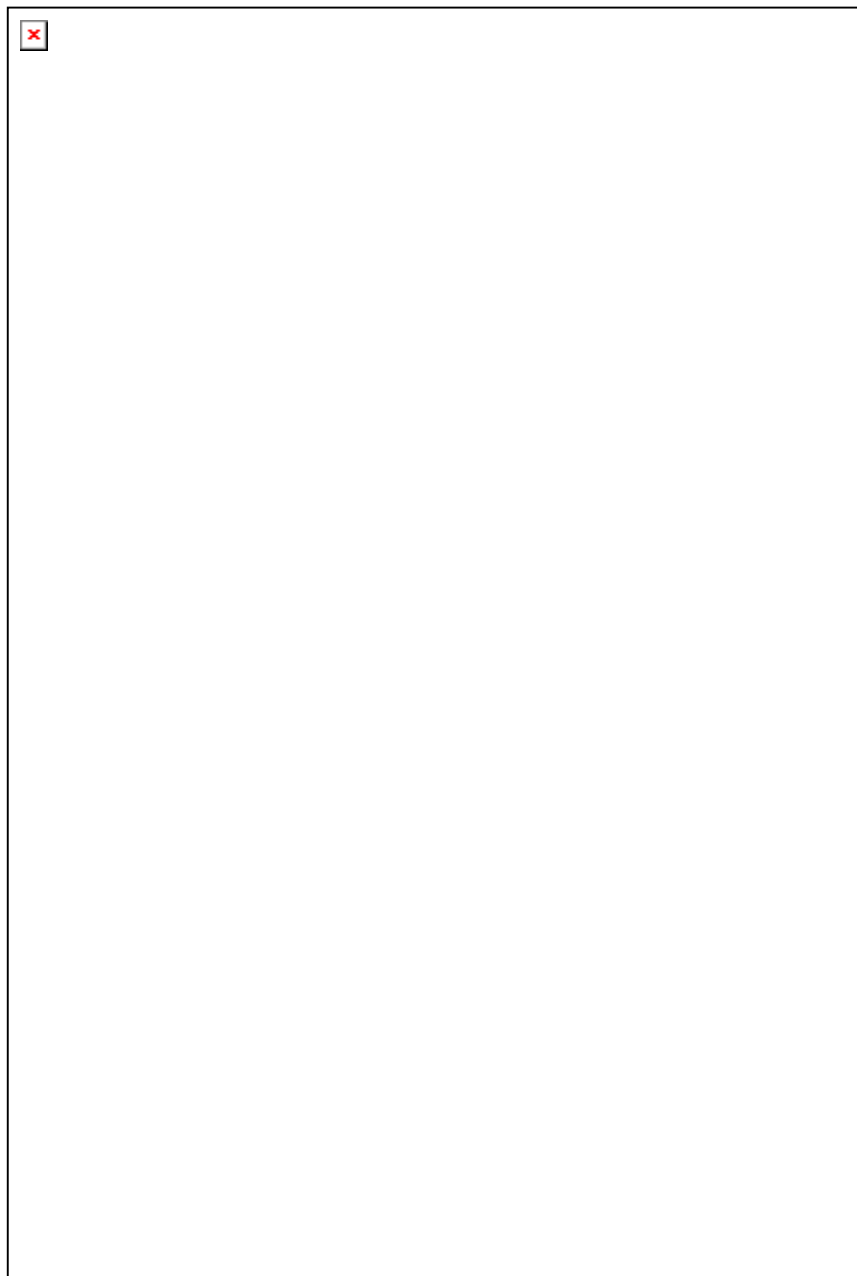
STRUCTURES OF THE AMINO ACID SIDE CHAINS

AND ATOM DESIGNATION (Continued)
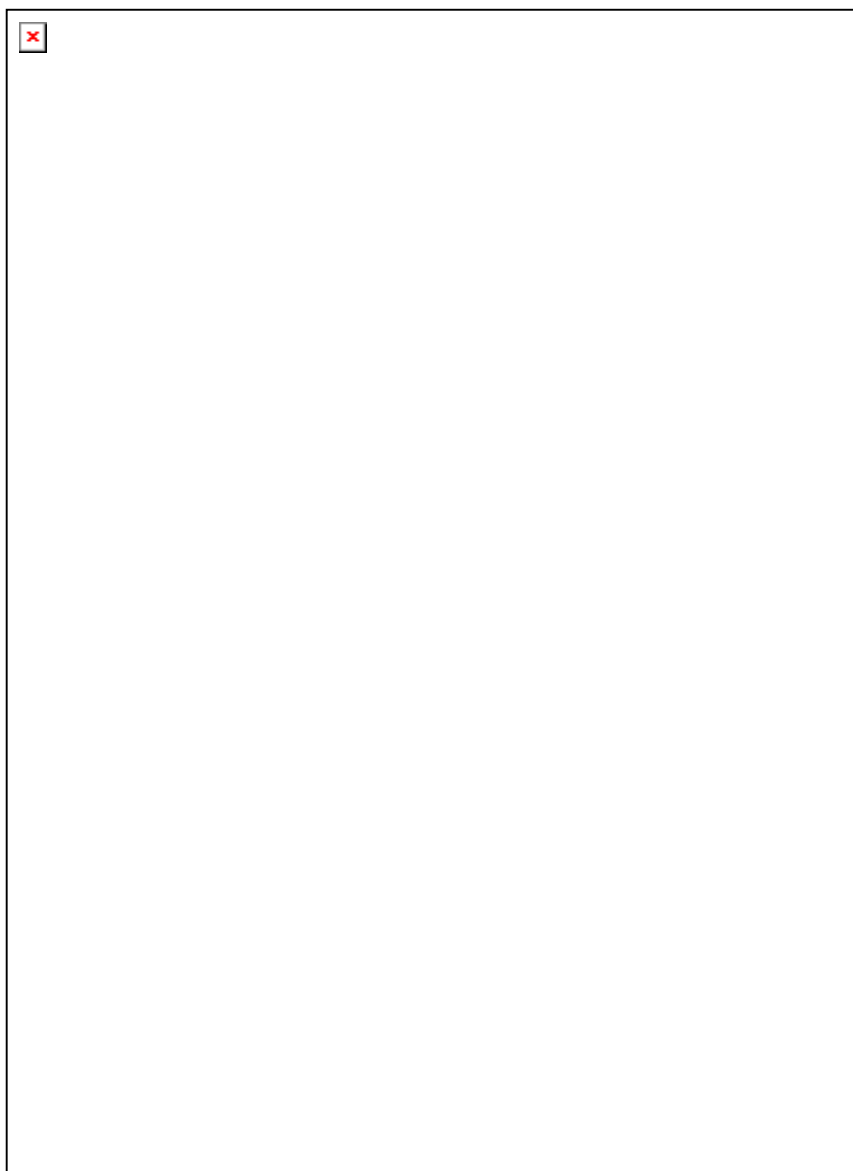
APPENDIX E

JOURNAL PUBLICATION

An endochitinase A from *Vibrio carchariae*: cloning, expression, mass and sequence analyses, and chitin hydrolysis

Wipa Suginta,[a,*] Archara Vongsuwan,[a] Chomphunuch Songsiriritthigul,[a] Heino Prinz,[b] Peter Estibeiro,[c] Rory R. Duncan,[d] Jisnuson Svasti,[e] and Linda A. Fothergill-Gilmore[f]

[a] *School of Biochemistry, Suranaree University of Technology, Nakhon Ratchasima 30000, Thailand*
[b] *Max Planck Institut für Molekulare Physiologie, Otto-Hahn-Str. 11, 44227 Dortmund, Germany*
[c] *ExpressOn BioSystems Ltd, Roslin BioCentre, Roslin EH25 9TT, UK*
[d] *Membrane Biology Group, University of Edinburgh, George Square, Edinburgh EH8 9XD, UK*
[e] *Center for Excellence in Protein Structure and Function, Department of Biochemistry, Faculty of Science, Mahidol University, Rama VI Road, Bangkok 10400, Thailand*
[f] *Institute of Cell and Molecular Biology, University of Edinburgh, Edinburgh EH9 3JR, UK*

Received 24 November 2003, and in revised form 25 January 2004

Abstract

We provide evidence that chitinase A from *Vibrio carchariae* acts as an endochitinase. The *chitinase A* gene isolated from *V. carchariae* genome encodes 850 amino acids expressing a 95-kDa precursor. Peptide masses of the native enzyme identified from MALDI-TOF or nanoESIMS were identical with the putative amino acid sequence translated from the corresponding nucleotide sequence. The enzyme has a highly conserved catalytic TIM-barrel region as previously described for *Serratia marcescens* ChiA. The M_r of the native chitinase A was determined to be 62,698, suggesting that the C-terminal proteolytic cleavage site was located between R^{597} and K^{598}. The DNA fragment that encodes the processed enzyme was subsequently cloned and expressed in *Escherichia coli*. The expressed protein exhibited chitinase activity on gel activity assay. Analysis of chitin hydrolysis using HPLC/ESI-MS confirmed the endo characteristics of the enzyme.
© 2004 Elsevier Inc. All rights reserved.

Keywords: Endochitinase; Gene isolation; Cloning; Gene sequence; TIM barrel; Gel activity assay; Chitin hydrolysis; HPLC-ESI MS

Chitin is a polymer of β-1,4 linked *N*-acetylglucosamine and is widely distributed in nature as a structural component of fungi, protozoa, insects, and crustaceans. Chitin is degraded by the sequential action of two hydrolytic enzymes: chitinases (EC 3.2.1.14), followed by *N*-acetylglucosaminidase (EC 3.2.1.30) [1]. Chitinases are a diverse family of enzymes found in a wide variety of organisms [2,3] and classified into glycosidase families 18 and 19, depending on their amino acid sequences [4,5]. Structural analyses of mutant chitinase A (SmChiA) from *Serratia marcescens* complexed with chitooligosaccharides [6] and of the fungal chitinase CiX1 from *Coccidioides immitis* complexed with a known chitinase inhibitor, allosamidin, [7] suggested a substrate-assisted catalytic mechanism for family 18 chitinases. The mechanism involves protonation of the leaving group by the catalytic residue (E^{315} in SmChiA or E^{171} in CiX1), followed by substrate distortion into a 'boat' conformation at subsite −1 and the stabilization of an oxazolinium intermediate by the sugar acetamido moiety. The experimental data that showed glycosidic bond cleavage by family 18 chitinases, yielding retention of β-anomeric configuration in the products, supported the mechanism obtained from the structural information [8–10]. The X-ray structures of the hevamine chitinase/lysozyme complexed with allosamidin [9] and of the *S. marcescens* ChiA mutants complexed with octa- and hexasaccharide substrates [6] indicated that the catalytic sites of these two enzymes contained six substrate binding subsites, designated subsites −4, −3, −2, −1, +1, and +2. The scissile glycosidic bond is located between subsites −1 and +1.

Two types of chitinases, exo- and endochitinases, have been distinguished and occur in both families. Exochitinase activity is defined as a progressive action that starts at the non-reducing ends of chitin chains and successively releases diacetylchitobiose units, while endochitinase activity involves random cleavage at internal points in chitin chains [11]. Based on the published 3D-structure information [12,13], the active site of family 18 endochitinases has a long, deep substrate-binding cleft with an opening on both sides. On the other hand, the active site of exochitinases has a tunnel-like morphology with a closure of the roof at the end of the tunnel [14,15].

The abundance of chitin has resulted in considerable interest in the possibilities of developing efficient bioconversion processes for recycling waste chitin based on chitinases. Marine bacteria are excellent sources of chitinases [16–19] and are potentially suitable sources of enzymes, especially for the recycling of waste crustacean chitin from the seafood industry. The highly insoluble polymer chitin is utilized rapidly as a sole source of carbon and nitrogen by marine bacteria, such as *Vibrios* [20]. The marine bacterium *Vibrio carchariae* is a particularly suitable source of chitinase A because it has been shown to express high levels of the enzyme within only 24 h of induction in the presence of chitin [21]. The enzyme is active as a monomer of M_t 63,000 as judged on SDS–PAGE. We report here the isolation of the gene encoding *V. carchariae* chitinase A and the determination of its sequence. The C-terminal proteolytic cleavage site of chitinase A was determined, permitting the gene that encodes chitinase A without the C-terminal proteolytic fragment to be cloned and functionally expressed in an *Escherichia coli* system.

Materials and methods

Bacterial strains and growth

A type strain of *V. carchariae* (LMG7890[T]) was obtained from the type culture collection at Laboratorium voor Microbiologie Gent, Rijksuniversiteit, Gent, Belgium, and was a gift from Professor B. Austin, Heriot-Watt University, Edinburgh, UK. It is relevant to mention that *V. carchariae* and *V. harveyi* are very similar taxonomically, and it has recently been proposed to combine them into a single species as *V. harveyi* [22]. However, we retain the designation *V. carchariae* because the two relevant type strains displayed different properties with regard to the expression of chitinase activity [21]. The bacterium was grown and kept in marine medium, pH 7.6 [23]. Swollen chitin [24] prepared from chitin flakes (Sigma Practical Grade from crab shells) was included in the culture media for induction of chitinase expression as indicated.

Immunological

Antisera against *V. carchariae* chitinase A were obtained from a female New Zealand rabbit. Purified chitinase (MonoQ fraction, 50 µl containing 150 µg chitinase) [21] was emulsified with 50 µl TiterMax Gold adjuvant (CytRx, Norcross, Georgia) according to the manufacturer's instructions and injected intramuscularly into two sites. Antisera were collected at the second, third, and fourth weeks after immunization, and no boosting injections were required. Western blotting was done with detection by enhanced chemiluminescence (ECL, Amersham).

Viscosity reduction assay

The viscosity reduction assay was carried out according to Khasin et al. [25]. The reaction mixture (0.5 ml) contained 2% (w/v) glycol–chitin solution [26], *V. carchariae* chitinase A (5 µg) purified according to Suginta et al. [21] or *S. marcescens* chitinase (Sigma) (5 µg), and 250 mM MES[1] buffer, pH 6.0. The reaction was incubated at room temperature in a viscometer No. 42 (0–0.16 ml), and the flow time of the reaction mixture was measured at time intervals: 0 min, 15 min, 30 min, 1 h, 2 h, 12 h, 24 h, and 48 h. Decrease in viscosity of glycol–chitin versus reaction times (h) was plotted by means of the average data values obtained from three separate experiments.

Construction of a V. carchariae expression library, cDNA cloning, and sequencing

DNA fragments of 4–7 kb were isolated from a partial *Sau*3 AI digest of *V. carchariae* genomic DNA prepared using the protocol of Ausubel et al. [27], ligated into the *Bam*HI site of pBluescript II KS(−), and transformed into *E. coli* type strain XL1 blue (Stratagene) by standard techniques. The library of 2100 transformants was screened for the expression of chitinase antigen using anti-chitinase A polyclonal antibodies. Positive clones were analyzed by restriction mapping, chitin plate assay, and Western blotting. Partial DNA sequencing was done manually by the dideoxy method according to the Sequenase PCR sequencing kit (USB) using T7 forward primer and SP6 reverse primer. Automated double-stranded DNA sequencing was carried out commercially by Oswel, Southampton, UK. The putative amino acid

---

[1] *Abbreviations used:* MES, 2-(4-morpholino)-ethanesulfonic acid; (GlcNAc)₂, *N,N'*-diacetylchitobioside; (GlcNAc)₃, *N,N',N''*-triacetylchitotrioside; (GlcNAc)₄, *N,N',N'',N'''*-tetraacetylchitotetraoside; IPTG, isopropylthiogalactoside; PMSF, phenylmethylsulfonyl fluoride; DMAB, *p*-dimethylaminobenzaldehyde; MALDI-TOF, matrix-assisted laser desorption ionizsation/time-of-flight; HPLC/ESI-MS, high performance liquid chromatography and electrospray mass spectrometry; SIM, single ion monitoring.

sequence of chitinase A was obtained from the back translation software in the DNA Star package. The signal peptide was predicted using SignalP V.1.1 program (http://www.cbs.dtu.dk/services/SignalP/). The nucleotide sequence of chitinase A has been deposited in the GenBank database under GenBank Accession No. Q9AMP1.

Amino acid sequence comparisons

The amino acid sequence alignment was made using "CLUSTALW" algorithm in a GCG package [28] and displayed using the Genedoc program (http://www.psc.edu/biomed/genedoc/). The putative *V. carchariae* chitinase A sequence was compared with three highly similar bacterial ChiA amino acid sequences available in the Swiss-Prot or TrEMBL database (http://us.expasy.org/). These sequences included *Altermonas* sp. strain O-7 (Accession No. P32823), *Pantoea* (*Enterobacter*) *agglomerans* (accession number P97034), and *S. marcescens* (accession number Q54275). Consensus motifs were analyzed based on the secondary structure of *S. marcescens* ChiA [13].

Mass analysis of the native chitinase A and its tryptic peptides

Chitinase A (2 μg) was applied in parallel onto a 12% SDS–PAGE gel using a Laemmli buffer system [29]. Following electrophoresis, protein was stained with Coomassie blue. After destaining, protein bands were excised from the gel and in-gel digested with trypsin (sequencing grade, Roche Diagnostics, Mannheim) using a standard protocol [30]. After overnight digestion at 37 °C, the peptides were extracted and dried in a SpeedVac vacuum centrifuge. A small fraction of these tryptic peptides was analyzed by high resolution MALDI-TOF MS (Voyager-DE Pro in reflective mode) in an α-cyano-4-hydroxycinnamic acid matrix for the peptide "mass fingerprinting". The majority was analyzed by nanoESI/MS (Thermo Finnigan LCQ Deca) using the proprietary "triple play" mode for obtaining MS/MS sequence information for the relevant peptides. Data bank searching was performed with "MS-Fit" (http://prospector.ucsf.edu/) for MALDI mass fingerprint data and with "Sequest search" (http://fields.scripps.edu/sequest/index.html). Mass spectra of intact protein were obtained with linear MALDI-TOF (Voyager-DE Pro) using sinapinic acid (3,5-dimethoxy-4-hydroxycinnamic acid) as the matrix.

Cloning of the DNA encoding C-terminally processed chitinase A

Two flanking primers were designed according to the nucleotide sequence of the *chitinase A* gene and com-

patible with cloning sites of the pQE60 expression vector (Qiagen). The forward primer included a *Nco*I cloning site, following the oligonucleotides that encode the chitinase A signal peptide. The reverse primer included a *Bgl*II cloning site, following the oligonucleotides encoding the C-terminal region starting from R[597]. The primer sequences are:

*Nco*I
N-terminal: 5′-TATGCCATGGTAATTCGATTTACCTATG-3′
C-terminal: 5′-GAAGATCTACGGTTTGGTGGGGTAACGAC-3′
*Bgl*II

Thirty cycles of PCR were carried out using *Taq* DNA polymerase (Promega) with the following temperature profile: denaturation at 95 °C for 30 s, annealing at 55 °C for 30 s, and extension at 72 °C for 1 min except for the final cycle where extension proceeded for 7 min. A 1.7-kb amplified PCR product was purified using a DNA gel extraction kit (Qiagen) following the manufacturer's instructions. The purified fragment (5 μg) was then ligated to the pDrive cloning vector (Qiagen) and transformed into *E. coli* DH5α. The recombinant plasmid was prepared using the plasmid miniprep kit according to Qiagen's standard protocol. The plasmid was digested with *Nco*I and *Bgl*II, and then inserted into the *Nco*I/*Bgl*II sites of the pQE60 vector. The chitinase A lacking the C-terminal proteolytic cleavage fragment was expressed under the T5 promoter/*lac* operator element in *E. coli* type strain M15. Using such a vector system, the protein contained six histidine residues tagged at the C-terminal region.

Purification of chitinase A

Chitinase A secreted by *V. carchariae* culture was purified according to Suginta et al. [21]. Briefly, *V. carchariae* was grown at 30 °C in a marine medium. Swollen chitin (2.5% (w/v)) was added to induce chitinase expression. After about 40 h, the growth medium was collected by centrifugation. Swollen chitin was also used in the first step of the enzyme purification using chitin affinity chromatography. Binding of the secreted chitinase to chitin was carried out batchwise by adding 25 g of swollen chitin to a 2-L growth medium of *V. carchariae* and stirred for 5 min at 4 °C, and then the chitinase-bound chitin was collected by centrifugation. After washing with sodium carbonate buffer (pH 8.5) followed by sodium acetate buffer (pH 5.5), the enzyme bound to chitin was eluted with 2 M guanidine HCl and dialyzed immediately against 20 mM sodium phosphate buffer, pH 7.0, to remove guanidine HCl. The protein precipitated by 35–80% saturated ammonium sulfate was dissolved in 2 ml of the dialysis buffer containing 100 mM NaCl and then applied to a Sephacryl S300 HR column. Fractions containing chitinase activity were pooled, concentrated, and then reapplied to the same Sephacryl S300 HR column to further remove minor

contaminants. Chitinase-containing fractions were combined, concentrated using a vacuum centrifuge concentrator, and then stored at −30 °C. Chitinase activity was determined colorimetrically using DMAB method [31]. Protein concentrations were determined by Bradford's method [32]. Unless otherwise stated, experiments were carried out at 4 °C throughout the purification steps. For purification of chitinase A expressed in *E. coli* M15, the bacterial cells carrying the recombinant pQE60 plasmid were grown at 37 °C in LB medium containing 100 µg/ml ampicillin to an OD_{600} of about 0.6, and then IPTG was added to a final concentration of 0.5 mM. Incubation was continued at 25 °C for 5 h with shaking before harvesting the cells by centrifugation at 2500g for 20 min. The cells were resuspended in 15 ml of 20 mM Tris–HCl buffer, pH 8.0, containing 150 mM NaCl, 1 mM PMSF, and 1 mg/ml lysozyme. The suspended cells were kept on ice and broke open using an ultrasonicator (30 s, 6–8 times). Unbroken cells and cell debris were removed by centrifugation. The supernatant containing soluble chitinase A was purified using Ni–NTA agarose chromatography according to Qiagen's protocol. Fractions eluted with 250 mM imidazole, which contained soluble chitinase A, were pooled and concentrated using Vivaspin membrane concentrators (MW cut-off 10,000). Further purification was performed using an ÄKTA purifier system (Amersham Biosciences) on a Superdex S-200 HR 10/30 column (1.0 × 30 cm) using 20 mM Tris–HCl buffer, pH 8.0, containing 150 mM NaCl as running buffer. A flow rate of 250 µl/min was applied and fractions of 500 µl were collected. Chitinase-containing fractions were combined and stored at −30 °C until use.

Chitinase activity assay following SDS–PAGE

Chitinase A expressed in *E. coli* (2 µg) was treated with gel loading buffer without β-mercaptoethanol and electrophoresed in 12% polyacrylamide gel containing 0.1% glycol–chitin. After electrophoresis, the gel was washed at 37 °C for 1 h with 250 ml of 150 mM sodium acetate, pH 5.0, containing 1% Triton X-100 and 1% skimmed milk, followed by the same buffer without 1% skimmed milk for another hour to remove SDS and to allow the proteins to refold. The gel was stained with Calcofluor white M2R (0.01%) (Sigma) in 500 mM Tris–HCl, pH 8.5, and visualized under UV [33].

HPLC/ESI-MS analysis of chitin hydrolysis of chitinase A expressed in E. coli

Chitin hydrolysis was carried out in 50 mM ammonium acetate buffer, pH 7.1, at 20 °C with shaking. The concentrations of chitinase A and colloidal chitin suspension [34] were 750 ng/µl and 100 µg/ml, respectively. The reactions were quenched with 10% (v/v) acetic acid. Following a centrifugation at 5 °C, the supernatant containing chitooligosaccharide products formed after 5 min was immediately injected into a 150 × 2.1 mm (5 µm) Hypercarb HPLC (ThermoQuest, USA). The column was connected to an Agilent Technologies 1100 series HPLC system under the control of a Thermo Finnigan LCQ DECA electrospray mass spectrometer. The HPLC was operated at particularly low temperature (10 °C) and detected by ESI-MS. ESI-MS was conducted in positive single ion mode (SIM mode). Mass-to-charge ratios (m/z) of expected oligosaccharides were selected as follows: GlcNAc (221.9), $(GlcNAc)_2$ (425.5), $(GlcNAc)_3$ (627.6), $(GlcNAc)_4$ (830.8), $(GlcNAc)_5$ (1034.0), $(GlcNAc)_6$ (1237.2), and $(GlcNAc)_7$ (1440.0). Identification of β- and α-anomers was assessed from previous experiments with equivalent reverse-phase HPLC system and ^{1}H NMR [8].

Results and discussion

V. carchariae chitinase A is an endochitinase

The rate of glycol–chitin hydrolysis by *V. carchariae* chitinase A was determined using the viscosity reduction assay (Fig. 1) [25]. Prior to hydrolysis, the viscosity of the reaction mixture was high due to the presence of very long chains of the substrate polymer. In the first hour after adding chitinase, the viscosity dropped rapidly due to digestion of chitin by the added chitinase enzyme, leading to rapid breakdown of the polymer chains. A subsequent more gradual decrease in the vis-
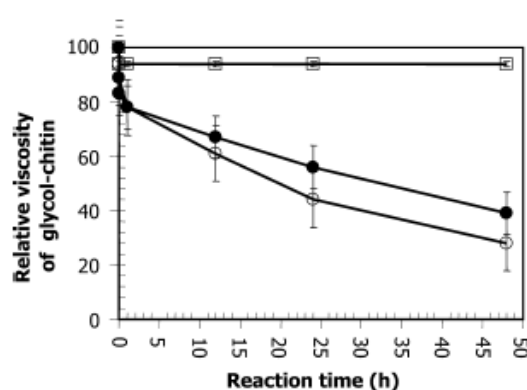
Fig. 1. Enzymatic viscosity reduction assay using glycol–chitin. Purified chitinase A (5 µg) was incubated with 2% (w/v) glycol–chitin solution at room temperature. The viscosity of glycol–chitin was measured at different time intervals from 0 min to 48 h. Reactions with *S. marcescens* chitinase (○), reactions with *V. carchariae* chitinase (●), and reactions without enzyme (□). Data are shown as means ± SEM (*n* = 3 for each protein).

cosity of the glycol–chitin solution was observed after 1 h of the hydrolytic reaction, at which time chitooligomers generated during initial hydrolysis were presumably further degraded into end products. However, the degradation of short intermediates appeared to have a less dramatic effect on the solution viscosity, compared to the initial viscosity change due to the hydrolysis of the long-chain substrate. After 48 h, the reaction became very slow and still did not reach complete hydrolysis. This might result from inhibition of the enzyme activity by high concentrations of the accumulated products.

A rapid reduction in viscosity at the very early stage of reaction indicated that the *V. carchariae* chitinase A has a characteristic endochitinase activity. The enzyme appears to be able to randomly cleave internal β-glycosidic bonds of the substrate polymer, leading to a rapid decrease in the chain length of the dissolved polymer and a rapid decrease in solution viscosity. Exochitinase activity, in contrast, would break down the polymer chains sequentially dimer by dimer from the non-reducing end, at a relatively constant rate over time [11]. Thus, a slow and steady reduction in viscosity would be expected upon addition of enzyme. Endochitinase activity was supported by results from paper chromatography (not shown) in which minor products: GlcNAc, $(GlcNAc)_3$, and $(GlcNAc)_4$, were detected along with the major product $(GlcNAc)_2$. These findings were later confirmed by analysis of the products of chitin hydrolysis by HPLC-MS, showing the production of chitosaccharide products ranging from GlcNAc to $(GlcNAc)_7$. The characteristic endochitinase activity was also observed for *S. marcescens* chitinase A (Fig. 1), which contrasts with a previous suggestion that *S. marcescens* chitinase A is an exochitinase [35].

Isolation of clones carrying the chitinase A gene

The genomic library consisting of 2100 colonies was screened for the expression of chitinase antigen, and six single colonies gave positive signals, and could be isolated. The library was estimated to correspond to 1.3 genome equivalents by assuming that the size of the *V.*

carchariae genome is the same as that of *E. coli* $(4.2 \times 10^6 \text{ bp})$ [36]. The positive clones were cultured individually in the presence or absence of swollen chitin, and samples of cell extracts and culture supernatants were examined by Western blotting (Fig. 2). It can be seen that all six clones expressed chitinase antigen in the cell extracts, with highest expression in the presence of the swollen chitin inducer (Fig. 2B and D). Clone P3C1 gave the highest expression, but apparently only in the presence of swollen chitin.

The M_r observed for the chitinase antigen expressed in *E. coli* was approx. 95,000, whereas that for chitinase purified from *V. carchariae* was 63,000 [21]. The expression pattern in the culture supernatants showed a much greater bias in favor of induced expression than the cell extracts, as only very faint signals were found in the absence of swollen chitin (Fig. 2A and C). Moreover, only four of the six clones (clones P2C1, P2C2, P2C3, and P3C1) appeared to give secretion into the culture supernatant, and only these four clones exhibited chitinase activity on a chitin agar plate (not shown). Immunoblotting of both fractions from untransformed *E. coli* cells showed no expression of chitinases upon induction with chitin (not shown). Expression of the 95-kDa chitinase in response to chitin implies that all the clones carried a DNA insert that contains the *chitinase A* gene with its own control element (a *ChiA* promoter) (Fig. 3).

Nucleotide sequence analysis

Restriction mapping with *Eco*RI showed that all the clones typically carried apparently identical 5.5-kb inserts, with the exception of clone P3C1 that had a 4.0-kb insert. Because P3C1 contained the smallest DNA fragment, it was therefore chosen for sequence analysis. DNA sequence determination of 100 bp at the 5′ end of the insert in clone P3C1 showed 76% sequence identity to the corresponding region of *ChiA* from *S. marcescens* [37]. The P3C1 clone was later fully analyzed to give the complete sequence (Fig. 3). The *chitinase A* gene contains a putative open reading frame of 2550 bases
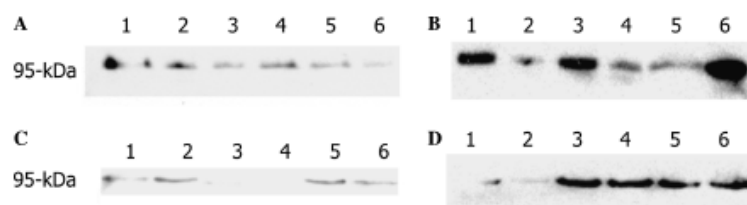
Fig. 2. Western blot analysis of clones expressing chitinase antigen. Single colonies were grown in the presence or absence of 1% (w/v) swollen chitin, and cell extracts and culture supernatants were prepared. The proteins present in these samples were analyzed by Western blotting. (A) Cell extracts, absence of swollen chitin; (B) cell extracts, presence of swollen chitin; (C) culture supernatants, absence of swollen chitin; and (D) culture supernatants, presence of swollen chitin. The tracks had the following clones: 1, P1C1; 2, P1C2; 3, P2C1; 4, P2C2; 5, P2C3; and 6, P3C1 (nomenclature: P refers to the number of the culture plate and C to the colony number).

W. Suginta et al. / Archives of Biochemistry and Biophysics 424 (2004) 171–180
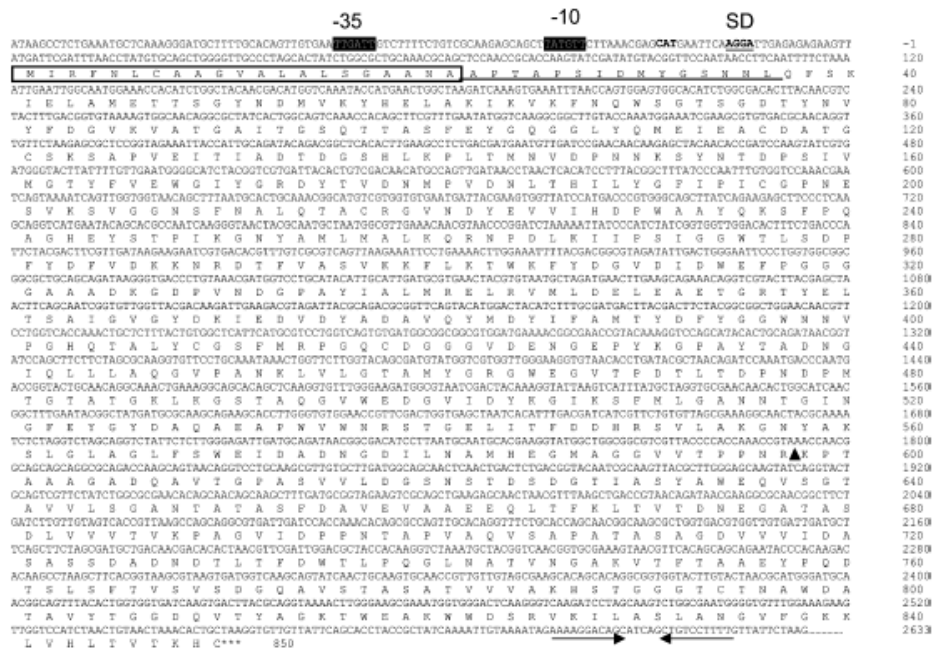
Fig. 3. Determination of the DNA sequence of the *V. carchariae* chitinase gene. Essential elements of the *chitinase A* gene comprise: (i) the −10 and −35 regions of a possible promoter sequence (highlighted); (ii) transcription start site (bold); (iii) the putative ribosome-binding site (AGGA) (bold and underline); (iv) the signal peptide containing 21 amino acids (boxed); (v) the structural *chitinase A* gene; (vi) the termination codon TAA (asterisks); and (vii) the putative inverted-repeat sequence downstream of the termination codon (horizontal arrows). The N-terminal sequence of secreted chitinase A determined by microsequencing [21] is underlined. The predicted C-terminal proteolytic cleavage site is indicated by a triangle.

starting at the ATG codon, ending with the stop codon TAA, and encodes 850 amino acid residues. The ATG initiation codon is preceded by a Shine–Dalgarno sequence (AGGA) that is identical to that of the ribosome binding site in the chitinase gene of *Enterobacter agglomerans* [38]. Typical promoter sequences [39] were found at the −35 region (TTGATT) and the −10 region (TATGTT), although the distance between these two sites is longer than customary (24 bp instead of 17 bp). The sequence at the −10 region is identical to that in the *E. coli lac* operon promoter. An inverted repeat sequence (AAAAGGACAGC- - - -GCTGTCCTTTT) is located 44 nucleotides downstream from the termination codon.

The chitinase precursor has a typical N-terminal secretion signal peptide of 21 residues with a positively charged arginine near the N-terminus followed by a hydrophobic region. It is especially rich in alanine (36%) and leucine (14%) [40]. A signal-sequence cleavage site was predicted by the Signal P V1.1 program as described in Materials and methods to be located between A^{21} and A^{22}, and corresponded precisely with the N-terminal sequence of the mature chitinase secreted by *V. carchariae* as determined by microsequencing [21]. Alanine has also been found to be on the N-terminal side of the

signal peptide cleavage site in other bacterial chitinases [38,41,42].

Amino acid sequence analysis

The deduced amino acid sequence of chitinase A from *V. carchariae* was compared with other bacterial ChiA sequences. The putative mature chitinase A showed highest identity with ChiA from *Vibrio parahaemolyticus* (94%), followed by ChiA from *Serratia liquefaciens* (48%), ChiA from *Alteromonas* sp. (47%), and ChiA from *Enterobacter* sp. (47%), ChiA from *S. marcescens* (47%), and ChiA from *Pantoea agglomerans* (44%). *V. carchariae* chitinase A aligned with ChiA from *Bacillus circulans* with low identity (18%). Fig. 4 shows the amino acid sequence comparison of *V. carchariae* chitinase A with *Alteromonas* sp ChiA, *P. agglomerans* ChiA, and *S. marcescens* ChiA. The secondary structure of the *S. marcescens* ChiA structure is also shown to locate the positions of an N-terminal chitin binding domain connected with a small hinge region, a typical $(\alpha/\beta)_8$ TIM barrel catalytic domain, and an extra $\alpha + \beta$ domain. As expected, bacterial chitinase A appears to be highly conserved in the catalytic region, with two completely conserved motifs SxGG (located in the β3
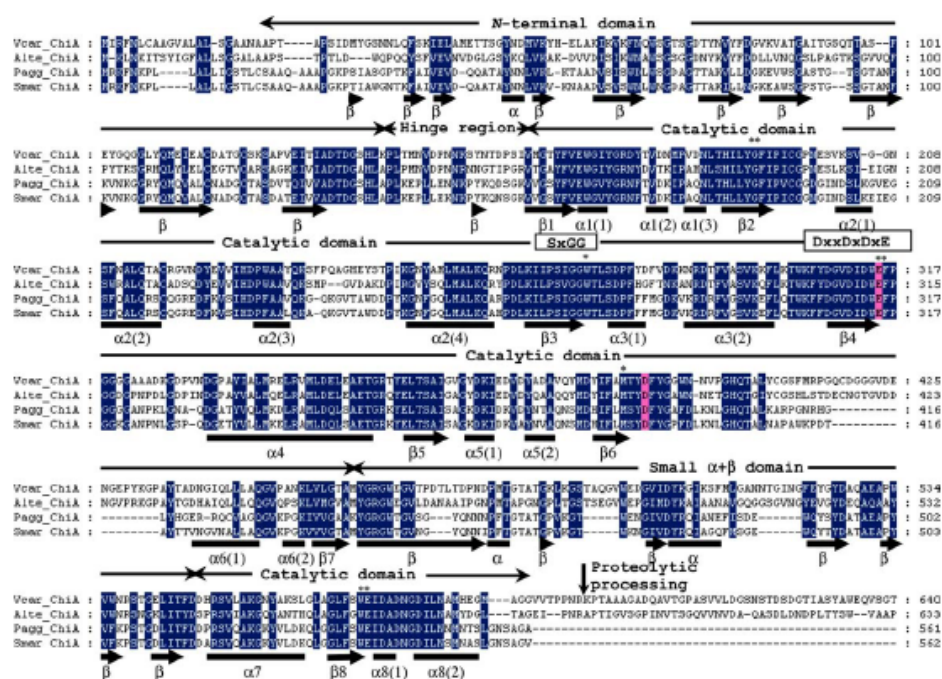
Fig. 4. Alignment of *V. carchariae* chitinase A with other bacterial chitinase A sequences. Bacterial chitinase A sequences were retrieved from the Swiss-Prot/TreEMBL protein databases, aligned using "CLUSTALW" and displayed in Gendoc. The secondary structure elements are those observed in the crystal structure of *S. marcescens* ChiA [13]. Completely conserved regions are shaded in dark blue and the catalytic residues in magenta. The amino acid residues that are suggested to form three cis peptide bonds or to provide hydrophobic environments in the active site of *S. marcescens* ChiA are indicated (asterisks). Key: Vcar_ChiA: chitinase A from *V. carchariae* (*harveyi*) (Q9AMP1); Alte_ChiA: ChiA from *Alteromonas* sp. strain O-7 (P32823); Pagg_ChiA: ChiA from *Pantoea* (*Enterobacter*) *agglomerans* (P97034); and Smar_ChiA: ChiA from *S. marcescens* (P07254, Q54275): ▶: β-strand ▬▬: α-helix.

strand) and DxxDxDxE (located in the β4 strand) within the TIM barrel catalytic domain. These motifs have been found in all family 18 chitinases [14].

Amino acid residues that were suggested to form three *cis* peptide bonds (equivalent to residues G^{190}–F^{191}, E^{315}–F^{316}, and W^{539}–E^{540}) or to provide hydrophobic environments (equivalent to residues F^{191}, W^{275}, F^{316}, and M^{388}) in the active site of *S. marcescens* ChiA are completely conserved in all the aligned sequences (Fig. 4).

C-terminal proteolytic cleavage site of V. carchariae chitinase A

The ensemble of peptides, which were eluted from in-gel digestion of chitinase A, was analyzed by means of MALDI-TOF or nanoESI mass spectrometry and subjected to a data-bank search. This process, commonly denoted as mass fingerprinting, resulted in an unambiguous match of this protein to the chitinase A gene (Table 1). Moreover, the molecular mass of peptide T1 (2040.7) agreed well with the theoretical mass (2040.0) of the N-terminal peptide identified previously by microsequencing [21]. In addition, peptide T39, identified as being

nearest to the C-terminus, had a mass of 551.0, which matched the mass of the tryptic peptide sequence GNYAK.

The chitinase A precursor had a calculated M_r of 90,249, which was slightly less than indicated by SDS–PAGE (95,000). Because the chitinase precursor was inactive and its molecular mass was approx. 23 kDa larger than the native enzyme, the precursor must be cleaved by a proteinase in *V. carchariae* to form the active 63-kDa enzyme. MALDI-TOF measurement yielded a peak of M_r 62,698 (Fig. 5), which corresponded to the mass of chitinase A predicted to end at R^{597} (calculated M_r 62,718.12). C-terminal processing has also been detected in other chitinases, for example, in two *Serratia* chitinases: a 52-kDa chitinase cleaved between F^{324} and K^{325} to produce an active proteolytic 35-kDa product, and a 54-kDa chitinase cleaved between I^{482} and T^{483} to produce an active proteolytic 22-kDa product [43,44]. The 59-kDa chitinase isolated from *Streptomyces olivaceoviridis* was also found to be proteolytically processed to a 47-kDa truncated chitinase lacking the chitin binding domain [45]. However, chitinases from *Aeromonas hydrophila* [46] and

Table 1
Mass identification of tryptic peptides of *V. carchariae* chitinase A by MALDI-TOF or nanoESI mass spectrometry

Position in the sequence[a]	Tryptic peptide	Expected mass	Observed mass	Peptide AA sequence
22–40	T1	2040.0	2040.7	APTAPSIDMYGSNNLQFSK
41–56	T2	1800.8	1800.5	IELAMETTSGYNDMVK
57–62	T3	759.4	759.3	YHELAK
67–86	T6	2284.0	2283.8	FNQWSGTSGDTYNVYFDGVK
124–151	T8	2976.5	2976.6	SAPVEITIADTDGSHLKPLTMNVDPNNK
152–173	T9	2554.2	2553.6	SYNTDPSIVMGTYFVEWGIYGR
204–218	T11	1523.7	1523.6	SVGGNSFNALQTAC
219–236	T12	2103.0	2102.8	GVNDYEVVIHDPWAAYQK
237–250	T13	1560.8	1560.7	SFPQAGHEYSTPIK
251–262	T14 + T15	1394.7	1394.5	GNYAMLMALKQR
268–288	T17 + T18	2397.2	2397.0	IIPSIGGWTLSDPFYDFVDKK
289–298	T19 + T20	1135.6	1135.6	NRDTFVASVK
303–326	T23 + T24	2601.2	2601.2	TWKFYDGVDIDWEFPGGGGAAADK
327–341	T25	1587.8	1587.6	GDPVNDGPAYIALMR
345–356	T27	1361.7	1361.7	VMLDELEAETGR
454–463	T31	1079.6	1079.6	LVLGTAMYGR
464–487	T32	2460.1	2460.1	GWEGVTPDTLTDPNDPMTGTATGK
488–505	T33 + T34	1965.0	1964.8	LKGSTAQGVWEDGVIDYK
509–538	T36	3377.5	3378.5	SFMLGANNTGINGFEYGYDAQAEAPWVWNR
539–550	T37	1389.7	1389.6	STGELITFDDHR
551–555	T38	516.3	516.5	SVLAK
556–560	T39	551.3	551.3	GNYAK

[a] Unidentified peptides are not included.
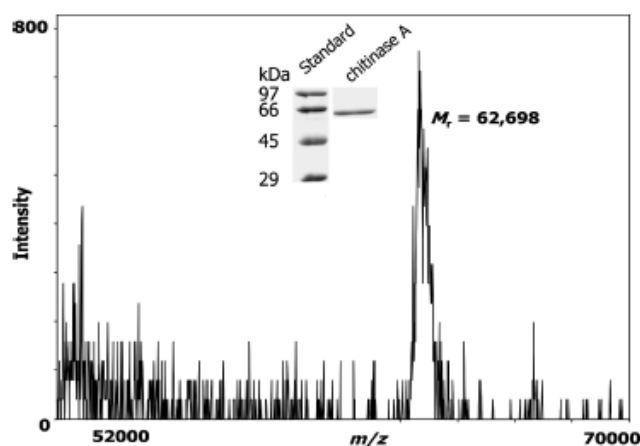
Fig. 5. MALDI-TOF spectrogram of chitinase A purified from *V. carchariae*. The purified *V. carchariae* chitinase A (2 μg) was mixed in serial dilutions (1/10) with sinapinic acid, 1 mg/ml in 0.3% TFA/ACN (1:1) and deposited on a stainless steel sample stage. After rapid drying, samples in crystalline form were submitted for Voyager Elite MALDI-TOF (linear mode).

Alteromonas sp. [41] are expressed as large proteins (866 and 820 residues, respectively), and apparently are not subjected to C-terminal processing.

Expression of chitinase A in E. coli

Chitinase A expressed in *E. coli* as the unprocessed precursor was much less active than the enzyme purified from *V. carchariae*. Taking advantage of the M_r of the native enzyme obtained from MALDI-TOF measurement, two oligonucleotides were designed to generate the mature protein without the 23-kDa C-terminal proteolytic peptide (see Materials and methods). A 1.7-kb DNA fragment encoding the C-terminally processed chitinase A was cloned into pDrive cloning vector and later transferred to the pQE60 expression vector. The protein was expressed under the T5 promoter in *E. coli* M15 under optimized conditions with high yield (~10 mg/100 ml culture).

Using such a system, the expressed chitinase was a hybrid protein with six histidines tagged at the C-terminus. The protein was purified using Ni–NTA agarose

affinity chromatography, followed by Superdex-S200 HR FPLC (Fig. 6, lane 1). Electrospray MS confirmed the M_r of the expressed protein to be 63,823 ($\pm$15), corresponding to the calculated M_r of the mature chitinase (62,718.12 Da) plus two additional amino acids: arginine and serine (260.27 Da). These amino acids were encoded by the six nucleotides (AGATCT) corresponding to the *Bgl*II cloning site following the codon of
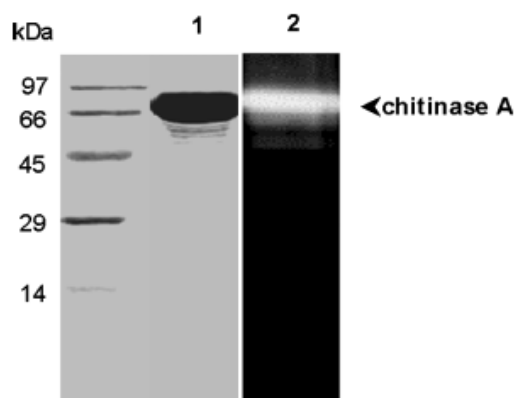

Fig. 6. Gel activity assay of the chitinase A expressed in *E. coli*. The purified chitinase A (3 μg) was electrophoresed in 12% SDS–PAGE. After electrophoresis, protein bands were stained with Coomassie blue (lane 1). In the case of the gel activity assay (lane 2), the protein was prepared in the absence of β-mercaptoethanol and was not heated prior to subjecting to SDS–PAGE gel in the presence of glycol–chitin. The gel was stained for chitinase activity using fluorescent Calcoflour white M2R.

R^{597} of the mature chitinase A (see Fig. 3) and formed a link to the C-terminal histidine tag residues (839.85 Da). The total calculated mass of the expressed protein is therefore 63,818.24 Da. The expressed protein exhibited chitinase activity using the gel activity assay with glycol–chitin substrate (Fig. 6, lane 2).

As analyzed by HPLC/ESI-MS, chitinase A expressed in *E. coli* was able to hydrolyze colloidal chitin. Fig. 7 shows a HPLC-MS chromatogram of chitooligosaccharide products acquired after 5 min of reaction time. The enzyme degraded chitin polymer releasing chitooligosaccharide products ranging from GlcNAc to $[GlcNAc]_7$ with $[GlcNAc]_2$ as the major product (>80% of the total products). Although $[GlcNAc]_5$ and $[GlcNAc]_7$ were not clearly seen in the HPLC-MS chromatogram, their molecular masses were certainly observed in the MS spectrum (Fig. 7 inset). The release of chitooligosaccharide products with various sizes confirmed the endo characteristic of *V. carchariae* chitinase A.

With the HPLC system used, the β- and α-anomers were also separated. The cleavage pattern was assessed from a separation profile of chitooligosaccharides as previously been published using reverse-phase HPLC and ^{1}H NMR [8]. The earlier appearing peak represented the β-anomer and the later peak corresponded to the α-anomer of the oligomeric products. Production of higher level of the β- over α-anomers at initial stage of reaction indicated that the hydrolysis of chitin polymer by chitinase A is employing a mechanism that is in an agreement with the substrate-assisted catalysis as suggested earlier [6,7].
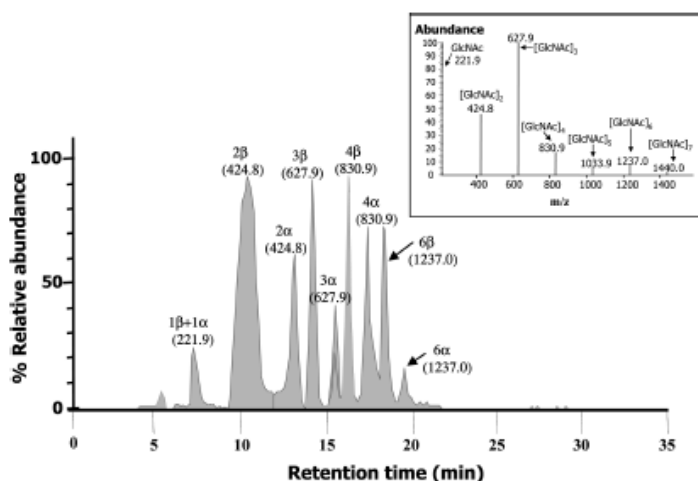
Fig. 7. A HPLC-MS chromatogram of hydrolytic products of chitinase A expressed in *E. coli*. Chitinase A (75 ng) was added to 100 μg/ml colloidal chitin and incubated at 20 °C for 5 min. After centrifugation, a 10-ml supernatant was immediately subjected to a hypercarb HPLC and eluted at 250 μl/min with a linear gradient from 5 to 40% acetronitrile into a LCQ ESI-MS. The relative abundance of the product peaks is plotted as a function of the elution time. Numbers indicate the amount of GlcNAc units in an oligomer, α, and β indicate their isoforms. The inset represents the MS signal recorded in the SIM mode set for m/z 222, 425, 628, 831, 1034, and 1237.

In conclusion, we provided evidence that *V. carchariae* chitinase A is an endochitinase. We also report gene isolation and sequence comparison based on the closely related *S. marcescens* ChiA. Determination of the C-terminal proteolytic site of the enzyme allowed the mature chitinase A to be generated in vitro, permitting successful expression of the functional protein in *E. coli*. This will lead to structural investigation and elucidation of the mode of enzyme action of *V. carchariae* chitinase A in great detail using both X-ray crystallographic and genetic engineering techniques, thus paving the way for the biotechnological application in bioconversion of chitin based on chitinase A.

Acknowledgments

References

[1] C. Jeuniaux, Methods Enzymol. 8 (1966) 644–650.
[2] R.A.J. Warren, Annu. Rev. Microbiol. 50 (1996) 183–212.
[3] R.S. Patil, V. Ghormade, M.V. Deshpande, Enzyme Microb. Technol. 26 (2000) 473–483.
[4] B. Henrissat, Biochem. J. 280 (1991) 309–316.
[5] B. Henrissat, A. Bairoch, Biochem. J. 316 (1993) 695–696.
[6] Y. Papanikolau, G. Prag, G. Tavlas, C.E. Vorgias, A.B. Oppenheim, K. Petratos, Biochemistry 40 (2001) 11338–11343.
[7] K. Bortone, A.F. Monzingo, S. Ernst, J.D. Robertus, J. Mol. Biol. 320 (2002) 293–302.
[8] S. Armand, H. Tomita, A. Heyraud, C. Gey, T. Watanabe, B. Henrissat, FEBS Lett. 343 (1994) 177–180.
[9] A.C. Terwisscha van Scheltinga, S. Armand, K.H. Kalk, A. Isogai, B. Henrissat, B.W. Dijkstra, Biochemistry 34 (1995) 15619–15623.
[10] C. Sasaki, A. Yokoyama, Y. Itoh, M. Hashimoto, T. Watanabe, T. Fukamizo, J. Biochem. (Tokyo) 131 (2002) 557–564.
[11] P.W. Robbins, C. Albright, B. Benfield, J. Biol. Chem. 263 (1998) 443–447.
[12] A.C. Terwisscha van Scheltinga, K.H. Kalk, J.J. Beintema, B.W. Dijkstra, Structure 2 (1994) 1181–1189.
[13] A. Perrakis, I. Tews, Z. Dauter, A.B. Oppenheim, I. Chet, K.S. Wilson, C.E. Vorgias, Structure 2 (1994) 1169–1180.
[14] D.M.F. van Aalten, B. Synstad, M.B. Brurberg, E. Hough, B.W. Riise, V.G.H. Eijsink, R.K. Wierenga, Proc. Natl. Acad. Sci. USA 97 (2000) 5842–5847.
[15] D.M.F. van Aalten, D. Komander, B. Synstad, S. Gaseidnes, M.G. Peter, V.G.H. Eijsink, Proc. Natl. Acad. Sci. USA 98 (2001) 8979–8984.
[16] B.L. Bassler, C. Yu, Y.C. Lee, S. Roseman, J. Biol. Chem. 266 (1991) 2476–2486.
[17] I. Hirono, M. Yamashita, T. Aoki, J. Appl. Microbiol. 84 (1998) 1175–1178.
[18] H. Tsujibo, Y. Yoshida, K. Miyamoto, Can. J. Microbiol. 38 (1992) 891–897.
[19] T. Lonhienne, K. Mavromatis, C.E. Vorgias, L. Buchon, C. Gerday, V. Bouriotis, J. Bacteriol. 183 (2001) 1773–1779.
[20] B.L. Bassler, P.J. Gibbons, C. Yu, S. Roseman, J. Biol. Chem. 266 (1991) 2468–2475.
[21] W. Suginta, P.A.W. Robertson, B. Austin, S.C. Fry, L.A. Fothergill-Gilmore, J. Appl. Microbiol. 89 (2000) 76–84.
[22] K. Pedesen, L. Verdonck, B. Austin, D.A. Austin, A.R. Blanch, P.A.D. Grimont, J. Jofre, S. Koblavi, J.L. Larsen, T. Tiainen, M. Vigneulle, J. Swings, Int. J. Syst. Bacteriol. 48 (1998) 749–758.
[23] R.T. Dando, E.P.S. Young, In the NCIMB Catalogue of Strains, Aberdeen University Press, Aberdeen, 1990.
[24] J. Monreal, E.T. Reese, Can. J. Microbiol. 15 (1968) 689–696.
[25] A. Khasin, I. Alchanati, Y. Shoham, Appl. Environ. Microbiol. 59 (1993) 1725–1730.
[26] E. Cabib, Methods Enzymol. 161 (1988) 425–435.
[27] F.M. Ausubel, R. Brent, R.E. Kingston, D.D. Moore, J.A. Smith, K. Strukh, Short Protocols in Molecular Biology, fourth ed., Wiley, New York, 1999.
[28] J.D. Thompson, D.G. Higgins, T.J. Gibson, Nucleic Acids Res. 22 (1994) 4673–4680.
[29] U.K. Laemmli, Nature 227 (1970) 680–685.
[30] A. Shevchenko, M. Wilm, Vorm, O.M. Mann, Anal. Chem. 68 (1996) 850–858.
[31] J.L. Reissig, J.L. Strominger, L.F. Leloir, J. Biol. Chem. 217 (1955) 959–966.
[32] M.M. Bradford, Anal. Biochem. 72 (1976) 248–254.
[33] J. Trudel, A. Asselin, Anal. Biochem. 178 (1989) 362–366.
[34] W.K. Roberts, C.P.J. Selitrennikoff, Gen. Microbiol. 134 (1988) 169–176.
[35] R.L. Roberts, E. Cabib, Anal. Biochem. 127 (1982) 402–412.
[36] K. Kaiser, N.E. Murray, P.A. Whittaker, in: D.M. Glover, B.D. Hames (Eds.), DNA Cloning 1: A Practical Approach, second ed., Oxford University Press, New York, 1996, pp. 37–84.
[37] J.D.G. Jones, K.L. Grady, T.V. Suslow, J.R. Bedbrook, EMBO J. 5 (1986) 467–473.
[38] L.S. Chernin, L. de la Fuente, V. Sobolev, S. Haran, C. Vorgias, A.B. Oppenheim, I. Chet, Appl. Environ. Microbiol. 63 (1997) 834–839.
[39] W.R. McClure, Annu. Rev. Biochem. 54 (1985) 171–204.
[40] G. von Heijne, Eur. J. Biochem. 133 (1983) 17–21.
[41] H. Tsujibo, H. Orikoshi, H. Tanno, K. Fujimoto, K. Miyamoto, C. Imada, Y. Okami, Y. Inamori, J. Bacteriol. 175 (1993) 176–181.
[42] H. Tsujibo, H. Orikoshi, K. Shiotani, M. Hayashi, J. Umeda, K. Miyamoto, C. Imada, Y. Okami, Y. Inamori, Appl. Environ. Microbiol. 64 (1998) 472–478.
[43] S.W. Gal, J.Y. Choi, C.Y. Kim, Y.H. Cheong, Y.J. Choi, J.D. Bahk, S.Y. Lee, M.J. Cho, FEMS Microbiol. Lett. 151 (1997) 197–204.
[44] S.W. Gal, J.Y. Choi, C.H. Kim, Y.H. Cheong, Y.J. Choi, S.Y. Lee, J.D. Bahk, M.J. Cho, FEMS Microbiol. Lett. 160 (1998) 151–158.
[45] H. Blaak, H. Schrempf, Eur. J. Biochem. 229 (1995) 132–139.
[46] J.P. Chen, F. Nagayama, M.C. Chang, Appl. Environ. Microbiol. 57 (1991) 2426–2428.

Enzymatic properties of wild-type and active site mutants of chitinase A from *Vibrio carchariae*, as revealed by HPLC-MS

Wipa Suginta[1], Archara Vongsuwan[1], Chomphunuch Songsiriritthigul[1,2], Jisnuson Svasti[3] and Heino Prinz[4]

1 School of Biochemistry, Institute of Science, Suranaree University of Technology, Nakhon Ratchasima, Thailand
2 National Synchrotron Research Center, Nakhon Ratchasima, Thailand
3 Department of Biochemistry and Center for Protein Structure and Function, Faculty of Science, Mahidol University, Bangkok, Thailand
4 Max Planck Institut für Molekulare Physiologie, Dortmund, Germany

The enzymatic properties of chitinase A from *Vibrio carchariae* have been studied in detail by using combined HPLC and electrospray MS. This approach allowed the separation of α and β anomers and the simultaneous monitoring of chitooligosaccharide products down to picomole levels. Chitinase A primarily generated β-anomeric products, indicating that it catalyzed hydrolysis through a retaining mechanism. The enzyme exhibited endo characteristics, requiring a minimum of two glycosidic bonds for hydrolysis. The kinetics of hydrolysis revealed that chitinase A had greater affinity towards higher M_r chitooligomers, in the order of $(GlcNAc)_6 > (GlcNAc)_4 > (GlcNAc)_3$, and showed no activity towards $(GlcNAc)_2$ and pNP-GlcNAc. This suggested that the binding site of chitinase A was probably composed of an array of six binding subsites. Point mutations were introduced into two active site residues – Glu315 and Asp392 – by site-directed mutagenesis. The D392N mutant retained significant chitinase activity in the gel activity assay and showed $\approx 20\%$ residual activity towards chitooligosaccharides and colloidal chitin in HPLC-MS measurements. The complete loss of substrate utilization with the E315M and E315Q mutants suggested that Glu315 is an essential residue in enzyme catalysis. The recombinant wild-type enzyme acted on chitooligosaccharides, releasing higher quantities of small oligomers, while the D392N mutant favored the formation of transient intermediates. Under standard hydrolytic conditions, all chitinases also exhibited transglycosylation activity towards chitooligosaccharides and pNP-glycosides, yielding picomole quantities of synthesized chitooligomers. The D392N mutant displayed strikingly greater efficiency in oligosaccharide synthesis than the wild-type enzyme.

Chitin is a homopolymer of $\beta(1,4)$-linked *N*-acetyl-D-glucosamine (GlcNAc) residues and a major structural component of bacteria, fungi, and insects. In the ocean, chitin is produced in vast quantities by marine invertebrates, fungi, and algae [1]. This highly insoluble compound is utilized rapidly, as the sole source of carbon and nitrogen, by marine bacteria such as *Vibrio* spp. [2,3]. Two types of enzymes are required for the hydrolysis of chitin. The first, chitinases, are the major enzymes, which degrade the chitin polymer into chitooligosaccharides and subsequently into the disaccharide, $(GlcNAc)_2$. $(GlcNAc)_2$ is then

further hydrolyzed by the second type of enzymes – β-glucosaminidases – to yield GlcNAc as the final product. Chitin catabolism through the carbohydrate catabolic cascade has rather complex signal transduction pathways and has been studied extensively in *Vibrio furnissi* [4–7].

Chitinases (EC 3.2.1.14) are classified into glycosyl hydrolase families 18 and 19, depending on their amino acid sequences [8–11]. All the known bacterial chitinases belong to the family 18 glycosidase. Structural data [12,13] and stereochemical studies of chitin hydrolysis [14–16] have revealed a substrate-assisted catalytic mechanism that involves substrate distortion, leading to glycosidic bond cleavage, to yield an oxazolinium intermediate and to retention of anomeric configuration in the products. Detailed characterization and kinetic analyses of chitinases, using chitin as a substrate, have been limited because enzyme-catalyzed reactions produce more than one species of oligosaccharide intermediate. Most kinetic studies of chitinases were obtained by using chitooligomers [GlcNAc$_n$, n = (2–6)] [16–20] or short chitooligomers coupled with p-nitrophenyl or 4-methylumbelliferyl groups [21–23].

We described, in a previous publication, the isolation of chitinase A from a marine bacterium, *V. carchariae* [24]. Chitinase A is highly expressed upon induction with chitin and is active as a monomer of M_r 62 700. Analysis of chitin hydrolysis by using the viscosity assay and HPLC-ESI MS suggested that the newly isolated chitinase acts as an endochitinase [25]. We also reported isolation of the gene encoding chitinase A and functional expression of the recombinant enzyme in an *Escherichia coli* system. In the present study, the hydro-

lytic activity of chitinase A resulting in the production of a broad range of chitooligosaccharide products was measured simultaneously by means of quantitative HPLC-ESI MS. Site-directed mutagenesis was also employed to elucidate the catalytic role of two active site residues. The hydrolytic and transglycosylation activities of the mutated enzymes were studied in comparison with the recombinant wild-type enzyme.

Results

Characterization of chitooligosaccharide products

Colloidal chitin was hydrolyzed by native chitinase A at 20 °C. After different reaction times, the reaction products were analyzed by using HPLC-ESI MS. Figure 1 shows an HPLC-MS chromatogram of chitooligosaccharide products after 2 h of reaction time. The mono-deacetylated dimer (m/z 383), trimer (m/z 586) and tetramer (m/z 789) were detected. Partial deacetylation typically occurred when chitin was prepared by treatment with acids [26]. Note that the mono-deacetylated trimer appeared at three different elution times. This corresponds to three different isomers (e.g. GlcNAc.GlcNAc.GlcN, GlcNAc.GlcN. GlcNAc, and GlcN.GlcNAc.GlcNAc), in accordance with the location of three acetyl moieties.

The signal-to-noise ratio improved significantly when the mass spectra were recorded in the single ion monitoring (SIM) mode corresponding to selected masses of reaction products [GlcNAc to (GlcNAc)$_6$]. The signal of ion clusters and deacetylated oligomers were thus excluded from the analysis. Figure 2 shows
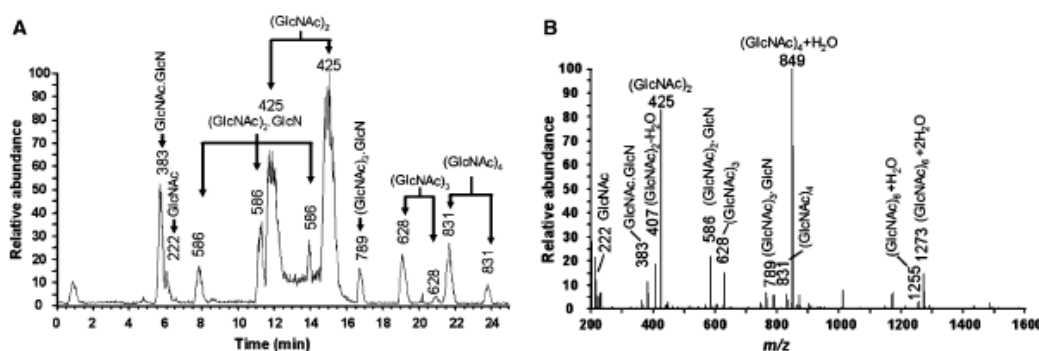
Fig. 1. Chitinase A catalyzes chitin hydrolysis. Native chitinase A (5 μg) was added to 10 mg·mL^{-1} colloidal chitin and incubated at room temperature (20 °C) for 2 h. Ten microlitres of the sample was added to a Hypercarb® column and eluted at 250 μL·min^{-1} with a linear gradient of 5–40% (v/v) acetonitrile into an LCQ ESI mass spectrometer. (A) An HPLC chromatogram representing chitin hydrolysis by chitinase A. The chitooligosaccharide masses are indicated on the corresponding peaks. (B) The mass spectrum averaged over the time range of the chromatogram in Fig. 1A is shown between 200 and 1600 m/z. All peaks are singly charged, as deduced from their isotope pattern. All clusters (two or three oligosaccharides with one proton) map to the chromatographic peaks of the respective molecules.
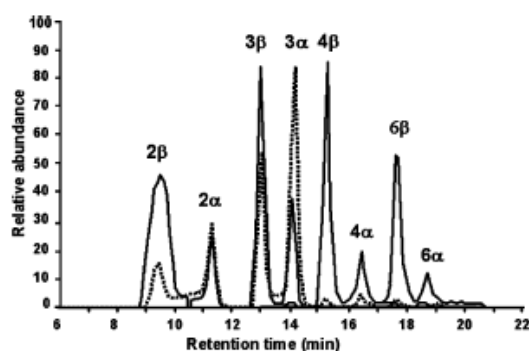
Fig. 2. Stereochemistry of chitin hydrolysis. Native chitinase A (75 ng) was added to 400 µg·mL^{-1} colloidal chitin and incubated at 20 °C for 5 min (solid line) and 60 min (dotted line). Ten microlitres of the sample was subjected to HPLC-MS. The signal was recorded in the single ion mode set for the masses 222, 425, 628, 831, 1034 and 1237. The relative intensity of the base peaks is plotted as a function of the elution time. Numbers indicate the amount of 2-amino-2-*N*-acetylamino-D-glucose (GlcNAc) units in an oligomer; β and α indicate their isoform.

the elution profile of the selected reaction products after 5 min (solid line) or 1 h (dotted line). Clearly, the longer oligomers are formed only transiently within the initial time of reaction, and then subsequently degraded over a longer incubation time.

Stereochemistry of chitin hydrolysis

Hydrophobic stationary phases of HPLC have been shown to bind preferentially to the α anomer, allowing both isomers to be separated and identified. The cleavage pattern was assessed from a previously published separation profile of chitooligosaccharides obtained by using reverse-phase HPLC and ^{1}H NMR [14,15]. The earlier peak represented the β anomer and the later peak corresponded to the α anomer of the oligomeric

products obtained at initial stage of reaction (Fig. 2, solid line). In order to evaluate which anomer was initially produced by chitinase A, we determined the peak ratio of oligomers immediately after hydrolysis of chitin and at equilibrium. The HPLC column was run at 10 °C and the sample was immediately loaded onto the column after 10 min of hydrolysis at 20 °C to minimize isomerization. Note that the peak ratio is related to the concentration ratio by a factor C [i.e. $(\beta/\alpha)_{concentrations} = C \times (\beta/\alpha)_{peaks}$], but this factor C disappears when ratios of ratios are calculated. The peak ratio β/α 'immediately' after hydrolysis divided by the peak ratio β/α at equilibrium was 6.9 for the dimer, 4.3 for the trimer, and 5.4 for the tetramer.

Quantitative analysis of chitooligosaccharide hydrolysis by native chitinase A

The hydrolysis of short chitooligosaccharides [(Glc-NAc)$_n$, $n = 2$, 3, 4 and 6] and colloidal chitin was studied further. The reaction was quenched by the addition of acetic acid, so that substrate decrease and product formation could be monitored at various timepoints. Quantification of the reaction products shown in Fig. 3 was obtained by means of separate calibration experiments using known concentrations of the oligomers, as described in the 'Experimental procedures'. This was mandatory, even for these chemically similar compounds, because MS ion counts were generally higher for longer oligomers than for shorter ones.

When chitinase A was incubated with (GlcNAc)$_2$, neither a decrease in (GlcNAc)$_2$ nor an increase in GlcNAc was observed upon incubation up to 57 h (Fig. 3A). In contrast, when (GlcNAc)$_3$ was the substrate, a slow decrease in (GlcNAc)$_3$ concentrations was already detected within the first 15 min of reaction (Fig. 3B). After 57 h, hydrolysis was complete, with
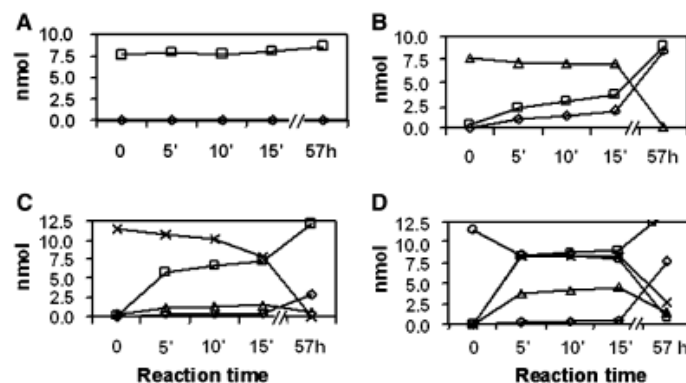
Fig. 3. Quantitative analysis of chitooligosaccharide hydrolysis. Native chitinase A (75 ng) was incubated at 20 °C with 2 mM of (A) (GlcNAc)$_2$, (B) (GlcNAc)$_3$, (C) (GlcNAc)$_4$, and (D) (GlcNAc)$_6$. The reaction was quenched by the addition of acetic acid to 10% and then applied to HPLC-ESI MS. For calibration of the HPLC peaks (α and β anomers) recorded at different masses in the single ion mode, mixtures of the same chitooligosaccharides and the monomer were applied at known concentrations. The calculated amounts of GlcNAc (◇), (GlcNAc)$_2$ (□), (GlcNAc)$_3$ (△), (GlcNAc)$_4$ (×), and (GlcNAc)$_6$ (○) are shown as a function of reaction times.

dimers and monomers being produced in equal amounts as the final products. Figure 3C represents the hydrolysis of $(GlcNAc)_4$. The enzyme hydrolyzed the tetramer mainly in the middle, so that dimers were formed. Trimers were also produced but in comparatively lower quantities ($< 20\%$ of the dimers at 15 min of reaction) and were degraded into dimers and monomers towards the end of the reaction. No monomer was detectable at the very early stages, but $\approx 20\%$ of monomers were obtained after the reaction was complete. The hydrolysis of $(GlcNAc)_6$ yielded predominantly $(GlcNAc)_4$ and $(GlcNAc)_2$ (Fig. 3D). The amount of transiently formed $(GlcNAc)_3$ was more than double that observed for tetramer hydrolysis. Tetramers and trimers were further hydrolyzed, again giving dimers and monomers as the end products.

The hydrolytic activity of chitinase A against colloidal chitin was also studied at various incubation times. All chitooligosaccharides, from monomers to hexamers, were observed, but dimers dominated the population of reaction intermediates. The monomer, GlcNAc, only appeared after a lag time of ≈ 30 min, and the larger oligomers – $(GlcNAc)_4$ and $(GlcNAc)_6$ – were only observed transiently within the first hour, with the levels of $(GlcNAc)_6$ being too low to be calculated. In contrast to these, the trimer $(GlcNAc)_3$ produced was rather stable and only further hydrolyzed after a few hours.

Steady-state kinetics of chitinase A with various substrates

HPLC-MS is a relatively complex technique compared to well-established colorimetric assays. In order to relate our findings to this standard methodology, hydrolysis of *p*-nitrophenol substrates was studied by using both methods. As with $(GlcNAc)_2$, chitinase A did not hydrolyze pNP-GlcNAc, but hydrolyzed pNP-$(GlcNAc)_2$ mainly into pNP $+ (GlcNAc)_2$ ($> 99\%$). For quantitative analysis, product concentrations were calculated directly by means of a pNP calibration curve in the case of the colorimetric assay, or by using a $(GlcNAc)_2$ calibration curve in the case of quantitative HPLC-MS. If pNP is used for monitoring the hydrolysis of pNP-$(GlcNAc)_2$, the other product will be $(GlcNAc)_2$, so that the results with both assays should be identical. Using linear regression plots, the K_m and k_{cat} values determined for the spectroscopic assay were 1.04 ± 0.10 mM and 5.78 ± 0.58 s^{-1}, and for the LC-MS assay were 1.05 ± 0.03 mM and 5.73 ± 0.16 s^{-1} (Table 1). The correlation coefficient between the two data sets was 0.997. The close similarity between the K_m and k_{cat} values obtained from the

Table 1. Kinetic parameters of chitinase A with various substrates. The hydrolysis of chitooligosaccharides and colloidal chitin at substrate concentrations of 0–2 mM was carried out with 75 ng of native chitinase A in 0.1 M ammonium acetate buffer (pH 7.1) at 20 °C for 5 min and quenched with 10% (v/v) acetic acid. The terminated reactions were then analyzed by using quantitative HPLC-MS. Kinetic parameters (K_m, k_{cat}, and k_{cat}/K_m) were obtained from Lineweaver–Burk plots, which were assessed by using a standard linear regression function. $(GlcNAc)_n$, β1–4 linked oligomers of GlcNAc residues where $n = 2$–6; $(GlcNAc)_n$-pNP, *p*-nitrophenol β-glycosides.

Substrate	K_m (mM)	k_{cat} (s^{-1})	k_{cat}/K_m (s^{-1}·M^{-1})
GlcNAc-pNP	No reaction	–	–
$(GlcNAc)_2$-pNP[a]	1.04 ± 0.10	5.78 ± 0.58	5.29×10^3
$(GlcNAc)_2$-pNP[b]	1.05 ± 0.03	5.73 ± 0.16	5.84×10^3
$(GlcNAc)_2$	No reaction	–	–
$(GlcNAc)_3$[b]	10.54 ± 1.40	9.71 ± 1.29	9.21×10^2
$(GlcNAc)_4$[b]	2.17 ± 0.29	0.63 ± 0.08	2.89×10^2
$(GlcNAc)_6$[b]	0.19 ± 0.01	5.81 ± 0.19	3.06×10^4
Chitin[b]	0.10 ± 0.02 mg·mL^{-1}	0.07 ± 0.006	–

[a] Determined by colorimetric assay, [b] determined by HPLC-ESI MS.

two methods confirms that the ESI MS assay is a reliable method for using to determine the kinetic parameters of chitinase A.

Having established confidence in the validity of the method, we systematically investigated, by using ESI MS, the kinetic properties of chitinase A with pNP-glycosides, chitooligosaccharides, and chitin. The initial velocity of the enzyme for concentrations of the substrates ranging from 0 to 2.0 mM was determined after 5 min of reaction. Given the fact that chitinase A produced $(GlcNAc)_2$ as the major end product, the initial velocity of all the substrates was calculated based on the release of $(GlcNAc)_2$.

Kinetic parameters (K_m, k_{cat}, and k_{cat}/K_m) were obtained from linear regression plots, as shown in Table 1. For chitooligomers, the K_m values decreased with increased length of oligomers [the K_m values for $(GlcNAc)_3$, $(GlcNAc)_4$, and $(GlcNAc)_6$ were 10.54 ± 1.40 mM, 2.17 ± 0.29 mM, and 0.19 ± 0.01 mM, respectively], indicating that the enzyme had greater affinity towards the higher M_r substrates.

The catalytic efficiency constant (k_{cat}/K_m) of pNP-$(GlcNAc)_2$ (5.84×10^3 s^{-1}·M^{-1}) was higher than that of $(GlcNAc)_3$ (9.21×10^2 s^{-1}·M^{-1}) or $(GlcNAc)_4$ (2.89×10^2 s^{-1}·M^{-1}), but lower than that of $(GlcNAc)_6$ (3.06×10^4 s^{-1}·M^{-1}). K_m and k_{cat} values for chitin were 0.10 ± 0.02 mg·mL^{-1} and 0.07 ± 0.006 s^{-1}. These values were similar to those measured for glycol-chitin with the 65 kDa chitinase from *Bombyx mori* (K_m, 0.13 mg·mL^{-1}; k_{cat}, 0.08 s^{-1}) [17].

Protein expression and hydrolytic activity of the wild-type chitinase A and mutants

We recently reported cloning and expression of the recombinant wild-type chitinase A as a $(His)_6$-tagged fusion protein [25]. As judged by a colorimetric assay using $pNP-(GlcNAc)_2$ as the substrate, the recombinant enzyme exhibited 117% of the specific activity of the native enzyme. The Quickchange Site-directed Mutagenesis Kit was used to generate three active site mutants using the clone carrying the recombinant wild-type DNA as template. The three mutated clones had changes of two amino acids, namely Glu315→Met (mutant E315M), Glu315→Gln (mutant E315Q), and Asp392→Asn (mutant D392N). Using the same expression and purification systems, the mutated and the wild-type enzymes were expressed in equivalent amounts, yielding ≈ 70 mg·L^{-1} of purified protein. SDS/PAGE analysis followed by staining with Coomassie blue showed single bands for the wild-type and mutants D392N and E315M, migrating with an M_r of $\approx 63\,000$ (Fig. 4A). In the case of the E315Q mutant, an additional faint band was also seen at an M_r of $\approx 43\,000$. This band appeared as a degradation product during freezing and thawing of the protein that was stored at −30 °C. As revealed by immunoblotting, all the mutants, as well as the wild-type, strongly reacted with polyclonal anti-(chitinase A) Ig (Fig. 4B), confirming that the expressed proteins were chitinase A. A gel activity assay using glycol-chitin displayed chitinase activity only for the wild-type and for the D392N mutant, with the mutant having much less activity. The E315Q and E315M mutants, by contrast, completely lacked hydrolytic activity (Fig. 4C).
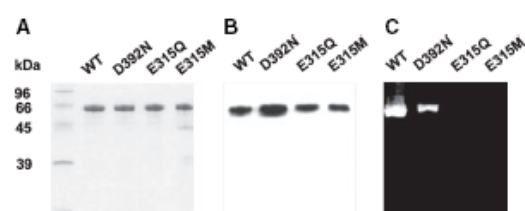

Fig. 4. SDS/PAGE analysis of the recombinant chitinase A and mutants. Purified chitinases (2 µg) were electrophoresed through a 12% (w/v) SDS polyacrylamide gel. After electrophoresis, protein bands were (A) stained with Coomassie blue, (B) immunoblotted and detected with polyclonal anti-(chitinase A), and (C) stained for chitinase activity with glycol-chitin using fluorescent Calcoflour white M2R. The tracks represent the following samples: 1, low-M_r standard proteins; 2, recombinant wild-type protein; 3, D392N mutant; 4, E315Q mutant; and 5, E315M mutant.

The products of chitooligosaccharide and colloidal chitin hydrolysis generated by recombinant wild-type and mutants were further analyzed as a function of time. No detectable products were seen when the chitin polymer was incubated with the mutants E315Q and E315M, even after 60 min. On the other hand, the D392N mutant was able to hydrolyze chitin with $\approx 20\%$ residual activity. As with the wild-type chitinase A, the D392N mutant released multiple species of hydrolytic products, varying from GlcNAc to $(GlcNAc)_6$.

After adjusting the concentration of the enzymes to yield similar activity, the hydrolytic activities of the wild-type protein and of the D392N mutant were assayed with $(GlcNAc)_{2-6}$. As expected, the enzymes failed to hydrolyze $(GlcNAc)_2$ and showed very low activity towards $(GlcNAc)_3$. With $(GlcNAc)_4$ as the substrate, both enzymes recognized the middle glycosidic bond of the tetrameric chain, releasing $(GlcNAc)_2$ as a major product (Fig. 5A). $(GlcNAc)_3$ appeared in small amounts only after $(GlcNAc)_2$ had accumulated. With $(GlcNAc)_5$ as the substrate, $(GlcNAc)_2$ and $(GlcNAc)_3$ were formed as the primary products, with the hydrolytic rate of the D392N mutant being much slower than that of the wild type. $(GlcNAc)_4$, measured in trace amounts, was probably formed through the reaction intermediates.

Both wild-type and D392N mutant cleaved $(GlcNAc)_6$ asymmetrically, mainly releasing $(GlcNAc)_2$ and $(GlcNAc)_4$ in equal amounts, followed by $(GlcNAc)_3$, and $(GlcNAc)_5$. At 60 min of reaction time, the yields of the trimer and the pentamer compared to the dimer were 34% and 30% for the wild-type, but 66% and 47% for the D392N mutant (Fig. 5B).

Oligosaccharide synthesis by chitinase A

Direct detection of molecular mass by HPLC-MS instantly identified higher M_r intermediates occurring in the course of hydrolysis. This transglycosylation was observed immediately with chitooligosaccharides, as well as with pNP-glycosides. Figure 6 demonstrates the quantitative analysis of polymerized (transglycosylation) products of $(GlcNAc)_4$ hydrolysis.

The transglycosylation reaction took place as early as 2 min after initiation, yielding picomole quantities of the elongated oligomers. The maximum yields of $(GlcNAc)_5$ and $(GlcNAc)_6$, synthesized relatively to the hydrolytic product, $(GlcNAc)_2$, were 3% and 9% for the wild-type enzyme and 11% and 12% for the D392N mutant. The synthesis of $(GlcNAc)_8$ was also detected, but with lower yields ($< 1\%$). All synthe-
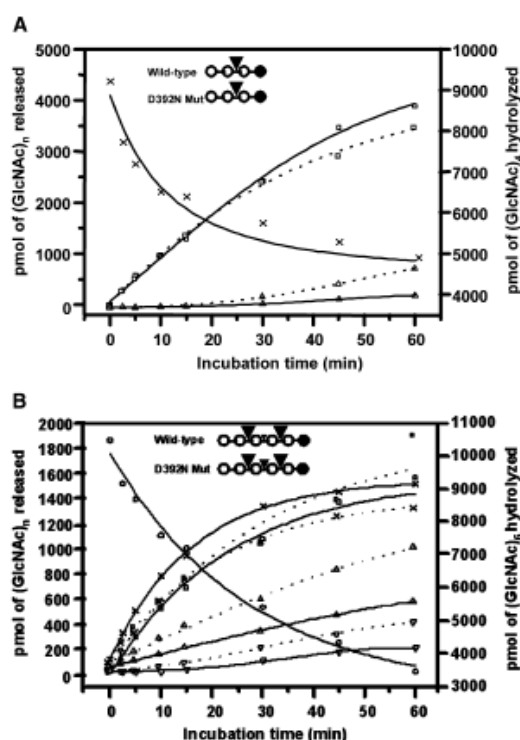
A

B

Fig. 5. Hydrolytic activity of the wild-type chitinase A and D392N mutant. The purified recombinant chitinase A (100 ng) or D392N mutant (500 ng) was added to a reaction mixture containing 1 mM (GlcNAc)$_n$ in 50 mM ammonium acetate buffer, pH 7.1. The reaction was quenched after the indicated reaction times at 20 °C by the addition of acetic acid to 10% and applied to calibrated HPLC-MS. For each substrate, the calculated concentrations of the products formed by the wild-type (solid line) and D392N mutant (broken line) are shown. (A) Hydrolysis of (GlcNAc)$_4$ and (B) hydrolysis of (GlcNAc)$_6$. □, (GlcNAc)$_2$; △, (GlcNAc)$_3$; ×, (GlcNAc)$_4$; ▽, (GlcNAc)$_5$; and ○, (GlcNAc)$_6$. The inset schematically shows the chitooligomers with the proposed cleavage sites (▼). The GlcNAc units at the reducing end are represented with filled circles (●).

sized oligomers were present only as reaction intermediates, which were utilized further within 30 min; (GlcNAc)$_5$, obtained with the D392N mutant, was the only exception – its concentration remained relatively steady up to 60 min. Similar patterns were also seen with other substrates. For instance, the tetramers, pentamers, and hexamers were formed during (GlcNAc)$_3$ hydrolysis, while hexamers, heptamers, and octamers were formed during (GlcNAc)$_5$ hydrolysis. Transglycosylation activity of chitinase A was also observed with pNP-glycosides, where (GlcNAc)$_3$ and (GlcNAc)$_4$ were detected during pNP-(GlcNAc)$_2$ hydrolysis and (Glc-
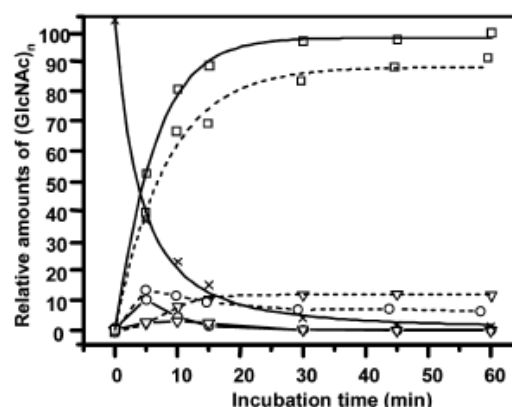
Fig. 6. Transglycosylation activity of the wild-type chitinase A and of the D392N mutant. The recombinant wild-type (100 ng) or the D392N mutant (500 ng) was added to a reaction mixture containing 1 mM (GlcNAc)$_4$ substrate in 50 mM ammonium acetate buffer, pH 7.1. The reaction was quenched after the indicated reaction times at 20 °C by the addition of acetic acid to a final concentration of 10% and the glycosylation products were analyzed by using the calibrated HPLC-MS. The chitooligomers formed by the wild-type enzyme are shown by solid lines and those formed by the D392N mutant in broken lines. □, (GlcNAc)$_2$; ×, (GlcNAc)$_4$; ▽, (GlcNAc)$_5$; and ○, (GlcNAc)$_6$.

NAc)$_4$, (GlcNAc)$_5$, and (GlcNAc)$_6$ were found during pNP-(GlcNAc)$_3$ hydrolysis.

Discussion

We have demonstrated the power of quantitative HPLC-MS when an enzymatic reaction with a large variety of products is investigated, such as the enzymatic reaction with chitinase A from *V. carchariae*. A combination of HPLC and ESI MS allowed the separation of α and β anomers and all chitooligosaccharide products to be monitored simultaneously. At the initial stage of reaction and low temperature, the enzyme yielded predominantly β anomers. The anomeric configurations gradually reached mutarotation equilibrium, where the ratio of β/α anomer peaks was similar among the different oligosaccharides. This clearly indicates that chitinase A has a stereo-selectivity for β anomers over α anomers. Chitinase A cleaved β-glycosidic linkages, retaining the anomeric form of the resulting products, which supports the substrate-assisted mechanism as described for family 18 chitinases [12].

Chitinase A had greater affinity towards higher M_r chitooligomers. The increase in affinity with chain

length of chitooligomers implies that the binding site must be composed of an array of subsites, probably six GlcNAc subsites. This corresponds to the structural data obtained for *Serratia marcescens* ChiA and the hevamine chitinase [12,15], in which a substrate-binding site extends over six GlcNAc subsites designated from -4 to $+2$.

Quantitative analysis showed that $(GlcNAc)_2$ was the main product of the hydrolytic reactions. The smallest substrates for chitinase A were trimers [(GlcNAc)_3 and pNP-(GlcNAc)_2], suggesting that the cleavage site is located asymmetrically in the substrate recognition sites, two of which form the product site. Hydrolysis of pNP-$(GlcNAc)_2$ with the chromophore attached at the reducing end of the sugar chain yielded $> 99\%$ $(GlcNAc)_2$, indicating that chitinase A cleaves the second bond from the nonreducing end. When $(GlcNAc)_3$ was produced as a reaction intermediate, it was relatively stable because its low affinity prevented rapid hydrolysis. Apparently, all monomers found as end products arose from these intermediate trimers. Indeed, the bond cleavage in the middle of $(GlcNAc)_6$, which produced two molecules of $(GlcNAc)_3$ in significant amounts, suggested that the catalytic cleft of the *Vibrio* enzyme has an open structure at both ends, giving long sugars access in a flexible manner. Such a feature can be expected from an enzyme with endo characteristics. The endo property of chitinase A is further verified by the formation of reaction intermediates of varying length (Fig. 2).

The role of two catalytic amino acid residues (Glu315 and Asp392) in the enzyme catalysis was also investigated. Of three newly generated chitinase A variants, the hydrolytic activity of E315M and E315Q mutants was entirely abolished. Apparently, structural modification of the carboxylate side-chain of Glu315 led to a loss of the hydrolytic activity, providing evidence that Glu315 is essential for catalysis. The catalytic role of the equivalent glutamic acid has been well demonstrated by the 3D structures of ChiA from *S. marcescens* [12,27] and of CiX1 from the pathogenic fungus *Coccidioides immitis* [28]. The D392N mutant retained significant hydrolytic activity with the tested substrates, implying that Asp392 does not have a direct catalytic function.

When the hydrolytic activity of the wild-type enzyme and the D392 mutant was investigated at various substrate concentrations, almost identical K_m values, but greatly decreased V_{max} values, were obtained for the D392N mutant. This may reflect influences of the mutation on the catalytic process, but not on the substrate-binding process. Site-directed mutagenesis and the 3D

structures of other chitinases showed that the equivalent Asp392 residues take part in the catalytic process by stabilizing the transition states flanking the oxazolinium intermediate and subsequently assisting the correct orientation of the 2-acetamido group in catalysis [13,29–31].

Chitooligosaccharide hydrolysis, as a function of time, revealed some differences between the nonmutated and mutated enzymes. As with native chitinase A, $(GlcNAc)_2$ did not act as a substrate and $(GlcNAc)_3$ was a poor substrate for both enzymes. These small M_r sugars are more likely to be generated as reaction products than to act as substrates. As judged by the patterns of the product formation, the release of dimers, trimers and tetramers from the hexamer was considered to result from direct action of the enzymes. On the other hand, the pentamer appeared to be formed by the condensation of smaller intermediates. Note that the wild-type enzyme prefers to degrade chitooligosaccharides, yielding direct formation of the primary products, while the mutant enzyme acted more efficiently on the transiently formed secondary products (Fig. 5).

The HPLC-MS method was sensitive enough to detect the low levels of oligosaccharides synthesized from chitinase A. Under specific conditions (low temperature, short reaction time and low substrate concentrations), oligosaccharide synthesis was likely to take place through transglycosylation reactions. The higher M_r oligomers, including pentamers, hexamers and octamers, were obtained from the hydrolysis of $(GlcNAc)_4$. These oligomers presumably arose from the condensation of two reaction intermediates, namely the pentamer from $(GlcNAc)_2 + (GlcNAc)_3$, the hexamer from $(GlcNAc)_2 + (GlcNAc)_4$ or $(GlcNAc)_3 + (GlcNAc)_3$, and the octamer from $(GlcNAc)_2 + (GlcNAc)_6$ or $(GlcNAc)_3 + (GlcNAc)_5$. The rates of formation were in the order of $(GlcNAc)_6 > (GlcNAc)_5 > (GlcNAc)_8$ for both enzymes. The ratios of the maximal yields of the synthesized products obtained by the mutant over the wild-type were $285 : 1$ for $(GlcNAc)_5$, $374 : 1$ for $(GlcNAc)_6$ and $3.7 : 1$ for $(GlcNAc)_8$. From these ratios, it was concluded that the D392 mutant was a more efficient enzyme in chitooligosaccharide synthesis.

In conclusion, we report, for the first time, the enzymatic properties of chitinase A as determined by using a suitably calibrated HPLC-ESI MS. This sensitive analytical method allowed a broad range of intermediate reaction products to be monitored simultaneously down to picomole levels and was therefore suitable for detailed characterization of chitinases, which is difficult to perform by using other methods.

Experimental procedures

Materials

The marine bacterium *V. carchariae* (LMG7890^T) was a gift from Dr Peter Robertson (Department of Biological Sciences, Heriot Watt University, Edinburgh, UK). All chemicals and reagents were of analytical grade and purchased from the following sources: reagents for bacterial media were from Scharlau Chemie S.A. (Barcelona, Spain); flake chitin (crab shell), chitooligosaccharide substrates and pNP-glycosides were from Sigma-Aldrich Pte., Ltd (Citilink Warehouse Complex, Singapore); SDS/PAGE chemicals from Amersham Pharmacia Biotech Asia Pacific Ltd (Bangkok, Thailand) and from Sigma-Aldrich Pte., Ltd; Sephacryl S300® HR resin was from Amersham Biosciences (Piscataway, NJ, USA); chemicals for buffers and reagents for protein preparation were from Sigma-Aldrich Pte., Ltd and from Carlo Erba Reagenti (Milan, Italy); and acetonitrile (HPLC grade) was from LGC Promochem GmbH (Wesel, Germany). All other reagents for LC-MS measurements were from Sigma-Aldrich (Munich, Germany).

Instrumentation

HPLC was operated on a 150×2.1 mm 5 µm Hypercarb® column (ThermoQuest, Thermo Electron Corporation, San Jose, CA, USA) connected to an Agilent Technologies 1100 series HPLC system (Agilent Technologies, Waldbronn, Germany) under the control of a Thermo Finnigan LCQ DECA electrospray mass spectrometer. The proprietary program XCALIBUR (Thermo Finnigan, Thermo Electron Corporation, San Jose, CA, USA) was used to control and calibrate HPLC-MS data.

Preparation of chitinase A

Native chitinase A secreted by *V. carchariae* culture was purified by chitin-affinity binding and gel filtration chromatography following the protocol described previously [24]. Recombinant wild-type chitinase A was obtained by cloning the chitinase A gene, lacking the C-terminal proteolytic fragment, into the pQE60 expression vector and expressing the protein in *E. coli* M15 cells [25]. For preparation of the recombinant enzyme, the bacterial cells were grown at 37 °C in 250 mL of Luria–Bertani (LB) medium, supplemented with 100 µg·mL^{-1} ampicillin, to an attenuance (*D*), at 600 nm, of ≈ 0.6, then isopropyl thio-β-D-galactoside (IPTG) was added to a final concentration of 0.5 mM. Incubation was continued at 25 °C overnight, with shaking, before the cells were harvested by centrifugation at 2500 *g* for 20 min. The cell pellet was resuspended in 15 mL of 20 mM Tris/HCl buffer, pH 8.0. containing 150 mM NaCl, 1 mM phenylmethanesulfonyl fluoride, and 1 mg·mL^{-1} lysozyme. The suspended cells were maintained

on ice and broken by using an ultrasonicator (30 s, six to eight times). Unbroken cells and cell debris were removed by centrifugation. The supernatant containing soluble chitinase A was purified by using Ni- nitrilotriacetic acid agarose chromatography, according to Qiagen's protocol (Qiagen, Valencia, CA, USA). Fractions eluted with 250 mM imidazole, which contained soluble chitinase A, were pooled, concentrated by using Vivaspin (Vivascience AG, Hannover, Germany) membrane concentrators (10 000 M_r cut-off), and further purified by gel filtration chromatography using an ĀKTA purifier system (Amersham Biosciences, Sweden) on a Superdex S-200 HR 10/30 column (1.0×30 cm). The running buffer was 20 mM Tris/HCl, pH 8.0, containing 150 mM NaCl. A flow rate of 250 µL·min^{-1} was applied and fractions of 500 µL were collected. Chitinase-containing fractions were combined and stored at −30 °C until use. Protein concentrations were determined by Bradford's method [32] and quantified using a standard calibration curve produced from BSA. Purity of the resultant protein was verified by SDS/PAGE operated under a Laemmli buffer system [33]. Unless otherwise stated, experiments were carried out at 4 °C throughout the purification steps.

Site-directed mutagenesis

Point mutations were introduced to the wild-type chitinase A DNA via pPCR-based mutagenesis using *Pfu* Turbo DNA polymerase (QuickChange Site-Directed Mutagenesis kit; Stratagene, La Jolla, CA, USA). Three chitinase A mutants were generated by using three sets of mutagenic oligonucleotides (Proligo Singapore Pte Ltd, Science Park II, Singapore). The forward oligonucleotide sequences designed for D392N, E315M, and E315Q mutants (sequences underlined) were 5′-CTTTGCGATGACTTAC AACTTCTACGGCGG-3′, 5′-GTAGATATTGACTGGAT GTTCCCTGGTGGCGGCG-3′ and 5′-GATATTGACTG GCAATTCCCTGGTGGCGGC-3′, and the reverse oligonucleotide sequences were 5′-CAGCCGCCGTAGAAGTT GTAAGTCATCGCAAAG-3′, 5′-CGCCGCCACCAGGG AACATCCAGTCAATATCTAC-3, and 5′-GCCGCCAC CAGGGAATTGCCAGTCAATATCTAC-3′, respectively. Confirmation of the mutated nucleotides by automated sequencing was carried out by the Bio Service Unit (BSU, Bangkok, Thailand). The oligonucleotide used for determining the nucleotide sequences of the three mutants was 5′-TTCTACGACTTCGTTGATAAGAAG-3′. The mutated proteins were expressed and purified under the same conditions as described for the wild-type enzyme.

Hydrolytic action of chitinase A on chitooligosaccharides and chitin

Hydrolysis of chitooligosaccharides by native chitinase A was carried out in 50 mM ammonium acetate buffer,

pH 7.1. Reactions containing 2.0 mM chitooligosaccharides, including $(GlcNAc)_2$, $(GlcNAc)_3$, $(GlcNAc)_4$, and $(GlcNAc)_6$, were incubated in the presence of 75 ng of purified enzyme at 20 °C with shaking. One-hundred microliter aliquots were taken at 5 min, 10 min, 15 min and 57 h and quenched with 10% (v/v) acetic acid. These terminated reaction mixtures (60 µL) were injected into a Hypercarb HPLC column, operated at 40 °C unless otherwise stated. A linear gradient of 0–40% (v/v) acetonitrile, containing 0.1% (v/v) acetic acid, was applied, and oligosaccharides separated from the column were immediately detected by ESI MS connected to the LC interface. ESI MS was conducted in positive SIM mode. The mass-to-charge ratio (m/z) of expected oligosaccharides were selected as follows: GlcNAc, 221.9; $(GlcNAc)_2$, 425.5; $(GlcNAc)_3$, 627.6; $(GlcNAc)_4$, 830.8; $(GlcNAc)_5$, 1034.0; $(GlcNAc)_6$, 1237.2; $(GlcNAc)_7$, 1440.0; pNP-GlcNAc, 342.3; pNP-$(GlcNAc)_2$, 545.5; and pNP-$(GlcNAc)_3$, 748.7. With chitin hydrolysis, reactions were carried out the same way as described for the hydrolysis of chitoligosaccharides, but with 200 µg·mL^{-1} colloidal chitin. The peak areas of chitinase A hydrolytic products obtained from MS measurements were quantified using the program XCALIBUR applying an MS Avalon algorithm for peak detection. A mixture of oligosaccharide containing $(GlcNAc)_n$, $n = 1$–6 was prepared by dilution in two ranges: 0–500 pmol and 50 pmol to 2 nmol. The calibration curves of each GlcNAc moiety were constructed separately and used to convert peak areas into molar quantities.

Hydrolysis of chitooligosaccharides by the recombinant wild-type and mutated chitinases A was carried out in 50 mM ammonium acetate buffer, pH 7.1. Reactions containing 1.0 mM chitooligosaccharide substrates, including $(GlcNAc)_2$, $(GlcNAc)_3$, $(GlcNAc)_4$, $(GlcNAc)_5$ and $(GlcNAc)_6$, were incubated with 50 ng·µL^{-1} enzyme at 20 °C with shaking. Aliquots of a 100 µL reaction mixture were taken at 0, 2.5, 5, 10, 30, 45 and 60 min, and quenched with 10% (v/v) acetic acid. The hydrolytic products were analyzed by HPLC-ESI MS as described for the native enzyme.

Kinetic measurements

Kinetic studies of native chitinase A using a colorimetric assay were performed in a microtiter plate reader (LabSystem, Helsinki, Finland). Reaction mixtures (100 µL) comprised 0–2 mM pNP-$(GlcNAc)$, pNP-$(GlcNAc)_2$ and pNP-$(GlcNAc)_3$ dissolved in dH$_2$O, chitinase A (75 ng), and 50 mM ammonium acetate buffer, pH 7.1. Release of pNP was monitored at an absorbance (A) of 405 nm every 15 s for 30 min at 25 °C, using a calibration curve of pNP in the same reaction buffer. Kinetic studies of chitinase A with chitooligosaccharide by LC-MS were carried out as described for the hydrolysis of chitooligosaccharides at substrate concentrations of 0.065–2 mM. This concentration range provided data points with sufficient quality, allowing

K_m and k_{cat} values to be calculated with reasonable confidence by using linear regression plots.

Kinetic parameters with pNP-$(GlcNAc)_2$, $(GlcNAc)_3$, $(GlcNAc)_4$, $(GlcNAc)_6$, and chitin substrates were also determined, based on the formation of $(GlcNAc)_2$ and the initial velocity of the enzyme, at 5 min of reaction at 20 °C. Kinetic values for the recombinant wild-type and D392N mutant were obtained at chitooligosaccharide substrate concentrations of 0–1 mM, as described for the native enzyme. The enzyme concentrations used in the reaction mixture were 100 ng for the purified wild-type and 500 ng for the D392N mutant.

Stereochemistry of product anomers

As the rate of mutarotation is temperature dependent, hydrolysis of chitin suspension (100 µg·mL^{-1}) by native chitinase A (75 ng) was carried out at low temperature (20 °C) in 50 mM ammonium acetate buffer, pH 7.1, with shaking. Products were monitored as quickly as possible and the reactions were quenched with 10% (v/v) acetic acid. After centrifugation at 5 °C, the supernatant containing chitooligosaccharide products formed after 5 min of incubation was immediately injected into a Hypercarb HPLC. The HPLC was operated at a particularly low temperature (10 °C) and detected by ESI MS in SIM mode with selected masses from monomer to hexamer. Identification of β and α anomers was assessed from previous experiments with equivalent reverse-phase HPLC system and ^{1}H NMR [14].

Transglycosylation of chitinase A

Reaction mixtures (100 µL) containing 1 mM $(GlcNAc)_4$, 100 ng of the wild-type enzyme or 500 ng of the D392N mutant, and 50 mM ammonium acetate, pH 7.1, were incubated at 20 °C. Transglycosylation activities of both enzymes were observed at 20 °C at time intervals of 0, 5, 10, 15, 30, 45 and 60 min. At the required time-points, aliquots (10 µL) were mixed with 90 µL of 20% (v/v) acetic acid, and 20 µL of the reaction mixture was then analyzed by HPLC-ESI MS. Quantification of the tranglycosylation products was conducted as described for chitinase A-catalyzed hydrolysis. Molecular ions of the products were monitored either in the scan mode (m/z 200–2000) or in the SIM mode with selected anticipated masses.

Immunodetection

Antisera against chitinase A were prepared with the purified chitinase A isolated from *V. carchariæ*, as described previously [24]. The purified wild-type and mutated chitinase A (2 µg) were electrophoresed on a 12% (w/v) SDS/PAGE gel, then transferred onto nitrocellulose membrane using a Trans-Blot® Semi-Dry Cell (BioRad, Hercules, CA,

W. Suginta *et al.*

USA). Immunodetection was carried out using enhanced chemiluminescence (ECL; Amersham Biosciences) according to the manufacturer's instructions. The primary antibody was polyclonal anti-(chitinase A) (1 : 2000 dilution) and the secondary antibody was horseradish peroxidase-conjugated anti-rabbit IgG (1 : 5000 dilution).

SDS/PAGE following the chitinase activity assay

The purified recombinant chitinase A (2 µg of each) were treated with gel loading buffer without 2-mercaptoethanol and electrophoresed through a 12% (w/v) polyacrylamide gel containing 0.1% (w/v) glycol chitin. After electrophoresis, the gel was washed at 37 °C for 1 h with 250 mL of 150 mM sodium acetate, pH 5.0, containing 1% (v/v) Triton X-100 and 1% (w/v) skimmed milk, followed by the same buffer without 1% (w/v) skimmed milk for a further 1 h to remove SDS and to allow the proteins to refold. The gel was stained with 0.01% (w/v) Calcoflour white M2R (Sigma, USA) in 500 mM Tris/HCl, pH 8.5, and visualized under UV [34].

Acknowledgements

References

1 Gooday GW (1990) The ecology of chitin degradation. In: *Advances in Microbial Ecology* (Marshall KC, ed.), pp. 387–430. Plenum Press, New York.

2 Yu C, Lee AM, Bassler BL & Roseman S (1991) Chitin utilization by marine bacteria: a physiological function for bacterial adhesion to immobilized carbohydrates. *J Biol Chem* **266**, 24260–24267.

3 Bassler BL, Gibbons PJ, Yu C & Roseman S (1991) Chitin utilization by marine bacteria: chemotaxins to chitin oligosaccharides by *Vibrio furnissii*. *J Biol Chem* **266**, 24268–24275.

4 Keyhani NO & Roseman S (1996) The chitin catabolic cascade in the marine bacterium *Vibrio furnissii*: molecular cloning, isolation, and characterization of a periplasmic chitodextrinase. *J Biol Chem* **271**, 33414–33424.

5 Keyhani NO & Roseman S (1996) The chitin catabolic cascade in the marine bacterium *Vibrio furnissii*: molecular cloning, isolation, and characterization of a periplasmic β-N-acetylglucosaminidase. *J Biol Chem* **271**, 33425–33432.

6 Keyhani NO, Li X-B & Roseman S (2000) The chitin catabolic cascade in the marine bacterium *Vibrio furnissii*: identification and molecular cloning of chitoporin. *J Biol Chem* **275**, 33068–33076.

7 Park JK, Keyhani NO & Roseman S (2000) The chitin catabolic cascade in the marine bacterium *Vibrio furnissii*: identification and molecular cloning, and characterization of a N, N'-diacetylchitobiose phosphorylase. *J Biol Chem* **275**, 33077–33083.

8 Warren RAJ (1996) Microbial hydrolysis of polysaccharides. *Annu Rev Microbiol* **50**, 183–212.

9 Patil RS, Ghormade V & Deshpande MV (2000) Review: Chitinolytic enzymes: an exploration. *Enzyme Microb Technol* **26**, 473–483.

10 Henrissat B (1991) A classification of glycosyl hydrolases based on amino acid sequence similarities. *Biochem J* **280**, 309–316.

11 Henrrisat B & Bairoch A (1993) New families in the classification of glycosyl hydrolases based on amino acid sequence similarities. *Biochem J* **293**, 781–788.

12 Papanikolau Y, Prag G, Tavlas G, Vorgias CE, Oppenheim AB & Petratos K (2001) High resolution structural analyses of mutant chitinase A complexes with substrates provide new insight into the mechanism of catalysis. *Biochemistry* **40**, 11338–11343.

13 Bortone K, Monzingo AF, Ernst S & Robertus JD (2002) The structure of an allosamidin complex with the *Coccidioides immitis* chitinase defines a role for a second acid residue in substrate-assisted mechanism. *J Mol Biol* **320**, 293–302.

14 Armand S, Tomita H, Heyraud A, Gey C, Watanabe T & Henrissat B (1994) Stereochemical course of the hydrolysis reaction catalysed by chitinase A1 and D from *Bacillus circulans* WL-12. *FEBS Lett* **343**, 177–180.

15 Terwissha van Scheltinga AC, Armand S, Kalk KH, Isogai A, Henrissat B & Dijkstra BW (1995) Stereochemistry of chitin hydrolysis by a plant chitinase/lysozyme and x-ray structure of a complex with allosamidin: evidence for substrate assisted catalysis. *Biochemistry* **34**, 15619–15623.

16 Sasaki C, Yokoyama A, Itoh Y, Hashimoto M, Watanabe T & Fukamizo T (2002) Comparative study of the reaction mechanism of family 18 chitinases from plants and microbes. *J Biochem* **131**, 557–564.

17 Koga D, Sasaki Y, Uchiumi Y, Hirai N, Arakane Y & Nagamatsu Y (1997) Purification and characterization of *Bombyx mori* chitinases. *Insect Biochem Mol Biol* **27**, 757–767.

18 Sakai K, Yokota A, Kurokawa H, Wakayama M & Moriguchi M (1998) Purification and characterization of three thermostable endochitinases of a noble Bacillus strain, MH-1, isolated from chitin-containing compost. *Appl Environ Microbiol* **64**, 3397–3402.

19 Bokma E, Barends T, Terwisscha van Scheltinga AC, Dijkstra BW & Beintema JJ (2000) Enzyme kinetics of hevamine, a chitinase from the rubber tree Hevea brasiliensis. *FEBS Lett* **478**, 119–122.

20 Fukamizo T, Sasaki C, Schelp E, Bortone K & Robertus JD (2001) Kinetic properties of Chitinase-1 from the fungal pathogen *Coccidioides immitis*. *Biochemistry* **40**, 2448–2454.

21 Hollis T, Honda Y, Fukamizo T, Marcotte E, Day PJ & Robertus JD (1997) Kinetic analysis of Barley chitinase. *Arch Biochem Biophys* **344**, 335–342.

22 Thompson SE, Smith M, Wilkinson MC & Peek K (2001) Identification of a chitinase antigen from *Pseudomonas aeroginosa* strain 385. *Appl Environ Microbiol* **67**, 4001–4008.

23 Honda Y, Kitaoka M, Tokuyasu K, Sasaki C, Fukamizo T & Hayashi K (2003) Kinetic studies on the hydrolysis of N-acetylated and N-deacytylated derivatives of 4-methylumbelliferyl chitobioside by the family 18 chitinases ChiA and ChiB from *Serratia marcescens*. *J Biochem* **13**, 253–258.

24 Suginta W, Robertson PAW, Austin B, Fry SC & Fothergill-Gilmore LA (2000) Chitinases from *Vibrio*: activity screening and purification of Chi A from *Vibrio carchariae*. *J Appl Microbiol* **89**, 76–84.

25 Suginta W, Vongsuwan A, Songsiriritthigul C, Prinz H, Estibeiro P, Duncan RR, Svasti J & Fothergill-Gilmore LA (2004) An endochitinase A from *Vibrio carchariae*: cloning, expression, mass and sequence analyses, and chitin hydrolysis. *Arch Biochem Biophys* **424**, 171–180.

26 Roberts WK & Selitrennikoff CP (1988) Plant and bacterial chitinases differ in antifungal activity. *J Gen Microbiol* **134**, 169–176.

27 Perrakis A, Tews I, Dauter Z, Oppenheim AB, Chet I, Wilson KS & Vorgias CE (1994) Crystal structure of a bacterial chitinase at 2.3 Å resolution. *Structure* **2**, 1169–1180.

28 Hollis T, Monzingo AF, Bortone K, Ernst S, Cox R & Robertus JD (2000) The X-ray structure of a chitinase from the pathogenic fungus *Coccidioides immitis*. *Protein Sci* **29**, 544–551.

29 Watanabe T, Kobori K, Miyashita K, Fujii T, Sakai H, Uchida M & Tanaka H (1993) Identification of glutamic acid 204 and aspartic acid 200 in chitinase A1 of *Bacillus circulans* WL-12 as essential residues for chitinase activity. *J Biol Chem* **268**, 18567–18572.

30 van Aalten DMF, Komander D, Synstad B, Gaseidnes S, Peter MG & Eijsink VGH (2001) Structural insights into the catalytic mechanism of a family 18 exo-chitinase. *Proc Natl Acad Sci USA* **98**, 8979–8984.

31 Synstad B, Gaseidnes S, van Aalten DMF, Vriend G, Nielsen JE & Eijsink VGH (2004) Mutational and computational analysis of the role of conserved residues in the active site of a family 18 chitinase. *Eur J Biochem* **271**, 253–262.

32 Bradford MMA (1976) Rapid and sensitive method for the quantitation of microgram quantities of protein utilizing the principle of protein-dye binding. *Anal Biochem* **72**, 248–254.

33 Laemmli UK (1970) Cleavage of structural proteins during the assembly of the head of bacteriophage T4. *Nature* **227**, 680–685.

34 Trudel J & Asselin A (1989) Detection of chitinase activity after polyacrylamide gel electrophoresis. *Anal Biochem* **178**, 362–366.

crystallization communications

Expression, purification, crystallization and preliminary crystallographic analysis of chitinase A from *Vibrio carchariae*

Chomphunuch Songsiriritthigul,[a,b] Jirundon Yuvaniyama,[c] Robert C. Robinson,[d] Archara Vongsuwan,[a] Heino Prinz[e] and Wipa Suginta[a]*

[a]School of Biochemistry, Suranaree University of Technology, Nakhon Ratchasima 30000, Thailand, [b]National Synchrotron Research Center, Nakhon Ratchasima 30000, Thailand, [c]Center for Excellence in Protein Structure and Function and Department of Biochemistry, Faculty of Science, Mahidol University, Bangkok 10400, Thailand, [d]Institute of Molecular and Cell Biology, Proteos, 61 Biopolis Drive, Singapore 138673, Singapore, and [e]Max-Planck Institut für Molekulare Physiologie, Otto-Hahn-Strasse 11, 44227 Dortmund, Germany

Correspondence e-mail: wipa@sut.ac.th
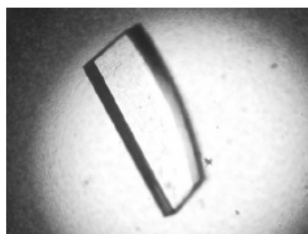
Chitinase A of *Vibrio carchariae* was expressed in *Escherichia coli* M15 host cells as a 575-amino-acid fragment with full enzymatic activity using the pQE60 expression vector. The yield of the highly purified recombinant protein was approximately 70 mg per litre of bacterial culture. The molecular mass of the expressed protein was determined by HPLC/ESI–MS to be 63 770, including the hexahistidine tag. Crystals of recombinant chitinase A were grown to a suitable size for X-ray structure analysis in a precipitant containing $10\%(v/v)$ PEG 400, $0.1\ M$ sodium acetate pH 4.6 and $0.125\ M$ CaCl$_2$. The crystals belonged to the tetragonal space group $P422$, with two molecules per asymmetric unit and unit-cell parameters $a = b = 127.64$, $c = 171.42$ Å. A complete diffraction data set was collected to 2.14 Å resolution using a Rigaku/MSC R-AXIS IV^{++} detector system mounted on an RU-H3R rotating-anode X-ray generator.

1. Introduction

Chitin, a β-1,4-linked *N*-acetylglucosamine (GlcNAc) polysaccharide, is a major structural component of fungal cell walls and the exoskeletons of invertebrates, including insects and crustaceans. This linear polymer may be degraded through the hydrolytic action of chitinases (EC 3.2.1.14). In correlation with the structural role of chitin, chitinases are important for biochemical and physiological functions in many organisms. In insects, chitinases are essential in the moulting process and may also affect gut physiology through their involvement in peritrophic membrane turnover (Merzendorfer & Zimoch, 2003), whereas plants produce chitinases as part of their defence mechanism against fungal pathogens (Herrera-Estrella & Chet, 1999; Melchers & Stuiver, 2000). Chitinases are thought to contribute to a number of morphogenetic processes in filamentous fungi, including spore germination, side-branch formation, differentiation into spores and autolysis (Gooday *et al.*, 1992). Many bacteria express chitinases that enable them to utilize chitin as the sole source of carbon and nitrogen (Yu *et al.*, 1991), whilst mammalian chitinases have been found to regulate the pathophysiological features of an allergic asthma (Wills-Karp & Karp, 2004).

On the basis of amino-acid sequence, chitinases are classified into glycosyl hydrolase families 18 and 19, which are unrelated, differing in structure and mechanism (Henrissat & Bairoch, 1993). Family 18 chitinases are present in a wide range of organisms, including bacteria, fungi, higher plants and humans. All family 18 chitinases share two short sequence motifs which form an $(\alpha/\beta)_8$ TIM-barrel active site. From accumulated structural information, it appears that family 18 enzymes catalyze the hydrolytic reaction by a substrate-assisted mechanism, in which protonation of the glycosidic oxygen leads to distortion of the sugar molecule at the scissile position. The resultant bond cleavage yields an oxazolinium intermediate and retention of anomeric configuration in the products (Papanikolau *et al.*, 2001; Bortone *et al.*, 2002; Armand *et al.*, 1994; Terwissha van Scheltinga *et al.*, 1995; Sasaki *et al.*, 2002). Family 19 chitinases have only been found in higher plants and in the Gram-positive bacterium *Streptomyces* (Cohen-Kupiec & Chet, 1998; Ohno *et al.*, 1996). In contrast to family 18 chitinases, the catalytic domains of family 19 chitinases have a bilobal $\alpha+\beta$ folding motif with a high α-helical content. The mode of catalytic action of this class of enzymes is a

crystallization communications

single displacement step, which results in an inversion of the anomeric configuration of the products (Brameld & Goddard, 1998; Robertus & Monzingo, 1999).

Chitinase A from a marine bacterium, *Vibrio carchariae*, is a 63 kDa family 18 glycosyl hydrolase (Suginta *et al.*, 2000). This monomeric enzyme acts as an endochitinase and has a broad range of substrate specificity with various chitin oligomers (Suginta *et al.*, 2004, 2005). Kinetic data implied greater affinity of chitinase A towards higher molecular-weight chitooligosaccharides, suggesting that the catalytic cleft of the enzyme comprises an array of binding subsites, most likely comparable to that of CiX1 from *Coccidioides immitis* (Fukamizo *et al.*, 2001; Sasaki *et al.*, 2002). The characteristic multiple binding subsite structure is commonly found in the active sites of hydrolytic enzymes that utilize biopolymers as substrates, such as proteases, lysozyme, cellulases and chitinases. We previously cloned a DNA fragment that encodes the functional chitinase A of *V. carchariae* into the pQE60 expression vector, with the corresponding recombinant protein expressed in *E. coli* M15 host cells (Suginta *et al.*, 2004). In the present study, we describe high-level expression and large-scale purification of the recombinant chitinase A from the same *E. coli* system. We also report the first crystals of chitinase A from marine bacteria and the preliminary analysis of their diffraction data.

2. Materials and methods

2.1. Expression and purification

The DNA fragment that encodes chitinase A (amino-acid residues 22–597, without the residue 598–850 C-terminal fragment) was previously cloned into the pQE60 expression vector (Suginta *et al.*, 2004) so as to express the 575-amino-acid fragment with a C-terminal $(His)_6$ sequence. In this study, high-level expression of this recombinant chitinase A in *E. coli* M15 host cells has been optimized. The cells were grown at 310 K in Luria–Bertani (LB) medium containing $100 \mu g \ ml^{-1}$ ampicillin and chitinase expression was induced by the addition of isopropyl thio-β-D-galactoside (IPTG) to a final concentration of 0.5 mM when OD_{600} of the cell culture reached 0.6. Cell growth continued at 298 K for 18 h and the cell pellet was collected by centrifugation at 4500 g for 30 min. The freshly prepared cell pellet was resuspended in 40 ml lysis buffer [20 mM Tris–HCl buffer pH 8.0 containing 150 mM NaCl, 1 mM phenylmethylsulfonylfluoride (PMSF) and $1 \ mg \ ml^{-1}$ lysozyme] and then lysed on ice using a Sonopuls Ultrasonic homogenizer with a 6 mm diameter probe (50% duty cycle; amplitude setting, 20%; total time, 30 s; 6–8 cycles). Unbroken cells and cell debris were removed by centrifugation at 12 000 g for 1 h. The supernatant was applied onto an Ni–NTA agarose affinity column (1.0 × 10 cm; Qiagen GmbH, Hilden, Germany) and chromatography was carried out gravitationally following the Qiagen protocol (http://www1.qiagen.com/literature/handbooks/INT/ProteinPurification.aspx). After loading, the column was washed with 50 ml 20 mM Tris–HCl buffer pH 8.0 containing 5 mM imidazole, followed by another 50 ml of the same buffer containing 10 mM imidazole. 0.5 ml fractions were collected and protein fractions eluted with 250 mM imidazole were concentrated using Vivaspin-20 ultrafiltration membrane concentrators (10 kDa molecular-weight cutoff, Vivascience AG, Hanover, Germany). Further purification was performed using an ÄKTA purifier system (Amersham Biosciences, Piscataway, NJ, USA) on a Superdex 200 HR 10/30 (1.0 × 30 cm) column. The running buffer was 20 mM Tris–HCl buffer pH 8.0 containing 150 mM NaCl. A flow rate of $250 \mu l \ min^{-1}$ was maintained and 0.5 ml fractions were collected and

assayed for chitinase activity. Chitinase-containing fractions were pooled and again concentrated using the same type of Vivaspin membrane concentrator. All purification steps were carried out at 277 K, unless otherwise stated. Protein concentrations were determined by Bradford's method (Bradford, 1976) using a standard calibration curve constructed from BSA (0–10 µg). The purity of chitinase A was verified by SDS–PAGE using a Laemmli buffer system (Laemmli, 1970). The accurate molecular mass of the recombinant chitinase A was determined by HPLC/ESI–MS (Thermo Finnigan, Thermo Electron Corporation, San Jose, CA, USA) operated under the conditions given previously (Suginta *et al.*, 2004). Chitinase activity was determined in a 100 µl assay mixture containing protein sample (35 µl), 1 mM pNP-$(GlcNAc)_2$ (25 µl) and 100 mM sodium acetate buffer pH 5.0 (40 µl). The reaction mix was incubated at 303 K for 10 min and the enzymatic reaction was terminated by the addition of 50 µl 1 M NaHCO$_3$. The amount of p-nitrophenol (pNP) released was determined spectrophotometrically at 405 nm. One unit of chitinase activity is defined as the amount of chitinase A that produces 1 nmol pNP per minute at 303 K.

2.2. Crystallization

Initial crystallization experiments were carried out by the micro-batch method in 96-well Impact plates (Hampton Research, Aliso Viejo, CA, USA) filled with 10 µl Al's oil (Hampton Research). For each crystallization drop, 0.5 µl chitinase A ($10 \ mg \ ml^{-1}$ in 20 mM Tris–HCl buffer pH 8.0 containing 150 mM NaCl) was added to 0.5 µl of each precipitant from Crystal Screen (Hampton Research) and JB Screen HTS I and HTS II (Jena Bioscience GmbH, Jena, Germany) without mixing. Small crystals were obtained after 4 d incubation at 277 K in condition A1 from JBScreen HTS I [15%(v/v) PEG 400, 0.1 M sodium acetate pH 4.6 and 0.1 M CaCl$_2$], condition H4 from JBScreen HTS I [30 %(w/v) PEG 8000, 0.2 M ammonium sulfate] and condition A10 from Crystal Screen [30%(w/v) PEG 4000, 0.1 M sodium acetate pH 4.6 and 0.2 M ammonium acetate]. Condition A1 was further optimized by the hanging-drop vapour-diffusion method in a 24-well VDX Plate (Hampton Research). A protein drop made up of 1 µl chitinase A solution ($10 \ mg \ ml^{-1}$ in 20 mM Tris–HCl buffer pH 8.0 containing 150 mM NaCl) mixed with 1 µl of various concentrations of precipitants [0–0.5 M CaCl$_2$ and 10–16 %(v/v) PEG 400 in 0.1 M sodium acetate pH 4.6] was equilibrated over 1.0 ml of the respective precipitant. The best single crystals were obtained with 10%(v/v) PEG 400, 0.1 M sodium acetate pH 4.6 and 0.125 M CaCl$_2$.

2.3. Data collection

The resultant crystals were immersed in a cryoprotectant solution [20 %(v/v) glycerol, 10% (v/v) PEG 400, 0.1 M sodium acetate pH 4.6 and 0.125 M CaCl$_2$] for roughly 10 s and then picked up with a nylon loop and quickly vitrified in a stream of nitrogen gas at 112 K. A single crystal diffracted X-rays to at least 2.2 Å resolution on a Rigaku/MSC R-AXIS IV^{++} detector mounted on an RU-H3R rotating-anode X-ray generator equipped with Osmic Blue confocal focusing mirrors and 0.3 mm collimator running at 50 kV and 100 mA. The crystal-to-detector distance was set to 190 mm, with all frames collected at 112 K. Diffraction data were recorded over a 65° rotation of the crystal around the φ axis in 260 diffraction images with a width of 0.25° per image. The data were processed with *Crystal-Clear/d*TREK* (Pflugrath, 1999).
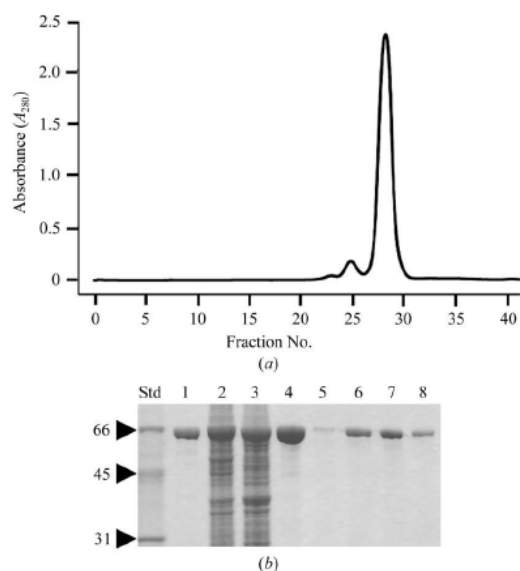
crystallization communications

Figure 1
Purification of chitinase A expressed from *E. coli* M15 cells. (*a*) Elution profile of recombinant chitinase A obtained from an ÄKTA purifier system with a Superdex 200 HR 10/30 (1.0 × 30 cm) gel-filtration column. The running buffer was 20 m*M* Tris–HCl buffer pH 8.0 containing 150 m*M* NaCl. A flow rate of 250 µl min^{-1} was maintained and 0.5 ml fractions were collected. (*b*) Chitinase A-containing fractions were subjected to SDS–PAGE analysis, followed by Coomassie Blue staining. Lanes: Std, low-molecular-weight standard proteins (serum albumin, ovalbumin and carbonic anhydrase); 1, purified native chitinase A; 2, crude cell lysate after 0.5 m*M* IPTG induction; 3, clear supernatant; 4, pooled fraction eluted with 250 m*M* imidazole during Ni–NTA agarose affinity chromatography; 5–8; eluted fractions 26, 27, 28 and 29 from the Superdex 200 HR column, respectively.

3. Results and discussion

In the present study, a *V. carchariae* chitinase A fragment [amino-acid residues 22–597, without the C-terminal sequence 598–850, but with a C-terminally attached (His)$_6$ tag to permit affinity chromatography on Ni–NTA-agarose] was highly expressed from *E. coli* M15 host cells. Purification of the recombinant chitinase A yielded ~70 mg highly purified protein per litre of bacterial culture. Fig. 1(*a*) shows an
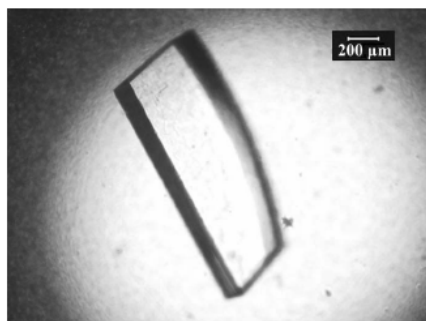

Figure 2
A crystal of recombinant chitinase A (dimensions 1100 × 400 × 100 µm) obtained from a hanging-drop vapour-diffusion setup using 0.1 *M* sodium acetate pH 4.6 containing 10%(*v/v*) PEG 400 and 0.125 *M* CaCl$_2$.

Table 1
Statistics for crystallographic data.

Values in parentheses are for the last shell.

Space group	*P*422
Unit-cell parameters (Å)	$a = b = 127.64$, $c = 171.42$
Solvent content (%)	55.1
Total No. of unique reflections collected	76752
No. of observed reflections	364202
Redundancy	4.75
Wavelength used (Å)	1.5418
Resolution range (Å)	54.16–2.14 (2.22–2.14)
Completeness (%)	97.2 (81.6)
R_{merge} † (%)	7.8 (24.3)
$\langle I/\sigma(I)\rangle$	5.4 (1.7)

† $R_{merge} = \sum_{hkl}\sum_i |I_i(hkl) - \langle I(hkl)\rangle| / \sum_{hkl}\sum_i I_i(hkl)$, where I_i is the intensity of the *i*th measurement of an equivalent reflection with indices *hkl*.

elution profile from FPLC on a Superdex 200 HR 10/30 gel-filtration column, representing a single peak corresponding to the band of apparent molecular weight 63 000 Da as shown on SDS–PAGE (Fig. 1*b*). The molecular mass of the purified protein was confirmed by HPLC/ESI–MS to be 63 770. This value matched, within a limit of 0.05% instrumentation error, the calculated molecular mass of the (His)$_6$-tagged chitinase A (63 784.23). The recombinant enzyme was fully active, giving a specific activity with *p*NP-(GlcNAc)$_2$ substrate of 1.49 nmol µg^{-1} min^{-1}, compared with 1.75 nmol µg^{-1} min^{-1} for the native enzyme (purified from *V. carchariae*).

With the hanging-drop vapour-diffusion method, the best crystals were obtained with a reservoir solution containing 10%(*v/v*) PEG 400 and 0.125 *M* CaCl$_2$. X-ray diffraction data of a single crystal with dimensions 1100 × 400 × 100 µm (Fig. 2) showed Laue group symmetry of 4/*mmm*.

The refined unit-cell parameters are $a = b = 127.64$, $c = 171.42$ Å and the crystal is likely to contain two molecules per asymmetric unit, with an estimated Matthews coefficient of 2.74 Å^3 Da^{-1} (Matthews, 1968). Diffraction statistics showed absences that could be characteristic of the tetragonal space groups *P*4$_1$22 or *P*4$_3$22. However, the data were initially scaled and merged in space group *P*422 in order to preserve all the data for subsequent confirmation of the correct space group by molecular-replacement calculations. The data were complete to 2.14 Å resolution; the final statistics for data collection and processing are summarized in Table 1.

A preliminary solution of the structure of *V. carchariae* chitinase was obtained by molecular-replacement calculations using the *AMoRe* (*CCP*4) program (Navaza, 1994) and the crystal structure of Chi A from *Serratia marcescens* (PDB code 1ctn; 49.3% identical to chitinase A from *V. carchariae*; Perrakis *et al.*, 1994) as the search model. A translation search using all space groups with 4/*mmm* symmetry (including *P*4$_1$22 and *P*4$_3$22) showed most compatibility with the *P*422 space group, giving an amplitude correlation coefficient of 32.4% and an *R* factor of 52.6% for the top solution, compared with 12.6–20.6% and 56.0–58.7%, respectively, for all others. Examination of the best solution revealed good crystal packing and no clashes between symmetry-related molecules. This preliminary model is currently being rebuilt and refined.

electronic reprint

crystallization communications

Function, Faculty of Science, Mahidol University, Bangkok 10400, Thailand.

References

Armand, S., Tomita, H., Heyraud, A., Gey, C., Watanabe, T. & Henrissat, B. (1994). *FEBS Lett.* **343**, 177–180.
Bortone, K., Monzingo, A. F., Ernst, S. & Robertus, J. D. (2002). *J. Mol. Biol.* **320**, 293–302.
Bradford, M. M. (1976). *Anal. Biochem.* **72**, 248–254.
Brameld, K. A. & Goddard, W. A. III (1998). *Proc. Natl Acad. Sci. USA*, **95**, 4276–4281.
Cohen-Kupiec, R. & Chet, I. (1998). *Curr. Opin. Biotechnol.* **9**, 270–277.
Fukamizo, T., Sasaki, C., Schelp, E., Bortone, K. & Robertus, J. D. (2001). *Biochemistry*, **40**, 2448–2454.
Gooday, G. W., Zhu, W. Y. & O'Donnell, R. W. (1992). *FEMS Microbiol. Lett.* **100**, 387–392.
Henrissat, B. & Bairoch, A. (1993). *Biochem. J.* **316**, 695–696.
Herrera-Estrella, A. & Chet, I. (1999). *EXS*, **87**, 171–184.
Laemmli, U. K. (1970). *Nature (London)*, **227**, 680–685.
Matthews, B. W. (1968). *J. Mol. Biol.* **33**, 491–497.
Melchers, L. S. & Stuiver, M. H. (2000). *Curr. Opin. Plant Biol.* **3**, 147–152.
Merzendorfer, H. & Zimoch, L. (2003). *J. Exp. Biol.* **206**, 4393–4412.
Navaza, J. (1994). *Acta Cryst.* A**50**, 157–163.
Ohno, T., Armand, S., Hata, T., Nikaidou, N., Henrissat, B., Mitsutomi, M. & Wanatabe, T. (1996). *J. Bacteriol.* **178**, 5065–5070.
Papanikolau, Y., Prag, G., Tavlas, G., Vorgias, C. E., Oppenheim, A. B. & Petratos, K. (2001). *Biochemistry*, **40**, 11338–11343.
Perrakis, A., Tews, I., Dauter, Z., Oppenheim, A. B., Chet, I., Wilson, K. S. & Vorgias, C. E. (1994). *Structure*, **2**, 1169–1180.
Pflugrath, J. W. (1999). *Acta Cryst.* D**55**, 1718–1725.
Robertus, J. D. & Monzingo, A. F. (1999). *EXS*, **87**, 125–135.
Sasaki, C., Yokoyama, A., Itoh, Y., Hashimoto, M., Watanabe, T. & Fukamizo, T. (2002). *J. Biochem. (Tokyo)*, **131**, 557–564.
Suginta, W., Robertson, P. A. W., Austin, B., Fry, S. C. & Fothergill-Gilmore, L. A. (2000). *J. Appl. Microbiol.* **89**, 76–84.
Suginta, W., Vongsuwan, A., Songsiriritthigul, C., Prinz, H., Estibeiro, P., Duncan, R. R., Svasti, J. & Fothergill-Gilmore, L. A. (2004). *Arch. Biochem. Biophys.* **424**, 171–180.
Suginta, W., Vongsuwan, A., Songsiriritthigul, C., Svasti, J. & Prinz, H. (2005). *FEBS J.* **272**, 3376–3386.
Terwissha van Scheltinga, A. C., Armand, S., Kalk, K. H., Isogai, A., Henrissat, B. & Dijkstra, B. W. (1995). *Biochemistry*, **34**, 15619–15623.
Wills-Karp, M. & Karp, C. L. (2004). *N. Engl. J. Med.* **351**, 1455–1457.
Yu, C., Lee, A. M., Bassler, B. L. & Roseman, S. (1991). *J. Biol. Chem.* **266**, 24260–24267.

Mutations of Trp275 and Trp397 altered the binding selectivity of *Vibrio carchariae* chitinase A

Wipa Suginta [a,*], Chomphunuch Songsiriritthigul [a,b], Archara Kobdaj [a], Rodjana Opassiri [a], Jisnuson Svasti [c]

[a] *School of Biochemistry, Institute of Science, Suranaree University of Technology, Nakhon Ratchasima 30000, Thailand*
[b] *National Synchrotron Research Center, P.O. Box 93, Nakhon Ratchasima 30000, Thailand*
[c] *The Department of Biochemistry and Center for Protein Structure and Function, Faculty of Science, Mahidol University, Bangkok, Thailand*

Abstract

Point mutations of the active-site residues Trp168, Tyr171, Trp275, Trp397, Trp570 and Asp392 were introduced to *Vibrio carchariae* chitinase A. The modeled 3D structure of the enzyme illustrated that these residues fully occupied the substrate binding cleft and it was found that their mutation greatly reduced the hydrolyzing activity against pNP-[GlcNAc]$_2$ and colloidal chitin. Mutant W397F was the only exception, as it instead enhanced the hydrolysis of the pNP substrate to 142% and gave no activity loss towards colloidal chitin. The kinetic study with the pNP substrate demonstrated that the mutations caused impaired K_m and k_{cat} values of the enzyme. A chitin binding assay showed that mutations of the aromatic residues did not change the binding equilibrium. Product analysis by thin layer chromatography showed higher efficiency of W275G and W397F in G4–G6 hydrolysis over the wild type enzyme. Though the time course of colloidal chitin hydrolysis displayed no difference in the cleavage behavior of the chitinase variants, the time course of G6 hydrolysis exhibited distinct hydrolytic patterns between wild-type and mutants W275G and W397F. Wild type initially hydrolyzed G6 to G4 and G2, and finally G2 was formed as the major end product. W275G primarily created G2–G5 intermediates, and later G2 and G3 were formed as stable products. In contrast, W397F initially produced G1–G5, and then the high-M_r intermediates (G3–G5) were broken down to G1 and G2 end products. This modification of the cleavage patterns of chitooligomers suggested that residues Trp275 and Trp397 are involved in defining the binding selectivity of the enzyme to soluble substrates.
© 2007 Elsevier B.V. All rights reserved.

Keywords: Active-site mutation; Chitin hydrolysis; Chitinase A; Chitooligosaccharide; Specific hydrolyzing activity; Thin layer chromatography; *Vibrio carchariae*

1. Introduction

Chitin is a β (1,4)-linked homopolymer of *N*-acetylglucosamine (GlcNAc or G1) and mainly found as a structural component of fungal cell walls and the exoskeletons of invertebrates, including insects and crustaceans. A complete hydrolysis of chitin usually requires three classes of glycosyl hydrolases. Endochitinases (EC 3.2.1.14) act randomly on chitin to give chitoligomers, then chitobioses ([GlcNAc]$_2$ or

G2) as the main products. Chitobiases (EC 3.2.1.52 or formally EC 3.2.1.30) and *N*-acetyl-β-hexosaminidases (EC 3.2.1.52) further hydrolyze the dimers and chitoligomers to yield *N*-acetylglucosamine (GlcNAc or G1) as the final product. Chitinases occur in a wide range of organisms, including viruses, bacteria, fungi, insects, higher plants, and humans. The presence of chitinases in such organisms is closely related to the physiological roles of their substrates. For example, bacteria express chitinases that enable them to utilize chitin biomass as the sole source of carbon and nitrogen [1], whilst chitinases in fungi are thought to have autolytic, nutritional and morphogenetic functions [2]. In insects, chitinases are essential in the moulting process, and may also affect gut physiology through their involvement in peritrophic membrane turnover [3]. Plant chitinases mainly act as biological control agents against fungal

pathogens and invading insects [4,5], while viral chitinases are involved in pathogenesis of host cells [6]. Chitinases in some vertebrates are mainly produced as part of their digestive tract and may also utilize the enzymes in their defense against pathogenic fungi and some parasites. Human chitinases are particularly associated with anti-inflammatory effect against the T helper-2 driven diseases, such as allergic asthma [7,8].

Chitin is the second most prominent polymer only after cellulose. Thus, the enzymatic degradation of chitin waste using chitinases has recently received much attention as an environmentally-friendly alternative to chemical methods. Chitin derivatives are highly biocompatible and offer a diverse range of applications in areas such as biomedicine, nutrition, food processing, and cosmetics. Chitinase A is a major chitinase produced at high levels by certain soil-born and marine bacteria. This enzyme could potentially serve as an efficient catalyst for the bioconversion of chitin into valuable derivatives for commercial use.

We previously reported the isolation of chitinase A from a Gram-negative marine bacterium, *Vibrio carchariae*, and the DNA that encodes the *Chi A* gene [9,10]. On the basis of amino acid sequence similarities, this M_r 63000 enzyme is classified as a member of family 18 chitinases [11]. Like other family-18 microbial enzymes [12–14], the catalytic domain of *V. carchariae* enzyme comprises two short sequence regions, which form an $(\alpha/\beta)_8$-TIM barrel active site. A completely conserved acidic amino acid (Glu315) located at the end of the conserved motif DxxDxDxE (in the β4 strand) is likely to be the catalytic residue [10]. The action of native chitinase A on chitin initially released a series of small chitooligomeric fragments, which were further hydrolyzed to G2 as the end product, suggesting that the enzyme acts as an endochitinase [15]. The retention of the β over α anomer of all the products observed at initial time of the reactions is in agreement with the substrate-assisted mechanism employed by the enzyme. As suggested by molecular simulation and X-ray structures of the family 18 glycosyl hydrolases [16–19], the catalytic acid equivalent to Glu315 is presumed to donate a proton to the glycosidic oxygen, which leads to a distortion of the sugar molecule at the scissile position into a boat conformation. The resultant bond cleavage yields an oxazolinium intermediate and the retention of anomeric configuration in the products. The higher affinity of *V. carchariae* chitinase A for higher M_r chitooligosaccharides [15] suggested that the catalytic cleft of the enzyme comprises an array of most probably six binding subsites, comparable to that of CiX1 from *Coccidioides immitis* [20,21] and chitinase A (*Sm*chiA) from *Serratia marcescens* [12,22].

A number of studies using site-directed mutagenesis of *Bacillus circulans* chitinase A1, *S. marcescens* 2170 chitinase A and B, and *Streptomyces griseus* chitinase C [23–26] suggested several surface exposed aromatic residues that were important for guiding the chitin chain to the catalytic cleft so that effective catalysis can take place. The effects of the active-site aromatic residues of *B. circulans* chitinase A1 on chitin hydrolysis were also well studied by Watanabe's group [27]. Since the amino acid alignment indicated that certain aromatic residues of *V. carchariae* chitinase A including Tyr171, Trp168, Trp275,

Trp397 and Trp570 are linearly aligned with the aromatic residues at the binding cleft of *B. circulans* chitinase A1 and of *S. marcescens* chitinase A, this research has employed site-directed mutagenesis to investigate the roles of these aromatic residues on the binding and hydrolytic activities of the enzyme towards insoluble chitin and soluble chitooligosaccharides.

2. Materials and methods

2.1. Bacterial strains and chemicals

Escherichia coli type strain DH5α was used for routine cloning, subcloning and plasmid preparation. Supercompetent *E. coli* XL1Blue (Stratagene, La Jolla, CA, USA) was the host strain for the production of mutagenized DNA. *E. coli* type strain M15 (Qiagen, Valencia, CA, USA) and the pQE 60 expression vector harboring *chitinase A* gene fragments were used for a high-level expression of recombinant chitinases. Chitooligosaccharides (G1–G6) and *p*NP-glycosides were obtained from Seikagaku Corporation (Bioactive Co., Ltd., Bangkok, Thailand). Flake chitin from crab shells was product of Sigma-Aldrich Pte Ltd., The Capricorn, Singapore Science Park II, Singapore). QuickChange Site-Directed Mutagenesis Kit including *Pfu* Turbo DNA polymerase was purchased from Stratagene. Aluminum sheets (Silica gel 60F$_{254}$, 20 × 20 cm) for thin-layer chromatography (TLC) were obtained from Merck Co. (Berlin, Germany). Restriction enzymes and DNA modifying enzymes were products of New England Biolabs, Inc. (Beverly, MA, USA). All other chemicals and reagents (analytical grade) were obtained from the following sources: reagents for bacterial media (Scharlau Chemie S.A., Barcelona, Spain.); chitin from crab shells and all chemicals for protein preparation and thin-layer chromatography (Sigma-Aldrich Pte Ltd., Singapore and Carlo Erba Reagenti SpA, Limito, Italy).

2.2. Homology modeling

The putative amino acid sequence of the mature *V. carchariae* chitinase A was submitted to Swiss-Model (http://swissmodel.expasy.org/) for the tertiary structure prediction using the X-ray structure of *S. marcescens* chi A E315L mutant complex with hexaNAG (G6) (PDB code: 1NH6) as structural template. The predicted structure was viewed and edited with Pymol (www.pymol.org). The residues at the substrate binding cleft of *V. carchariae* chitinase A were located by superimposing 459 residues of *V. carchariae* chitinase A with the equivalent residues of *S. marcescens* chi A mutant docked with G6 coordinates, using the program Superpose available in the CCP4 suit [28].

2.3. Mutant design and site-directed mutagenesis

Point mutations were introduced to the wild-type *chitinase A* DNA that was previously cloned into the pQE expression vector by PCR technique [10], using the QuickChange Site-Directed Mutagenesis Kit, according to the Manufacturer's protocols. Active-site chitinase A variants were generated using oligonucleotides synthesized from Proligo Pte Ltd. (Helios, Singapore) and Bio Service Unit (BSU) (Bangkok, Thailand). Oligonucleotide sequences used for site-directed mutagenesis are listed in Table 1. Single mutants (W168G, Y171G, W275G, W397F, W570G and D392N) were constructed using the DNA fragment encoding wild-type chitinase A as template. A double mutant (W397F/W570G), a triple mutant (W397F/W570G/ W275G), and a quadruple mutant (W397F/W570G/W275G/Y171G) were produced using mutants W570G, W397F/W570G, and W397F/W570G/W275G, respectively, as DNA templates.

The success of newly-generated mutations was confirmed by automated DNA sequencing (BSU, Thailand). The programs used for nucleotide sequence analyses were obtained from the DNASTAR package (DNASTAR, Inc., Madison, USA).

2.4. Protein expression and purification

The DNA fragment that encodes wild-type chitinase A (amino acid residues 22–597, without the 598–850 C-terminal fragment) was cloned into

Table 1
Primers used for mutagenesis

Name	DNA template	Sequence[a]
W168G	*Chitinase A* wild-type	forward 5′-CTTATTTTGTTGAAGGAGGCATCTACGG-3′
		reverse 5′-CCGTAGATGCCTCCTTCAACAAAATAAG-3′
Y171G	*Chitinase A* wild-type	forward 5′-GAATGGGGCATCGGAGGTCGTGATTACAC-3′
		reverse 5′-GTGTAATCACGACCTCCGATGCCCCATTC-3′
W275G	*Chitinase A* wild-type	forward 5′-CATCTATCGGTGGTGGAACACTTTCTGAC-3′
		reverse 5′-GTCAGAAAGTGTTCCACCACCGATAGATG-3′
D392N	*Chitinase A* wild-type	forward 5′-CTTTGCGATGACTTACAACTTCTACGGCGG-3′
		reverse 5′-CAGCCGCCGTAGAAGTTGTAAGTCATCGCAAAG-3′
W397F	*Chitinase A* wild-type	forward 5′-GACTTCTACGGCGGCTTCAACACAACGTTCC-3′
		reverse 5′-GGAACGTTGTTGAAGCCGCCGTAGAAGTC-3′
W570G	*Chitinase A* wild-type	forward 5′-GCAGGTCTATTCTCTGGAGAGATTGATGC-3′
		reverse 5′-GCATCAATCTCTCCAGAGAATAGACCTGC-3′
Double mutant	W570G mutant	forward 5′-GACTTCTACGGCGGCTTCAACACAACGTTCC-3′
		reverse 5′-GGAACGTTGTTGAAGCCGCCGTAGAAGTC-3′
Triple mutant	double mutant	forward 5′-CATCTATCGGTGGTGGAACACTTTCTGAC-3′
		reverse 5′-GTCAGAAAGTGTTCCACCACCGATAGATG-3′
Quadruple mutant	triple mutant	forward 5′-GAATGGGGCATCGGAGGTCGTGATTACAC-3′
		reverse 5′-GTGTAATCACGACCTCCGATGCCCCATTC-3′

[a] Sequences underlined indicate mutated codons.

the pQE60 expression vector and highly expressed in *E. coli* M15 cells as the 576-amino acid fragment with a *C*-terminal (His)$_6$ sequence [10]. For recombinant expression, the cells were grown at 37 °C in Luria Bertani (LB) medium containing 100 μg/ml ampicillin until OD$_{600}$ of the cell culture reached 0.6. After that, the cell culture was cooled down on ice to 25 °C before chitinase expression was induced by the addition of isopropyl thio-β-ᴅ-galactoside (IPTG) to a final concentration of 0.5 mM. Cell growth was continued at 25 °C for 18 h, and the cell pellet was collected by centrifugation at 4500×*g* for 30 min. The freshly-prepared cell pellet was resuspended in 40 ml of lysis buffer (20 mM Tris–HCl buffer, pH 8.0, containing 150 mM NaCl, 1 mM phenylmethylsulphonyl fluoride (PMSF), and 1.0 mg/ml lysozyme), then lysed on ice using a Sonopuls Ultrasonic homogenizer with a 6-mm-diameter probe (50% duty cycle; amplitude setting, 20%; total time, 30 s, 6–8 times). Unbroken cells and cell debris were removed by centrifugation at 12,000×*g* for 1 h. The supernatant was immediately applied to a Ni-NTA agarose affinity column (1.0×10.0 cm) (QIAGEN GmbH, Hilden, Germany), and the chromatography was carried out gravitationally at 25 °C, following the Qiagen's protocol. After loading, the column was washed with 100 ml of loading buffer (20 mM Tris–HCl buffer, pH 8.0) containing 5 mM imidazole, followed by another 50 ml of 10 mM imidazole in the loading buffer. Ni-NTA-bound proteins were then eluted with 250 mM imidazole in the same buffer. Eluted fractions of 0.5 ml were collected and 6 μl of each fraction was analyzed on a 12% SDS-PAGE, according to the method of Laemmli [29], to confirm purity. Fractions that possessed chitinase activity were pooled and then subjected to several rounds of membrane centrifugation using Vivaspin-20 ultrafiltration membrane concentrators (*M*$_r$ 10,000 cut-off, Vivascience AG, Hannover, Germany) for a complete removal of imidazole. A final concentration of the protein was determined by Bradford's method [30] using a standard calibration curve constructed from BSA (0–25 μg). The freshly-prepared proteins were either immediately subjected to functional characterization or stored at −30 °C in the presence of 15% glycerol until used.

2.5. Chitinase activity assays

Chitinase activity was determined by colorimetric assay using *p*NP-[GlcNAc]$_2$ as substrate or by reducing sugar assay using colloidal chitin as substrate. The *p*NP assay was determined in a 96-well microtiter plate and a 100-μl assay mixture contained protein sample (10 μl), 500 μM *p*NP-(GlcNAc)$_2$ (25 μl), and 100 mM sodium acetate buffer, pH 5.0 (65 μl). The reaction mixture was incubated at 37 °C for 10 min with constant agitation, then the enzymatic reaction was terminated by the addition of 50 μl 1.0 M Na$_2$CO$_3$. The amount of

p-nitrophenol (*p*NP) released was determined spectrophotometrically at 405 nm in a microtiter plate reader (Applied Biosystems, Foster City, CA, USA). The molar concentrations of *p*NP were calculated from a calibration curve constructed with varying *p*NP from 0 to 30 nmol.

The reducing sugar assay was carried out by modifying the chitinase microassay protocol developed by Bruce et al. [31]. The reaction mixture (400 μl), containing 20 mg of colloidal chitin (prepared based on Hsu and Lockwood, 1975 [32]) in 0.1 M sodium acetate buffer, pH 5.0 and 80 μg chitinase A, was incubated at 37 °C with shaking in a Thermomixer comfort (Eppendorf AG, Hamburg, Germany). After 60 min, the reaction was terminated by boiling at 100 °C for 5 min, and then centrifuged at 2795×*g* for 5 min to precipitate the remaining chitin. A 150-μl supernatant was transferred to a new tube, to which was added 30 μl of 0.8 M potassium tetraborate, followed by boiling for 3 min. After cooling, 900 μl of a freshly prepared *p*-dimethylaminobenzaldehyde (DMAB) solution was added and then incubated at 37 °C for 20 min. A release of reducing sugars was detected by measuring the absorbance at 585 nm (*A*$_{585}$). Specific hydrolyzing activity against colloidal chitin was calculated by converting *A*$_{585}$ to μmoles of reducing sugars using a standard calibration curve constructed with varying G2 from 0 to 4.0 μmol.

2.6. Circular Dichroism (CD) spectroscopy

The purified chitinases were diluted to 0.40 to 1.40 mg/ml in 20 mM Tris/HCl buffer, pH 8.0. CD spectra over three scans were measured using a Jasco J-715 spectropolarimeter (Japan Spectroscopic Co., Japan) at near UV (190 to 250 nm) regions. CD measurements were performed at 25 °C with a scan speed of 20 nm/min, 2 nm bandwidth, 100 mdeg sensitivity, an average response time of 2 s and an optical path length of 0.2 mm. The baseline buffer for all the proteins was 20 mM Tris/HCl buffer, pH 8.0. The baseline was measured and subtracted from each spectrum before the raw data were transformed to mean residue ellipticity (MRE) using the equation: $[\Theta] = (73.33 \, m°)/([\text{prot}]_{\text{mM}} \, l_{\text{cm}} \, n)$, where $[\Theta]$ is the MRE in deg cm^2 d/mol, *n* is the number of amino acids in the polypeptide chain, *m°* is the measured ellipticity, and l is the path length in centimeters. The intensity of JASCO standard CSA (non-hygroscopic ammonium (+)-10-camphorsulfonate) at wavelength 290 nm was about 45 units. Therefore, the conversion factor was calculated to be 3300/CSA intensity at 290 nm or 73.33 using the equation above. The molecular weight of each protein was calculated from number of amino acids×mean residue weight. After noise reduction and concentration adjustment, the measured ellipticity was converted to the molar ellipticity, which was plotted versus wavelength.

2.7. Kinetic measurements

Kinetic studies of chitinase A mutants were performed by colorimetric assay in a microtiter plate reader (Applied Biosystems, USA). The reaction mixture (100 μl), containing 0–500 μM pNP-(GlcNAc)$_2$, dissolved in 100 mM sodium acetate buffer, pH 5.0, and dH$_2$O, was pre-incubated at 37 °C for 10 min. After the enzyme (400 ng) was added, the reaction was continued for additional 10 min at 37 °C and then terminated with 50 μl of 1 M Na$_2$CO$_3$. Release of p-nitrophenol (pNP) was monitored at A_{405}, which was subsequently converted to molar quantities using a calibration curve of pNP (0–30 nmol). The kinetic values (K_m, V_{max}, and k_{cat}) were evaluated from three independent sets of data by the nonlinear regression function of the GraphPad Prism software (GraphPad Software Inc., San Diego, CA).

2.8. Chitin binding assay

Chitin binding studies were carried out using flake chitin prepared from crab shells (Sigma-Aldrich Pte Ltd., Singapore). Fine particles of insoluble chitin were suspended in dH$_2$O to yield 10 mg/ml stock solution (the suspension was continuously stirred with a magnetic stirrer in order to obtain consistent amounts when pipetting). A reaction mixture (2.0 ml), containing 2.5 mg/ml flake chitin and 200 μg/ml chitinase in 100 mM sodium acetate buffer, pH 5.0, was shaken continuously at 4 °C. At different time points (0, 5, 10, 15, 30, 60, 90, 120, and 180 min), a 150-μl aliquot was taken and spun twice in a microcentrifuge at 9660×g for 3 min to precipitate the chitin particles. Then the unbound chitinase A remaining in the supernatant was measured spectrophotometrically at 280 nm (A_{280}).

2.9. Product analysis by thin-layer chromatography

Hydrolysis of chitooligosaccharides (G2–G6) by wild-type and mutants D392N, W168G, Y171G, W275G, and W397F was carried out in a 80-μl reaction mixture, containing 0.1 M sodium acetate buffer, pH 5.0, 2.5 mM substrate and 800 ng purified enzyme. The reaction was incubated at 30 °C with shaking for 60 min, and then terminated by boiling for 5 min. For product analysis, each reaction mixture was applied five times (one μl each) to a silica TLC plate (7.0×10.0 cm), and then chromatographed three times (1 h each) in a mobile phase containing n-butanol: methanol: 28% ammonia solution: H$_2$O (10:8:4:2) (v/v), followed by spraying with aniline-diphenylamine reagent and baking at 180 °C for 3 min [33].

In the time course of G6 hydrolysis by wild-type, W275G and W397F were measured in the same way as described for the hydrolysis of G2–G6, but the reaction was incubated at 30 °C at interval times of 2, 5, 10, 15, 30, 60 min, and 18 h prior to termination. Examination of the time course of chitin hydrolysis by the three chitinase variants was carried out in a 400-μl reaction mixture, containing 0.1 M sodium acetate buffer, pH 5.0, 20 mg colloidal chitin, and 80 μg purified enzyme. The reaction was incubated at 30 °C at the same time intervals as for G6 hydrolysis, and then terminated by boiling for 5 min. Products released from the reactions were subsequently analyzed by TLC using the conditions described above.

3. Results and discussion

3.1. Sequence analysis and homology modeling

A comparison of the deduced amino acid sequence of *V. carchariae* chitinase A with seven other family-18 chitinases suggested that Glu315 and Asp392 are completely conserved (data not shown). However, we previously employed site-directed mutagenesis to demonstrate that only Glu315 was important for catalysis [15]. The alignment also showed that five aromatic residues, including Trp168, Tyr171, Trp275, Tyr435, and Trp570 in the sequence of *V. carchariae* chitinase A are linearly aligned with the equivalent aromatic residues of other bacterial sequences. Trp397 is the only residue for which phenylalanine is replaced in the sequences of *S. marcescens*, *B. cepacia*, and *A. punctata*. In an attempt to locate these amino acids in the structure of *V. carchariae* chitinase A, its 3D-structure was modeled based on the X-ray structure of *S. marcescens* Chi A E315L mutant complexed with G6 (see Materials and methods). The target residues, which extend over the substrate binding cleft at the top of the TIM-barrel domain, are shown in Fig. 1A.

Fig. 1B displays the superimposition of the active site of *V. carchariae* chitinase A on that of *S. marcescens* Chi A E315L mutant. It can be seen that Trp168, Tyr171, Trp231, Trp 275, Tyr435, Trp570, Glu315 and Asp392 of the *Vibrio* enzyme completely overlay Trp167, Tyr170, Phe232, Trp275, Trp539, Glu315 and Asp391, respectively, of the *Serratia* enzyme with an R.M.S. value of 0.032 Å. In contrast, Trp397 overlaid Phe396 residue of the *Serratia* enzyme with the orientation of their hydrophobic faces lying perpendicular to each other.

Since the positions of the binding cleft residues of *V. carcharia* and *S. marcescens* chitinases were nearly identical, most of the conformations of the sugar rings bound in the catalytic cleft of the template's structure are likely to be adopted by the modeled structure. Based on this assumption, Tyr171 is likely to be located at the edge of the binding cleft beyond subsite −4 (the non-reducing end), whereas Trp168, Trp570, and Trp275 should stack against the pyranosyl rings of GlcNAc units at subsites −3, −1, and +1, respectively. Trp397 should be located near the GlcNAc unit at subsite +2 (the reducing end). The presence of Glu315 at the scissile bond between the GlcNAcs at subsites −1 and +1 seems to explain the catalytic role of this residue. Asp392 appears to be further away from the cleavage site, but in close contact with the GlcNAcs at subsites +1 and +2. This supports our previous finding that this residue did not play a direct role in catalysis [15].

3.2. Recombinant expression, purification and secondary structure determination

To investigate the influence of Tyr171, Trp168, Trp275, Trp397, Trp570 on the binding and hydrolytic activities of *V. carchariae* chitinase A, these residues were mutated using PCR-based site-directed mutagenesis. Replacement of Asp392 with Asn was previously described by Suginta et al. [15]. After confirming the genetic modification of the target bases by automatic DNA sequencing, the recombinant proteins were highly expressed in *E. coli* M15 host cells. The six histidine residues tagged at the *C*-terminus allowed the proteins to be readily purified using Ni-NTA agarose affinity chromatography. SDS/PAGE analysis showed that the purified proteins migrated to ∼63 kDa (Fig. 2A). This molecular weight corresponded well to that of wild-type. The yields obtained from this expression system were approx. 10–15 mg of highly purified protein per liter of bacterial culture.

Prior to further investigating the effects of point mutations on the binding and hydrolytic activities, the folding states of the *E. coli* expressed chitinase A were examined by means of CD spectroscopy. Fig. 2B shows that the spectra of the mutated
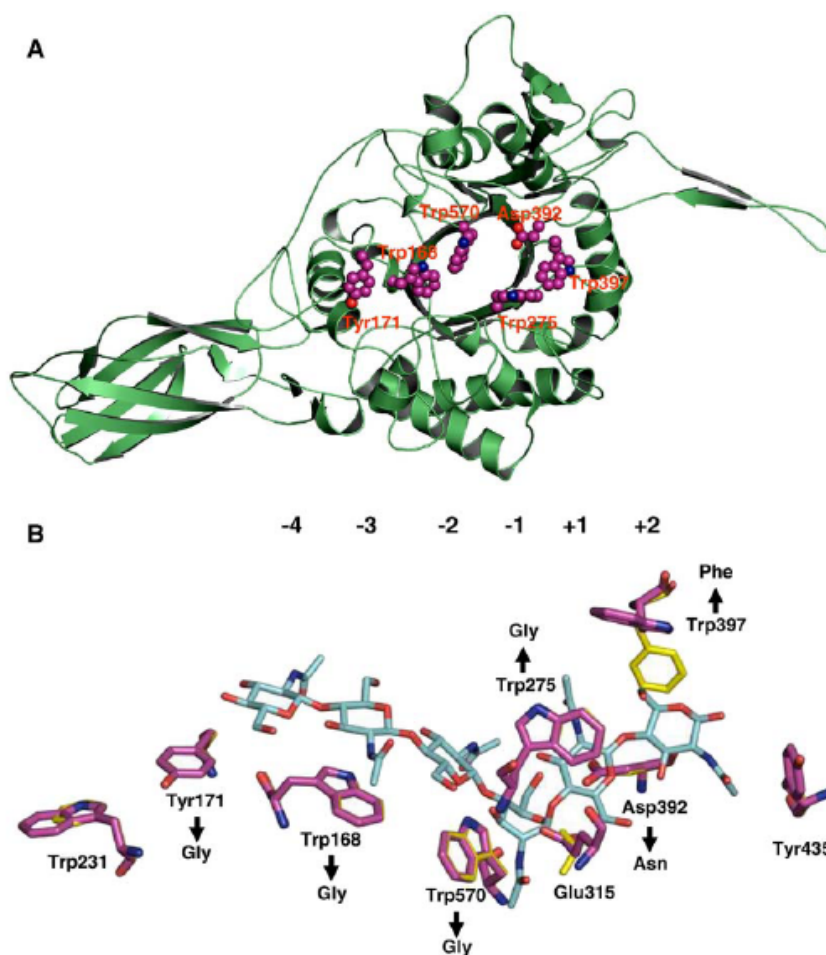
Fig. 1. The Swiss-Model 3D-structure of *V. carchariae* chitinase A. (A) A ribbon representation of the 3D-structure of *V. carchariae* chitinase A (in green) was modeled based on the X-ray structure of *S. marcescens* Chi A E315L mutant as described in the text. The target aromatic residues (in magenta) that line within the substrate-binding cleft are shown in space-filling model. (B) A stick model of the putative binding cleft of *V. carchariae* chitinase A (in magenta) was superimposed on that of *S. marcescens* Chi A E315L mutant (in yellow) complexed with G6 (in cyan). N atoms are shown in blue and O atoms are shown in red. (For interpretation of the references to colour in this figure legend, the reader is referred to the web version of this article.)

proteins nicely overlaid the spectrum of the wild-type. This demonstrated the overall similarity of the conformations of mutated and non-mutated enzymes.

3.3. Effects of the mutations on the chitin binding equilibrium and the specific hydrolyzing activity of chitinase A

Initial studies of the chitin binding activity of single mutants were performed using flake chitin prepared from crab shells. To minimize hydrolysis of the enzyme bound to the chitin substrate, the assay mixture was maintained at 4 °C throughout the experiment. For each reaction, a decrease in the concentration of the unbound enzyme was monitored at various time points as indicated in Materials and methods. The results (Fig. 3) showed that the binding behaviors of wild-type enzyme and mutants W168G, Y171G, W275G, and W397F were indistinguishable. In general, the binding process took place quite rapidly, and reached equilibrium within 15 min. However, a difference was seen with mutant D392N for which the binding took a much longer time, about 60 min, to reach equilibrium. Apparently, mutations of the aromatic side chains did not markedly affect the binding equilibrium.

When the specific hydrolyzing activity of the different chitinase variants towards pNP-[GlcNAc]$_2$ and colloidal chitin were examined (Table 2), similar results were seen
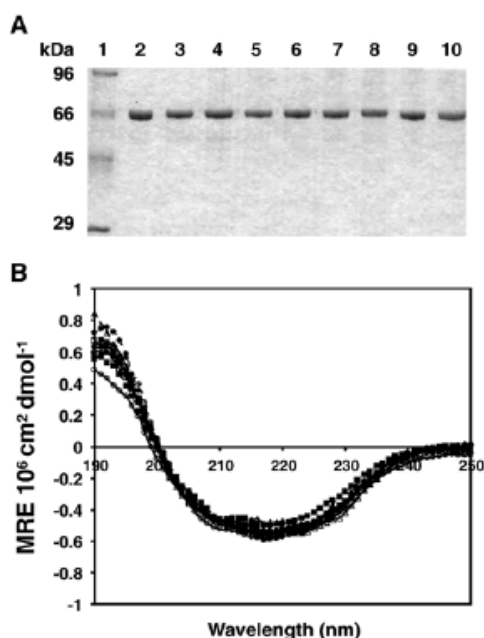
Fig. 2. SDS/PAGE analysis and CD spectra of chitinase A variants. (A) Purified chitinases (2 μg) were electrophoresed using 12% SDS/PAGE gel and then were stained with Coomassie blue. (B) Chitinase A and its mutants were purified by Ni-NTA agarose affinity chromatography, and then dialyzed extensively to remove imidazole. The proteins were solubilized in 20 mM Tris/HCl buffer, pH 8.0 to final concentrations of 0.40 to 1.40 mg/ml. CD spectra of chitinase variants were obtained with a Jasco J-715 spectropolarimeter. A solution of 20 mM Tris/HCl, pH 8.0 was used for background subtraction. Symbols: —O—, wild-type; —□—, D392N; —△—, W168G; —●—, Y171G, —■—, W275G; —▲—, W397F; ---O---, W570G; ---□---, double mutant; ---△---, triple mutant; and ---●---, quadruple mutant.
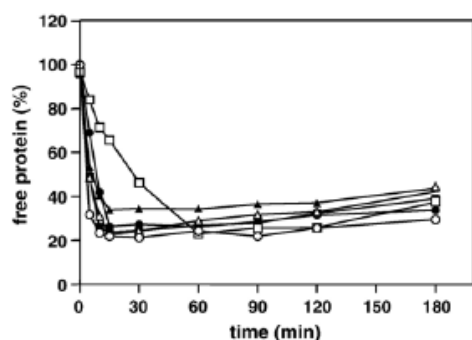

Fig. 3. Time-course studies of binding of chitinase A and mutant enzymes to colloidal chitin. Chitinases (200 μg/ml in 100 mM sodium acetate buffer, pH 5.0) were incubated with 2.5 mg/ml flake chitin at 4 °C to minimize chitin hydrolysis. Decreases in free enzyme concentration were monitored at different time points from 0 to 180 min by measuring A_{280}. Each data value was calculated from triplicate experiments. Symbols: O, wild-type; □, D392N; △, W168G; ●, Y171G, ■, W275G; and ▲, W397F.

Table 2
Specific hydrolyzing activity of chitinase A and mutants against pNP-[GlcNAc]$_2$ and colloidal chitin

Chitinase A variant	Specific hydrolyzing activity	
	($\times 10^{-3}$ μmol pNP/min/μg)[a]	(μmol reducing sugars/min/μg)[b]
Wild-type	1.84±0.05 (100)[c]	1.99±0.018 (100)
D392N	0.61±0.09 (33.4)	n.d.[d]
W168G	0.24±0.03 (13.0)	n.d
Y171G	0.36±0.00 (19.5)	n.d.
W275G	0.20±0.00 (11.1)	0.10±0.001 (5.0)
W397F	2.61±0.08 (141.8)	2.04±0.061 (102.5)
W570G	0.11±0.00 (5.6)	n.d.
Double mutant (W570G/W397F)	0.10±0.002 (5.5)	n.d.
Triple mutant (W570G/W397F/W275G)	0.01±0.001 (0.6)	n.d.
Quadruple mutant (W570G/W397F/W275G/Y171G)	0.01±0.001 (0.6)	n.d.

For colorimetric assay A 100-μl assay mixture, containing 400 ng chitinase, 500 μM pNP-(GlcNAc)$_2$, and 0.1 M sodium acetate buffer, pH 5.0, was incubated at 37 °C for 10 min, and then terminated by the addition of 50 μl of 1.0 M Na$_2$CO$_3$. The amount of pNP released was determined by A_{405}. The μmole amount of pNP was calculated from a calibration curve of pNP (0–30 nmol). With the reducing sugar assay, the reaction mixture (400 μl), containing 20 mg of colloidal chitin, 0.1 M sodium acetate buffer, pH 5.0 and 80 μg chitinase A, was incubated at 37 °C with continuous shaking. After 60 min, the reaction was boiled at 100 °C for 5 min, and then centrifuged to remove the insoluble chitin. Release of reducing sugars was determined according to DMAB method as described in Materials and methods. The μmol amounts of the reducing sugars were estimated using a standard calibration curve of G2 (0–4.0 μmol).
[a] Chitinase activity was measured using pNP-[GlcNAc]$_2$, and release of pNP was detected by the colorimetric method.
[b] Chitinase activity was measured using colloidal chitin, and release of reducing sugars was detected by the DMAB method.
[c] Values in brackets represent relative activity compared to that of wild-type (set as 100).
[d] n.d. represents no detectable activity.

with both substrates. Mutations of Trp168, Tyr171, Trp570, and D392N completely abolished the hydrolyzing activity against colloidal chitin, and greatly reduced the hydrolyzing activity against the pNP substrate. As previously seen with *B. circulans* ChiA1, mutations of the equivalent aromatic residues (Trp53, Tyr56, and Trp433, respectively) to alanine also resulted in a drastic decrease in the hydrolyzing activity of *B. circulans* ChiA1, especially against crystalline β-chitin or colloidal chitin [27]. As proposed by Watanabe [23,27,34], Trp53 and Tyr56 (the equivalent residues of Trp168 and Tyr171 of the *Vibrio* chitinase) participate in the feeding process that brings the incoming chitin chain through the binding cleft.

At this point, it is difficult to draw a conclusion why mutations of Trp168 and Tyr171 also affected the hydrolyzing activity against the pNP substrate, as the [GlcNAc]$_2$ moieties could only bind to subsites −2 and −1 to allow the pNP aglycone to bind at subsite +1 for further cleavage.

Of all single mutants, W570G showed most severe effects on the hydrolyzing activity, having no activity against colloidal chitin and least activity (5% remaining activity) against pNP-[GlcNAc]$_2$. In the modeled 3D structure (see

Table 3
Kinetic parameters of wild-type and mutants of chitinase A

Chitinase A variants	$K_m{}^a$ (μM)	V_{max} (nmol/min/μg chitinase)	k_{cat} (s^{-1})	k_{cat}/K_m (s^{-1} M^{-1})
Wild-type	288±26.0	1.94±0.09	2.15	7.16×10^2 (100)[b]
D392N	71±5.5	0.29±0.01	0.31	4.34×10^2 (61)
W168G	278±28.2	0.10±0.01	0.11	3.82×10^1 (5)
Y171G	115±10.2	0.20±0.001	0.21	1.85×10^2 (26)
W275G	62±10.8	0.11±0.001	0.12	1.89×10^2 (26)
W397F	315±26.7	2.44±0.11	2.59	8.23×10^2 (114)

The hydrolysis of pNP-[GlcNAc]$_2$ at varying concentrations of 0–500 μM was carried out with 400 ng native chitinase A in 100 mM sodium acetate buffer, pH 5.0 for 10 min at 30 °C, and then the reaction was terminated with 50 μl of 1 M Na$_2$CO$_3$. Release of pNP, monitored at A$_{405}$, was converted to molar quantities using a calibration curve of pNP (0–30 nmol). The kinetic values (K_m, V_{max}, and k_{cat}) were determined by nonlinear regression using GraphPad Prism software (GraphPad Software Inc., San Diego, CA).

[a] Kinetic assays were preformed with pNP-[GlcNAc]$_2$ as described in Materials and methods. Results are average of three independent experiments.

[b] Numbers in brackets reveal relative k_{cat}/K_m values of the generated mutants by comparing with the wild-type value (set to 100).

Fig. 1B), Trp570 was closest to the sugar ring at subsite-1. Like Trp539 in the *Serratia* structure [22], this residue is likely to be responsible for holding the GlcNAc ring at this position in place so that cleavage of the glycosidic bond between subsites −1 and +1 can occur.

Trp397 was an exception. Its mutation to Phe, instead, enhanced hydrolyzing activity towards the pNP substrate to 142% but increased the activity towards colloidal chitin only slightly to 102.5%. Although the elevated activity against pNP-[GlcNAc]$_2$ cannot be explained at this stage, the lack of change in the hydrolyzing activity towards the chitin polymer implied that Trp397 did not participate directly in the hydrolytic process.

In addition, the triple and quadruple mutants yielded non-detectable activity against colloidal chitin and less than 1% remaining activity against pNP-[GlcNAc]$_2$. This may be seen as the cumulative effects of multiple point mutations on the hydrolyzing activity of *Vibrio* chitinase A.

3.4. Steady-state kinetics of chitinase A variants against pNP-[GlcNAc]$_2$

The kinetic parameters of the hydrolytic activity of wild-type and its single mutants (except for W570G) were further explored with pNP-[GlcNAc]$_2$. As shown in Table 3, the active-site modifications resulted in impairment of both K_m and k_{cat} of the enzyme. Mutants D392N, Y171G and W275G particularly reduced the K_m values to 0.24, 0.4 and 0.2 times, respectively, of the wild-type's value, while mutant W168G did not significantly change the K_m value against the pNP substrate. It is visible that the same mutants also greatly reduced the k_{cat} values to 5–14% of that of the wild-type. Overall, the mutations varied the k_{cat}/K_m values of the enzyme. W168G displayed the least value (5%), followed by Y171G and W275G (approx. 26%), and D392N (61%), compared to the value obtained for wild-type.

On the other hand, mutant W397F gave no significant changes in the kinetic parameters of the enzyme with pNP-[GlcNA]$_2$. Its K_m and k_{cat} values were found to be 1.1 and 1.2 fold of that of the wild-type. These data suggested that Trp397 did not take part in the hydrolysis of this substrate.

3.5. TLC analysis of the hydrolytic activity of chitinase variants

The effects of the mutations on the hydrolytic activities against chitooligomers (G2–G6) and colloidal chitin were further studied by thin layer chromatography (TLC). The cleavage patterns of each mutant were initially observed at a single point in time (60 min). As expected, none of the mutants hydrolyzed G2 substrate, as it only acts as the end product of the enzyme action [15]. With G3 substrate (Fig. 4A), W397F was the only mutant that degraded G3 to G1 and G2, while the wild-type and other mutants did not utilize G3 at all. Our recent study showed high K_m value (10.54 mM) of the native enzyme towards G3, indicating that G3 was a poor substrate for *V. carchariae* chitinase [15].

Distinct patterns of product formation became visible with longer-chain oligomers (G4–G6). With G4 substrate (Fig. 4B), the formation of G2 was seen at higher levels with mutants
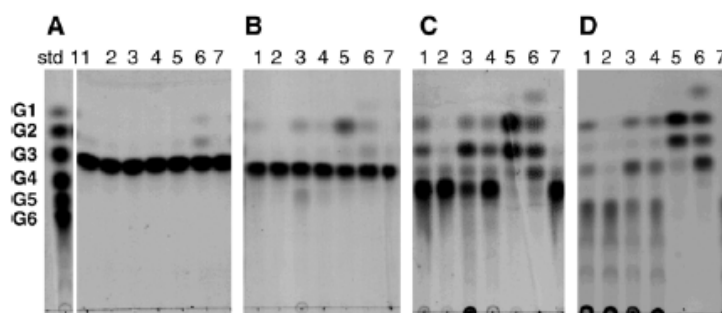

Fig. 4. TLC analysis of chitooligosaccharide hydrolysis of chitinase A and mutants. A reaction mixture, containing 400 ng chitinase and 2.5 mM substrate (G2–G6) in 100 mM sodium acetate buffer, pH 5.0, was incubated for 60 min at 30 °C. After boiling, the reaction solution (5 μl) was analyzed on TLC and sugar products detected with aniline-diphenylamine reagent. (A) Hydrolysis of G3 substrate, (B) Hydrolysis of G4 substrate, (C) Hydrolysis of G5 substrate, and (D) Hydrolysis of G6 substrate. Lanes: std, standard mix of G1–G6; 1, wild-type; 2, D392N; 3, W168G; 4, Y171G, 5, W275G; 6, W397F; and 7, substrate control.
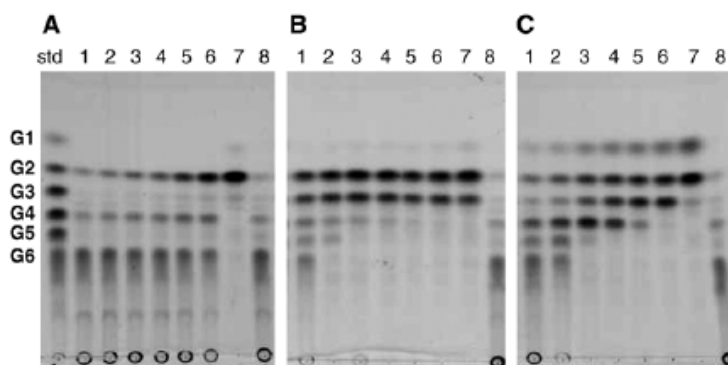
Fig. 5. Time-course of G6 hydrolysis by wild-type and mutants W275G and W397F. A reaction mixture (80 μl), containing 800 ng wild-type (A), W275G (B), or W397F (C) and 2.5 mM G6 in 0.1 M sodium acetate buffer, pH 5.0, was incubated at various times at 30 °C, and then analyzed by TLC. Sugar products were detected with aniline-diphenylamine reagent. Lanes: std, a standard mix of G1–G6; 1–7, incubation at 2, 5,10, 15, 30, 60 min and 18 h, respectively; and 8, substrate control.

Y171G, W275G, and W397F (with W275G having the most prominent signal). In G4 hydrolysis, an extra band corresponding to G5 was detected in the reaction with W168G, most likely due to be some tranglycosylation occurring concurrently with hydrolysis. Enhanced glycosylation was also recently found by Aronson et al. [35] in point mutation of the non-reducing end residue (Trp167 to Ala) for *S. marcescens* chitinase A.

With G5 and G6 substrates (Fig. 4C and D), the aromatic side chain mutants in general created more hydrolytic products than the wild-type enzyme. The breakdown of these substrates to G2 and G3 was best achieved by W275G, whereas the release of G1–G4 intermediates was preferred by W397F. On the other hand, W168G and Y171G seemed to behave similarly to the wild-type homologue, by releasing a small amount of G4 and greater amounts of G3 and G2 in the reactions with G5 substrate, while releasing comparable amounts of G4 and G2 in the reactions with G6 substrate.

The discrimination in substrate hydrolysis between wild-type and its mutants W275G and W397 was confirmed by time course experiments. Fig. 5A–C show the products formed by hydrolysis of G6 with the three variants at different times of reaction. Noticeably, both W275G and W397F hydrolyzed G6 much more efficiently than wild-type chitinase A. The reactions of W275G and W397F with G6 were already complete at 5 and 10 min, while substantial amounts of G6 were still present at these time points in the reaction mixture containing wild-type.

A further observation was that the three enzymes clearly adopted different modes of action on G6 substrate. This claim is supported by the fact that wild-type initially hydrolyzed G6 to G4 and G2. At the end of the reaction, G2 was produced as the major product (Fig. 5A). In contrast, W275G generated reaction intermediates of various lengths from G2 to G5 at initial times. Later, almost equal amounts of G2 and G3 were formed and this remained stable in course of reaction (Fig. 5B). On the other hand, W397F gave most distinct results by releasing a full range of G1–G5 products at early reaction times, eventually yielding G1 and G2 at the end (Fig. 5C).
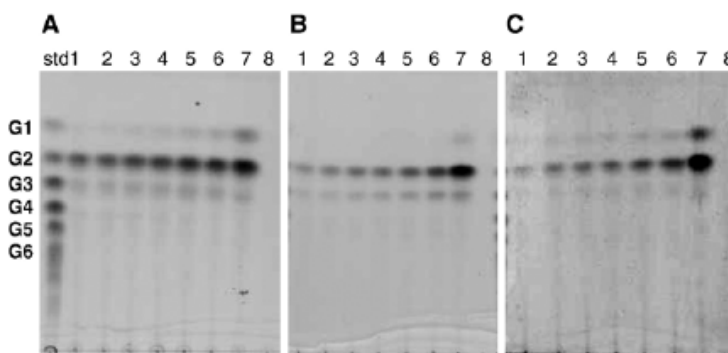

Fig. 6. Time-course of colloidal chitin hydrolysis by wild-type and mutants W275G and W397F. A reaction mixture (400 μl), containing 80 μg wild-type (A), W275G (B), or W397F (C) and 20 mg colloidal chitin in 0.1 M sodium acetate buffer, pH 5.0, was incubated at various times at 30 °C, and then analyzed by TLC using the same conditions as described for chitooligosaccharide hydrolysis. Lanes: std, standard mix of G1–G6; 1–7, incubation at 2, 5,10, 15, 30, 60 min and 18 h, respectively; and 8, substrate control.

The difference in cleavage patterns was not visible when the three enzymes were used to hydrolyze colloidal chitin (Fig. 6A–C). Over the first 60 min of incubation, the three enzymes essentially degraded chitin to G2 as the major product, with trace amounts of G3. Then, after 18 h, G2 and G1 were produced as the major end products, with some G3 also being present in the reaction of the W275G mutant.

The 3D-structure of *S. marcescens* chitinase A E315L mutant complexed with hexaNAG revealed that the oligosaccharide occupied subsites −4 to +2. An almost superimposition of the substrate binding clefts of *Vibrio* and *Serratia* enzymes (Fig. 2B) led to the assumption that oligosaccharide substrates would occupy the binding cleft of the *Vibrio* chitinase A in a similar manner as it was observed with the *Serratia* enzyme. Further investigation of the products released from penta- and hexaNAG hydrolyses by *S. marcescens* wild-type chitinase A demonstrated that both substrates only occupied subsites −2 to +2 with additional sugars extend beyond the substrate-binding cleft at the reducing end [22]. Such a four subsite binding mode seemed to also be the case for *B. circulans* chitinase A1 [27]. Even though the binding mode of the *Vibrio* enzyme cannot be specified at this point in time, the shift in the degradation patterns against chitooligomers upon particular point mutations gave indication that Trp275 and Trp397 are both important in the selective binding of soluble substrates.

A mutation of Trp397 to Phe results in an entire change in the cleavage patterns of the enzyme towards G6 and it can thus be assumed that Trp397 is involved in defining the primary binding sites for the incoming sugars so that the G2 and G4 will mainly be produced from the G6 substrate (Fig. 5A). Mutation of Trp397 to a less hydrophobic residue (Phe) seemed to loosen the binding affinity at this subsite. As a result, the incoming oligosaccharide had more freedom to assemble itself in the binding cleft, thus permitting various bonds to be exposed to the cleavage site (Fig. 5C). This finding is in a good agreement with the previous observations on *Serratia* and *Bacillus* chitinases [22,27]. Based on the −2 to +2 binding mode, Aronson et al. [22] suggested that the loss of binding affinity of the subsite +2 residue as a result of amino acid replacement (Trp396 to Ala) shifted the primary binding sites at least one position towards the non-reducing end.

Mutation of the +1 binding residue (Trp275) to Gly led to a major change in the hydrolysis of higher M_r oligosaccharides (as seen in Fig. 4B–D and Fig. 5B) by allowing the second and the third bonds of G6 from the non-reducing end (in the four subsite binding mode) to be equally accessed, confirming that Trp275 is involved in the specific binding of GlcNAc units around the cleavage site.

With colloidal chitin, no significant change in the cleavage patterns was seen as a result of the specific mutations of Trp275 and Trp397, which suggested that the two residues did not play the same role as in chitooligosaccharide degradation. According to "the feeding-sliding theory" suggested by Watanabe's group [23,27,34], a chitin polymer would enter the binding cleft unidirectionally from the non-reducing end rather than enter randomly like small substrates. Under these conditions, binding would be more influenced by a cluster of the surface-exposed amino acid residues that stretch along the *N*-terminal chitin binding domain through the substrate binding cleft than by particular residues.

References

[1] C. Yu, A.M. Lee, B.L. Bassler, S. Roseman, Chitin utilization by marine bacteria. A physiological function for bacterial adhesion to immobilized carbohydrates, J. Biol. Chem. 266 (1991) 24260–24267.

[2] D.M. Rast, M. Horsch, R. Furter, G.W. Gooday, A complex chitinolytic system in exponentially growing mycelium of *Mucor rouxii*: properties and function, J. Gen. Microbiol. 137 (1991) 2797–2810.

[3] H. Merzendorfer, L. Zimoch, Chitin metabolism in insects: structure, function and regulation of chitin synthases and chitinases, J. Exp. Biol. 206 (2003) 4393–4412.

[4] A. Herrera-Estrella, I. Chet, Chitinases in biological control, EXS 87 (1999) 171–184.

[5] L.S. Melchers, M.H. Stuiver, Novel genes for disease-resistance breeding, Curr. Opin. Plant Biol. 3 (2000) 147–152.

[6] R.S. Patil, V.V. Ghormade, M.V. Deshpande, Chitinolytic enzymes: an exploration, Enzyme Microb. Technol. 26 (2000) 473–483.

[7] L.E. Donnelly, P.J. Barnes, Acidic mammalian chitinase—A potential target for asthma therapy, TRENDS Pharmacol. Sci. 25 (2004) 509–511.

[8] M. Wills-Karp, C.L. Karp, Chitin checking-novel insights into asthma, N. Engl. J. Med. 351 (2004) 1455–1457.

[9] W. Suginta, P.A. Robertson, B. Austin, S.C. Fry, L.A. Fothergill-Gilmore, Chitinases from *Vibrio*: activity screening and purification of chiA from *Vibrio carchariae*, J. Appl. Microbiol. 89 (2000) 76–84.

[10] W. Suginta, A. Vongsuwan, C. Songsiririthigul, H. Prinz, P. Estibeiro, R.R. Duncan, J. Svasti, L.A. Fothergill-Gilmore, An endochitinase A from *Vibrio carchariae*: cloning, expression, mass and sequence analyses, and chitin hydrolysis, Arch. Biochem. Biophys. 424 (2004) 171–180.

[11] B. Henrissat, A. Bairoch, New families in the classification of glycosyl hydrolases based on amino acid sequence similarities, Biochem. J. 293 (1993) 781–788.

[12] A. Perrakis, I. Tews, Z. Dauter, A.B. Oppenheim, I. Chet, K.S. Wilson, C.E. Vorgias, Crystal structure of a bacterial chitinase at 2.3 Å resolution, Structure 2 (1994) 1169–1180.

[13] T. Hollis, A.F. Monzingo, K. Bortone, S. Ernst, R. Cox, J.D. Robertus, The X-ray structure of a chitinase from the pathogenic fungus *Coccidioides immitis*, Protein Sci. 9 (2000) 544–551.

[14] K. Suzuki, M. Taiyoji, N. Sugawara, N. Nikaidou, B. Henrissat, T. Watanabe, The third chitinase gene (chiC) of *Serratia marcescens* 2170 and the relationship of its product to other bacterial chitinases, Biochem. J. 343 (1999) 587–596.

[15] W. Suginta, A. Vongsuwan, C. Songsiririthigul, J. Svasti, H. Prinz, Enzymatic properties of wild-type and active site mutants of chitinase A from *Vibrio carchariae*, as revealed by HPLC-MS, FEBS J. 272 (2005) 3376–3386.

[16] I. Tews, A.C. Terwisscha van Scheltinga, A. Perrakis, K.S. Wilson, B.W. Dijkstra, Substrate-assisted catalysis unifies two families of chitinolytic enzymes, J. Am. Chem. Soc. 119 (1997) 7954–7959.

[17] K.A. Brameld, W.A. Goddard III, Substrate distortion to a boat conformation at subsite −1 is critical in the mechanism of family 18 chitinases, J. Am. Chem. Soc. 120 (1998) 3571–3580.

[18] A.C. Terwisscha van Scheltinga, S. Armand, K.H. Kalk, A. Isogai, B. Henrissat, B.W. Dijkstra, Stereochemistry of chitin hydrolysis by a plant chitinase/lysozyme and X-ray structure of a complex with allosamidin: evidence for substrate assisted catalysis, Biochemistry 34 (1995) 15619–15623.

[19] D.M. van Aalten, D. Komander, B. Synstad, S. Gaseidnes, M.G. Peter, V.G. Eijsink, Structural insights into the catalytic mechanism of a family 18 exo-chitinase, Proc. Natl. Acad. Sci. U. S. A. 98 (2001) 8979–8984.

[20] C. Sasaki, A. Yokoyama, Y. Itoh, M. Hashimoto, T. Watanabe, T. Fukamizo, Comparative study of the reaction mechanism of family 18 chitinases from plants and microbes, J. Biochem. (Tokyo) 131 (2002) 557–564.

[21] T. Fukamizo, C. Sasaki, E. Schelp, K. Bortone, J.D. Robertus, Kinetic properties of chitinase-1 from the fungal pathogen *Coccidioides immitis*, Biochemistry 40 (2001) 2448–2454.

[22] N.N. Aronson Jr., B.A. Halloran, M.F. Alexyev, L. Amable, J.D. Madura, L. Pasupulati, C. Worth, P. Van Roey, Family 18 chitinase-oligosaccharide substrate interaction: subsite preference and anomer selectivity of *Serratia marcescens* chitinase A, Biochem. J. 376 (2003) 87–95.

[23] T. Watanabe, A. Ishibashi, Y. Ariga, M. Hashimoto, N. Nikaidou, J. Sugiyama, T. Matsumoto, T. Nonaka, Trp122 and Trp134 on the surface of the catalytic domain are essential for crystalline chitin hydrolysis by *Bacillus circulans* chitinase A1, FEBS Lett. 494 (2001) 74–78.

[24] T. Uchiyama, F. Katouno, N. Nikaidou, T. Nonaka, J. Sugiyama, T. Watanabe, Roles of the exposed aromatic residues in crystalline chitin hydrolysis by chitinase A from *Serratia marcescens* 2170, J. Biol. Chem. 276 (2001) 41343–41349.

[25] F. Katouno, M. Taguchi, K. Sakurai, T. Uchiyama, N. Nikaidou, T. Nonaka, J. Sugiyama, T. Watanabe, Importance of exposed aromatic residues in chitinase B from *Serratia marcescens* 2170 for crystalline chitin hydrolysis, J. Biochem. (Tokyo) 136 (2004) 163–168.

[26] Y. Itoh, J. Watanabe, H. Fukada, R. Mizuno, Y. Kezuka, T. Nonaka, T. Watanabe, Importance of Trp59 and Trp60 in chitin-binding, hydrolytic, and antifungal activities of *Streptomyces griseus* chitinase C, Appl. Microbiol. Biotechnol. 72 (2006) 1176–1184.

[27] T. Watanabe, Y. Ariga, U. Sato, T. Toratani, M. Hashimoto, N. Nikaidou, Y. Kezuka, T. Nonaka, J. Sugiyama, Aromatic residues within the substrate-binding cleft of *Bacillus circulans* chitinase A1 are essential for hydrolysis of crystalline chitin, Biochem. J. 376 (2003) 237–244.

[28] Collaborative Computational Project, Number 4, The CCP4 suit: programs for protein crystallography, Acta Cryst. D50 (1994) 760–763.

[29] U.K. Laemmli, Cleavage of structural proteins during the assembly of the head of bacteriophage T4, Nature 227 (1970) 680–685.

[30] M.M. Bradford, A rapid and sensitive method for the quantitation of microgram quantities of protein utilizing the principle of protein-dye binding, Anal. Biochem. 72 (1976) 248–254.

[31] A. Bruce, U. Srinivasan, H.J. Staines, T.L. Highley, Chitinase and laminarinase production in liquid culture by *Trichoderma* spp. and their role in biocontrol of wood decay fungi, Int. Biodeterior. Biodegrad. 35 (1995) 337–353.

[32] S.C. Hsu, J.L. Lockwood, Powdered chitin agar as a selective medium for enumeration of actinomycetes in water and soil, Appl. Microbiol. 29 (1975) 422–426.

[33] T. Tanaka, S. Fujiwara, S. Nishikori, T. Fukui, M. Takagi, T. Imanaka, A unique chitinase with dual active sites and triple substrate binding sites from the hyperthermophilic Archaeon *Pyrococcus kodakaraensis* KOD1, Appl. Environ. Microbiol. 15 (1999) 5338–5344.

[34] T. Imai, T. Watanabe, T. Yui, J. Sugiyama, Directional degradation of beta-chitin by chitinase A1 revealed by a novel reducing end labelling technique, FEBS Lett. 510 (2002) 201–205.

[35] N.N. Aronson Jr., B.A. Halloran, M.F. Alexyev, X.E. Zhou, Y. Wang, E.J. Meehan, L. Chen, Mutation of a conserved tryptophan in the chitin-binding cleft of *Serratia marcescens* chitinase A enhances transglycosylation, Biosci. Biotechnol. Biochem. 70 (2006) 243–251.

CURRICULUM VITAE

NAME Mrs. Chomphunuch Songsiriritthigul

DATE OF BIRTH 21 December 1972

PLACE OF BIRTH Bangkok, Thailand

+

INSTITUTION ATTENDED

Kasetsart University, Bangkok, Thailand, 1991-1994,

Bachelor of Science (Chemistry)

Mahidol University, Bangkok, Thailand, 1995-1997,

Master of Science (Applied Analytical and Inorganic

Chemistry)

Suranaree University of Technology, Nakhon Ratcha-

sima, Thailand, 2002-2007,

Doctor of Philosophy (Biochemistry)

AWARDS AND SCHOLARSHIPS

Postgraduate Scholarship for M.Sc. Degree from the

National Science and Technology Development

Agency (NSTDA) : Funding via Institutional

Strengthening Program (ISP)